

TE  
662  
.A3  
no.  
FHWA-  
RD-  
74-68  
C.2

Dept. Of Transportation  
JUN 16 1975  
Library

No. FHWA-RD-74-68

# TERMINATION OF THE IN-SITU STATE OF STRESS IN SOIL MASSES

P. J. Huck, H. J. Pincus, et al.



September 1974

Final Report

This document is available to the public  
through the National Technical Information  
Service, Springfield, Virginia 22161

Prepared for  
**FEDERAL HIGHWAY ADMINISTRATION**  
Offices of Research & Development  
Washington, D.C. 20590

## NOTICE

This document is disseminated under the sponsorship of the Department of Transportation in the interest of information exchange. The United States Government assumes no liability for its contents or use thereof.

The contents of this report reflect the views of the contracting organization, which is responsible for the facts and the accuracy of the data presented herein. The contents do not necessarily reflect the official views or policy of the Department of Transportation. This report does not constitute a standard, specification, or regulation.

Sufficient copies of this report are being distributed by FHWA Bulletin to provide a minimum of two copies to each regional office, one copy to each division office, and two copies to each State highway agency. Direct distribution is being made to the division offices.

1. Report No. FHWA-RD-74-68		2. Government Accession No.		3. Recipient's Catalog No.	
4. Title and Subtitle DETERMINATION OF THE IN-SITU STATE OF STRESS IN SOIL MASSES,		5. Report Date September 1974		6. Performing Organization Code	
		8. Performing Organization Report No. D6083			
7. Author(s) Peter J. Huck, Howard J. Pincus Madan M. Singh, Y. P. Chugh		10. Work Unit No. (TRAIS) FPC35B2-0052		11. Contract or Grant No. DOT-FH-11-8082	
9. Performing Organization Name and Address IIT Research Institute 10 West 35th Street Chicago, Illinois 60616		13. Type of Report and Period Covered Final Report		14. Sponsoring Agency Code SD340	
		12. Sponsoring Agency Name and Address Department of Transportation Federal Highway Administration, Office of Research Washington, D.C. 20590			
15. Supplementary Notes FHWA Contract Manager: Dr. Steven I. Majtenyi					
16. Abstract <p>The mass behavior of soil and the loadings imparted to civil engineering works by soil masses are strongly influenced by the naturally existing in-situ soil stresses. The determination of in-situ stresses in soil masses is a difficult problem which, in some cases, requires extensive and subtle evaluation if even an approximate determination is to be made.</p> <p>These studies were conducted to review and assess techniques. Methods for estimating in-situ stress from a knowledge of the soil and assumed stress history, as well as direct measurement methods are identified and described. All known methods for determining in-situ stresses are summarized. Recommendations are made for the development of (a) more sophisticated hardware, (b) transfer and development of fabric analysis technology to soil mechanics, and (c) long range development of magnetic resonance techniques.</p>					
17. Key Words Soil Mechanics Tunneling Subsurface Investigation Stresses			18. Distribution Statement No restrictions. This document is available through the National Technical Information Service, Springfield, Virginia 22151.		
19. Security Classif. (of this report) unclassified		20. Security Classif. (of this page) unclassified		21. No. of Pages 316	
				22. Price	





## FOREWORD

This project was funded by the Department of Transportation, Federal Highway Administration Office of Research under Contract DOT-FH-11-8082. This support and the guidance of the technical monitor, Dr. S.I. Majtenyi, are gratefully acknowledged.

Mr. Huck acted as principal investigator, with overall technical and administrative direction provided by Dr. M. Singh. Major contributions were made by Dr. H. Pincus in Fabric Analysis, by Mr. F. Jarke in Electroparamagnetic Resonance, and by Drs. T. Liber and Y.P. Chugh in analytic modeling. A number of investigators outside geotechnical disciplines contributed to the studies. Dr. H. O'Neill and Mr. R. Semmler conducted the efforts on electron beam and gamma-ray techniques, and Mr. H. Hegner, L. Townsend and H. Tobin conducted the efforts on electromagnetic applications. Consultation was provided by Dr. R. Ohlhaber in electron microscopy and by Dr. P. Toulas in infrared. Mr. S. Varadhi assisted in the review and evaluation of the geotechnical literature.

Considerable assistance was obtained from correspondence and conversations with investigators both in this country and abroad. We hope the work of these men is treated accurately and fairly in this report.

# TABLE OF CONTENTS

<u>Section</u>	<u>Page</u>
1. INTRODUCTION	1
2. EXISTING TECHNOLOGY	5
2.1 State of Stress	5
2.1.1 Soil Stresses	5
2.1.2 Earth Pressure at Rest	6
2.2 Evaluation of $K_o$	9
2.2.1 Theoretical Evaluation-Normally Consolidated	12
2.2.2 Empirical Evaluation - Overconsolidated	16
2.3 Laboratory Determination of Stresses	18
2.3.1 Special Triaxial Tests	22
2.3.2 $K_o$ Devices	28
2.3.3 Laboratory Tests for In-Situ Stresses	32
2.4 In-Situ Determination of Stresses	43
2.4.1 Acoustic Wave Propagation	43
2.4.2 Borehole Deformation Techniques	51
2.4.3 Stress Probe	60
2.4.4 Hydraulic Fracturing Methods	62
2.4.5 Vane Shear Tests	70
2.4.6 Comparison of Field Determinations	74
2.5 Evaluation of Anisotropic Properties	78
2.5.1 Introduction	78
2.5.2 Hydraulic Permeability	82
2.5.3 Electrical Conductivity	88
2.5.4 Electron Microscopy	93
2.5.5 Infrared	98
2.5.6 Gamma Radiation	99
2.5.7 X-Rays	100
2.5.8 Electron Beam Techniques	101
2.5.9 Summary of Anisotropic Properties Measurements	105

# TABLE OF CONTENTS (cont.)

<u>Section</u>	<u>Page</u>
3. FABRIC ANALYSIS	107
3.1 Introduction	107
3.2 Expectations of Fabric Analysis	107
3.3 Statistical Methods	116
3.4 Anticipated Behavior of Various Soil Types	138
3.5 Orientation of Measuring Devices with Respect to Soil Fabric	140
3.6 Experimental Work to Investigate Relations Among Changes in Fabric, Stress History, and Initial Fabric and Composition	146
3.7 Plans for Mapping and Analyzing Soil Fabrics	174
3.8 Field Sampling	194
3.9 Recommendations	198
4. ELECTROMAGNETIC RESONANCE	205
4.1 Introduction	205
4.2 Nuclear Magnetic Resonance	205
4.3 Nuclear Quadrupole Resonance	208
4.4 Electron Paramagnetic Resonance	209
4.5 Experimental Results	211
4.6 Recommendations	212
5. RECOMMENDED IN-SITU STRESS GAGE DEVELOPMENT	214
5.1 Criteria and Capabilities	214
5.2 Analysis of Insertion Disturbance	215
5.2.1 Analysis Methods and Assumptions	215
5.2.2 Vertical Stress Below Probe	219
5.2.3 Driving Shear Stress	223
5.2.4 Lateral Perturbations While Driving	226
5.2.5 Release of In-Situ Shear Stress	230
5.3 Stress Measurement Concepts	234
5.3.1 Menard Pressuremeter	234
5.3.2 Self-Boring Pressuremeter	237

# TABLE OF CONTENTS (cont.)

<u>Section</u>	<u>Page</u>
5.3.3 Zone Pressurization	240
5.4 Summary of Probe Requirements	247
5.5 Proposed Development Plan for In-Situ Stress Gage	248
6. SUMMARY	254
6.1 Overview	254
6.2 Currently Existing Techniques	254
6.3 Recommended Development	255
APPENDIX A --SOIL STRESSES	258
A.1 Stress Tensor	258
A.2 Effective Stress Concept	266
A.3 Stress Transformation Equations	266
A.4 Discontinuous In-Plane Stresses In a Layered Semi-Infinite Body	269
APPENDIX B --FABRIC ANALYSIS GLOSSARY	280
APPENDIX C --ELECTRON MICROSCOPY: SPECIMEN PREPARATION	288
BIBLIOGRAPHY	292

# LIST OF FIGURES

<u>Figure</u>		<u>Page</u>
2-1	Stress History for $K_o$ Overconsolidated Site	8
2-2	Stress History for Normally Consolidated Site with Lateral Stress Relief	8
2-3	Stress Path: Normally Consolidated Plane Strain	10
2-4	Stress Path: Overconsolidated Isotropic	10
2-5	Stress Distribution for Constant $K_o$ in Normally and Overconsolidated Soils	11
2-6	Stress Distribution for $K_o = K_p$ Overconsolidated Soil	11
2-7	Equilibrium of Wedge Shaped Soil Mass	13
2-8	Reported Values of $K_o$ Compared with Theoretical Approximations	15
2-9	Precompression Ratio vs $K_o$ for Seattle Clay	17
2-10	Liquid Limit vs $\lambda$ and $\alpha$	17
2-11	Reported Relationships Between Overconsolidation Ratio and $K_o$	19
2-12	Relationship Between $K_o$ , $\phi'$ and OCR	20
2-13	Relationship Between $K_o$ , PI and OCR	21
2-14	$K_o$ Test Cell	23
2-15	Non-Contacting Capacitive Lateral Strain Gage	25
2-16	Circumferential Strain Gage	27
2-17	Interpolation of $K_o$ from Constant Stress Ratio Tests	29
2-18	$K_o$ Test Cell	30
2-19	Axial and Radial Stress History for $K_o$ Test on Bearpaw Shale	31



# LIST OF FIGURES (cont.)

<u>Figure</u>		<u>Page</u>
2-20	Axial and Radial Stresses for Bearpaw Shale	31
2-21	Obrcian's $K_o$ Device	33
2-22	Obrcian's $K_o$ vs Axial Stress Data (typical)	33
2-23	Axial and Radial Stresses Back Computed from Obrcian's Data	34
2-24	University of Washington Stress-Meter	35
2-25	$K_o$ Relationships Obtained with U of W Stress-Meter	35
2-26	Horizontal Consolidation Test Data - $K_o = 0.5$	37
2-27	Horizontal Consolidation Test Data - $K_o = 1.0$	38
2-28	Effect of Sampling Disturbance on Horizontal Consolidation Test	39
2-29	Variation of $K_o$ and $K_p$ with Depth at Bradwell	42
2-30	Velocity Ellipse and Principal Stress Directions	45
2-31	Shear Wave Velocity Data in Dry Ottawa Sand	47
2-32	Cross-Borehole Shooting Methods	48
2-33	Refraction Corrections for Cross-Borehole Shooting Method	49
2-34	Classic Menard Pressuremeter	53
2-35	Idealized Menard Pressuremeter Data	54
2-36	Pressuremeter Component of Cambridge In-Situ Test Device	56
2-37	Self-Boring Pressuremeter	58
2-38	Cambridge Stress Probe	61

# LIST OF FIGURES (cont.)

<u>Figures</u>		<u>Page</u>
2-39	Cambridge Stress Probe Lab and Field Data	63
2-40	Lateral Stresses at King's Lynn	64
2-41	Hydraulic Fracturing Idealization	65
2-42	Hydraulic Fracturing Data in Rock	66
2-43	Bjerrum Hydrofrac Apparatus	68
2-44	Hydrofrac Data in Soil	69
2-45	Vanes Used in Anisotropic Vane Shear Test	71
2-46	Anisotropic Vane Shear Data	73
2-47	Predicted Crack Profiles	80
2-48	Actual Crack Patterns	80
2-49	Distribution of Crack Inclinations	81
2-50	Effect of Specimen Orientation on $A_f$	83
2-51	Pore Size Distributions	85
2-52	Pore Size Distributions	86
2-53	Electrical Dispersion Data	89
2-54	Effect of Stress Reversal on Conductivity Parallel to Shear Plane	91
2-55	DC Conductivity vs Shear Deformation	92
2-56	Effect of Triaxial Test on Grain Orientation Distribution	95
2-57	Stress Ratio vs Orientation Parameter $S_z/S_x$	96
2-58	Distribution of Contact Angles in Direct Shear Test	97
2-59	Preferred Orientation Ratio by Meade's X-ray Diffraction Method	102
2-60	Orientation Ratio by Martin's X-ray Diffraction Method	103

# LIST OF FIGURES (cont.)

<u>Figures</u>		<u>Page</u>
2-61	Orientation Ratio vs Strain	104
3-1	Kinematic and Dynamic Petrofabrics	109
3-2	External and Internal Factors Influencing Deformation	109
3-3	Types of Fabric Symmetry	110
3-4	Relation Between Homogeneity and Scale	113
3-5	Discontinuities in the Same Body at Different Scales	113
3-6	Physical Features Defining Foliations	115
3-7	Physical Features Defining Lineations	115
3-8	Generation of Stereographic and Lambert Projections	122
3-9	Contouring of a Point Diagram	122
3-10	Types of Fabric Diagrams	123
3-11	Axial Subfabrics and Orthorhombic Subfabrics Illustrated by Contoured Equal-Area Projections	123
3-12	Monoclinic and Triclinic Subfabrics Illustrated by Equal-Area Projections	124
3-13	Idealized Shear and Extension Fractures Associated with a Fold	124
3-14	Optical Diffraction Apparatus	126
3-15	Relation of Diffraction Pattern to Distribution Parameters of Input	127
3-16	Idealized Optical Diffraction Input and Output	128
3-17	Optical Diffraction of Intersection Lines	129
3-18	Spatial Frequency Analysis by Diffraction	130
3-19	Fourier Transforms of Simple Functions	131

# LIST OF FIGURES (cont.)

<u>Figures</u>		<u>Page</u>
3-20	Fourier Transforms of Truncated Functions	132
3-21	Equipment Lay-Out for Optical Diffraction	133
3-22	Flow Charts for Production of Transform and Filtered Image	134
3-23	Idealized Input and Outputs	135
3-24	Filtering of Polar Coordinate Paper	136
3-25	Grain Alignment in Experimentally Deformed Clays	143
3-26	Transforms of Particles Having Varying Sphericity and Roundness	150
3-27a	Grain Size Chart	151
3-27b	Transform of Grain Size Drawings	152
3-28a	Half-Tones of Grain Size Chart	153
3-28b	Transforms of Grain Size Half-Tones	154
3-29	Typical Reference Inputs and Transforms	155
3-30	Filtering of Quartzite Photomicrograph	156
3-31	Calibration Transform	157
3-32	Macropeds of Similar Size and Shape-- Input and Transform	158
3-33	Cuneate Macropeds of Dissimilar Size with Inclined Joint Planes -- Input and Transform	159
3-34	Macropeds of Dissimilar Size and Shape with Craze Planes--Input and Transform	160
3-35	Apedal Soil--Input and Transform	161
3-36	Irregular Ortho-Joint Planes--Input and Transform	162
3-37	Craze Planes--Input and Transform	163

# LIST OF FIGURES (cont.)

<u>Figures</u>		<u>Page</u>
3-38	Simple Free Grain Argillans with Strong Continuous Orientation	164
3-39	Simple Skew-Plane Argillan with Straited Orientation -- Input and Transform	165
3-40	Vugh and Plane Argillans and Chalcedans - Input and Transforms	166
3-41	Compound Crystal Chamber - Input and Transform	167
3-42	Fecal Pellet - Input and Transform	168
3-43	Mosepic Plasmic Fabric-Input and Transform	169
3-44	Clino-Bimasepic Plasmic Fabric--Input and Transform	170
3-45	Omnisepic Plasmic Fabric-Input and Transform	171
3-46	Surfaces of Discontinuity or Heterogeneity	177
3-47	Methods of Marking Oriented Hand Specimens	180
3-48	Orientation and Marking of Hand Specimens and Thin Sections	180
3-49a	Rectangularly Stacked Ovals with Varying Axial Ratios	181
3-49b	Transform of Figure 3-49a	182
3-50a	Rhombic Stacking of Ovals	184
3-50b	Transform of Figure 3-50a	185
3-51	Transform Profiles of Tennessee Marble Under Uniaxial Compression	186
3-52	Graphical Analysis of Transform Profiles	188
3-53a	Uniaxially Loaded Specimens of Tennessee Marble	192
3-53b	Transforms of Figure 3-53a	193



# LIST OF FIGURES (cont.)

<u>Figures</u>		<u>Page</u>
3-54	Triaxially Loaded Tennessee Marble - Input and Transform	195
4-1	EPR Spectrum of $\gamma$ -Irradiated Kaolin	213
5-1	Components of Self-Boring Devices	218
5-2	Finite Element Mesh Used for Analysis	220
5-3	Comparison of FEM and Closed Form Solution Analysis	221
5-4	Shear Contours Generated by FEM Analysis	222
5-5	Insertion Shear Stresses	225
5-6	Insertion Shear Stress vs Interface Shear Resistance	227
5-7	Stresses Resulting from Lateral Perturbation	228
5-8	Release of In-Situ Lateral Shear Stress	231
5-9	Effect of Interface Shear Resistance on Release of Lateral Shear Stress	233
5-10	Concept - Driving Through Lubricated Membrane	235
5-11	Concept - Non Circular Geometry	235
5-12	Radial Deflections for Classic Borehole Pressuremeter	236
5-13	Behavior of Self-Boring Pressuremeter in Biaxial Lateral Stress Field	238
5-14	Radial Deflections for Self-Boring Pressuremeter	239
5-15	Concept - Hydraulic Zone Pressurization	241
5-16	Stresses Associated with Zone Pressurization	243
5-17	Stress Circle Obtained from Zone Pressurization Concept	244
5-18	Hydraulic Zone Pressurization Gage Response	246
5-19	Recommended Hardware Development Work Plan	249

# LIST OF FIGURES (cont.)

<u>Figures</u>	<u>Page</u>
A-1      Normal and Shear Stresses in the x-y Plane	259
A-2      Development of the Stress Concept	261
A-3      Principal Stresses in a Plane	262
A-4      Mohr's Circle for Stresses	264
A-5      Stress Ellipse	265
A-6      Layered Semi-Infinite Continuous Elastic Body	270
A-7      Example of Stresses and Strains in Three Layer Semi-Infinite Body	276

## LIST OF TABLES

<u>Table</u>	<u>Page</u>
2.1      Applicability of Existing Field Methods to Various Geotechnical Conditions	75
2.2      Characteristics of Existing In-Situ Devices	76
3.1      Deformation Indicators Related to Soil Types	141
3.2      Deformation Indicators Related to Fabric Components	142
3.3      Scaling Relationships via Measurements on Inputs and Outputs	172
3.4      Elongations of Rectangularly Stacked Ovals	183
3.5      Proposed Fabric Analysis Work Plan Outline	199
3.6      Recommended Fabric Analysis Plan-Objectives, Milestones and Results	202
4.1      NMR Active Isotopes	206
5.1      Interface Shear Resistance Parameters	224
5.2      Level of Effort for Recommended Hardware Development Work Plan	253
6.1      Characteristics of Various In-Situ Techniques	255
D.1      Use of Various Specimen Preparation Techniques for Investigations of Soil Microstructure	290

# NOMENCLATURE

A	Skempton's pore pressure coefficient
$\bar{A}$	alternate form of Skempton's pore pressure coefficient given by $\bar{A} = AB$
$\bar{A}_f$	Skempton's pore pressure coefficient at failure
$\overline{\Delta A}$	change in area
a	interface adhesion at soil/construction material interface (psi or N/m <sup>2</sup> )
B	Skempton's pore pressure parameter defined by $B = [(\Delta u)/(\Delta \sigma_3)]$
C	capacitance (Farads)
$C_a$	shape factor for hydraulic flow through soil medium
c'	soil cohesion in terms of effective stress (psi or N/m <sup>2</sup> )
D	diameter
E	modulus of elasticity (psi or N/m <sup>2</sup> )
$E_d$	dynamic elastic modulus (psi or N/m <sup>2</sup> )
e	void ratio
$F(u,v)$	Fourier transform representing the complex amplitude as a function of position coordinates (u,v) in the transform plane (back focal plane)
f	focal length of lens
$f(x,y)$	input function as a function of position coordinates (u,v) in the transform plane (back focal plane)
$f_c$	interface shear resistance factor for cohesion $f_c = a/c$ (psi or N/m <sup>2</sup> )
$f_\phi$	interface shear resistance factor for friction $f_\phi = \delta/\phi$ (psi or N/m <sup>2</sup> )
$f_o$	characteristic frequency (Hz)

# NOMENCLATURE (Cont'd.)

$G_d$	dynamic shear modulus (psi or $N/m^2$ )
$H$	height
$\Delta H$	fluid head loss
$I_o(\kappa)$	a Bessel function of the first kind of pure imaginary argument
$i$	D.C. current flow (amps)
$k$	dielectric constant
$K_a$	active earth pressure coefficient that defines the stress ratio at failure
$k_H$	hydraulic permeability coefficient
$K_o$	coefficient of earth pressure at rest
$K_p$	passive earth pressure coefficient that defines the stress ratio at failure
$n$	porosity
$P_I$	internal pressure (psi or $N/m^2$ )
$P_r$	overconsolidation ratio
$P_s$	instantaneous shut in pressure for hydraulic fracture (psi or $N/m^2$ )
$Q$	hydraulic flow rate (volume per unit time)
$R_H$	hydraulic radius
$r_a$	number of spikes between D.C. (zero frequency) and the first order spike with height $\geq$ some constant specified fraction of the height of the first order spike, for load a.
$r_b$	same as for $r_a$ , for load b
$\bar{r}_a$	mean value of $r_a$ for both sides of the profiles
$\bar{r}_b$	mean value of $r_b$ for both sides of the profiles



# NOMENCLATURE (Cont'd.)

S	shear strength (psi or $N/m^2$ )
$S_v$	vertical shear strength (psi or $N/m^2$ )
$S_h$	horizontal shear strength (psi or $N/m^2$ )
$S_{ij}$	total stress tensor (psi or $N/m^2$ )
T	torque required to shear vanes of various aspect ratio (lb-ft or N-m)
u	pore pressure in the sample (psi or $N/m^2$ )
$u_o$	initial pore pressure at depth Z (psi or $N/m^2$ )
V	measured velocity (ft/sec or m/sec)
$V_p$	dilatational wave velocity (ft/sec or m/sec)
$V_s$	distortional wave velocity (ft/sec or m/sec)
$\Delta V$	impressed voltage (volts)
x,y,z	cartesian coordinates
$\alpha_g$	angle coordinate of center of gravity of distribution
$\bar{\alpha}$	angle coordinate of center of gravity of sample taken as maximum likelihood estimate of $\alpha_g$
$\gamma$	density ( $lb/ft^3$ or $kg/m^3$ )
$\gamma_w$	unit weight of water
$\delta$	interface friction angle
$\delta_{\beta\gamma}$	Kronecker's delta
$\delta_{\alpha\gamma}$	Kronecker's delta
$\epsilon_v, \epsilon_h$	vertical and horizontal strains
$\epsilon_o$	permittivity constant (Farads/meter)
$\eta$	viscosity of fluid
$\kappa$	a measure of concentration about the mean

# NOMENCLATURE (Cont'd.)

$\lambda$	wavelength of incident light (meter)
$\nu$	Poisson's ratio
$\nu_d$	dynamic Poisson's ratio
$\rho$	mass density (slug/ft <sup>3</sup> or kg/m <sup>3</sup> )
$\sigma_1, \sigma_2, \sigma_3$	principal stresses (psi or N/m <sup>2</sup> )
$\sigma_o$	confining pressure
$\sigma_{ij}$	tensor representing the three dimensional state of stress at a point
$\sigma_m$	mean stress
$\sigma_n$	normal stress
$\sigma_v, \sigma_h$	vertical and horizontal normal stress (psi or N/m <sup>2</sup> )
$\sigma_x, \sigma_z$	normal stress in x and z directions
$\sigma_{DC}$	DC conductivity (mho/m)
$\sigma_{AC}$	AC conductivity (mho/m)
$\sigma'_v, \sigma'_h$	effective vertical and horizontal normal stress
$\tau_I$	Interface shear resistance
$\tau_{xz}, \tau_{r\theta}$	shear stress in xz or $r\theta$ plane
$\emptyset$	angle of internal friction
$\emptyset'$	angle of friction based on effective stress notation
$\psi$	critical angle to vertical for crack propagation



# DETERMINATION OF IN-SITU STRESSES IN SOIL MASSES

## 1. INTRODUCTION

The behavior of a soil mass under loading or during excavation depends upon the stress field that naturally exists in-situ. This stress field defines the extent to which the soil shear strength may be already mobilized and the origin of the stress paths that will be followed on subsequent additional loading, unloading and changes of the boundaries of the soil masses. Usually, the in-situ state of stress at a point in the soil mass is not the result of elastic or plastic equilibrium alone but also is influenced by the stress history and other factors (e.g., chemical, temperature).

At present computer methods allow us to estimate ground movements and changes in the state of stress during and after the construction of structures. The reliability of the computation and, in particular, the evaluation of stability conditions, the estimation of ground movements and stresses on the structures depend equally upon a realistic soil model and the initial stress state. A realistic soil model itself requires knowledge of all the stresses, including the intermediate stresses. The significance of the intermediate stress on soil behavior has been pointed out by Henkel (1958), Duncan (1966) and others. The factor of safety depends on the initial stress state, the degree to which the soil strength is mobilized and the origin of the subsequent loading path. It is necessary that the full in-situ stress tensor existing in the field be known.

Movements predicted by modern mathematical techniques are sensitive to the initial stresses input into the program. Current practice is to make simplifying assumptions regarding the existing in-situ stresses, and under some geotechnical conditions these assumptions are justified. The assumptions

often are hidden within the programming, so that the geotechnical engineer may not be aware that initial in-situ stress levels are based on estimated values of elastic moduli. In-situ stresses should be measured by geotechnical engineers--not estimated by computers.

This study addresses the problem of the in-situ state of stress in soils. Under simple conditions, such as a uniform, normally consolidated soil under a horizontal ground surface, the state of stress can be determined from theoretical considerations. In other cases, it should be measured in the field or in laboratories.

A number of field methods for measuring in-situ stresses exists: hydraulic fracturing, borehole pressuremeter, anisotropic vane shear test, acoustic velocity measurements and others. The use of these techniques permits us to make measurements in-situ of the least principal stress, the mean stress in the horizontal plane, or the stress ratio  $\sigma_h/\sigma_v$ . In-situ stresses may be also estimated by laboratory tests in combination with some knowledge of the stress history of the site. A typical procedure is to determine the overconsolidation ratio by standard means and to determine the ratio  $K_0$  for the particular type of soil under consideration through a load-release cycle to achieve the same overconsolidation ratio as exists in-situ.

Existing field and laboratory methods are limited. In-situ methods measure only single components of the stress tensor or a stress ratio. Laboratory techniques are too dependent on information that may not be available, and the assumption that the geologic history of a site may be reproduced on a laboratory time scale.

New methods and hardware capable of measuring the complete in-situ stress tensor are required to take full advantage of modern analysis tools. The studies reported herein were designed as a first definitive step in the



fulfillment of these needs. The scope includes evaluation of existing stress measurement methods and the development of improved concepts for determining the full stress tensor. The specific objectives were to:

- (A) Summarize current methods applicable to the determination of the state of stress in soils. Included are in-situ field determination of in-situ normal and shear stresses, and the principal stress directions, as well as field and lab methods for the estimation of stress history. This is discussed in Section 2 of this report.
- (B) Study the feasibility of applying fabric analysis in soils for determining the in-situ stresses. A number of subordinate objectives were included to define the extent to which fabric analysis can be applied to soils and the results which may be expected. This is discussed in Section 3 of this report.
- (C) Evaluation of the feasibility of utilizing anisotropic properties of undisturbed soil for determining in-situ stresses. The following technologies were reviewed for this purpose.
  - o Soil mechanics
  - o Water permeability
  - o Sound conduction
  - o X-rays
  - o Gamma-rays
  - o Electric conductivity
  - o Electron beam
  - o Electromagnetic resonance
  - o Infrared
  - o Electron microscopy

These are discussed in Section 2.5 and Section 4.

- (D) Bring to the level of a conceptual design the novel technique most promising for the determination of in-situ stresses. Included are theoretical analysis, development, evaluation and the delivery of preliminary drawings together with a work plan to realize the projected hardware. This is discussed in Section 5.

Because all users of this report will not be geotechnical engineers, brief reviews of soil stress notation and a glossary of fabric analysis terms are appended.

## 2. EXISTING TECHNOLOGY

### 2.1 STATE OF STRESS

#### 2.1.1 SOIL STRESSES

The three dimensional state of stress at a point may be expressed as a second-order symmetric tensor by

$$\sigma_{ij} = \begin{bmatrix} \sigma_{11} & \sigma_{12} & \sigma_{13} \\ \sigma_{21} & \sigma_{22} & \sigma_{23} \\ \sigma_{31} & \sigma_{32} & \sigma_{33} \end{bmatrix}$$

where  $\sigma_{AA}$  are normal stresses on three mutually perpendicular planes and  $\sigma_{AB} = \sigma_{BA}$  are the corresponding shear stresses on the same planes. If these planes are normal to the principal stress directions, the tensor becomes

$$\sigma_{ij} = \begin{bmatrix} \sigma_{11} & 0 & 0 \\ 0 & \sigma_{22} & 0 \\ 0 & 0 & \sigma_{33} \end{bmatrix}$$

in which the  $\sigma_{AA}$  are the principal stresses, and the shear stresses  $\sigma_{AB}$  are zero.

Several options are available in the determination of the stress tensor. The shear and normal stresses on three arbitrary orthogonal planes may be determined or the principal stresses and their directions may be determined. The choice in any given case depends on the technique used to make the measurement. Because direct measurements of shear stress in-situ are usually difficult, direct measurement techniques are generally used to monitor normal stress. Certain indirect techniques, e.g., fabric analysis, deal with shear stresses more effectively.

Traditionally, the intermediate principal stress has not been considered important in geotechnical applications. Its role is now the subject of an increasing amount of attention (Shibata and Karube, 1965; Broms and Casbarian, 1965; Saada and Zamani 1969) and it is important that methods of measuring the full stress tensor in-situ be developed to make use of these and other efforts.

The geologic events that lead to anisotropy of in-situ stresses are numerous. Any event that changes the conditions of lateral constraint, such as river valley erosion, tectonic movements, or nonlevel ground surface may be expected to result in modification of the lateral stresses. For this reason, a knowledge of the geologic history alone is not sufficient to estimate in-situ stresses.

#### 2.1.2 EARTH PRESSURE AT REST

The coefficient of earth pressure at rest,  $K_0$ , is defined as the ratio of horizontal to vertical effective stresses, for the case where the principal directions are vertical and horizontal and the lateral strain is zero. For example, "at rest" conditions may be obtained in a tri-axial test with the appropriate stress ratio, or in a natural deposit constrained against lateral deflection. To the extent that sidewall friction exists,  $K_0$  conditions are not present in a consolidation apparatus or a silo. An infinite slope or inclined strata do not, of course, impose restraint conditions for zero lateral strain.

The range of values that may be assumed by  $K_0$  is limited by the strength of the soil to

$$K_a \leq K_0 \leq K_p$$

where  $K_a$  and  $K_p$  are the active and the passive earth pressure coefficients that define the stress ratios at failure. For

a soil having cohesion  $c'$ , friction  $\phi'$ , and density  $\gamma$ , these active and passive limits are

$$K_a = \tan^2 \left( 45 - \frac{\phi'}{2} \right) - \frac{2c'}{\gamma z} \tan \left( 45 - \frac{\phi'}{2} \right)$$

$$K_p = \tan^2 \left( 45 + \frac{\phi'}{2} \right) + \frac{2c'}{\gamma z} \tan \left( 45 + \frac{\phi'}{2} \right)$$

at depth  $z$ . The term  $\gamma z$  replaces the major principal stress  $\sigma_1$  in the cohesion terms because  $K_0$  is defined only when the principal directions are vertical and horizontal.

Alternatively,  $K_0$  may be expressed in terms of Poisson's ratio  $\nu$  as

$$K_0 = \frac{\nu}{1-\nu}$$

Although Poisson's ratio is frequently assumed to lie between zero and one-half, soil is not an elastic material and  $K_0$  values greater than one often occur.

The history of a site is of major importance in the magnitude of  $K_0$ . For a history of monotonically increasing vertical stress, as in a normally consolidated soil, the value of  $K_0$  must be less than one and is frequently near the value  $K_0 = 1/2$ . If the vertical stresses are decreased by the removal of overburden, the horizontal stresses tend to remain locked in at relative high levels. For heavily over-consolidated soils,  $K_0$  may approach the passive failure condition  $K_p$ . Such a stress history is indicated in Figure 2-1. Alternatively, the horizontal stresses may be released, as by river down cutting, so that the active failure condition is approached as indicated in Figure 2-2. Tectonic stresses, changes in ground water level and other events may also modify the in-situ stresses.

The behavior of a soil mass is strongly dependent upon the existing in-situ stresses. Bjerrum (1967) suggested that progressive slope failure is encouraged by conditions of high lateral stress and low residual strength. Henkel (1970) used a simple stress space to indicate the influence

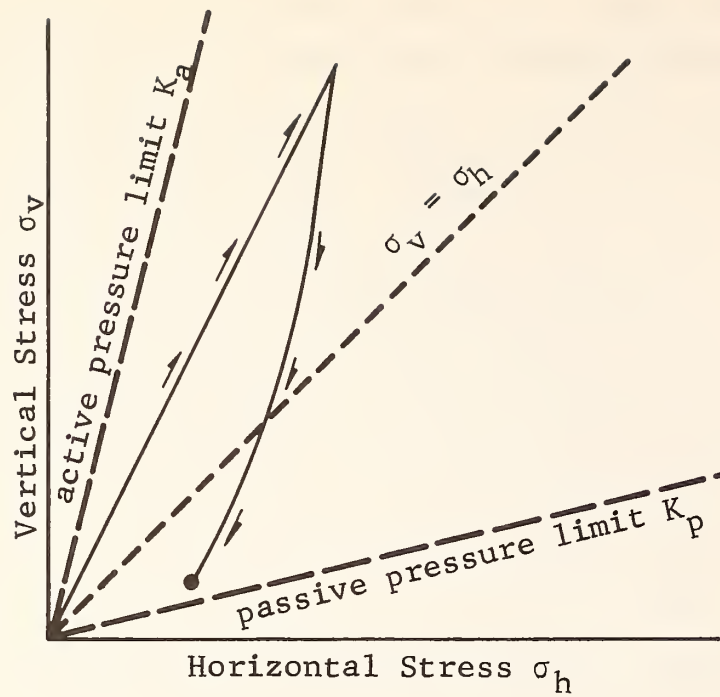


Figure 2-1. Stress History for  $K_0$  Overconsolidated Site

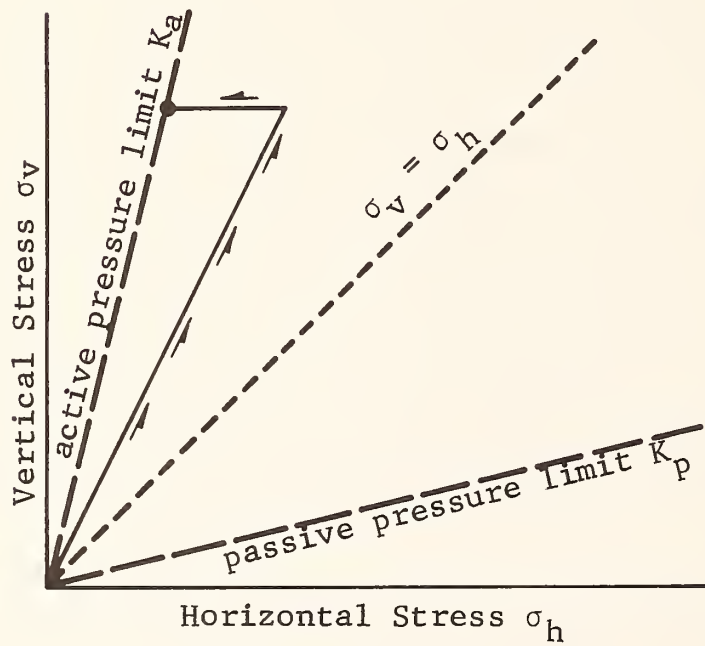


Figure 2-2. Stress History for Normally Consolidated Site with Lateral Stress Relief



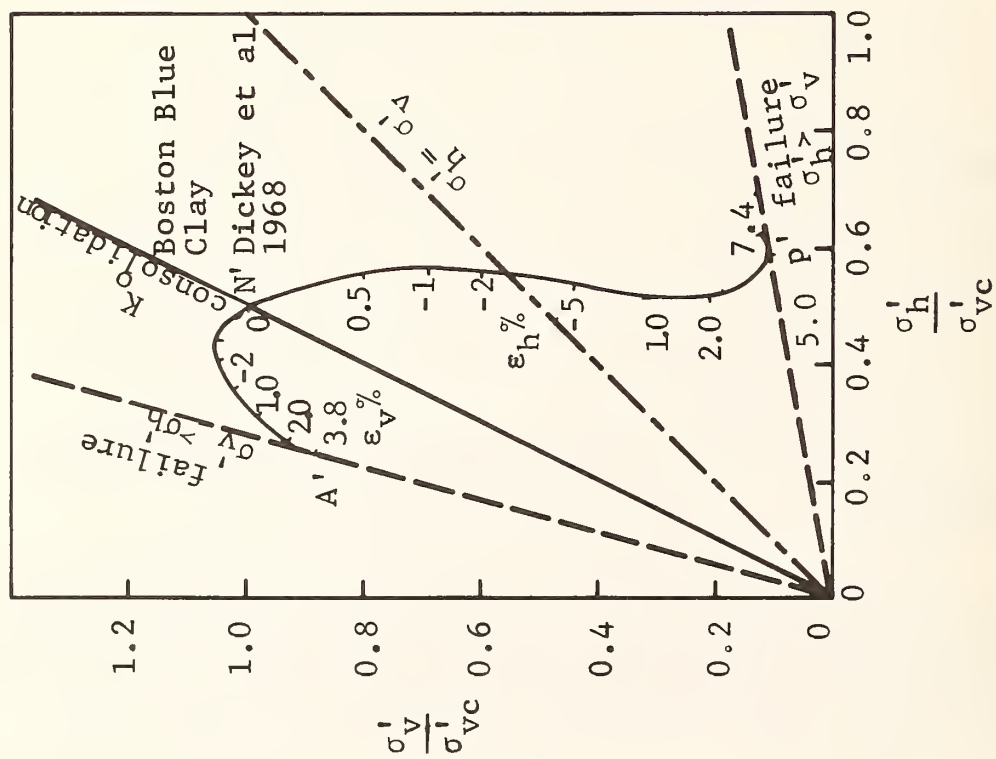
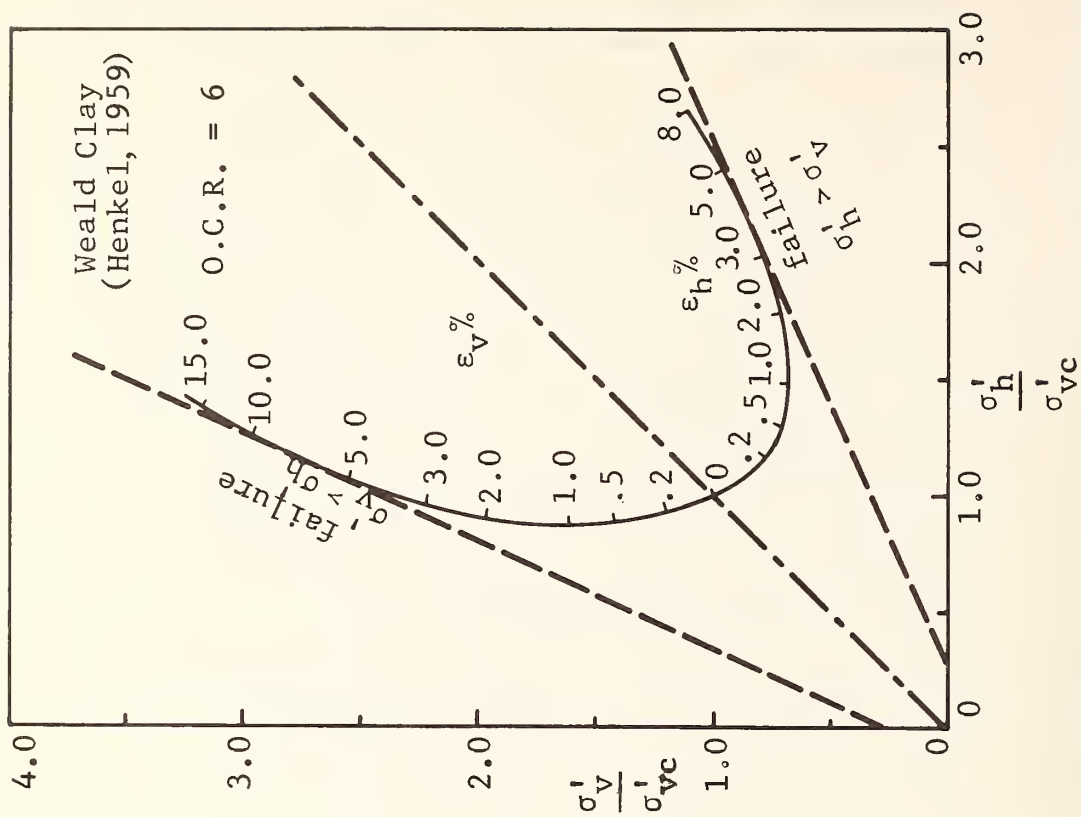
of initial stresses and stress path and soil behavior. His curves are combined in Figures 2-3 and 2-4. Typical stress paths for normally consolidated and overconsolidated soils are shown for both active and passive conditions. The differences in behavior that result from the different stress conditions and stress paths are obvious. Duncan and Dunlop (1969) present finite element simulations of excavation in a normally consolidated soil ( $K_o = 0.81$ ) and in a heavily overconsolidated soil ( $K_o = 1.60$ ). Predicted shear stresses were found to depend strongly on the value of  $K_o$ . This may be expressed by the factor of safety necessary for the  $\phi_u = 0$  analysis if shear stresses are to be everywhere less than the shear strength. The equilibrium of the normally consolidated soil ( $K_o = 0.81$ ) required a safety factor of 3; the equilibrium of the overconsolidated soil ( $K_o = 1.60$ ) required a safety factor of 5. The  $K_o$  values were held constant with depth in this analysis, as indicated in Figure 2-5. A highly overconsolidated soil may approach passive failure conditions, as was the case of Bradwell (Skempton, 1961). In such a case,  $K_o$  would decrease with depth to the limiting value given by:

$$K_o = K_p = \tan^2 \left( 45 + \frac{\phi}{2} \right) + \frac{2c}{\gamma z} \tan \left( 45 + \frac{\phi}{2} \right)$$

and the stress distribution would be as shown in Figure 2-6. At Bradwell,  $K_o$  behaved in a more complex fashion increasing with depth to a maximum value then decreasing. In such an extreme case, the analysis of Duncan and Dunlop would doubtless have indicated even greater differences between the equilibrium requirements of the normally and overconsolidated cases.

## 2.2 EVALUATION OF THE COEFFICIENT OF THE EARTH PRESSURE AT REST

If the stress history of a soil mass is known to be normally consolidated, or overconsolidated without lateral strain, and the vertical is a principal stress direction, an estimate of  $K_o$  may be obtained from the soil properties.



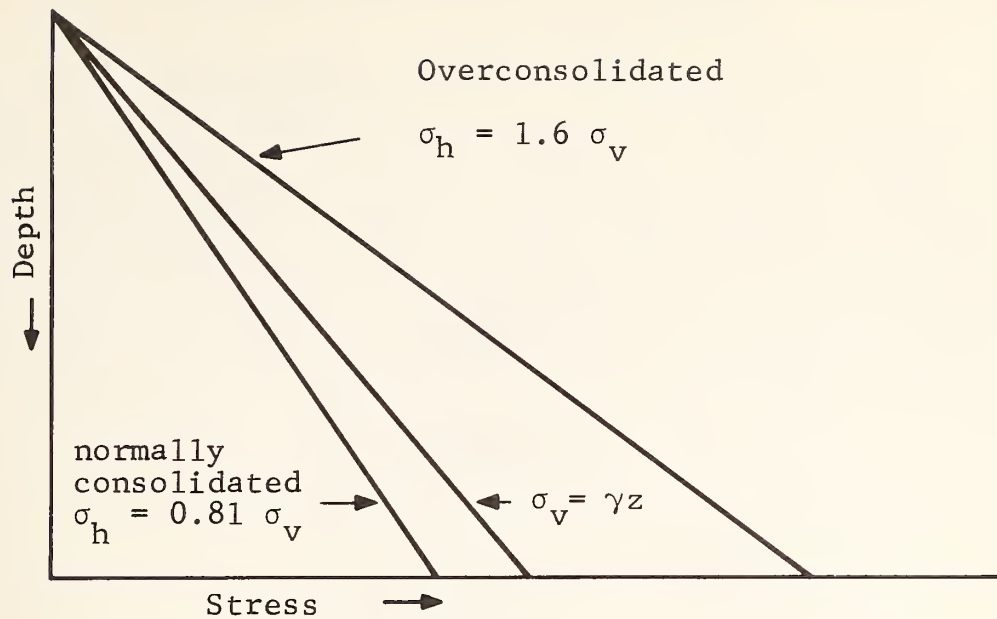


Figure 2-5. Stress Distribution for  $K_o$  Constant with Depth in Normally and Overconsolidated Soils

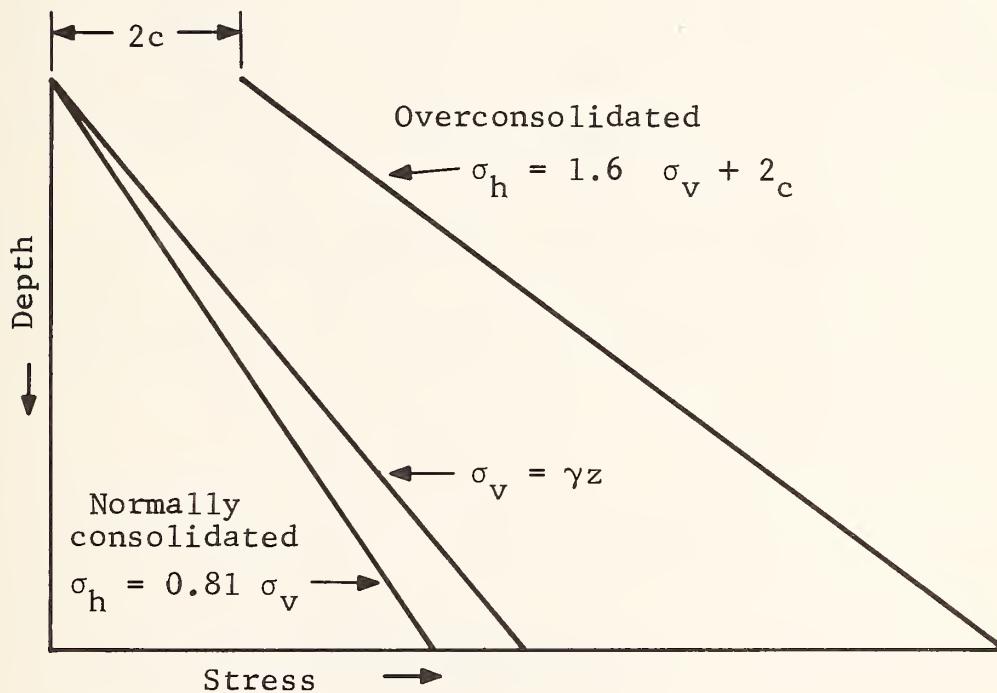


Figure 2-6. Stress Distributions for Normally Consolidated ( $K_o$  constant) and for Overconsolidated ( $K_o = K_p$ ) Soils

### 2.2.1 THEORETICAL EVALUATION, NORMALLY CONSOLIDATED $K_0$

The approximation of Jaky's expression  $K_0 = 1 - \sin \phi$  is frequently used for normally consolidated soils. The development of this expression (Keszdi) is based on the equilibrium of a wedge-shaped mass (Figure 2-7) with side slopes at an inclination  $\phi$ . Two zones, ABO and CDO, exist in which the shear strength is fully mobilized. These zones must be in plastic equilibrium, with the state of stress known:

$$\sigma_z = \tau \frac{1 + \sin^2 \phi}{\sin \phi \cos \phi}$$

$$\sigma_x = \tau \cot \phi$$

$$\tau_{xz} = \tau = \gamma z \sin \phi \cos \phi - x \sin^2 \phi$$

Between the two plastic zones there is a transition zone BOC in which the shear strength is not fully mobilized. The stresses within this wedge are computed on the basis of

- 1) the continuity of shear stresses across the boundaries BO and CO.
- 2) assumption that the shear stress  $\tau_{xz}$  is distributed parabolically in the  $x$  direction.
- 3) equilibrium and compatibility conditions.

On the surface BO, with  $x_1 = z \tan (45^\circ - \phi/2)$

the stresses are given by:

$$\sigma_z = \gamma x_1 \left[ \frac{1 + \sin^2 \phi}{\cos \phi} \right]$$

$$\sigma_x = \gamma x_1 \cos \phi$$

$$\tau_{xz} = x_1 \gamma \sin \phi$$

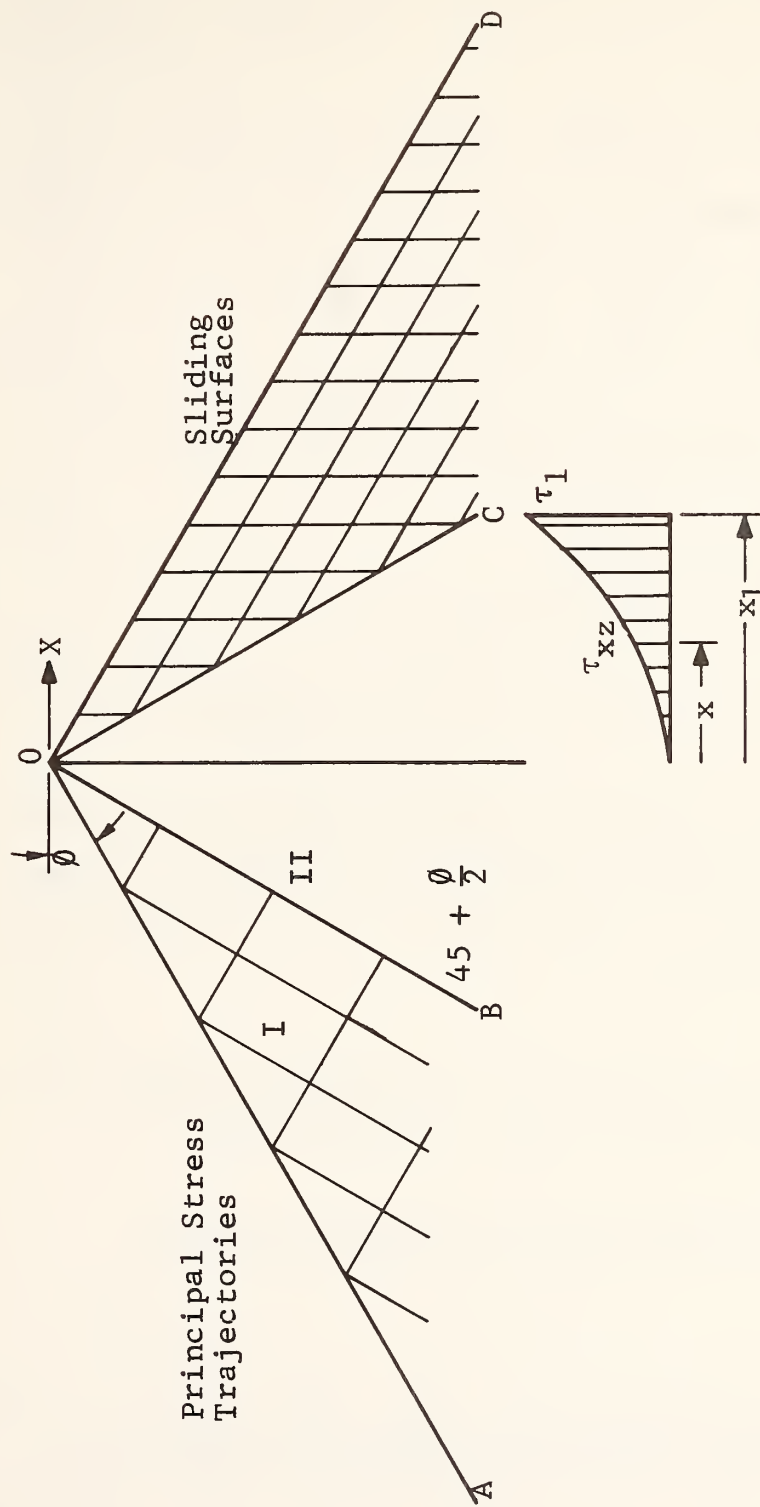


Figure 2-7. Equilibrium of Wedge Shaped Soil Mass Used by Kezdi to Display Jaky's Approximation  $K_o = 1 - \sin \phi$

The stresses in BOC are not known, but  $\tau_{xz} = 0$  at  $x = 0$  and  $\tau_{xz} = x\gamma \sin \emptyset$  on OB and OC. A parabolic distribution is assumed:

$$\tau_{xz} = \tau_1 x^2/x_1^2$$

The equilibrium condition

$$\frac{\partial \sigma_z}{\partial z} + \frac{\partial \tau_{xz}}{\partial x} = \gamma$$

gives the condition  $\sigma_z = \gamma z$  at  $x = 0$ . From

$$\frac{\partial \sigma_x}{\partial x} = - \frac{\partial \tau_{xz}}{\partial z}$$

the condition  $\sigma_x = \gamma z (1 - \sin \emptyset) \frac{1 + 2/3 \sin \emptyset}{1 + \sin \emptyset}$  on  $x = 0$ .

Jaky and his followers assumed that the  $x = 0$  plane has zero lateral strain because of symmetry conditions. He formed the ratio  $\sigma_x/\sigma_y$  which, if this assumption is valid, is the ratio  $K_o$ :

$$K_o = \frac{\sigma_x}{\sigma_y} = (1 - \sin \emptyset) \frac{1 + (2/3) \sin \emptyset}{1 + \sin \emptyset}$$

Various approximations of this expression are

$$K_o = 1 - \sin \emptyset \quad \text{and} \quad K_o = 0.9 (1 - \sin \emptyset).$$

These are plotted in Figure 2-8. The simple  $K_o = 1 - \sin \emptyset$  is the form most frequently employed to estimate  $K_o$ . The plane  $x = 0$  may not be truly in the at-rest condition, the zero deflection condition at  $x = 0$  being the result of



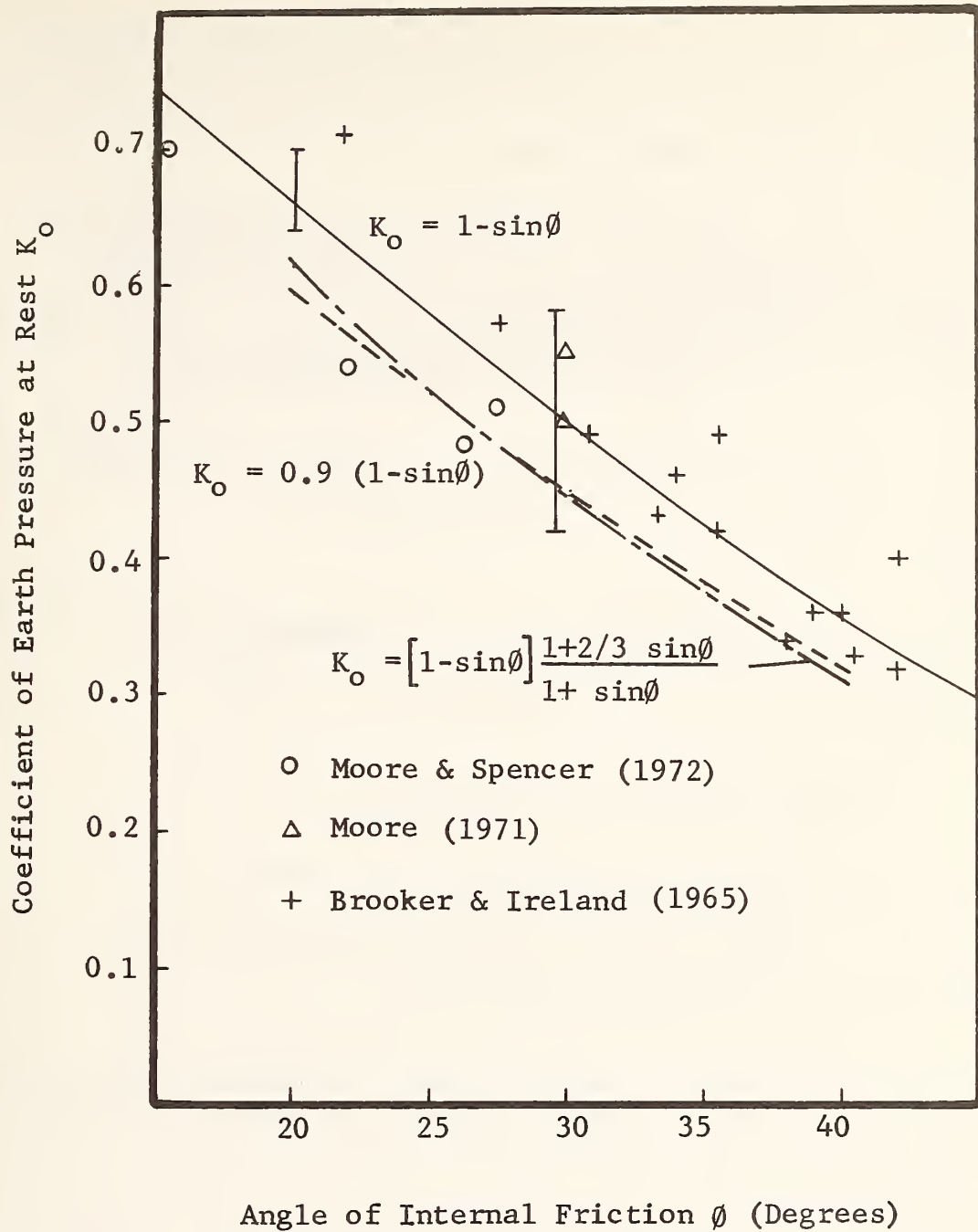


Figure 2-8. Reported Values of  $K_o$  Compared With Jaky's Relationship and Its Approximations

symmetry rather than necessarily representing a state of zero lateral strain. The scatter in reported  $K_o$  values is greater than the difference in the two expressions and the simpler form is commonly used.

### 2.2.2 EMPIRICAL EVALUATION, OVERCONSOLIDATED $K_o$

Considerable data have been published relating lateral stresses to overconsolidation ratio and soil index properties. Typical relationships include:

$$K_o = \lambda + \alpha (P_r - 1) \quad \text{Sherif and Strazer (1973)}$$

and

$$K_o = (K_o^{nc} P_r^h) \quad \text{Schmidt (1973)}$$

in which

$$K_o^{nc} = \text{normally consolidated } K_o$$

$$P_r = \text{overconsolidation ratio}$$

$$\lambda, \alpha, h = \text{empirical constants.}$$

Sherif and Strazer generate the empirical parameters  $\alpha$  and  $\lambda$  by plotting  $K_o$  as a function of overconsolidation ratio (Figure 2-9). Values of  $\alpha$  and  $\lambda$  for various soils are plotted in Figure 2-10. If Figure 2-10 is used to predict  $\alpha$  and  $\lambda$ , errors are in the range of  $\pm 0.1$  and  $\lambda \pm 0.02$  for  $\alpha$ . Then

$$\Delta K_o = \Delta \lambda + (P_r - 1) \Delta \alpha$$

$$\Delta K_o = \pm 0.1 \pm .02 (P_r - 1)$$

and for very high overconsolidation ratios, the variation in  $\alpha$  may become important.

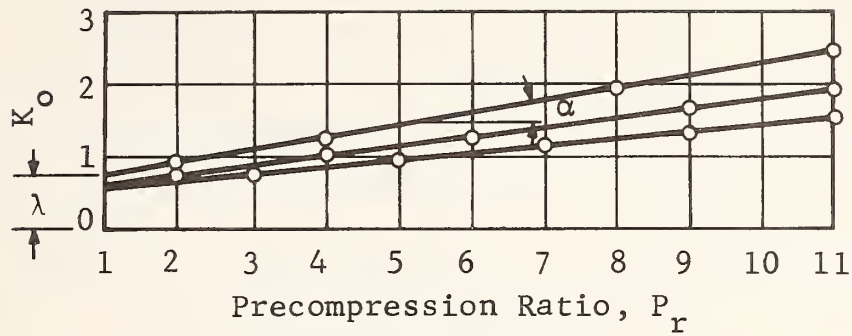


Figure 2-9. Precompression Ratio  $P_r$  Versus  $K_o$  for Seattle Clay (During Overconsolidation) (Sherif & Strazer 1973)

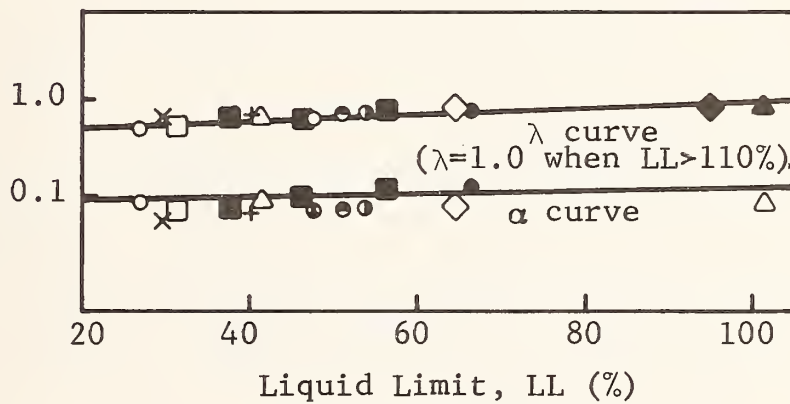


Figure 2-10. Liquid Limit Versus  $\lambda$  and  $\alpha$  (Sherif & Strazer 1973)

The parameter  $h$  of the representation suggested by Schmidt is found as the slope of a log-log plot of  $K_o$  against overconsolidation ratio. Its value ranges between 0.3 and 0.6.

The  $K_o$  vers.  $P_r$  data of several investigators are plotted in Figure 2-11. The influence of soil type is most apparent at large overconsolidation ratios. Both Skempton (1961) and Yudhbir and Prasad (1973) indicate maximum  $K_o$  values when  $P_r$  is in the range 20 to 40; in Skempton's case this was attributed to surface weathering and cracking at the Bradwell site. The maximum value of  $K_o$  is limited by the passive earth pressure  $K_p$ , indicating that the continuously upward trends of the data of Sherif and Strazer and of Brooker and Ireland must at least level off at high  $P_r$  values. If  $K_o$  approaches  $K_p$ , vertical swelling of the soil deposit acts to cause unloading along the  $K_p$  yield surface, as indicated in the typical stress trajectory inset in Figure 2-11. The Brooker and Ireland (1965) data were originally shown as functions of plasticity index (Figures 2-12 and 2-13).

It can be seen that an approximate value of  $K_o$  may be determined if the soil mass is known not to have experienced lateral deflection. In some areas, local experience may provide guidance if knowledgeably applied. However, in-situ lateral stresses can be modified radically by localized conditions and more direct methods of estimating their actual value are needed.

### 2.3 LABORATORY DETERMINATION OF STRESSES

A number of techniques are available to estimate in-situ stresses. Some measure the soil behavior under  $K_o$  conditions and require the following assumptions:

- o Principal stresses are vertical and horizontal
- o The soil mass has a history of zero lateral strain
- o The vertical stress history is known
- o The soil response over geological periods are reflected in short-term laboratory tests.

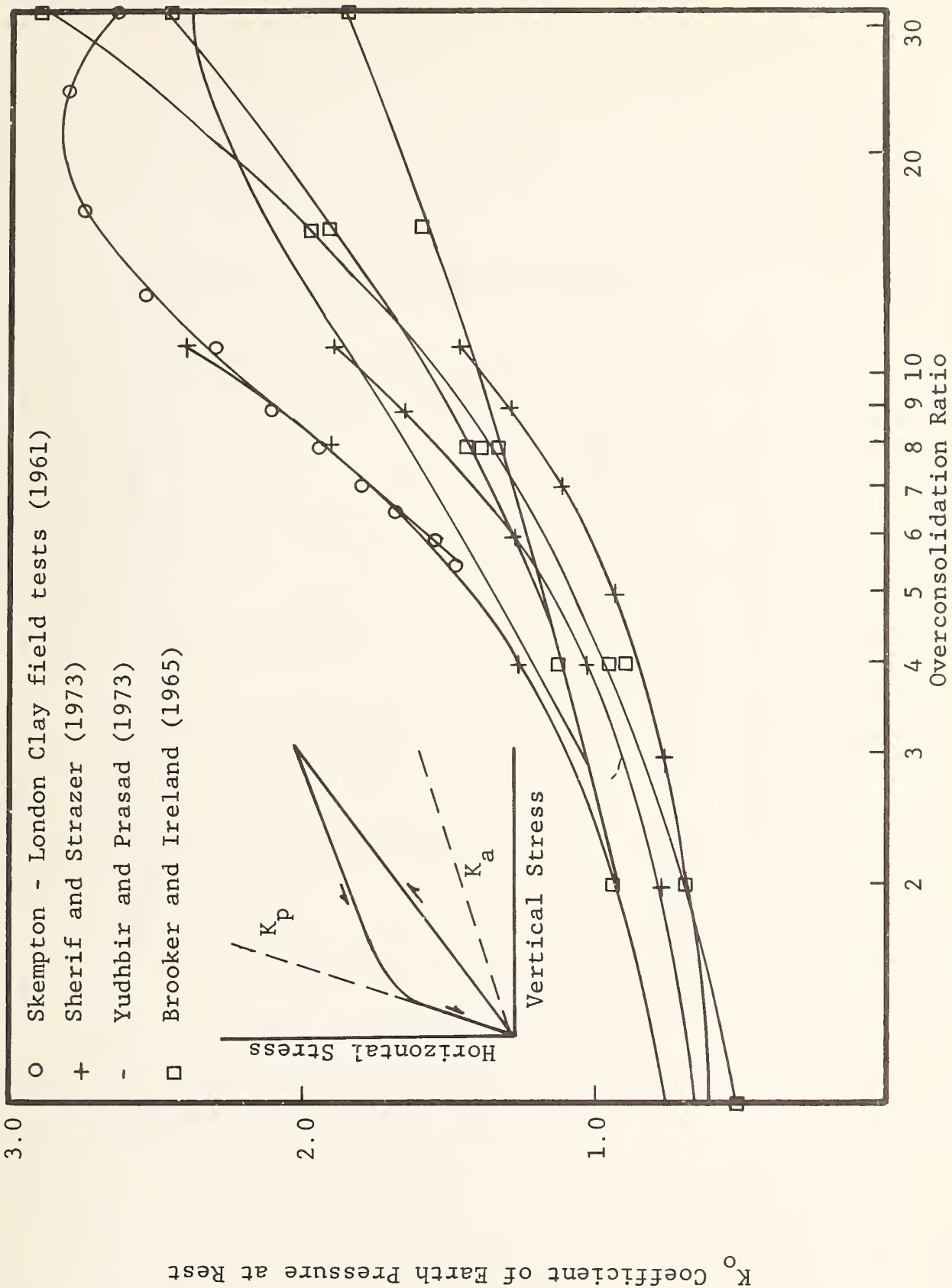


Figure 2-11 Relationship Between  $K_o$  and Overconsolidation Ratio

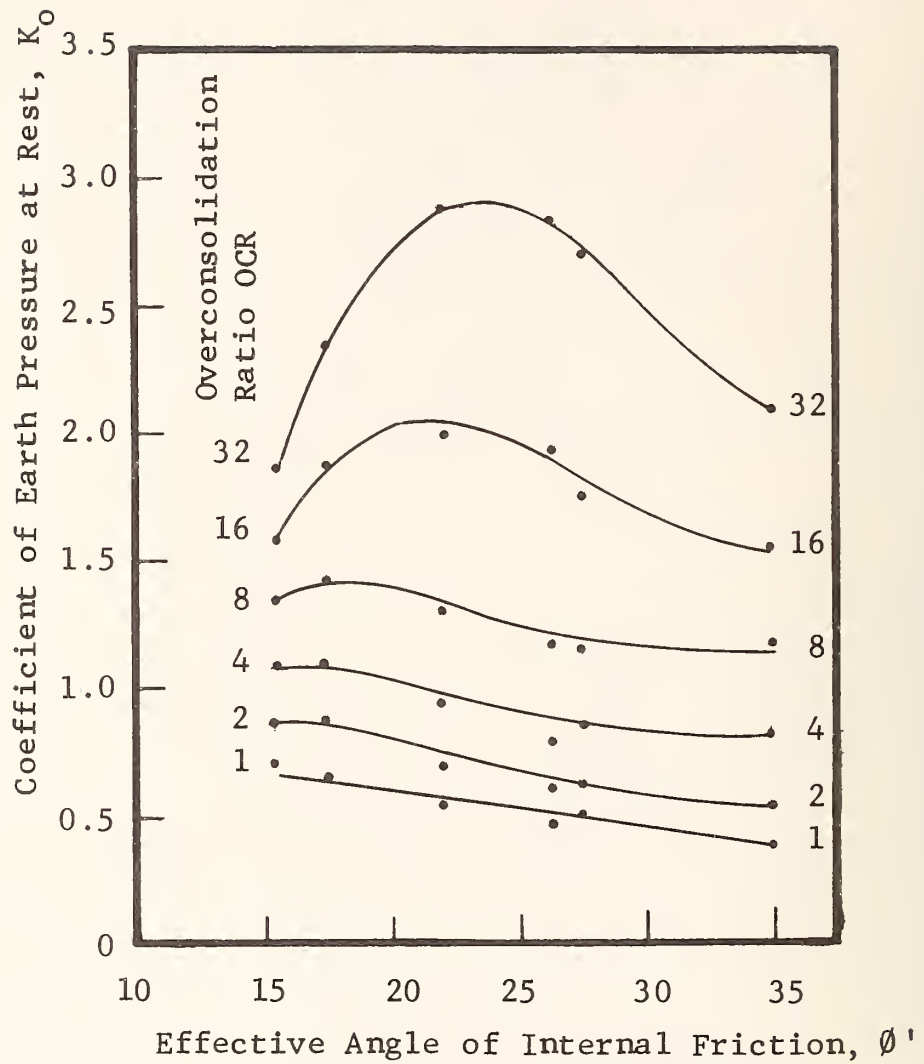


Figure 2-12. Relationship Between  $K_o$ ,  $\phi'$ , and OCR (After Brooker and Ireland, 1965)



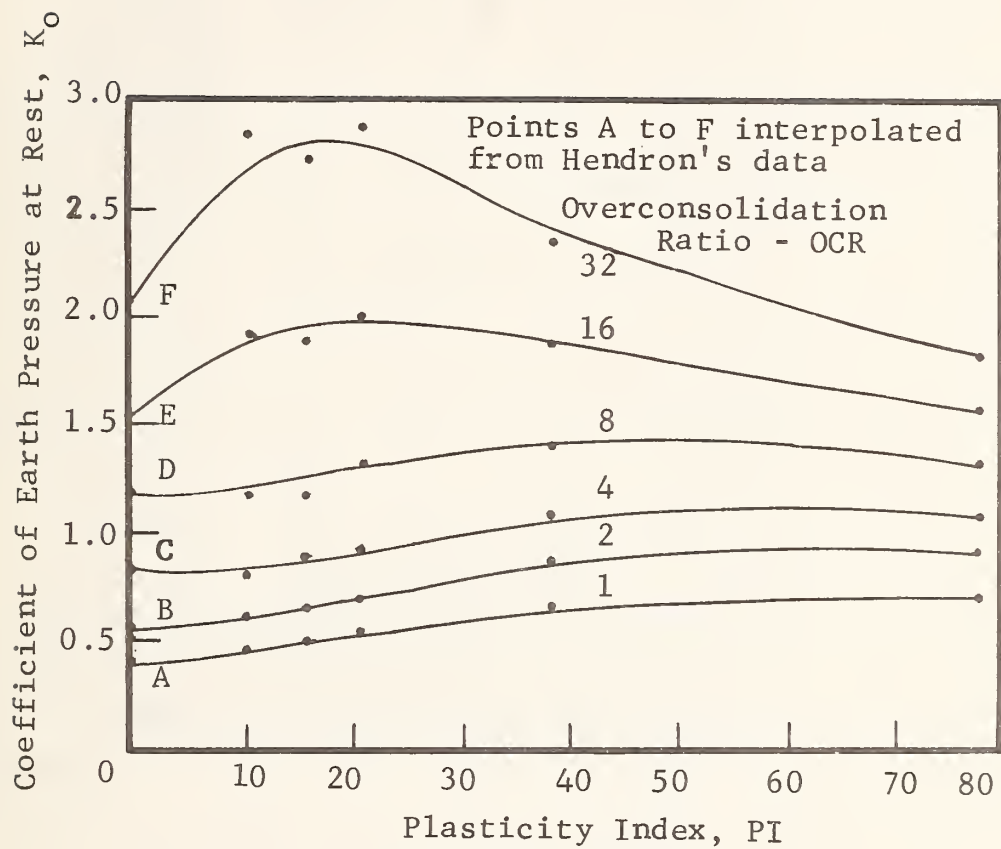


Figure 2-13. Relationship Between  $K_o$ , PI and OCR (After Brooker and Ireland, 1965)

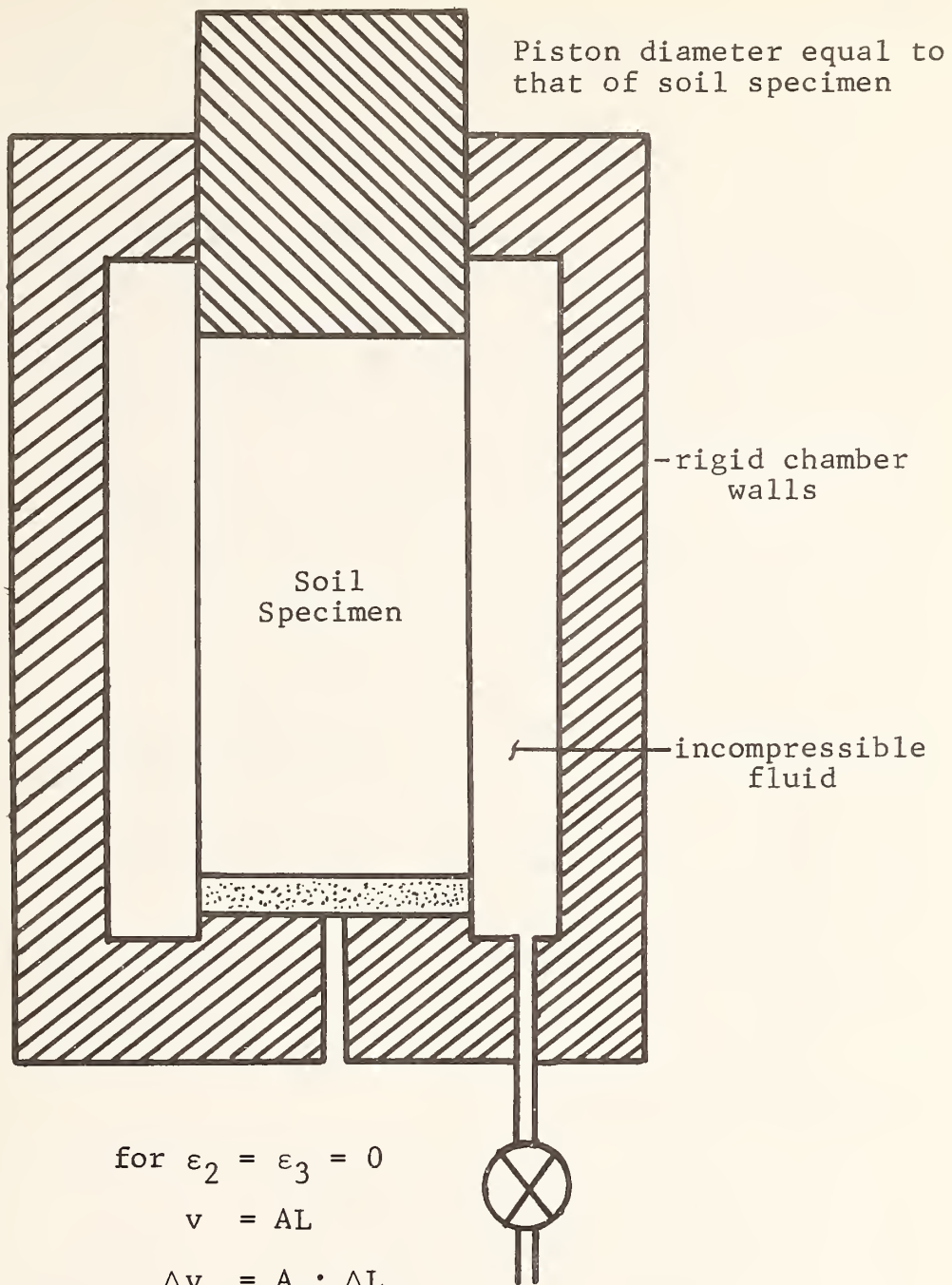
Others measure some property of the sample that reflects the stresses experienced in-situ.

### 2.3.1 SPECIAL TRIAXIAL TESTS

The value of  $K_0$  may be estimated by laboratory tests under conditions of zero lateral deflection. At the 1958 Brussels Earth Pressure Conference, Bishop (1958) described triaxial tests to maintain zero lateral deflection. The basis of one method rests on the equality between vertical and volumetric strains when lateral strains are zero. This is applied in the  $K_0$ -test cell shown schematically in Figure 2-14. As long as the chamber and confining fluid may be considered as allowing no lateral strain in the soil, the equality of vertical and volumetric strains in the soil is enforced by the fact that the loading piston and soil specimen diameters are identical. The test is invalid if pore pressure gradients are established in the soil or if the soil is not homogeneous since either condition may induce localized nonzero lateral strains in the sample. Bishop stated that previous investigators were unsuccessful in applying this technique. Bishop's second method includes monitoring the lateral strain across the specimen diameter and manipulating the stress ratio to maintain zero lateral strain and uses a number of devices (Bishop and Henkel, 1961). Other workers have developed sensitive lateral strain sensors in standard triaxial cells to maintain  $K_0$  loading conditions. Another method mentioned by Bishop was the measurement of overconsolidation ratios in both the horizontal and vertical directions on undisturbed samples.

Altschaeffl and Mishu (1970) used a steel ring surrounding the soil specimen as a noncontacting radial deflection capacitive transducer. The capacitance,  $C$ , between coaxial cylinders of radius  $a$  and  $b$  is given by

$$C = \frac{2\pi\epsilon_0 Lk}{\ln\left[\frac{b}{a}\right]}$$



$$\text{for } \epsilon_2 = \epsilon_3 = 0$$

$$v = AL$$

$$\Delta v = A \cdot \Delta L$$

$$\epsilon_v = \frac{\Delta v}{v} = \frac{\Delta L}{L}$$

$$\epsilon_v = \epsilon_1$$

Figure 2-14. Uniaxial Triaxial Apparatus ( $K_0$  Test Cell)

where

- $\epsilon_0$  = permittivity constant =  
8.85 x 10<sup>-12</sup> Farads/meter
- k = dielectric constant
- L = length of the shorter cylinder

For a given set-up, the capacitance depends on the radius, a, of the soil sample. The gage was driven by a standard capacitance bridge as shown in Figure 2-15. An alternative electronics package for this type of noncontacting probe exists in the form of proximity gage electronics. Such a system provides a DC voltage analog to the change in capacitance, without requiring continuous manual nulling and phase balancing. The capacitance bridge package should perform well in  $K_0$  testing since the intent is to avoid any changes in the radius of the soil specimen. With proper control of the stress ratios, the capacity of the ring-soil capacitor should not change except with changes in the k of the fluid with temperature or pressure. Geometries other than the sample in a ring used by Altschaeffl and Mishu are also useful. Proximity gage transducers frequently use the capacitance between a sharp point and a conductive plane to make local measurements. In these cases, a mechanical micrometer is included to calibrate the system directly.

In general, capacitive transducers have the following advantages:

- o a large sensing area to average minor point-to-point variations
- o sensitivity and range that is easily scaled by the probe geometry. (Extremely sensitive transducers may be designed if a small operating range is permitted.)
- o zero contact force.

Their disadvantages are that:

- o careful shielding is required to avoid extraneous signals resulting from the capacity of the probe with respect to its environment, and
- o calibration needs may be extensive.

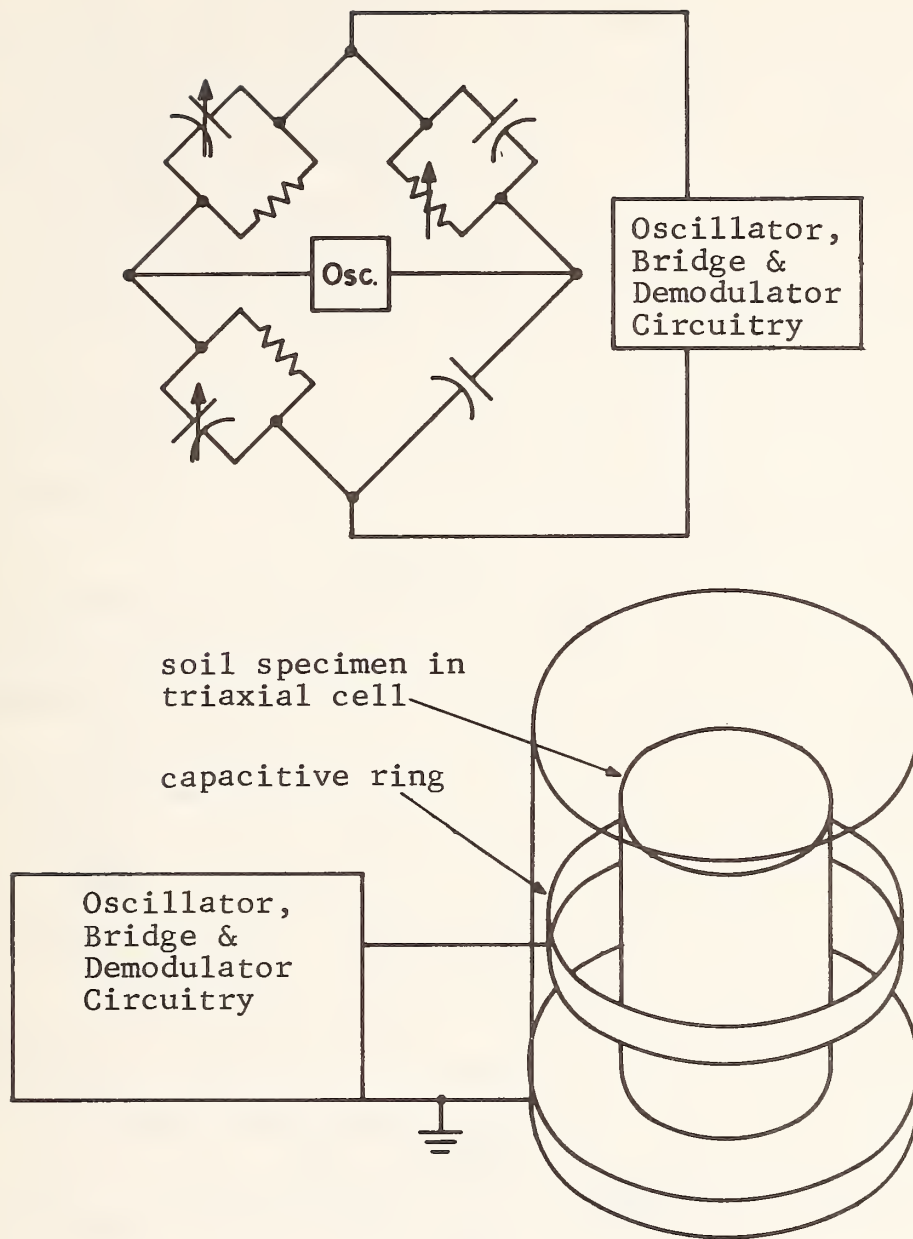


Figure 2-15. Capacitance Bridge and Schematic of Non-contacting Lateral Strain Sensor (Altschaeffl and Mishu, 1970)



The optical methods suggested by Dudley (1971) include photogrammetry and optical tooling techniques to monitor the sample diameter in a triaxial cell. The optical tooling technique provides real time measurement of specimen diameter, as needed for a  $K_0$  test. Two 10-second theodolites were set up 47 in. (1.2 m) from the specimen center, to monitor the angles subtended by two specimen diameters. This system is said to determine the specimen dimension to an accuracy of 0.005 in. ( $13 \times 10^{-5}$  m). This is equivalent to an uncertainty of about 0.2% strain for the 2.42-in. ( $61.5 \times 10^{-3}$  m) diameter specimens used. Dudley suggests that the accuracy might be increased to 0.001 in. ( $3 \times 10^{-5}$  m) by improved methods. The triaxial cell wall acts as an optical lens, increasing sensitivity.

C.A. Moore (1971) used foil strain gages mounted on a foil band to monitor radial strain in  $K_0$  tests on soils containing mica. The sensor (Figure 2-16) is simply a gaged foil band wrapped around the specimen, tightened by an attached tubing clamp. The pin and hole arrangement constitutes a remotely operated release to permit removal of the transducer from the specimen before soil failure. Moore used his lateral strain sensor to provide a feedback signal in a closed loop stress control system for his triaxial apparatus. The confining pressure was increased at a constant rate while the axial stress was automatically controlled for zero lateral strain. The closed loop system was added to avoid the cumulative effect of incremental loading steps and re-adjustments that may be expected in a less sophisticated system.

The problem of accumulating errors as a zero deflection control system hunts for the correct stress ratio was approached differently by Andrawes and El-Sohby (1972, 1973). These authors conduct several constant stress ratio tests at slightly different stress ratios. The stress ratio at which axial and volumetric strains are equal is interpolated as shown in Figures 2-17. Figure 2-17(a) indicates that the



Electrical Strain Gages  
Active & Dummy

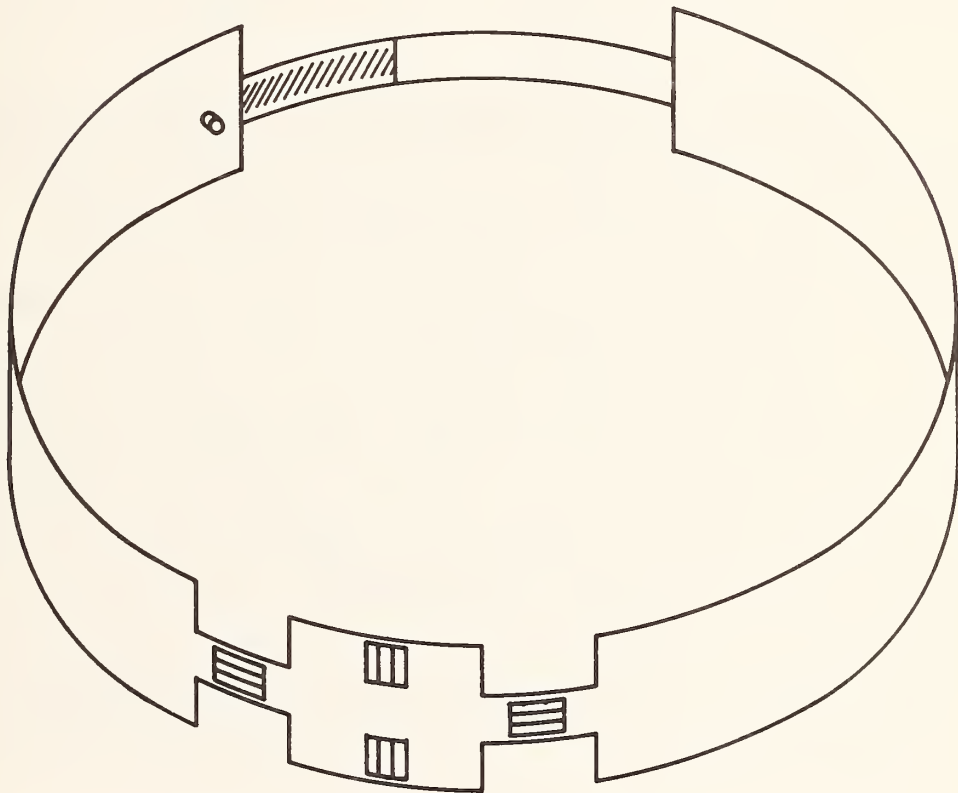
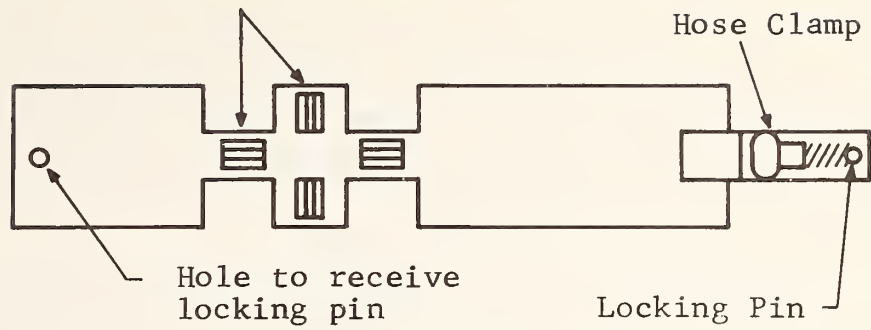


Figure 2-16. Circumferential Strain Gage  
(Moore, 1971)

value of  $K_0$  for the dense sand is between 1/2.3 and 1/3.0. Interpolation to zero-strain ratio in Figure 2-17(b) yields the value of  $K_0 = 1/2.9 = .34$ . Accuracy as great as justified by the apparatus and instrumentation being used may be obtained by additional triaxial tests at stress ratios closer to the interpolated value of  $1/K_0$ . Andrawes and El-Sohby (1973) measured axial strain by dial indicator and volumetric strain by burette.

Utilization of  $K_0$  triaxial tests to estimate in-situ stresses requires that the soil mass be consolidated under  $K_0$  conditions, that the major principal stress be known, and that the triaxial test adequately simulate the stress-strain history of the soil mass.

### 2.3.2 $K_0$ DEVICES

Special test devices have been designed to enforce conditions of zero lateral strain (Brooker and Ireland, 1965; Obricjan, 1969; and Sherif and Strazer, 1973). These devices are characterized by rigid sidewalls, instrumented for lateral stress but permitting little or no lateral strain. Unlike  $K_0$  triaxial tests in which variations in lateral strain may occur which average to zero over the measured portion of the specimen, the rigid sidewalls force the lateral strain to remain zero. This advantage is countered by the disadvantage that the rigid sidewalls cannot be made perfectly frictionless, thus may induce shear stress on what should be a principal stress plane. For this reason, the specimen height is made small relative to the diameter, as is done in one-dimensional consolidometers for the same reason.

The apparatus described by Brooker and Ireland (1965) employs a steel membrane to restrict lateral strain as shown in Figure 2-18. Foil strain gages on the rear of the membrane monitor circumferential strain, which is maintained within about 10 microstrains by oil pressure on the back. Typical data obtained are indicated in Figures 2-19 and 2-20.

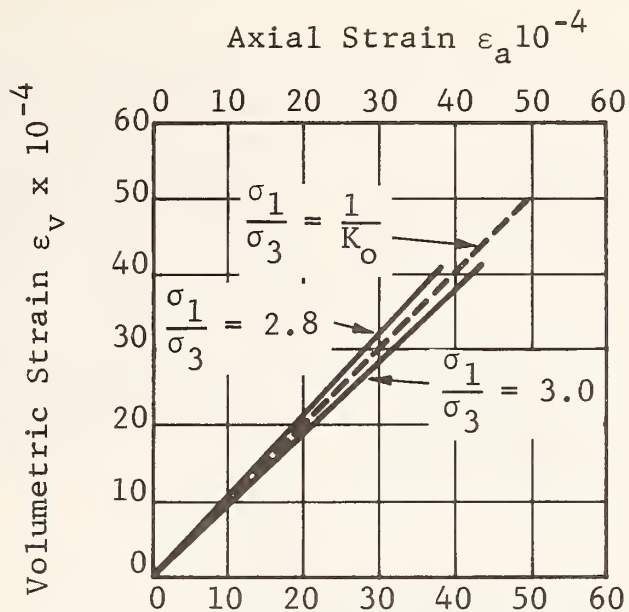


Figure 2-17(a). Constant Stress Ratio Tests for Dense Sand

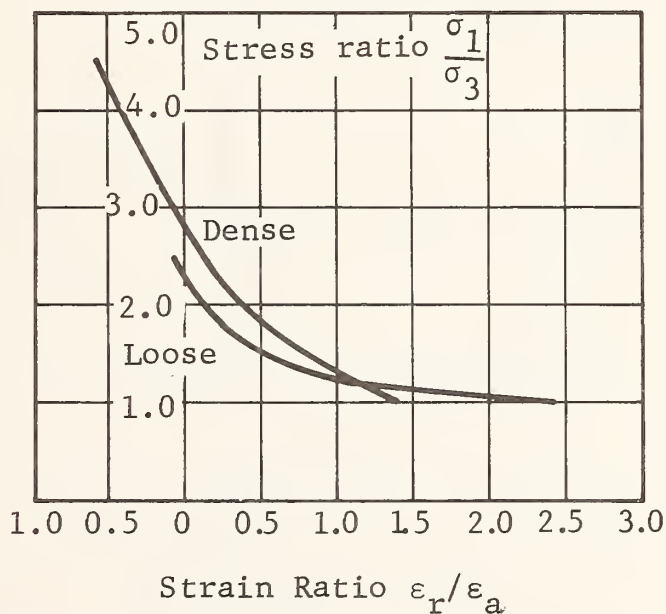


Figure 2-17(b). Relations Between Stress Ratios and Strain Ratios for Tests Conducted Under Constant Stress Ratios

Figure 2-17. Measurement of  $K_0$  by Interpolation from Constant Stress Ratio Tests (Andrawes & El-Sohby; 1972,1973)

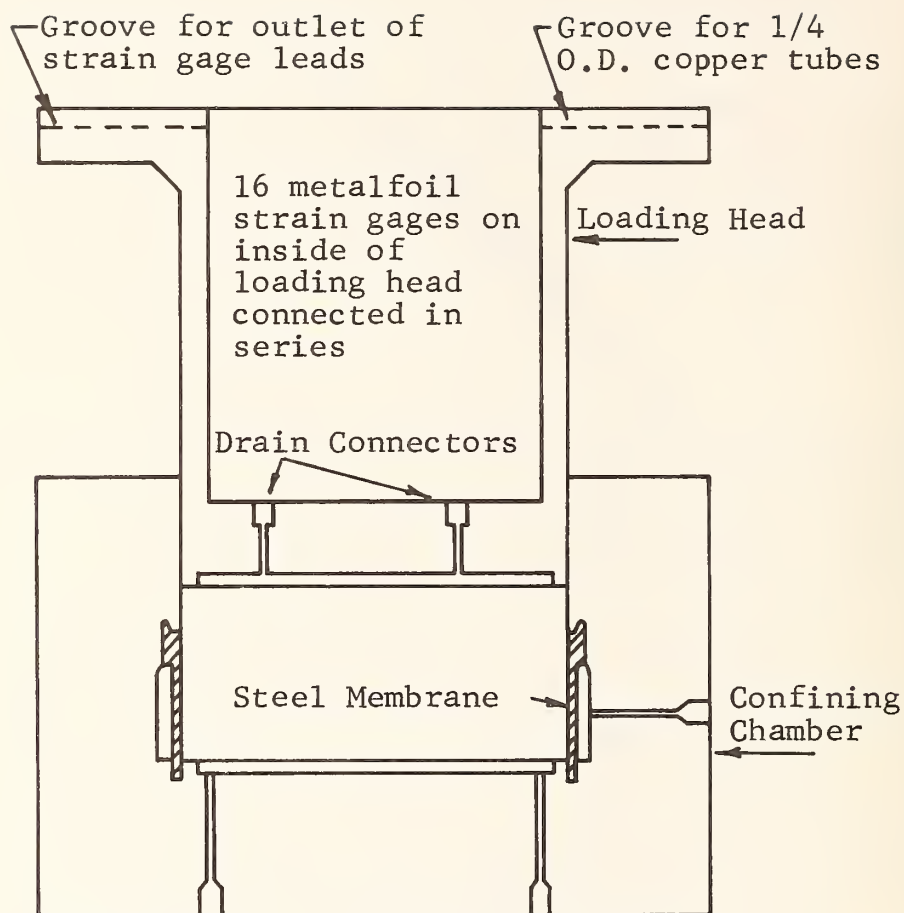


Figure 2-18. Assembly of Test Cell  
(Brooker & Ireland, 1965)

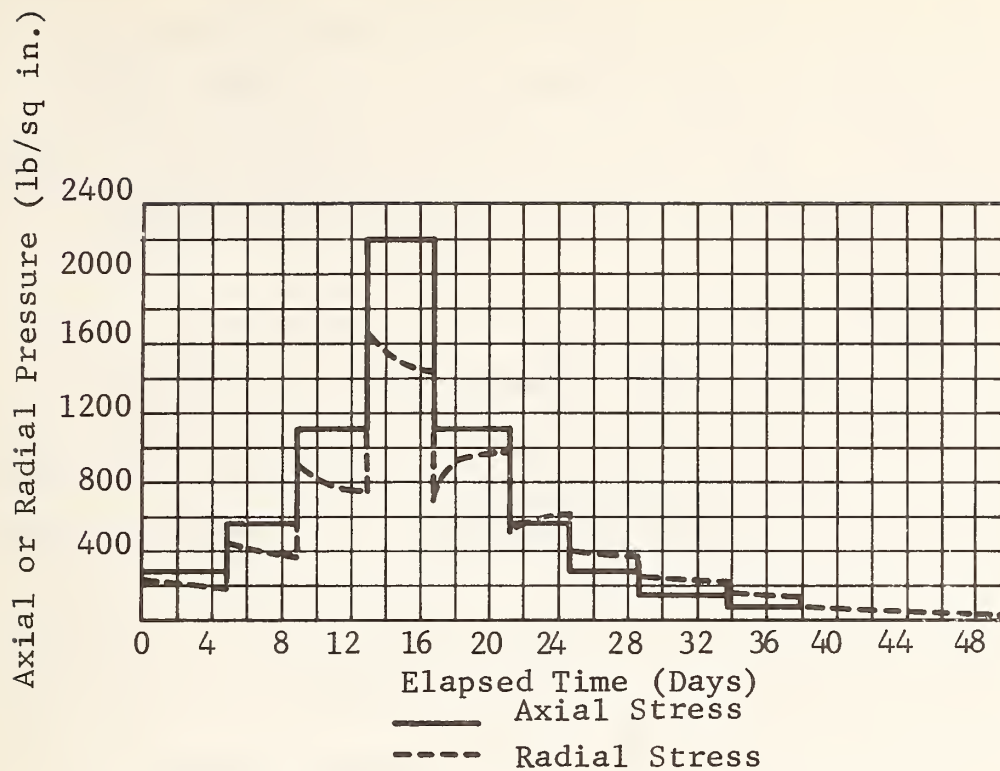


Figure 2-19 Variation of Axial and Radial Pressure with Time: Bearpaw Shale

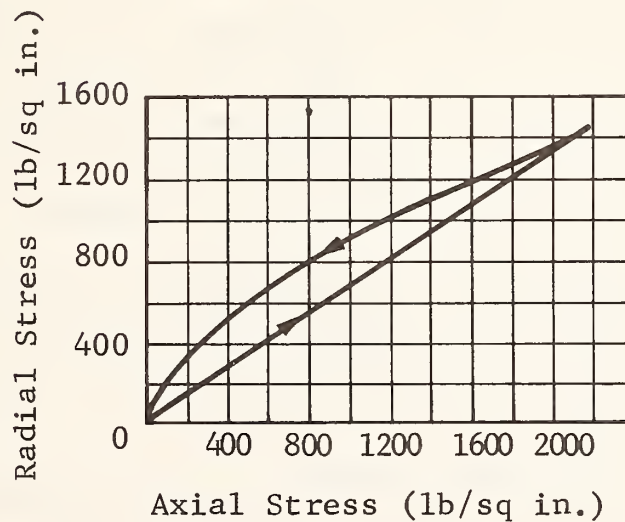


Figure 2-20. Axial and Radial  $K_0$  Stresses for Bearpaw Shale (Brooker & Ireland, 1965)



The stress-time curve in Figure 2-19 indicates the pore pressure decay at each loading step. The stress path in Figure 2-20 was constructed using the stresses at 100% consolidation. This figure also shows that initial loading  $K_0$  is constant for this material to at least 2200 psi ( $15 \times 10^6$  Newton/meter<sup>2</sup>).

Obrcian (1969) employed a  $K_0$  device (Figure 2-21) having a heavy wall split confining ring instrumented to monitor lateral stress and side wall friction. These data indicate that mean shear stresses induced on the confining ring were on the order of 10 percent of the major principal stress, that is, roughly 1/4 to 1/3 the magnitude of the minor principal stress at the  $K_0$  values reported. Typical data shown in Figure 2-22 appear to indicate a decrease in  $K_0$  values with increasing stress. Obrcian points out that this behavior is consistent with increasing density at higher stress levels, yet this appears to conflict with investigators who find that  $K_0$  is constant for virgin loadings. If the data in Figure 2-22 are used to back calculate the lateral stresses, the relationships in Figure 2-23 emerge, indicating that the hyperbolic relationship between  $K_0$  and  $\sigma_1$  may be the result of a seating error of approximately 1.5 psi ( $10^4$  N/m<sup>2</sup>) in the lateral stress. Thus there appears to be no significant discrepancy between the Obrcian's data and the findings of other investigators that on initial or virgin loading  $K_0$  is constant.

Sherif and Strazer (1973) employed the University of Washington Stress-Meter (Figure 2-24) in their work. Typical data obtained with this  $K_0$  device are shown in Figure 2-25.

### 2.3.3 LABORATORY TESTS FOR IN-SITU STRESSES

At least two techniques that use laboratory tests to evaluate the stresses to which the soil sample is subjected in situ are available.



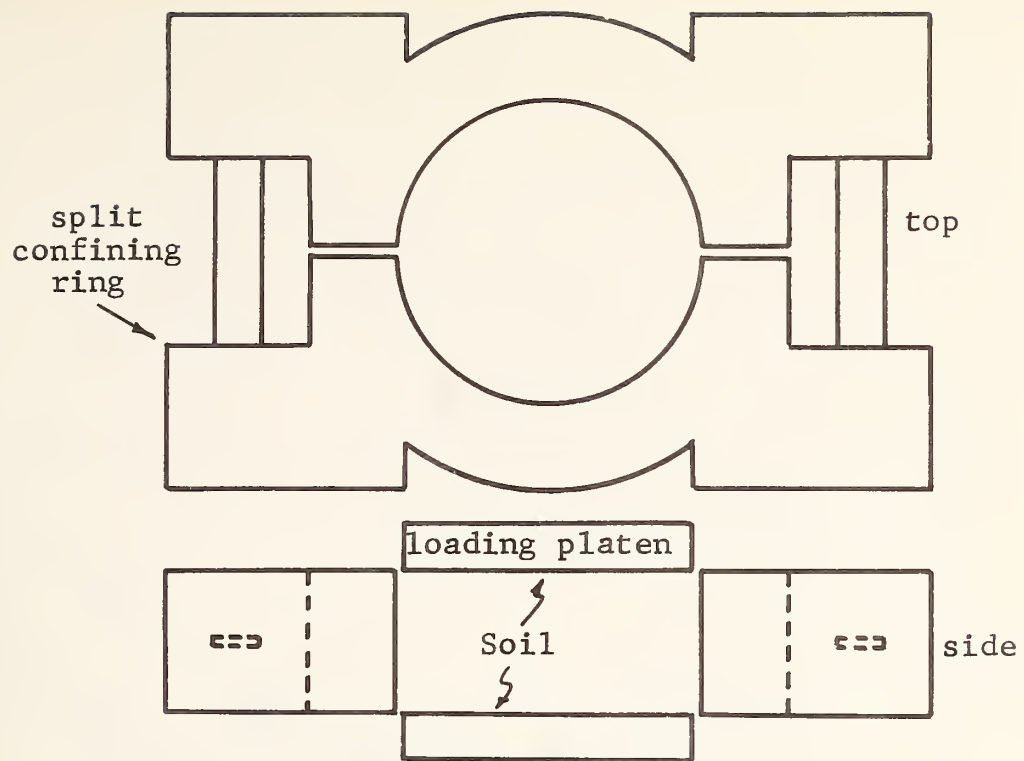


Figure 2-21. Schematic of  $K_0$  Device (Obrcian, 1969)

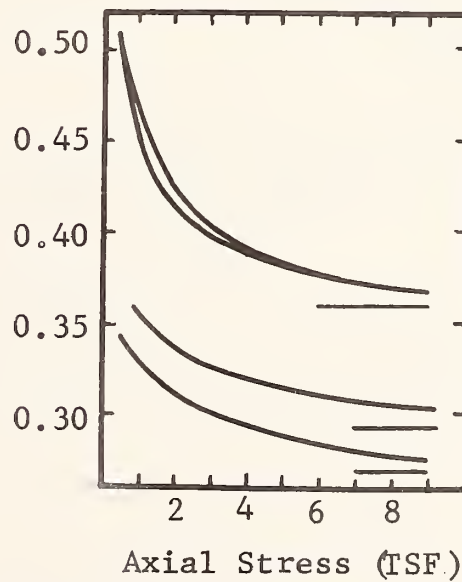


Figure 2-22. Relationship Between  $K_0$  and Axial Stress for Sand With Silt (Obrcian, 1969)

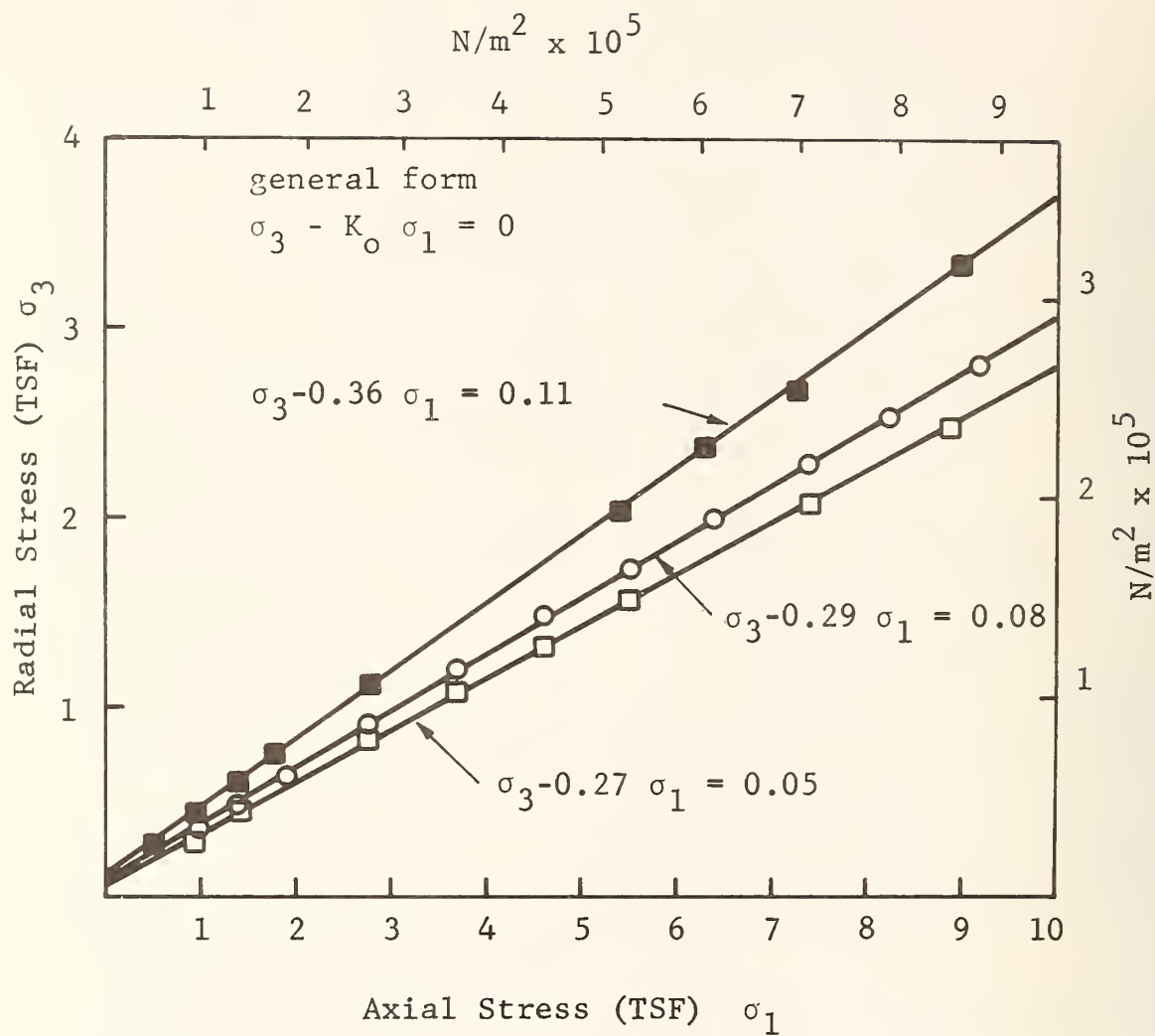


Figure 2-23. Axial and Radial Stresses Computed From Obrcian's Data

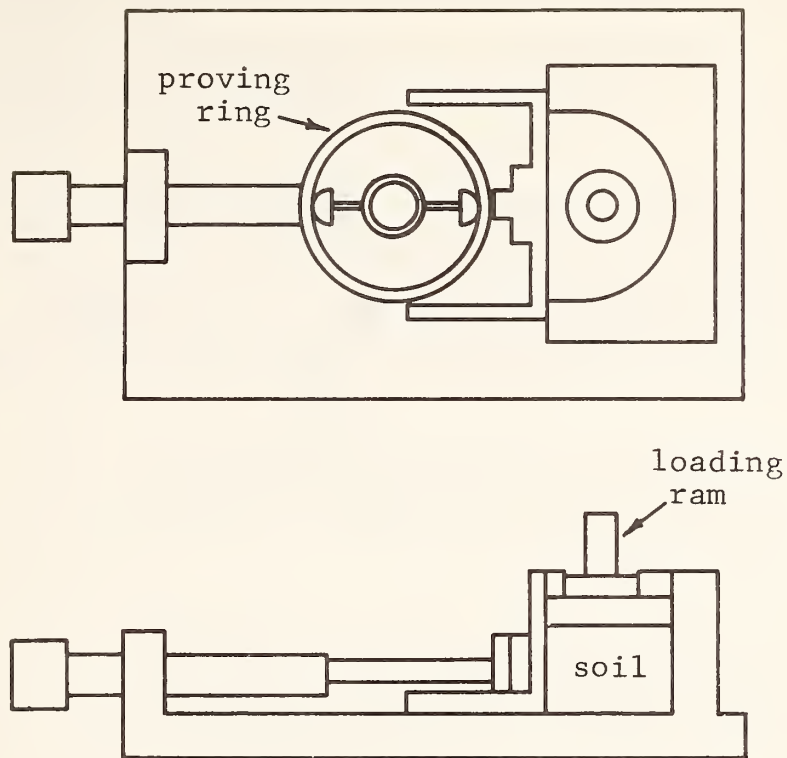


Figure 2-24. University of Washington Stress-Meter  
(Sherif & Strazer, 1973)

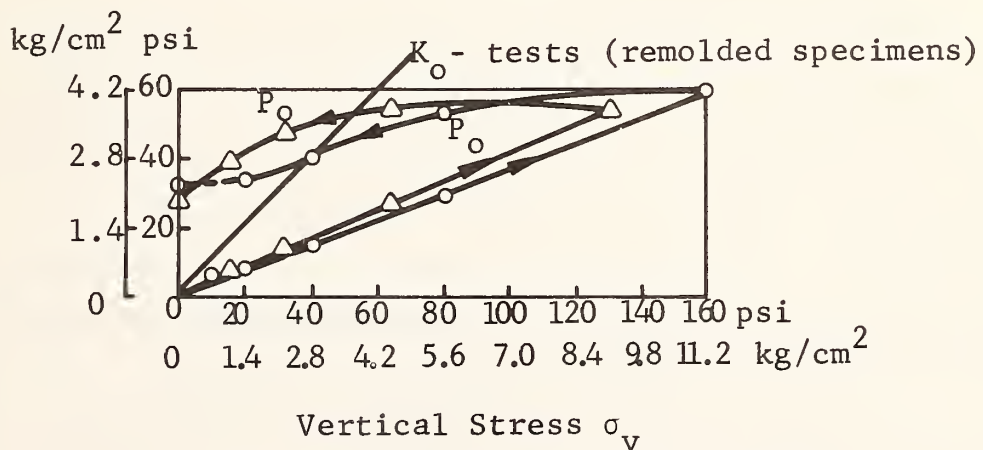


Figure 2-25.  $K_o$  Relationships  
Obtained with University of Washington  
Stress-Meter  
(Sherif & Strazer, 1973)

The lateral consolidation test mentioned by Bishop (1958) appears to have been developed by Poulos and Davis (1970, 1972). The procedure is to consolidate an undisturbed sample in the horizontal direction while holding the vertical stress at its assumed in-situ value.

- o A triaxial specimen is loaded to the estimated in-situ vertical stress value using a low stress ratio. The confining pressure should be sufficiently large to just prevent failure, and must be less than the anticipated value of  $K_0$ .
- o The confining pressure is gradually increased while the axial stress is held constant at the in-situ vertical stress level.
- o The observed void ratio is plotted against confining pressure. The plot should resemble an  $\epsilon$ -log P consolidation curve and display a break near the in-situ lateral stress.
- o The sequence may be repeated using specimens of varying disturbance. If the estimated lateral stress is plotted against disturbance ratio, the results may be extrapolated back to zero disturbance.

Degree of disturbance is defined as  $\Delta e / (\Delta e)_{\max}$  where  $\Delta e$  is the difference between the field void ratio and that of the laboratory specimen at the preconsolidation pressure and  $(\Delta e)_{\max}$  is the difference between the field void ratio and that of a remolded specimen at the preconsolidation pressure. Typical data on laboratory-consolidated Kaolin are shown in Figures 2-26 through 2-28. Even samples remolded at constant moisture content (disturbance ratio = 1.0) retain a "memory" of the in-situ stress. Note that the test series consolidated at  $K_0 = 1.0$  displays a less distinct break relative to the  $K_0$ -consolidated test series. The method cannot be used for heavily overconsolidated clays.

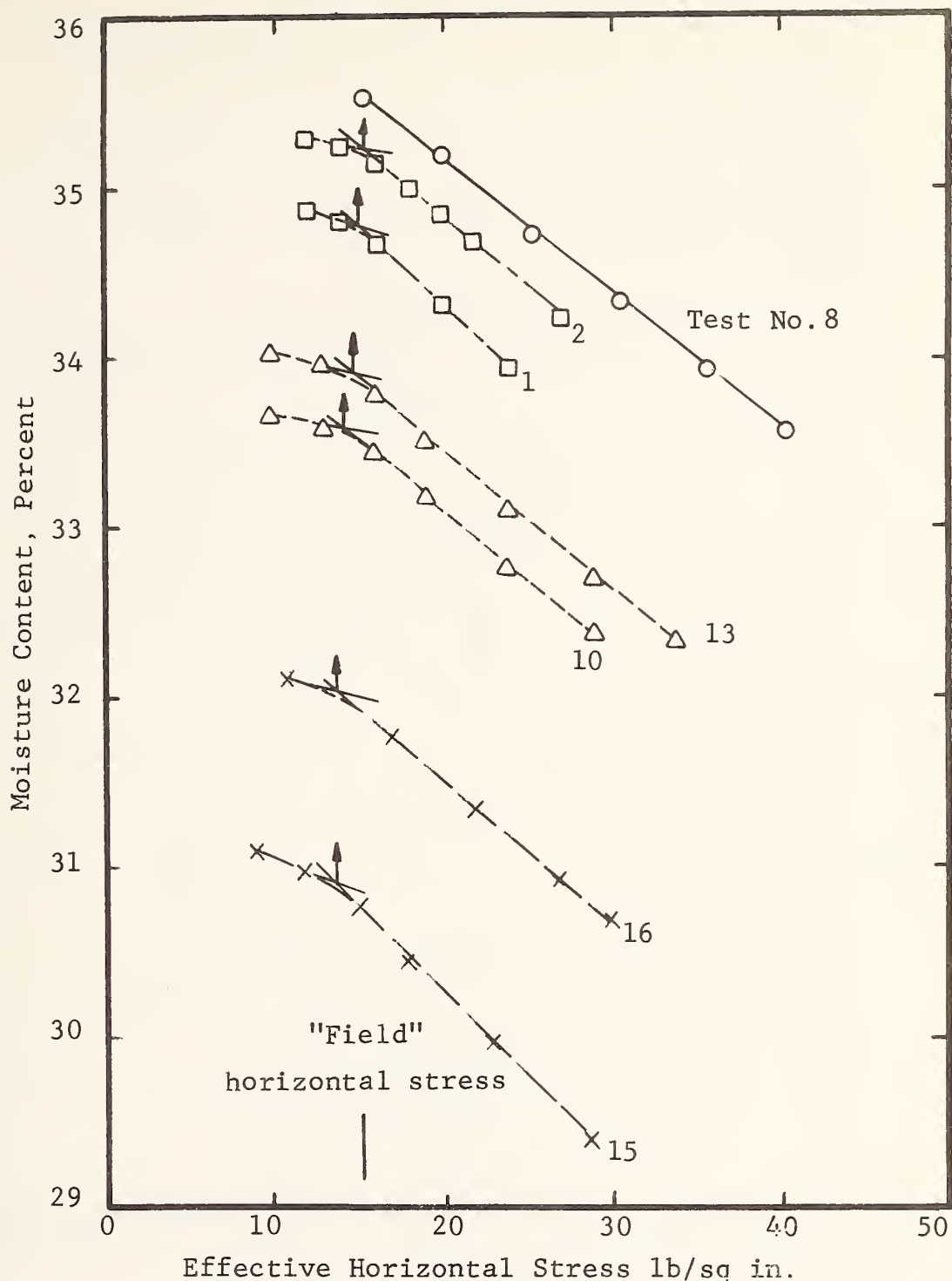


Figure 2-26 Moisture Content vs Effective Horizontal Stress Normally Consolidated Kaolin,  $K_0$  Consolidated to  $\sigma_{vo}' = 30$  lbs/sq in. ( $2.07 \times 10^5$  N/m<sup>2</sup>) (Poulos and Davis, 1970)

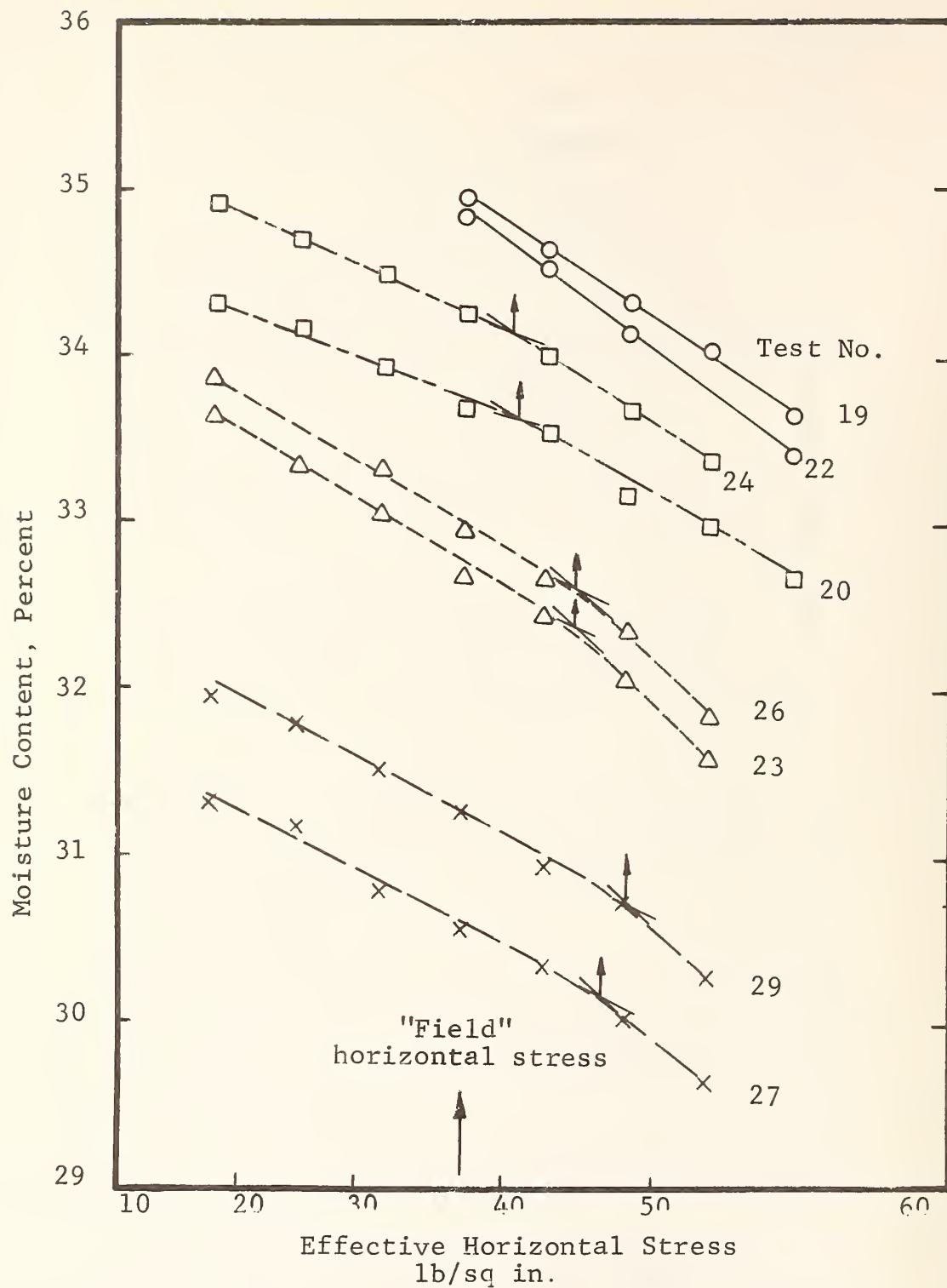


Figure 2-27 Moisture Content vs Effective Horizontal Stress. Consolidated to  $\sigma_{ho}' = \sigma_{vo}' = 30$  psi ( $2.07 \times 10^5$  N/m<sup>2</sup>) (Poulos and Davis, 1970)



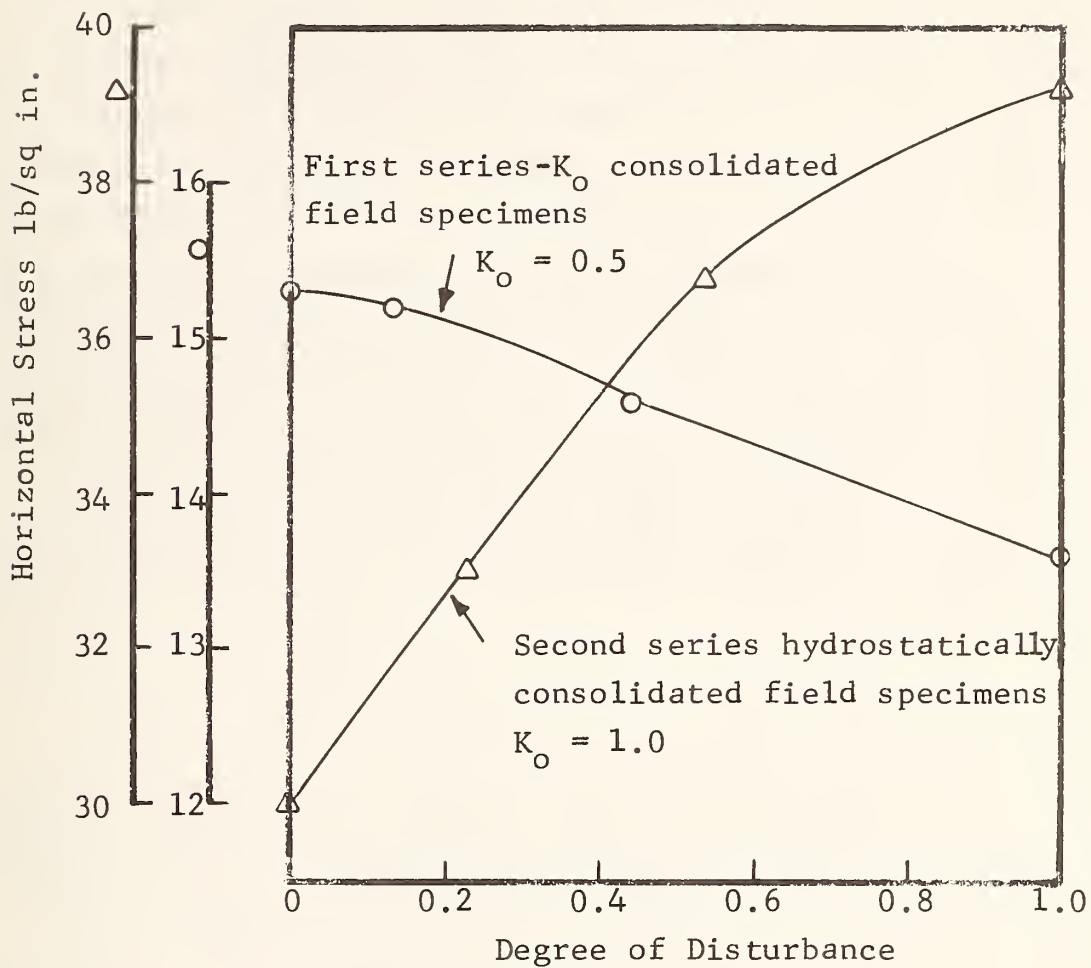


Figure 2-28. Effect of Sampling Disturbance On Deduced In-Situ Horizontal Stress (Poulos and Davis, 1970)

A rather indirect method for dealing with over-consolidated clays was employed by Skempton (1961) at the Bradwell site. In this case, the value of  $K_o$  was determined by an indirect stress-relief method employing the transfer of lateral effective stress to neutral stress that occurs during the sampling procedure itself. Briefly, when a sample is removed from the soil mass, the total stress in the sample is reduced to zero. The relative compressibilities of the soil matrix and the pore water result in a transfer of effective stress from the soil to tension in the pore water.

That is, when the sample is removed from the ground, the total stress on the sample is reduced from the in-situ value to zero. The soil matrix expands slightly, inducing tension in the pore water. Thus we have a change in stress (caused by removing the sample from the ground) that is related to a change in pore pressure, and can make use of Skempton's pore pressure coefficient  $A$ . The total stresses in-situ are:

$$\sigma_v = \sigma'_v + u_o$$

$$\sigma_h = (\sigma_v - u_o) K_o + u_o = \sigma'_v K_o + u_o$$

in which  $u_o$  is the pore pressure at depth  $z$ . After removal from the ground, the effective stress in the sample is  $-u$  where  $u$  is the pore pressure in the sample. The sample pore pressure is given by

$$u = u_o + \Delta u$$

$$u = u_o + 1/3 (\Delta\sigma_1 + 2\Delta\sigma_3) + (A - 1/3) \left| \Delta\sigma_1 - \Delta\sigma_3 \right|$$

The change in stress due to the release of the in-situ stress is:

$$\Delta\sigma_1 = -\sigma_v = -u_o - \sigma'_v$$

$$\Delta\sigma_3 = -\sigma_h = -\sigma'_v K_o - u_o$$

leading to

$$K_o = \frac{(u/\sigma_v') + A}{A - 1} \quad \text{for } K_o > 1$$

$$K_o = \frac{-(u/\sigma_v') + (A - 2/3)}{A + 1/3} \quad \text{for } K_o < 1$$

in which A is the appropriate pore pressure coefficient and the other symbols take their accepted meanings. An extensive series of tests was conducted at the Bradwell site to determine the neutral stress both in-situ and in samples. The resulting  $K_o$  values are shown in Figure 2-29. The decrease in  $K_o$  at depths less than 20 ft (6m) is attributed to the reduction of lateral stress resulting from weathering and softening of the London clay prior to the disposition of the post-glacial Marsh clay. At depths near 30 ft (9m),  $K_o$  is near the approximate value of  $K_p$ , indicating a possible failure zone. The method employed by Skempton at the Bradwell site was in part a solution in response to a specific problem. Although it has since been applied by other investigators, e.g., Blight (1969), it may be somewhat elaborate for routine site investigation programs.

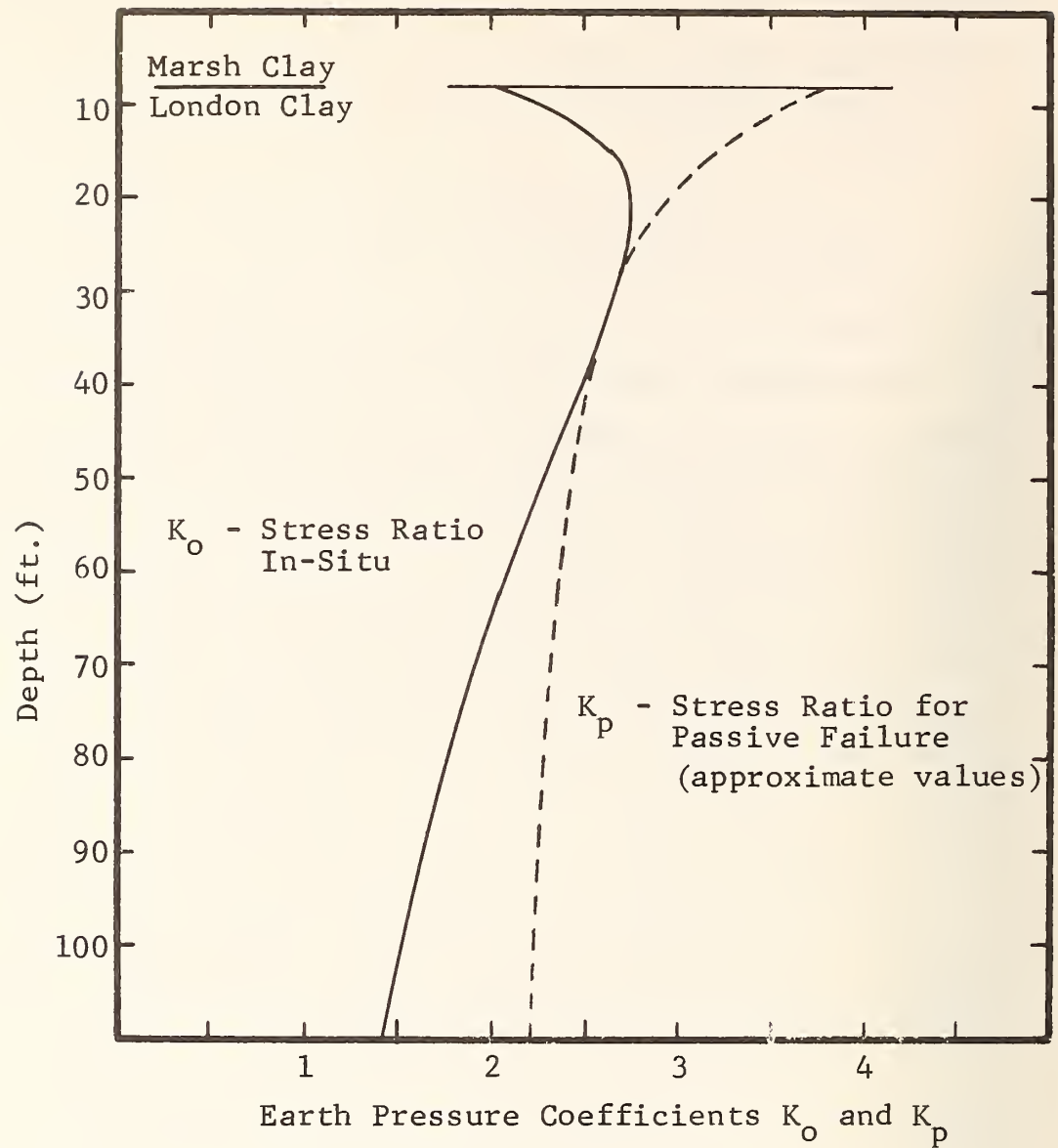


Figure 2-29. Variation of Stress Ratio  $K_o$  and Failure Stress Ratio  $K_p$  with Depth for London Clay at Bradwell (After Skempton, 1961)

## 2.4 IN-SITU DETERMINATION OF STRESSES

Several techniques that may be used in-situ for stress measurement are discussed below. These devices measure, in-situ, some soil property or effect that may be related to one or more components of the in-situ stress field. Pre-knowledge of the stress history or over-consolidation ratio is not generally required in a direct in-situ technique.

### 2.4.1 ACOUSTIC WAVE PROPAGATION

The words acoustic and sonic are taken as descriptive of low amplitude waves which may be of any convenient frequency. The propagation velocity of such waves in a continuum is given by:

$$v_p = \left[ \frac{E_d}{\rho} \left( 1 + \frac{2\nu_d^2}{1-\nu_d-2\nu_d^2} \right) \right]^{1/2}$$

for the dilatational wave velocity and by

$$v_s = \left[ \frac{E_d}{\rho} \left[ \frac{1}{2(1+\nu_d)} \right] \right]^{1/2} = \sqrt{\frac{G_d}{\rho}}$$

for the distortional wave velocity, in which

$E_d$  = dynamic elastic modulus

$\nu_d$  = dynamic Poisson's ratio

$G_d$  = dynamic shear modulus

$\rho$  = mass density

Acoustic velocity measurements are frequently used to determine dynamic elastic moduli (e.g., Afifi and Richart, 1973; Bamert, et al., 1965). Because the elastic moduli of rock and soil are typically stress-dependent, the wave propagation velocities may be correlated directly with in-situ stress. Johnson and Nelson (1970) report a seismic field study that included determination of elastic

moduli in several directions at a rock site. The velocity data and a corresponding in-situ velocity ellipse are shown in Figure 2-30. It is assumed that the velocity ellipse corresponds to the in-situ stress ellipse.

Hardin and Richart (1963) conducted resonant column tests on Ottawa sand, crushed quartz sand and crushed quartz silt to determine the parameters influencing wave velocities. They proposed correlations having the form

$$V_s = (A - Be) \sigma_o^C$$

in which  $V_s$  = shear wave velocity.

$e$  = void ratio

$\sigma_o$  = confining pressure

A, B & C = empirical constants.

For dry sands, gradation and relative density had no effect except in so far as the void ratio changed. Crushed quartz silt exhibited a dependency on time when measurements were made one hour after loading. Substituting the empirical constants, the shear wave velocities,  $V_s$ , were found to be:

For dry Ottawa sand:

$$V_s = (170 - 78.2 e) \sigma_o^{1/4} \quad \text{for} \quad (\sigma_o > 2000 \text{ psf})$$

$$V_s = (119 - 56.0 e) \sigma_o^{3/10} \quad \text{for} \quad (\sigma_o \leq 2000 \text{ psf})$$

For dry crushed quartz sand:

$$V_s = (159 - 53.5 e) \sigma_o^{1/4}$$

For dry crushed quartz silt (not overconsolidated):

$$V_s = (167 - 87.8 e) \sigma_o^{1/4}$$



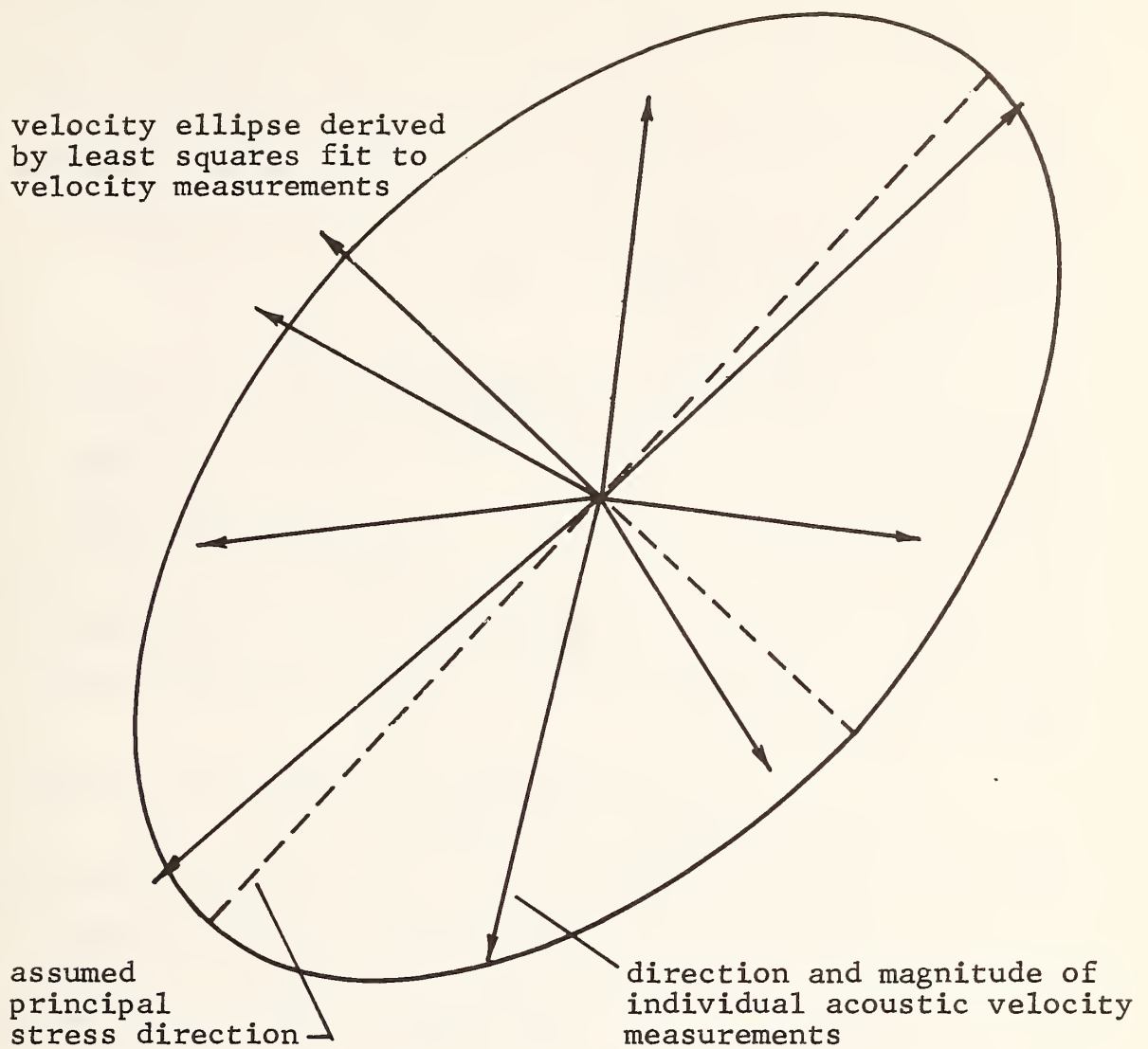


Figure 2-30. Velocity Ellipse Derived From Measurements of Acoustic Velocity at San Bernardino Tunnel Intake Tower Site (Johnson and Nelson, 1970)

Typical data for Ottawa sand are shown in Figure 2-31. The velocity data are predicted to within about  $\pm 10\%$  by the correlations noted. If the correlations are reversed, i.e., measured velocity data used to predict stresses, the associated errors would be on the order of  $\pm 40\%$  since  $\partial\sigma/\sigma = 4 \partial V/V$ . For overconsolidated quartz silt, there is little variation of wave velocity with confining pressure, so that the correlation given holds only for normally consolidated quartz silt.

The relationships of Hardin and Richart were applied by Stokoe and Woods (1972) in the cross-borehole method shown in Figure 2-32. These investigators measured shear wave velocity between boreholes. As pointed out by Haupt (1973) in a discussion of this paper, refraction of the wave path as indicated in Figure 2-33 makes necessary corrections when measurements at shallow depths are attempted. The required corrections to the Stokoe and Woods data are shown in Figure 2-33(b).

The one-fourth-root dependence of acoustic velocity is an unattractive feature of the concept because the experimental error in determination of velocity is reflected in an error four times as large in the inferred stresses, i.e., 5 percent error in the velocity measurement results in a 20 percent error in the reported stress;  $\Delta\sigma/\sigma = 4(\Delta V_s/V_s)$ . Compounding this is the number of other parameters that affect the acoustic velocity. Circumvention of this problem would require development of an in-situ calibration capability. This could be accomplished by direct measurement of in-situ stress in the formation being mapped, or by pressurizing a section of the borehole wall in which a localized velocity versus stress calibration may be computed. The major advantages of the cross borehole concept are its rapidity, and the fact that measurements are conducted on the undisturbed soil far from the boreholes. In all, it appears

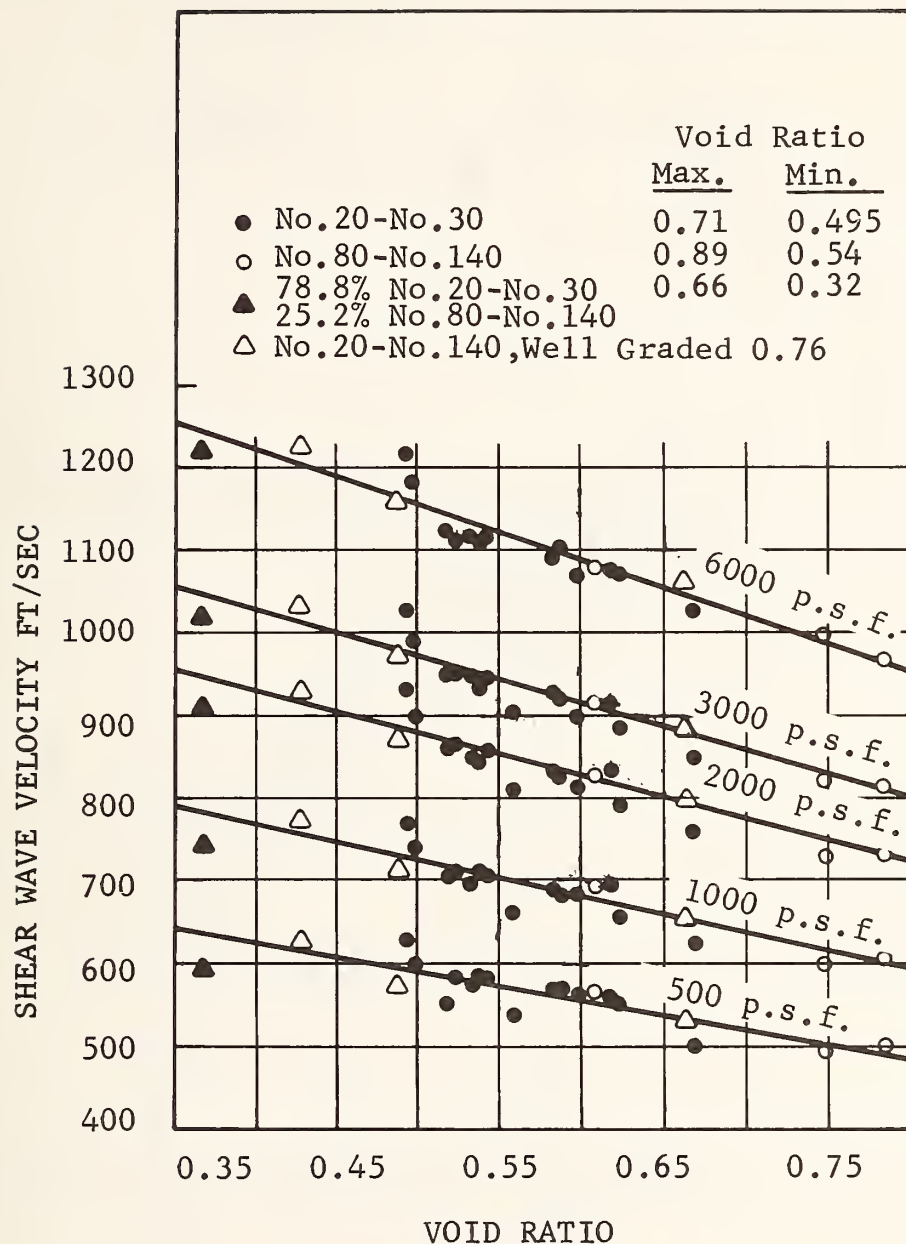


Figure 2-31. Variation of Shear Wave Velocity with Void Ratio for Various Confining Pressures, Grain Sizes, and Gradations in Dry Ottawa Sand (Series I) (Richart & Hardin, 1963)

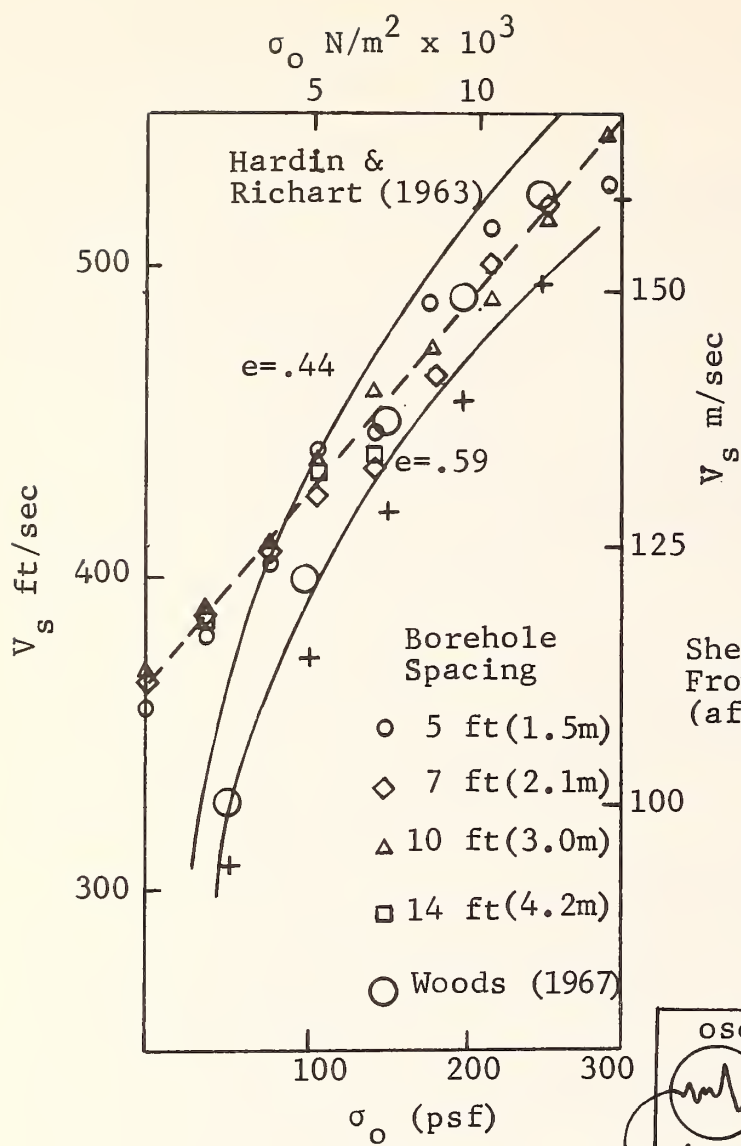
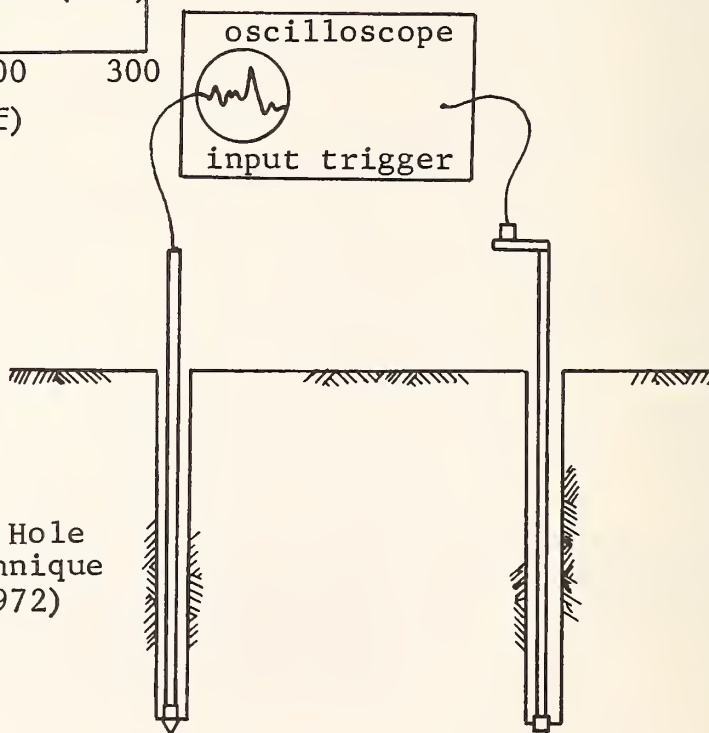


Figure 2-32

Shear Wave Velocity Profile  
From Cross-Hole Shooting  
(after Stoke & Woods)

Schematic of Cross Hole  
Seismic Survey Technique  
(Stokoe & Woods, 1972)



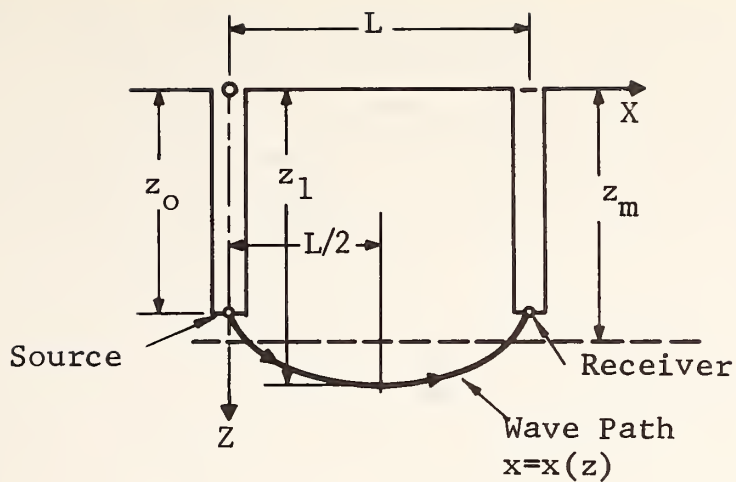


Figure 2-33(a). Curved Wave Path

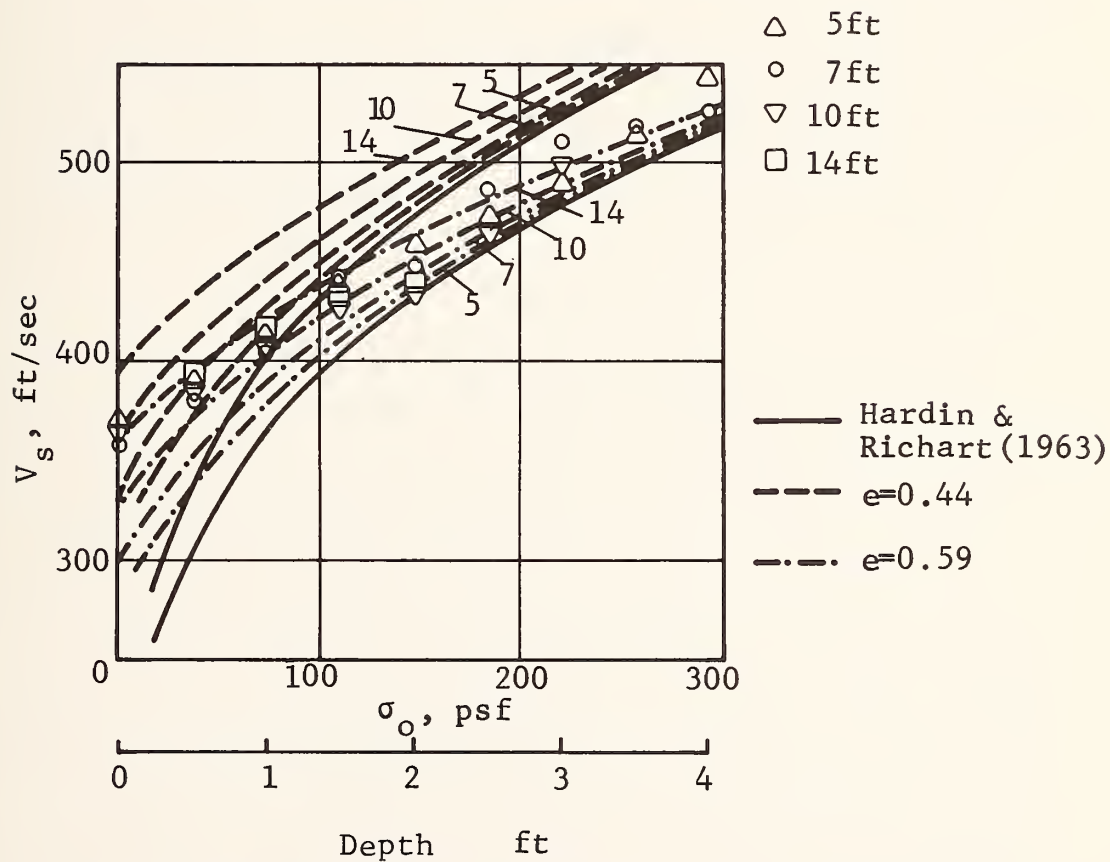


Figure 2-33(b). Shear Wave Velocity Profile

Figure 2-33 Refraction Correction for Cross-Borehole Shooting (Haupt 1973)

to be a good technique for obtaining a generalized view of the gross stress field, but will not give results of great precision in any localized volume. As such, it would be especially valuable when used in conjunction with another method capable of detailed and precise measurements in small volumes.



#### 2.4.2 BOREHOLE DEFORMATION TECHNIQUES

A number of techniques based on deformation measurements in boreholes or shafts have been suggested or used. In rock mechanics, these include overcoring, (Obert and Duvall, 1967, and Jaeger and Cook, 1964) and flat or curved jacks, (Glossop, 1968). It is difficult to visualize overcoring or stress relief methods being applied to soil although it should not be immediately discarded. The major difficulty results from the changes in the stress field near a borehole, particularly in the case of yielding. If rock yields during coring (or overcoring) the phenomenon of core discing occurs, but at least an estimate of the in-situ stresses may be recovered (Obert and Duvall, 1967). Applications of borehole deformation techniques in soils include the jacking of plates or semi-cylindrical sleeves (Glossop, 1968; Sherif and Strazer, 1973). Many investigators have reported on the development or application of various types of pressure-meters.

The reported jacking tests (Glossop; Sherif and Strazer) were directed toward the measurement of in-situ deformation moduli. However, since the opening of a borehole or a shaft implies stress relief of the radial component at the wall, the initial phase of a jacking test, if properly conducted, results in an estimate for the in-situ lateral stress, much as the odometer test provides a value for the vertical consolidation stress. This would be subject to the same constraints as a consolidation test, which measures the maximum historical applied stress. Such tests have been described by Obert and Duvall (1967), Glossop (1968), Wroth and Hughes (1972, 1973), Menard (1967), Shepherd and Charleson (1971), Baguelin, et al., (1972), Higgins (1969), Meigh and Greenland (1965), Smith and Smith (1968), Gibson and Anderson (1961), and Campbell and Hudson (1969). Although earlier work was done in Germany, the development of the pressuremeter appears to rest with Menard.

Recently major improvements were made at Cambridge by Wroth and Hughes and in France by Baguelin and Jezequel. The classical Menard pressuremeter (Figure 2-34) is simply an inflatable probe which is lowered into an open borehole and expanded against the soil.

The data are typically a plot of probe volume or diameter as a function of pressure and, usually, time. The probe pressure is increased in increments and the volume measured at specified intervals after the application of each increment. Idealized results are indicated in Figure 2-35. The "creep" curve is the volume change recorded between readings taken 30 and 60 seconds after each pressure increment. The P-V curve represents the 60-second volume readings and the "inertia" curve represents the pressure-volume relationship for the pressuremeter itself. The in-situ stress may either be estimated directly from the curve or it may be evaluated from theoretical cavity expansion analysis. The pressure-volume curve may provide an estimate, since most authors make a statement such as "the initial sloping portion of the curve results from the restoration of the earth pressure to the undisturbed condition prior to the removal of the soil from the hole," (Campbell and Hudson, 1969). Also, the first knee on the P-V curve appears to correspond roughly to an abrupt decrease in the creep values. Such an abrupt increase in modulus would be expected at the level of the lateral in-situ stresses. Seldom, however, do data as clean as these idealized curves result from actual testing. This is partially due to the fact that most investigators are interested in modulus and ultimate strength values, so that the initial portions of the P-V curve may be completely missed.

The classical approach to the stress problem is to deal with the ultimate pressure at which indefinitely large deflections occur. This is dealt with by theoretical analysis of the expanding cavity problem (Menard, 1957;

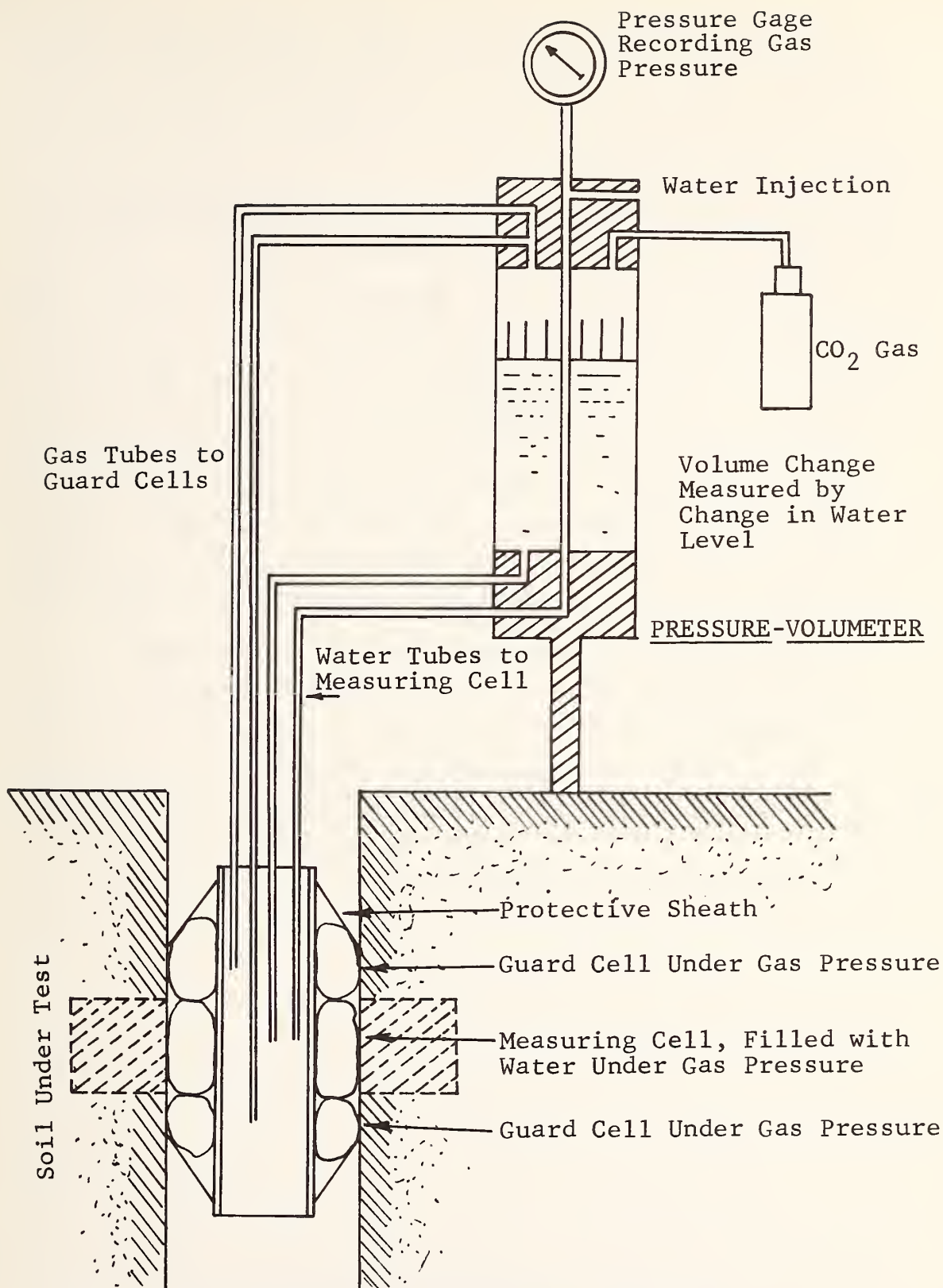


Figure 2-34. Classic Menard Pressuremeter (Campbell 1969)

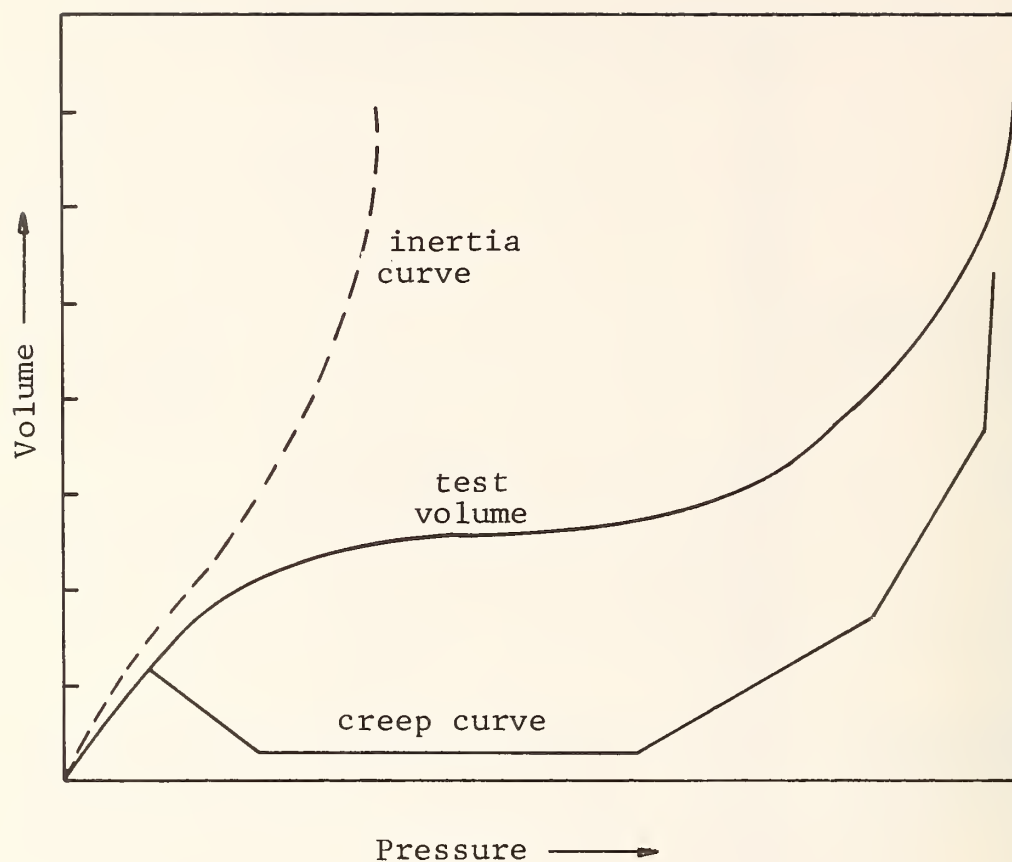


Figure 2-35. Idealized Pressuremeter Data  
(Higgins, 1969)



Gibson and Anderson, 1961; Wroth and Hughes, 1972; and Vesic, 1972), which relates the ultimate pressure to the in-situ stress. Assumptions regarding the soil behavior are made, and mathematical models are developed to predict the pressure. The result is a relationship between the limit pressure and the soil properties and volumetric behavior, and other parameters considered appropriate by the particular investigator. The problem is made more difficult by the post-yield behavior of the soil near the pressuremeter. A plastic zone is formed early in the test which modifies the stress distribution around the pressuremeter. The radius of the plastic zone is considered by Vesic (1972). Such analysis requires detailed knowledge of the post-yield soil behavior, which may be lacking. This is a problem that requires a certain amount of experience and judgment if confidence is to be placed in the results.

Many of the tests conducted with the pressuremeter in this country were directed toward the evaluation of specific hardware. Thus, many of the disadvantages cited by some authors are not inherent in the concept, but reflect hardware developmental problems. This may be a factor in the lack of general acceptance of this device. Hardware development is, in fact, continuing, as demonstrated by the efforts of the Cambridge group under Wroth and Hughes, and the French group under Baguelin and Jezequel.

Both devices avoid the problem of stress relief and disturbance by drilling into the soil without an open borehole. The Cambridge probe, shown schematically in Figure 2-36, resembles a vertical mole. The auger level should be maintained such that there is no tendency for the soil to yield, either into or ahead of the advancing probe. The thin membrane is held flat against the probe body by a slight vacuum during insertion of the probe into the soil. Note that the membrane is approximately the same thickness as

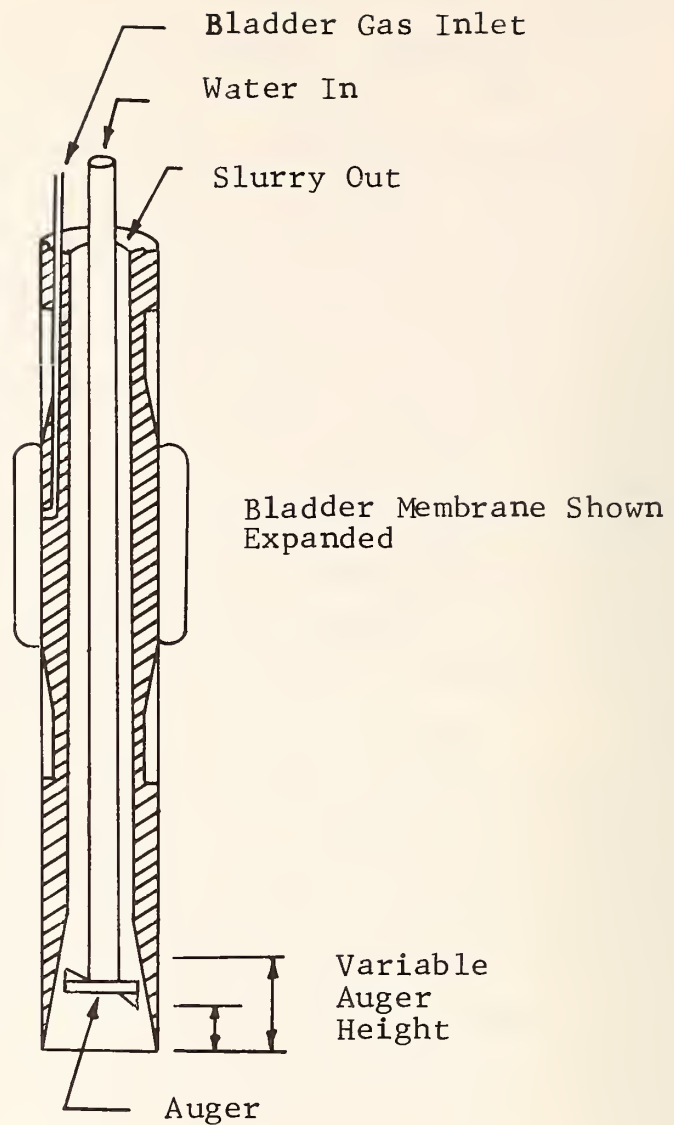


Figure 2-36. Pressuremeter Component of Cambridge Stress Probe  
(Wroth and Hughes, 1972)



a standard triaxial membrane, about 0.012 inch ( $3 \times 10^{-4}$  m) This is much thinner than the membrane used for the Menard borehole pressuremeter and can be so because the membrane is everywhere supported by the soil since it is not in an over-size borehole. An additional difference is that the membrane is inflated by gas rather than water. This allows use at greater depths since the pressure due to a high head of water in the drill string is avoided. Deflection is measured by feeler gages acting on the interior of the bladder. The Cambridge device may be used in conjunction with a companion direct lateral stress measurement device which is said to be more accurate than the pressuremeter for stress measurements. However, when using the pressuremeter alone, the in-situ lateral stress should be the level at which expansion is initiated.

The French device, shown in Figure 2-37, differs from the Cambridge device in the following respects. The membrane is supported by a thin water layer during insertion. The parameter monitored during a test is the volumetric expansion of the probe rather than the measurement of radial deflection. The pressure behind the probe is monitored during insertion and can provide certain indications if the slurry pressure is so high as to force mud up around the outside of the probe. Should this occur, the soil is already disturbed and a test at the same location would be useless. Because the membrane is fluid-backed, any inequality between the lateral stresses tends to redistribute during insertion.

During insertion, disturbance to the in-situ stresses may be caused by interface shear stresses induced at the surface of the probe. This shear stress is reduced by the use of polished steel instrument surfaces. Potyondy (1961) reported shear resistance for soil-polished steel in terms of frictional and cohesive parameters  $f_{\phi} = \delta/\phi$  and  $f_c = a/c$  in which  $\delta$  is the interface friction angle:  $a$  is the interface

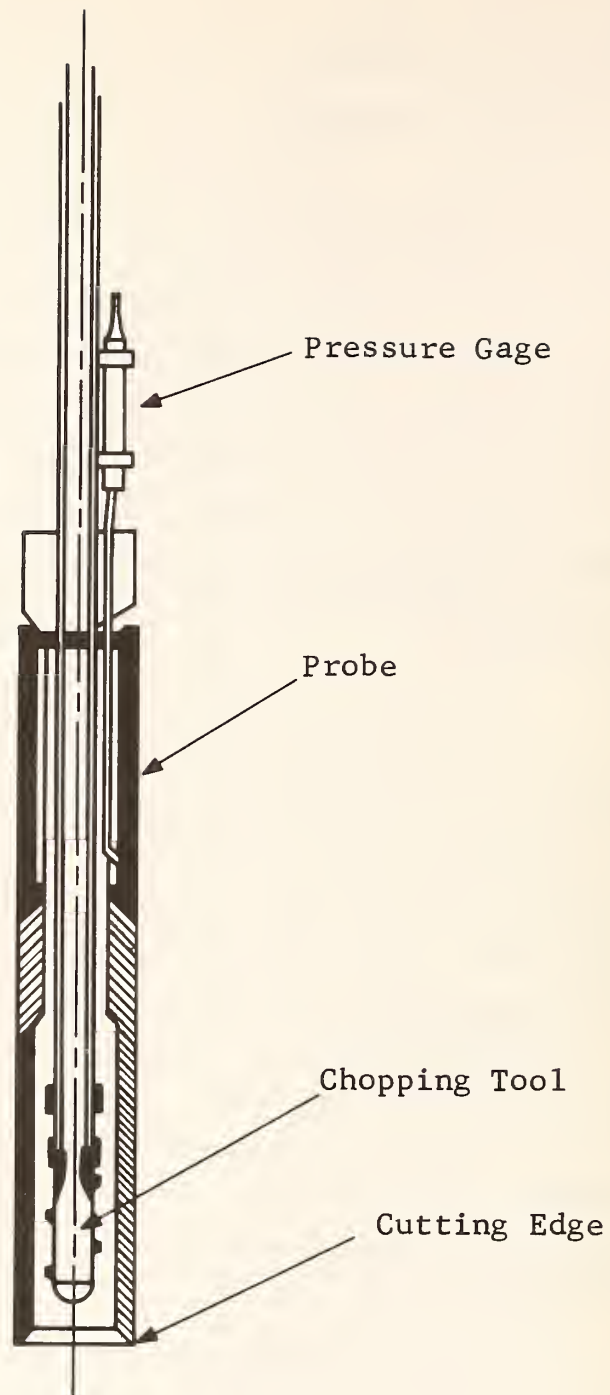


Figure 2-37      Sketch of "Autoforeuse" Probe  
(Baguelin et al. 1972)

adhesion. Thus, the Mohr failure curve may be expressed in terms of the soil shear strength parameters  $\phi$  and  $c$  by  $\tau = c f_c + \sigma \tan (\phi f_\phi)$ . Potyondy recommends the following values for use with polished steel:

	$f_\phi$	$f_c$
dry dense sand	0.54	--
saturated dense sand	0.64	--
dry dense cohesionless silt	0.79	--
saturated dense cohesionless silt	0.68	--
saturated loose cohesionless silt	0.40	--
cohesive granular soil	0.40	--
clay	0.50	0.50

Leonards (1965) reports work that included the effect of lubricants on soil-polished steel interface shear resistance in terms of a coefficient of friction  $\mu = \tau/\sigma$ . Since  $\mu = \tan \delta$ , these data can be cast into the same form as that of Potyondy, giving the following results:

	20-30 sand $f_\phi$	60-80 sand $f_\phi$
polished steel	0.47	0.55
teflon coated steel	0.46	0.76
graphite coated steel	0.34	0.45

This indicates that a teflon coating may actually increase the shear resistance of a steel-sand interface, whereas graphite performs better as a lubricant. Potyondy's data show that polished steel surfaces introduce shear stresses into the soil that range from 40 to 80 percent of the soil shear strength. For dense silt a polished steel surface is little better than a wholly rough surface.

Pressuremeters have been used in rock and granular soils, but the Cambridge and the French devices are considered most reliable in the softer clays.

### 2.4.3 STRESS PROBE

A direct approach to the in-situ stress measurement problem is to somehow insert a stress gage into the ground with so little disturbance that accurate measurements can be made. It should be noted that the problem of making stress measurements, even in artificial specimens where the gage may be placed with practically zero disturbance, is not itself trivial. Nonetheless quite effective soil stress gages are commercially available.

The first attempt at a stress probe may have been undertaken by Kenney (1967) while at the Norwegian Geotechnical Institute. The device was an open bottom tube built up from sheet piling sections, in all approximately 10 meters in length. Total stress and pore pressure gages were placed flush with the outer surface at several locations along the tube. The device was allowed to sink into the quick clay under its own weight. Although the clay was observed to displace into the tube, certain disturbance along the outside was inevitable as the tube entered the soil. Stress measurements were made over a long period as the clay relaxed against the tube. Kenney pointed this out and did not use the term  $K_0$  in his report. This device was intended to resolve a discrepancy between reported laboratory values of  $K_0$  and reported shear strength parameters for Norwegian normally consolidated quick clays. In fact, in-situ lateral stresses were shown to be greater than laboratory  $K_0$  tests had indicated, so that the stress probe successfully dealt with the specific question it was designed to answer.

The current extension of the stress probe is embodied in the device, Figure 2- 38, designed at Cambridge (Wroth and Hughes; 1972, 1973). This is a heavy wall open tube carrying flush mounted lateral stress gages and an internal auger to reduce insertion disturbance. The time required

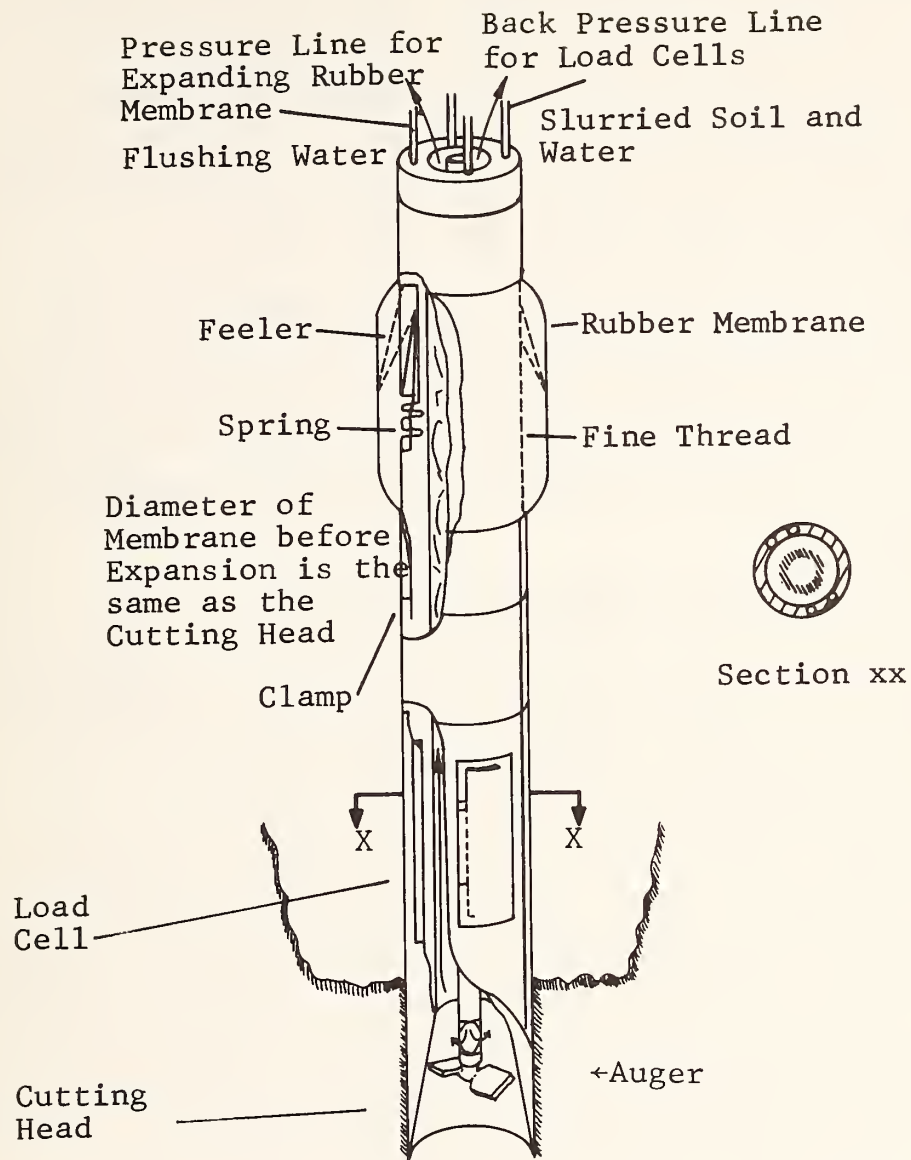


Figure 2-38 Main Details of Cambridge In-Situ Instrument Showing Stress Gages (Wroth and Hughes 1972)



for the soil stresses to relax is on the order of 10 hours as opposed to up to 10 days for the NGI stress probe. Typical data are shown in Figures 2-39 and 2-40. The device is similar to the Cambridge pressuremeter in its manner of insertion. At one point, both the pressuremeter and stress probe units were mounted end to end. Because of the difference in test duration, the pressuremeter is probably more efficiently used in a separate probe even if both units are used at the same site.

The stress probe configurations reported in the literature surveyed monitor lateral stress in only one direction. If the lateral stresses are not equal and the principal directions are not known, the devices have to be rotated in the ground to make three separate sequential measurements.

#### 2.4.4 HYDRAULIC FRACTURING METHODS

A common stress measurement tool in rock mechanics is hydraulic fracturing (Haimson, 1968, 1971, 1972; Kehle, 1964; Obert and Duvall, 1967). Initially employed as a technique to improve well production by fracturing the near-by-strata, the technique may be extended to measure the least principal stress and rock tensile strength. The technique as mathematically idealized by Kehle is shown in Figure 2-41. A section of the well borehole is isolated by packers and pressurized at sufficiently high levels to open a tensile fracture normal to the least principal stress. The shut-in pressure  $P_s$  in Figure 2-42 is shown to approximate the least principal stress. If the least principal stress happens to be vertical, little information is gained since this stress component is generally known, given the density of overburden material. Haimson describes the stress information that can be retrieved from a knowledge of the fracture direction and pressures:



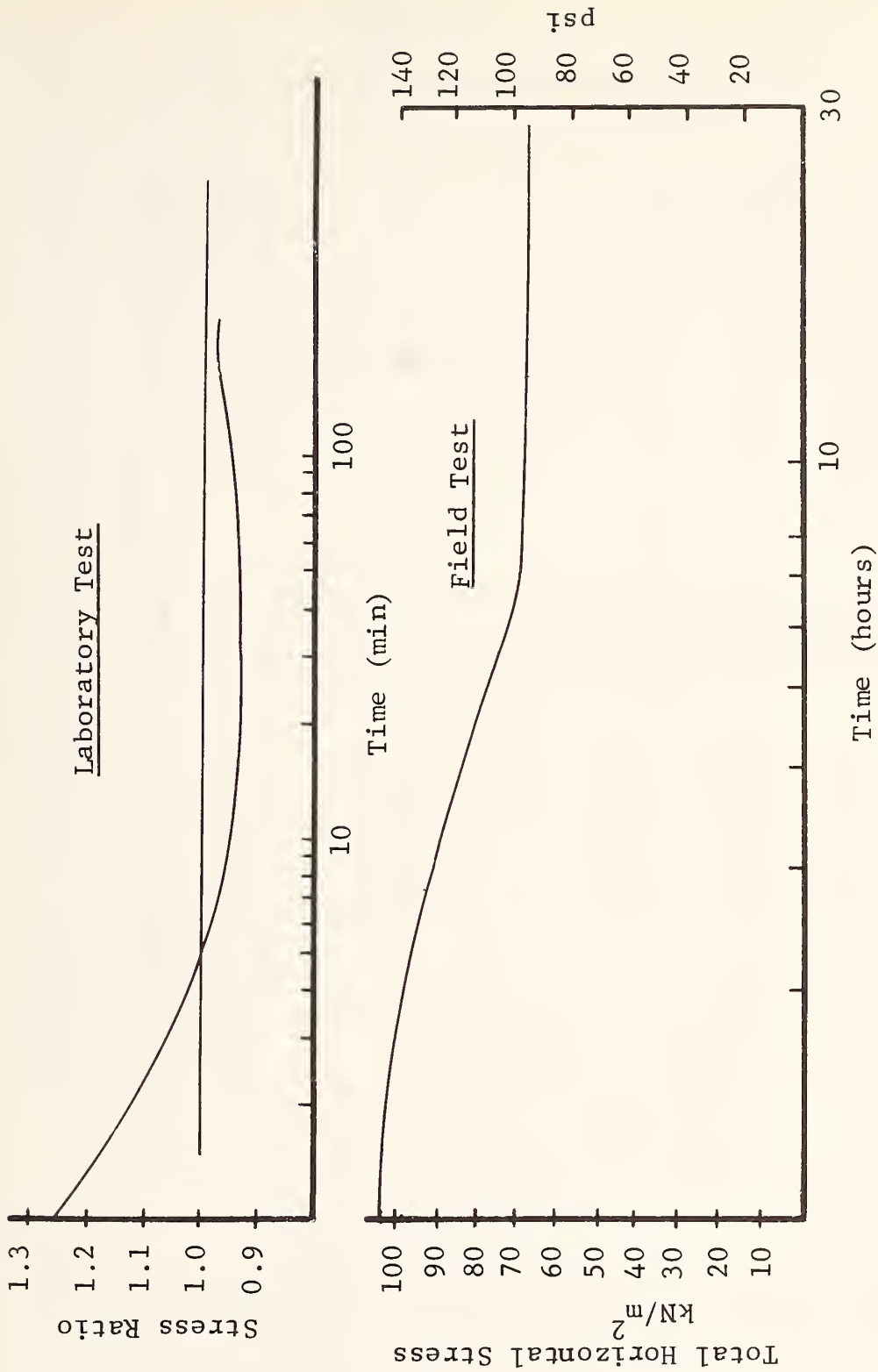


Figure 2-39. Change of Lateral Stress Recorded by Cambridge Stress Probe With Time (Wroth and Hughes, 1972)

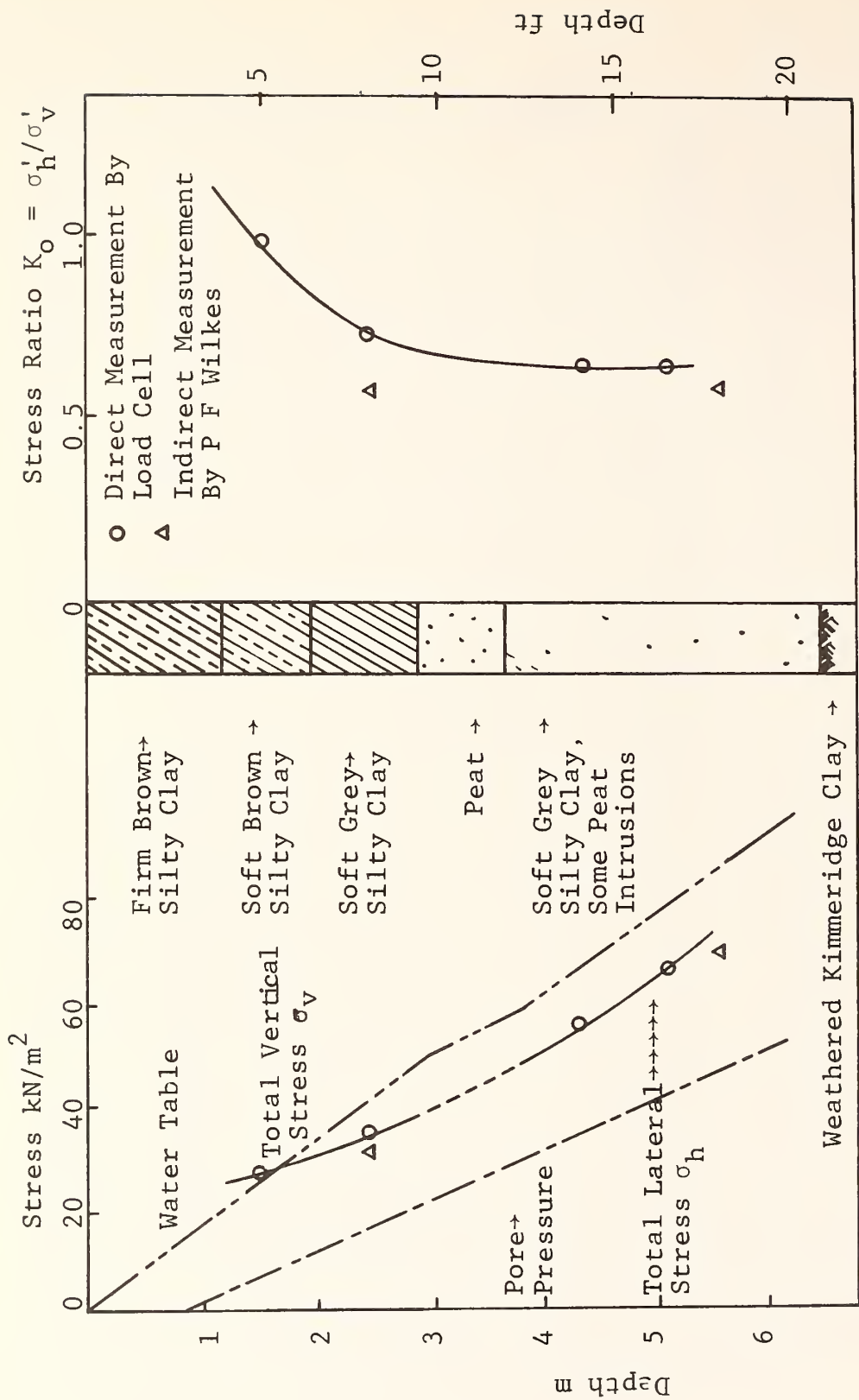


Figure 2-40 Measurements of Lateral Stress at Different Depths for One Profile in a Field Test at King's Lynn. (Wroth and Hughes 1972)

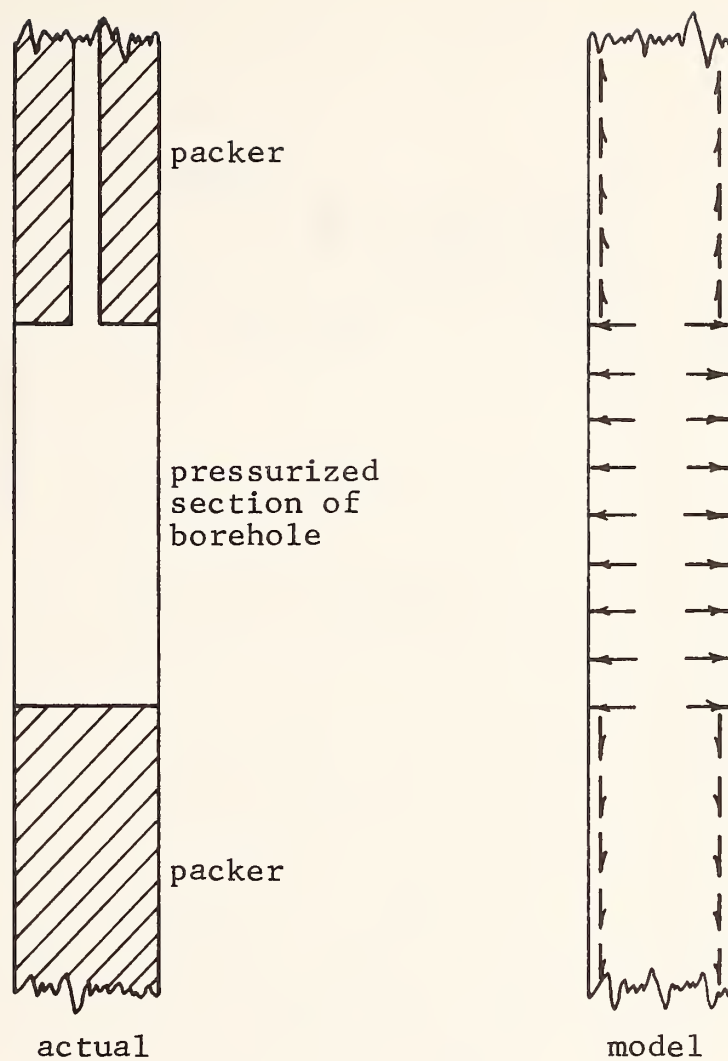


Figure 2-41. Idealization of Hydraulic Fracturing  
In Rock  
(Kehle 1964)

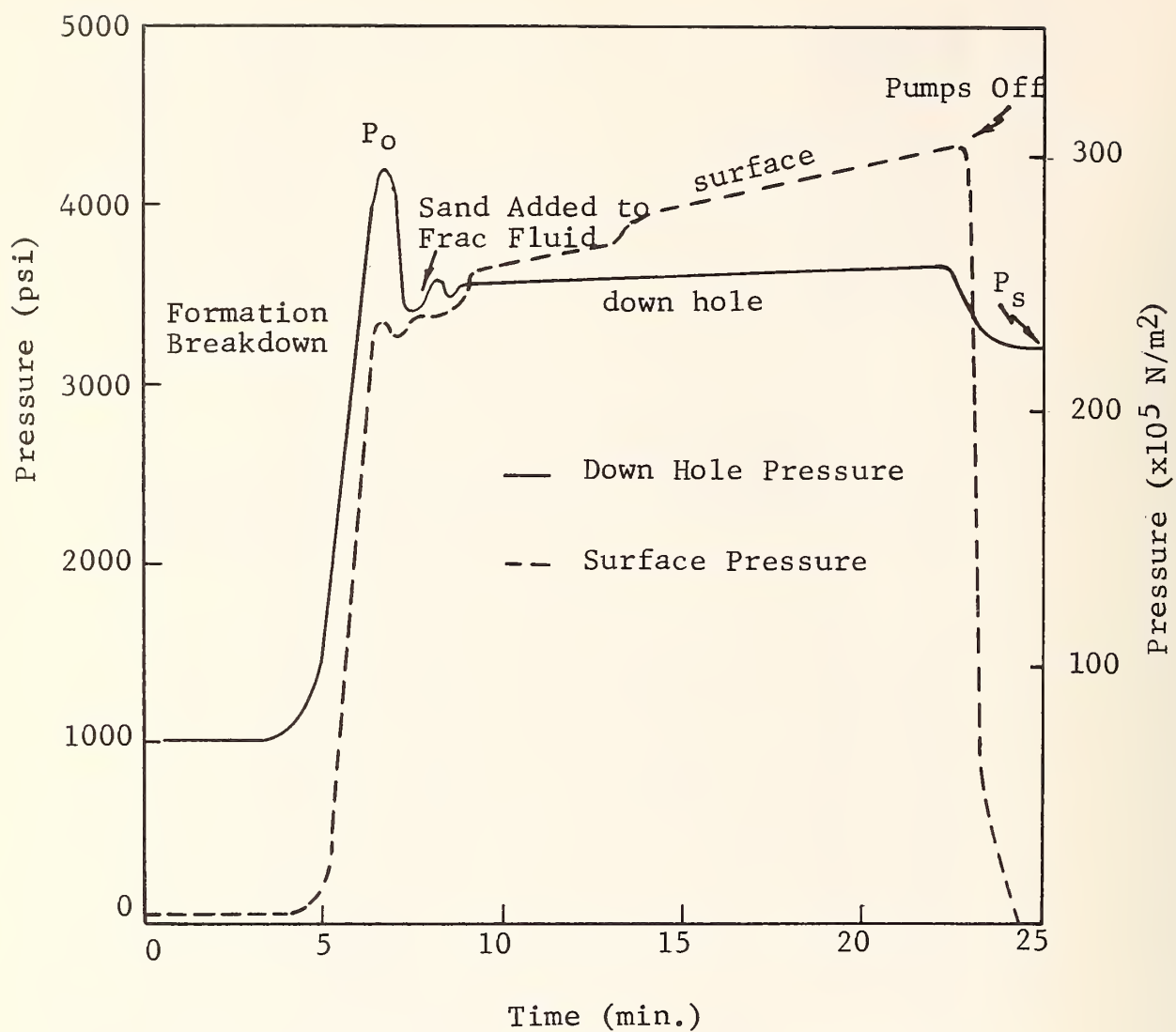


Figure 2-42. Schematic of Pressure Versus Time Graph From a Typical Well-Fracturing Operation

		Fracture Initiation Direction	
		Horizontal	Vertical
Fracture Extension Direction	Horizontal	$S_{11} = ?$	$S_{11} = S_{22} = S_H$ (assume)
		$S_{22} = ?$	
		$S_{33} = -P_s$	
	Vertical	$S_{11} = ?$ $S_{22} = -P_s$ $S_{33} = f(S_{22})$	$S_{11} = f(S_{22})$ $S_{22} = -P_s$ $S_{33} = f(\gamma D)$

For the most common case of vertical fracture initiation and extension, the in-situ stress field is well defined.

The use of hydraulic fracturing in soils apparently results from investigations of anomalous values of field permeability values reported by Bjerrum and Anderson (1972) and Bjerrum, et al., (1972). Bozozuk of the National Research Council of Canada (NRC) and Schmertmann, recently at NRC, are extending the method. This work employs standard piezometers that are backpressured to fracture the soil. Bjerrum's field apparatus and data are shown in Figures 2-43 and 2-44. If paraffin is used as a fracturing fluid there is no flow until the fracture actually occurs. If water is used, minor flow into the soil occurs before fracture. This is the pressure range that would be employed in a permeability test. When fracture does occur, the flow rate is drastically increased.

Bozozuk's considerably refined apparatus is said to be capable of measuring lateral stress and tensile strength for depths down to 125 ft in fine grained soils

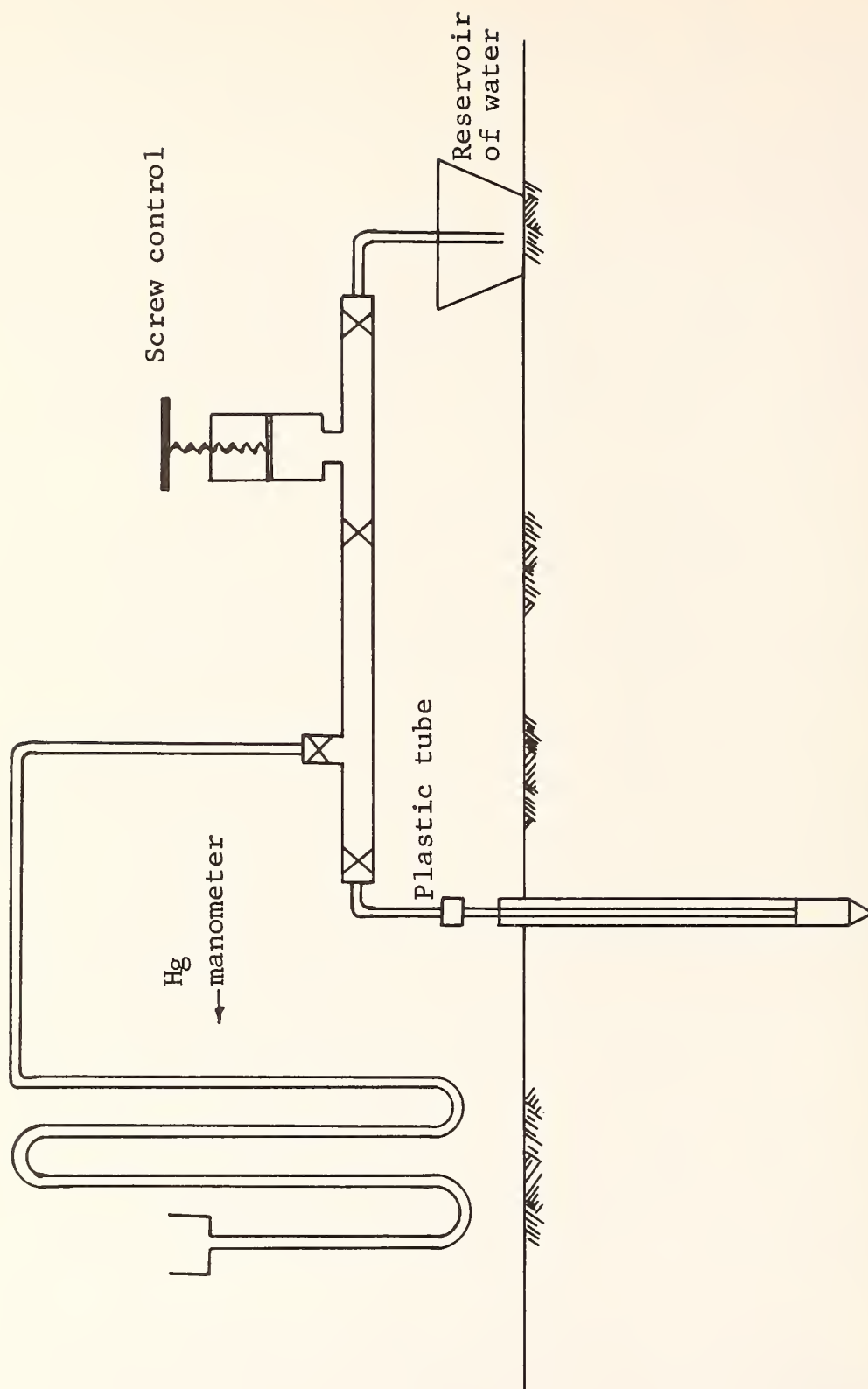


Figure 2-43. Sketch of Bjerrum's Hydraulic Fracturing Field Apparatus



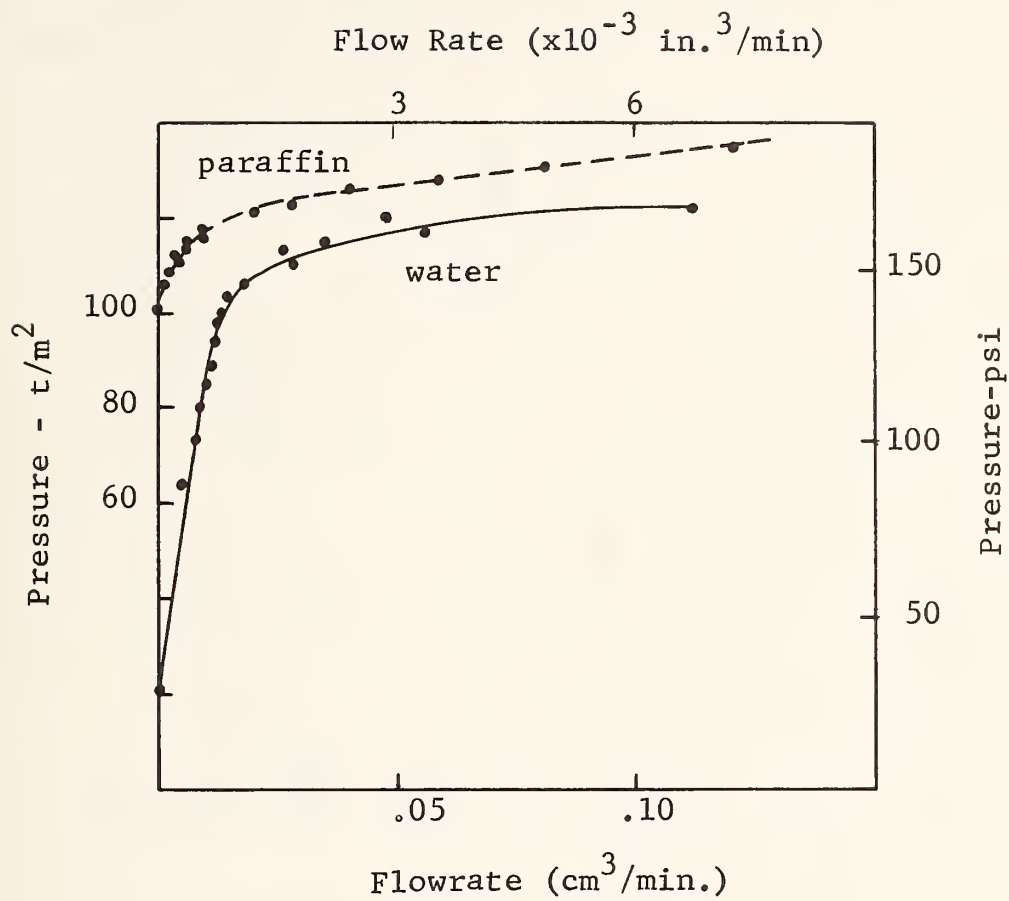


Figure 2-44. Hydraulic Fracturing Data in Soil (Bjerrum and Anderson, 1972)

having  $K_0$  as high as 1.25. In general, lateral stresses in excess of the overburden pressure can be measured only if the soil has some tensile strength. One of the major advantages of the technique is the rapidity with which measurements can be made once the piezometers are established in place.

Hydraulic fracturing would be highly recommended for fine grained soils if the in-situ stresses are to be monitored at a point during some period of time. Once the probe is in place and the soil stresses have relaxed, measurements can be made at the rate of 20 a day. It would appear that major earthwork operations particularly lend themselves to this technique for monitoring soil stress build-up, if the degree of compaction is not so great as to result in the minor principal stress being in the vertical direction.

Successful use of the technique in coarse-grained soils is limited in that the piezometer tip should have high permeability as compared with the soil. Certain approaches are obvious, such as the use of a relative viscous fracturing fluid in an open ported piezometer tip. It is not known if these developments have been attempted.

#### 2.4.5 VANE SHEAR TESTS

The strength anisotropy of a soil mass may be measured by means of multiple vane shear tests (Aas, 1965, 1967; and Blight, 1971) using vanes of different aspect ratio. The concept is shown in Figure 2-45. The torque  $M$  required to rotate a vane of diameter  $D$  and height  $H$  is written in terms of the horizontal and vertical shear strengths  $S_h$  and  $S_v$ :

$$M = \pi D H \frac{D}{2} S_v + 2 \frac{\pi D^2}{4} \frac{D}{3} S_h \quad (\text{after Aas})$$

$$M \left[ \frac{2}{\pi D^2 H} \right] = S_v + S_h \left[ \frac{D}{3H} \right]$$

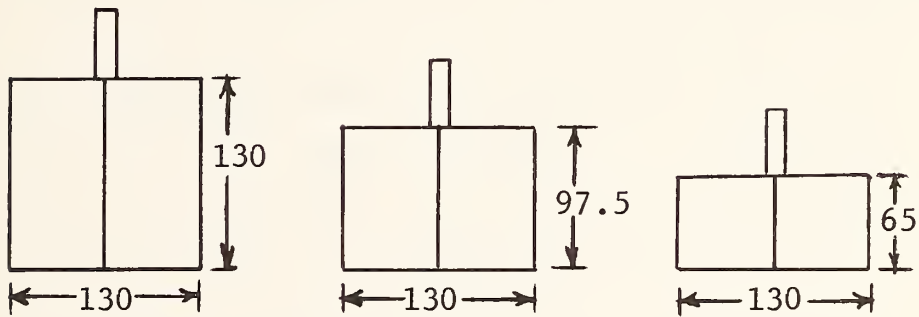
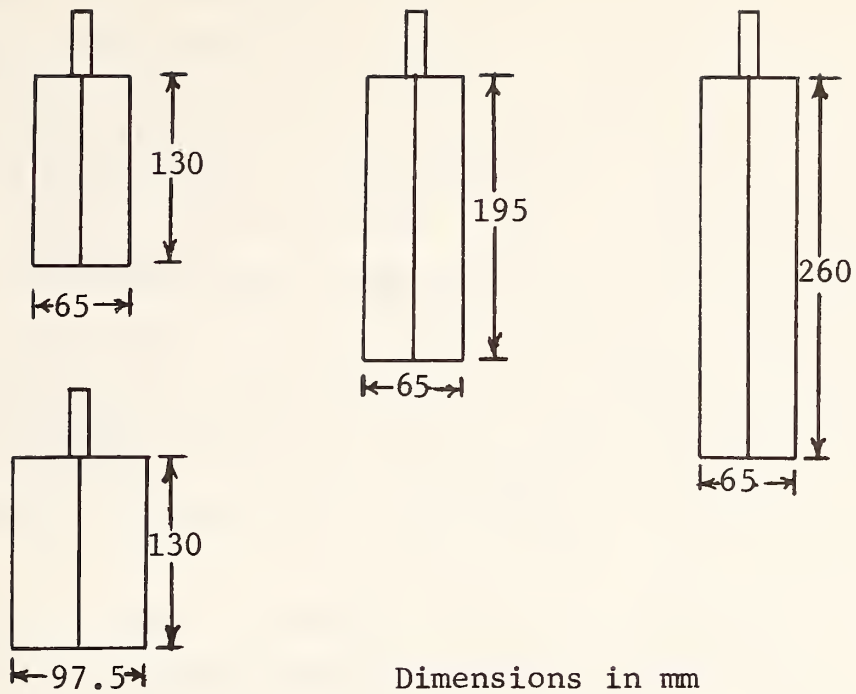


Figure 2-45. Vanes Used in Anisotropic Vane Shear Test (Aas 1965)

Then if vane shear tests having different aspect ratios  $D/H$  are plotted on  $2M/\pi D^2 H - D/3H$  coordinates, the result should be a straight line having intercepts of  $S_v$  and  $S_h/S_v$  on the two axes. Data from four Norwegian sites as reported by Aas are shown in Figure 2-46. It can be seen that the straight line relationship holds except for high aspect ratios ( $D/H = 1/6$ ). The values for  $S_v/S_h = 1/(S_h/S_v)$  range from about 1/2 for normally consolidated sites to 1 for slightly overconsolidated sites. These are roughly the expected values of  $K_0$ , so it appears that the measured strength anisotropy may reflect in-situ stress ratios. Aas states that this is supported by tests in a vane-triaxial apparatus; i.e., a triaxial cell into which a miniature vane is inserted.

A somewhat different analysis is made by Blight (1971). The torque required to shear vanes of various aspect ratios is written in terms of the cohesion, friction angle and vane dimensions. The following notation is used:

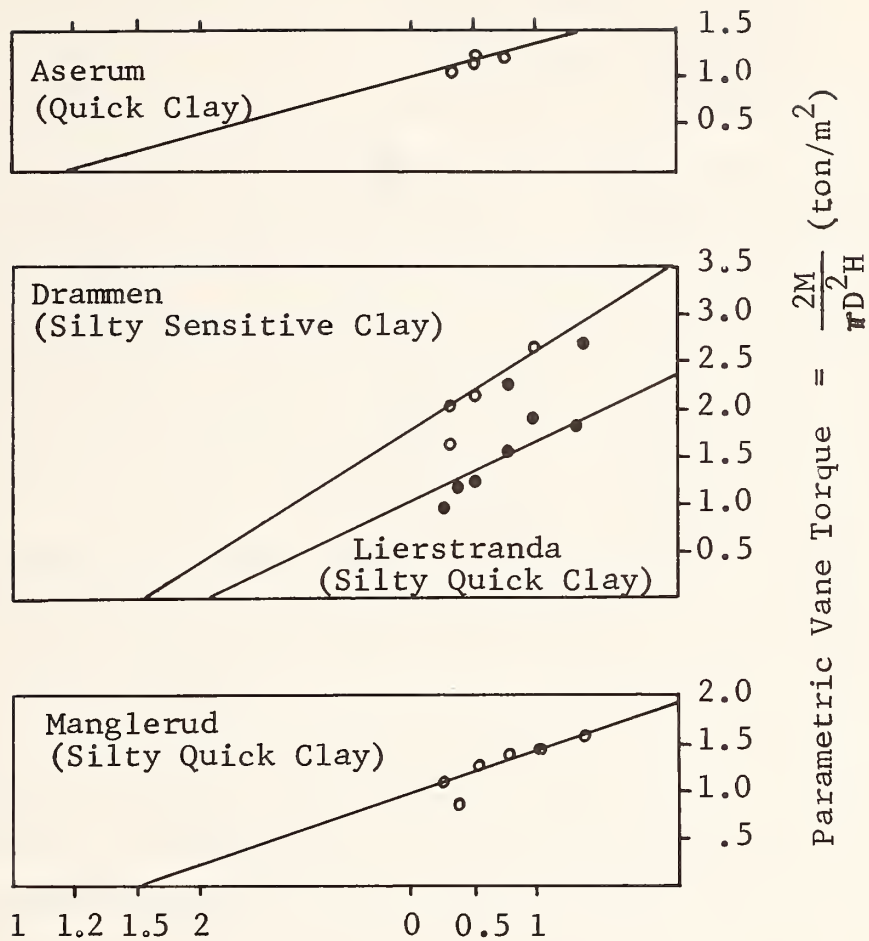
$$\begin{aligned} T(D) &= \text{torque for vane aspect ratio of 1} \\ T(D/3) &= \text{torque for vane aspect ratio of 1/3} \\ T(2D) &= \text{torque for vane aspect ratio of 2} \\ R &= \text{strength ratio } S_v/S_h \end{aligned}$$

$$R = \frac{T(D) - T(D/3)}{3T(D/3) - T(D)} \quad \text{or} \quad R = \frac{T(2D) - T(D/3)}{6T(D/3) - T(2D)}$$

If  $\phi$  is assumed isotropic and  $c$  is assumed negligible in comparison with  $\sigma \tan \phi$ , then

$$R = \frac{c + \sigma_h \tan \phi}{c + \sigma_v \tan \phi} = \frac{\sigma_h}{\sigma_v}.$$

Blight cautions that his assumptions may only be valid for intrinsically isotropic soils in which cohesion may be ignored.



$$M \left[ \frac{2}{\pi D^2} \right] = S_v + S_h \left[ \frac{D}{3H} \right]$$

$$\text{for } M \left[ \frac{2}{\pi D^2} \right] = 0, \quad \frac{S_h}{S_v} = - \frac{1}{D/3H}$$

Figure 2-46. Anisotropic Vane Shear Data  
(Aas 1965)

## 2.4.6 COMPARISON OF FIELD DETERMINATIONS

Five in-situ techniques currently available for determining in-situ field stresses are:

- acoustic velocity
- borehole pressuremeter
- borehole stress probe
- hydraulic fracturing
- anisotropic vane shear

The choice of a particular technique for use at a specific site depends largely on the circumstances and must be made after a number of factors have been considered. The geotechnical applicability of each field technique is indicated in Table 2.1. Matrix locations marked X indicate geotechnical conditions for which a technique is particularly suited, conditions noted N/A indicate geotechnical conditions under which a technique is not appropriate. Selection of a technique for use at a particular site requires judgements that cannot be included in a simple table -- engineering judgement requires familiarity with the method, the site and the apparatus available.

Some of the characteristics of the existing in-situ methods are summarized in Table 2.2. The accuracy of each method obviously depends on the circumstances of the test, and the ratings applied may change if the geotechnical conditions are not appropriate to the test method being used. The range of each test is more easily identified. The borehole and anisotropic vane shear devices respond to local effects near the test apparatus, and will require great care to avoid insertion disturbance. Acoustic velocity and hydraulic fracturing are long range tests that tend to average over a large volume of soil and be less influenced by local disturbance. The uniformity of the soil mass must also be considered in terms of the sampling range, since a long range technique will not resolve the detailed changes in stress that may be expected if more than one soil type is present in the volume sampled.



Table 2.1

APPLICABILITY OF FIELD METHODS TO  
VARIOUS GEOTECHNICAL CONDITIONS

Soil Type	Fine Grained			Course Grained			
STRESS HISTORY	lateral stresses equal		Full $\sigma_1 \neq \sigma_2 \neq \sigma_3$ Triaxial	lateral stresses equal		Full $\sigma_1 \neq \sigma_2 \neq \sigma_3$ Triaxial	Quantity Obtained
	K <sub>o</sub> Normally Consolidated	K <sub>o</sub> Over-Consolidated		K <sub>o</sub> Normally Consolidated	K <sub>o</sub> Over-Consolidated		
Acoustic Velocity	X	X	X	X	X	X	$\sigma_n$
Borehole Pressuremeter	X	X	N/A			N/A	$\sigma_h$
Borehole Stressprobe	X	X		X	X		$\sigma_n$
Hydraulic Fracturing	X	N/A	X	N/A	N/A	N/A	$\sigma_3$
Anisotropic Vane Shear			N/A	X	X	N/A	K <sub>o</sub>

## STRESS CODE

$$K_o = \sigma_h / \sigma_v$$

$$\sigma_h = \text{mean horizontal stress}$$

$$\sigma_m = \text{mean stress}$$

$$\sigma_n = \text{normal stress}$$

$$\sigma_3 = \text{least principal stress}$$

Table 2.2

## CHARACTERISTICS OF IN-SITU STRESS DEVICES

	Relative Accuracy Low-Medium-High	Volume Sampled Small-Large	Equipment Costs Low-Medium-High	Indicates Principal Stress Directions
Acoustic Velocity	L	L	L-M	Yes
Borehole Pressuremeter	M	S	H	No
Borehole Stressprobe	H	S	H	Yes
Hydraulic Fracturing	H	L	L-M	No
Anisotropic Vane Shear	L	S	L	No

The costs associated with the various methods include the capital expenditures and the time required to conduct the actual testing. The anisotropic vane shear test requires only several special vanes in addition to standard equipment. The capital cost associated with this method is noted as negligible in Table 2.2, indicating costs less than \$100. The capital costs associated with the cross-borehole shooting and hydraulic fracturing methods range from minor cabling to more significant recording and transducer purchases. The following major items are suggested for the two methods:

cross-borehole shooting hardware

- acoustic receiver (geophone)
- acoustic transmitter
- oscilloscope (preferably dual beam)
- adjustable delay line
- cabling

hydraulic fracturing hardware

- standard piezometer tip
- electrical pressure transducer (mounted down hole)
- conditioning electronics for transducer (bridge balance)
- recorder (X-Y or chart recorder)
- variable-flow fluid source (e.g., pressurized gas bottle, precision regulator, fluid bottle and metering valve)
- flowmeter

hydraulic fracturing hardware (shallow depths only)

- standard piezometer tip
- mercury manometer
- screw volume control

Obviously the capital expenditures depend on the instrumentation available and the sophistication desired. Total system costs range from several hundred to several thousand dollars.

The techniques requiring the most expensive hardware are the cross-borehole pressuremeter and the stress probe. In addition to instrumentation requirements, a sophisticated down hole device is required. Both techniques employ

self-boring probes and presently only one model of each is known to be on the market.

The operating costs associated with each technique depend on the structure and work load of the field crew. Cross-borehole shooting probably requires only several minutes per test plus drilling time to reach the desired level. The anisotropic vane shear technique is considered equivalent to three standard vane shear tests. Hydraulic fracturing requires less than 1/2 hour per test after the piezometers are established and excess pore pressures due to driving are allowed to dissipate. The self-boring pressuremeter requires 1/2 to several hours per test whereas the stress probe requires one to four days. The latter two instruments also require drill rig and augering support for insertion at the desired horizon.

## 2.5 EVALUATION OF ANISOTROPIC PROPERTIES

### 2.5.1 INTRODUCTION

Because soil fabric tends to become more oriented with increasing consolidation or deformation, the stress history is inferred, at least in part, from the degree and orientation of anisotropic behavior in a soil mass. The fabric elements that display stress dependency thus are of interest vary considerable in size. For example, Blight (1971) applied the Griffith criterion to determine the fracture patterns expected in shrinking or swelling clays. By this criterion, the angle  $\psi$  to the vertical at which cracking occurs is given by:

$$\cos 2\psi = \frac{\sigma_v' - \sigma_h'}{2(\sigma_v' + \sigma_h')} \quad \text{shrinking}$$

$$\cos 2(90^\circ - \psi) = \frac{\sigma_h' - \sigma_v'}{2(\sigma_h' + \sigma_v')} \quad \text{swelling.}$$

The case of shrinking is given by a mass of initially intact clay, saturated throughout, but with the water table a distance  $h$  below the surface. The pore water tension in the saturated clay at the surface is given by  $u = \alpha \gamma_w gh$ . The factor  $\alpha$  tends toward unity if evaporation ceases, and increases above unity if the evaporation rate increases. The resulting shrinkage stress, which depends on the stiffness of the soil, may be defined by  $\sigma_s = \beta \gamma_w gh$ , in which  $\beta$  will probably be equal to or greater than  $\alpha$ . The effective and total stresses may now be computed, giving for the Griffith criterion

$$\cos 2\psi = \frac{\beta}{2(2\alpha - \beta)} \quad \text{at the surface}$$

$$\cos 2\psi = \frac{\gamma z(K_o - 1) - \beta \gamma_w (h - z)}{2 [\gamma z(K_o + 1) - (2\alpha - \beta) \gamma_w (h - z)]} \quad \text{at depth } z$$

or if it is assumed that  $K_o = \frac{1}{2}$  and  $\gamma = 2\gamma_w$

$$\cos 2\psi = \frac{-[z + \beta(h - z)]}{2 [3z - (2\alpha - \beta)(h - z)]} \quad \text{at depth } z$$

Predicted crack profiles for two values of  $\alpha$  and  $\beta$  are shown in Figure 2-47, a corresponding actual crack pattern in Figure 2-48.

If shrinkage cracks become filled by material washed down from the surface and the soil subsequently swells, horizontal swelling will be restrained and horizontal swelling pressures may become large. Two sets of fissures may be expected to form in soil that alternately shrinks and swells. The swelling cracks will form at orientations of 50 to 60 degrees if the cracks form at a total stress ratio of  $3 < \sigma'_h / \sigma'_v < 6$ . In Figure 2-49, a frequency distribution



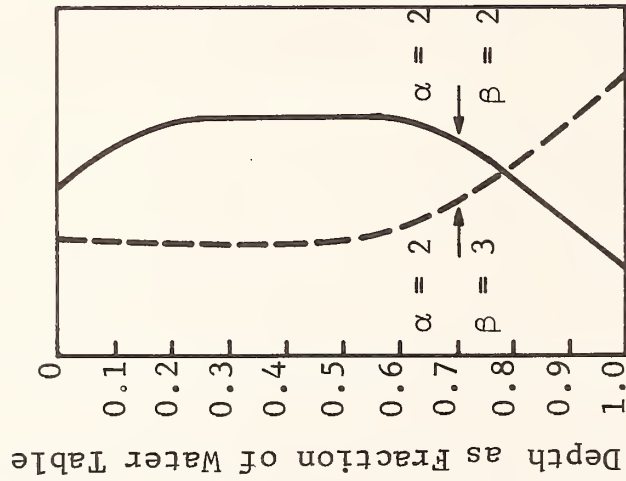


Figure 2-47. Typical Predicted Profiles of Cracking (Blight, 1971)

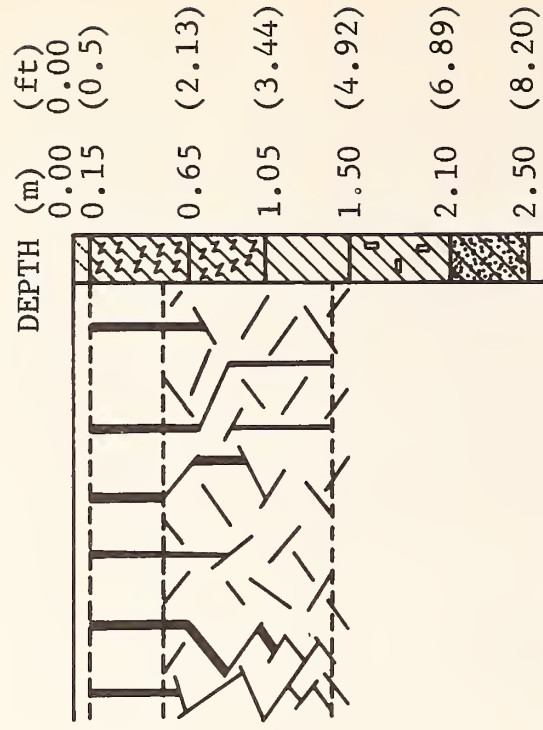


Figure 2-48. Simplified Pattern of Cracks and Fissures in a Soil Profile Near Onderstepoort (Blight, 1971)



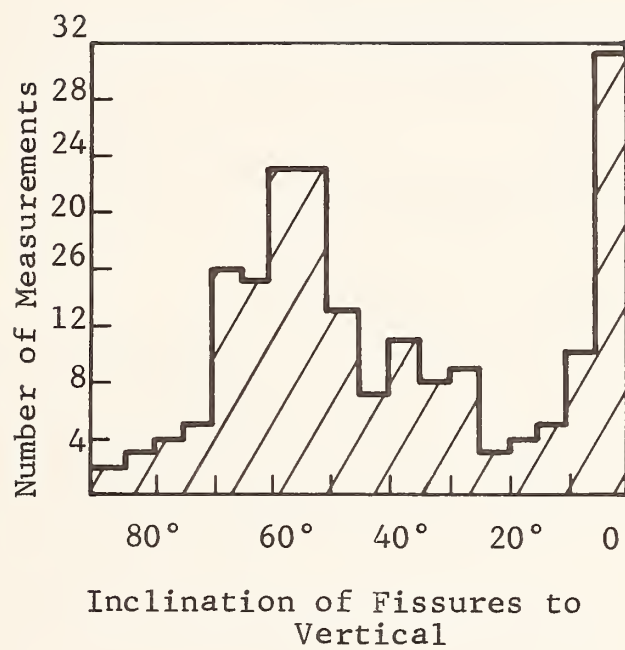


Figure 2-49. Distribution of Crack Inclinations  
(Blight, 1971)

of fissure angles shows a concentration of shrinkage cracks at  $\psi = 30$  degrees and swelling cracks at  $\psi = 57$  degrees. It can be seen that, although anisotropy is generally considered to be the result of the orientation of small fabric elements such as soil grains, fabric elements many times larger may be useful in deducing the history of a soil mass.

The following tools and disciplines were reviewed to evaluate their potential use with respect to fabric analysis and the broader goal of in-situ stress determination.

- o hydraulic permeability
- o electrical conductivity
- o acoustic propagation
- o electron microscopy
- o infrared
- o gamma rays
- o electron beam
- o electromagnetic resonance

#### 2.5.2 HYDRAULIC PERMEABILITY

Hydraulic permeability is a parameter routinely measured both in-situ and in the laboratory. The anisotropy of permeability has been shown to significantly influence soil properties. Ingles and Lee (1971) argue that strength anisotropy in fine-grained soils results from the influence of macropore anisotropy on minimum energy fracture paths. Duncan and Seed (1966) show that anisotropy in Skempton's pore pressure coefficient at failure  $\bar{A}_f$ ,

$$\Delta u = B (\Delta \sigma_3) + \bar{A}(\Delta \sigma_1 - \Delta \sigma_3)$$

is associated with anisotropy of undrained strength. Experimental data given show that  $\bar{A}_f$  for horizontal samples is consistently greater than  $\bar{A}_f$  for vertical samples as indicated in Figure 2-50. Since  $\bar{A}_f$  depends on the soil matrix stiffness and pore geometry, the different  $\bar{A}_f$  values in the two directions indicate the corresponding

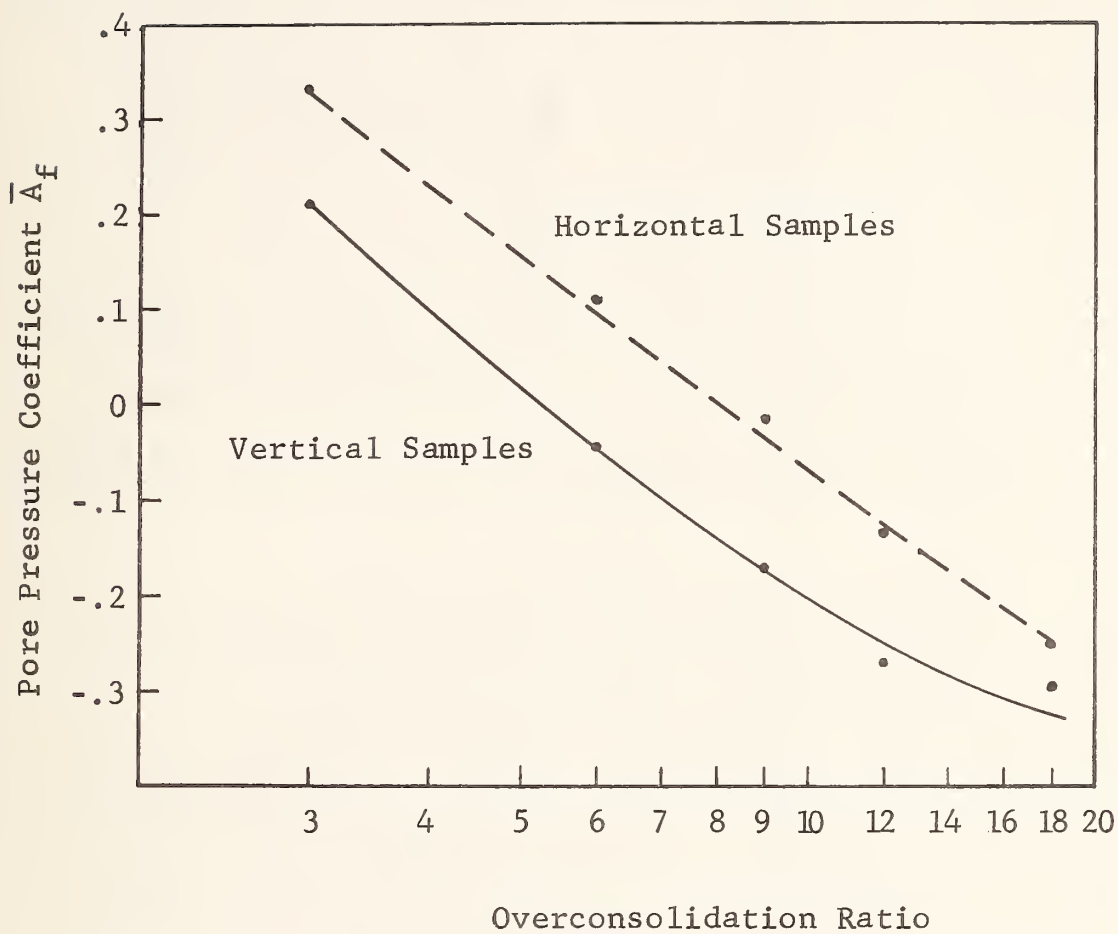


Figure 2-50. Effect of Specimen Orientation on Measured  $\bar{A}_f$  in Bay Mud  
(Duncan & Seed 1966)

differences in fabric and stresses. It is anticipated that the soil pore fabric may prove to be a more sensitive stress indicator than the soil grain fabric.

Mercury intrusion techniques were employed by Diamond (1970) and Sridharan, Altschaeffl and Diamond (1971) to determine pore size distribution curves. As static compactive effort increases, the larger voids are sequentially eliminated, the smaller voids being largely unaffected. The pore size distribution for sedimented clay is significantly different from that in compacted clay, with few voids larger than the grain size (Figures 2-51 and 2-52). Pore size distributions in cohesionless material were determined by Windisch and Soulie (1970) by manual measurements on thin sections of epoxy treated specimens. Few data except a pore size distribution are given in this paper which is basically the description of a fabric analysis technique.

Possible methods by which pore fabric may be evaluated include microscopy, hydraulic permeability and electrical conductivity. Hydraulic permeability is determined in the laboratory by various techniques or by piezometric measurements in the field. The anisotropy of permeability is commonly treated by assigning separate values to the permeability coefficient in the horizontal and vertical directions. Taylor (1967) gives a model for the hydraulic permeability coefficient  $k_H$  as

$$k_H = C_s \gamma_w n R_H^2 / \eta$$

The electrical analog for laminar flow is employed by Long and Zimmie (1973) to evaluate the shape factor  $C_s$  and estimate the hydraulic radius  $R_H$ . The DC electrical flow in a porous plug can be expressed by

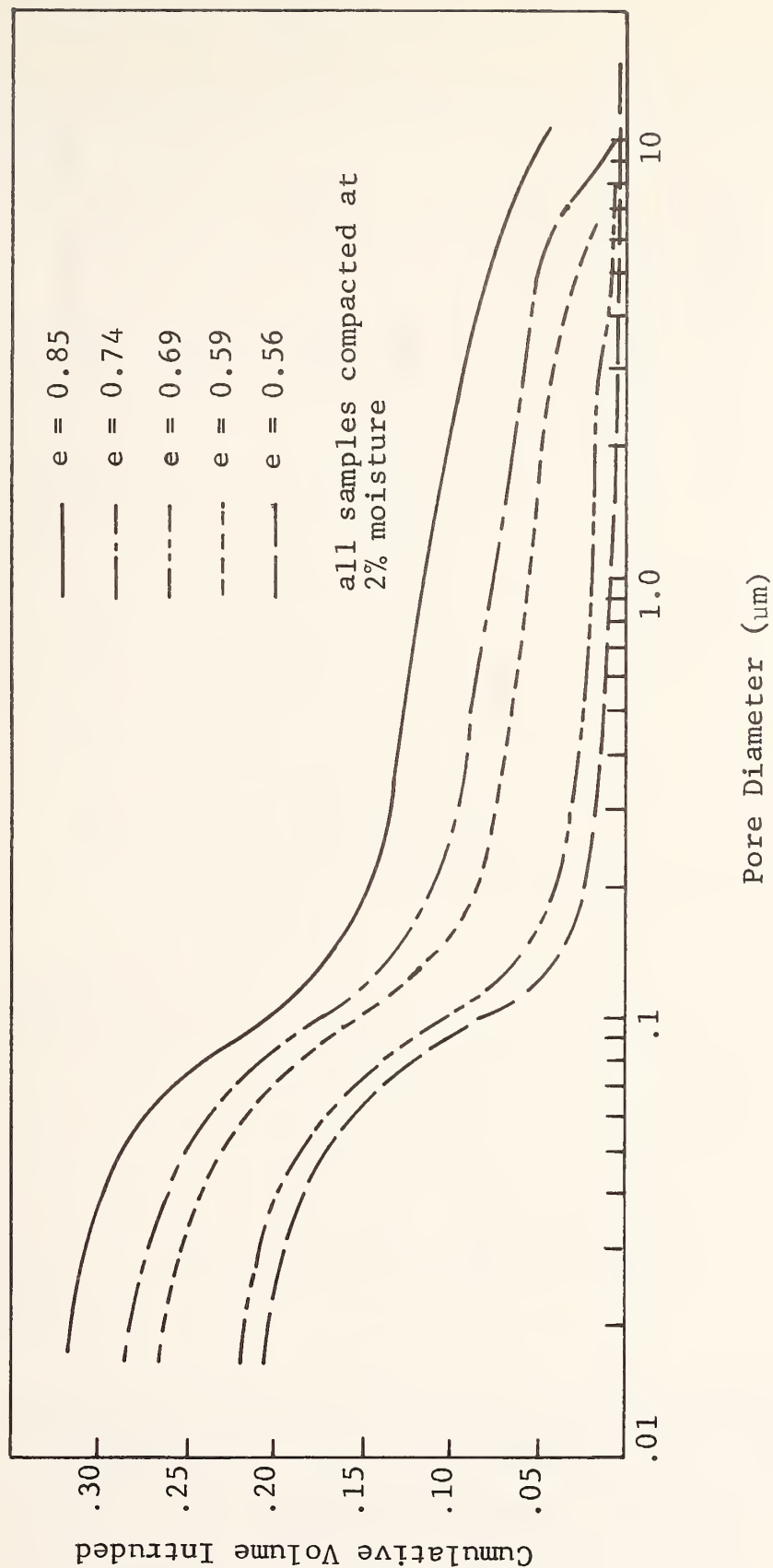


Figure 2-51. Effect of Degree of Compaction on Pore-Size Distribution of Statically-Compacted Kaolinite

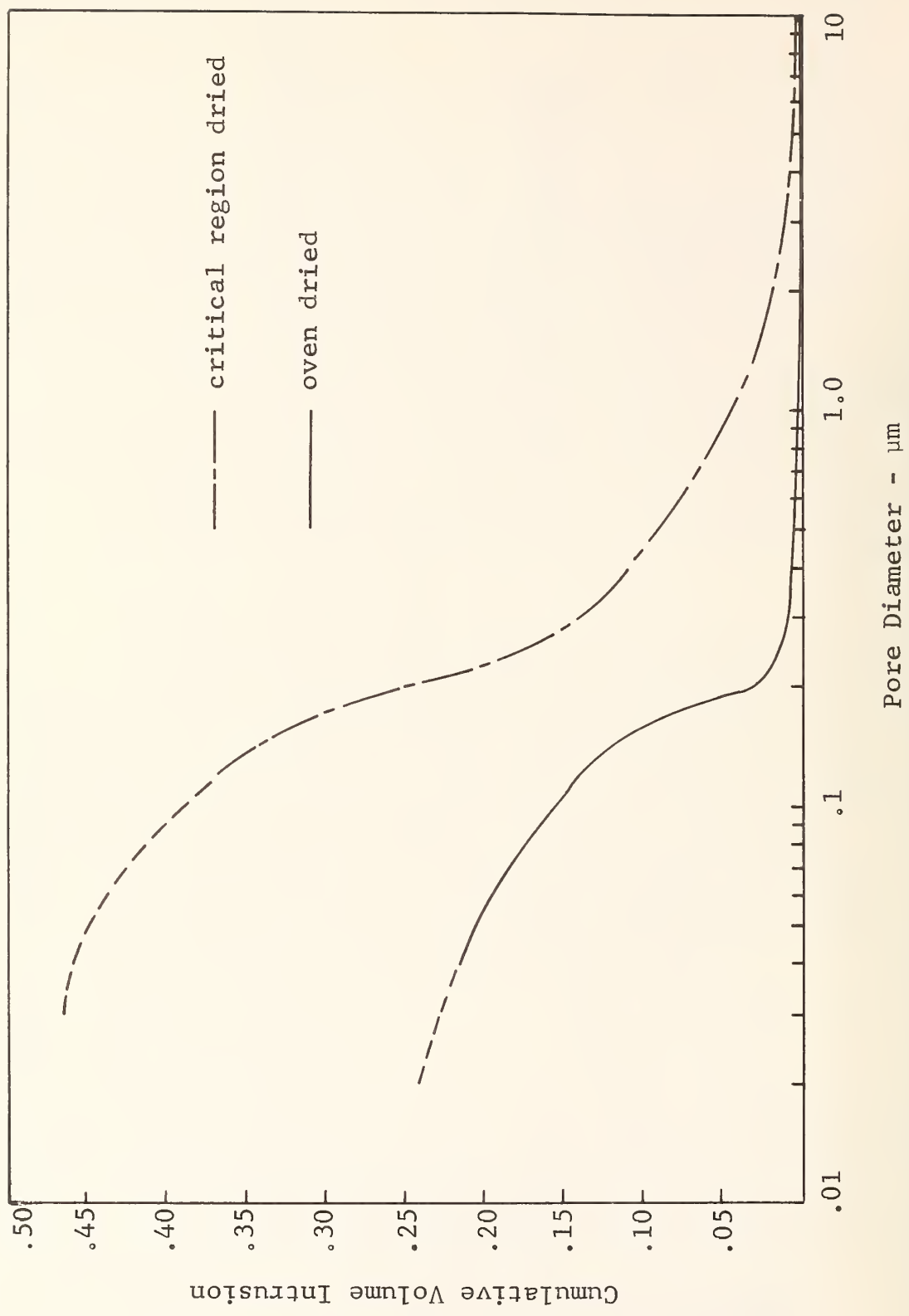


Figure 2-52. Pore-Size Distributions for Artificially-Sedimented Kaolinite Samples



$$C_s n = \frac{Li}{\Delta v \lambda A}$$

This may be compared with the fluid flow as follows:

$$C_s n = \frac{i}{\Delta v} \frac{L}{A} \frac{1}{\lambda} = \frac{Q}{\Delta H} \frac{L}{A} \frac{\eta}{\gamma_w R_H^2}$$

$$\text{or } R_H^2 = \frac{Q}{i} \frac{\Delta v}{\Delta H} \frac{\eta \lambda}{\gamma_w}$$

in which  $R_H$  = hydraulic radius

$L$  = sample length

$Q$  = hydraulic flow rate =  $k_H \frac{\Delta H}{L} A$

$\Delta H$  = fluid head loss

$\eta$  = viscosity of fluid

$\gamma_w$  = unit weight of fluid

$i$  = DC current flow

$\Delta v$  = impressed voltage

$\lambda$  = specific conductivity of electrolyte

$n$  = porosity

$A$  = area

Sequential measurements of fluid flow and DC current were made. Tests on fretted glass disks were conducted and found to compare reasonable well with mercury intrusion data and the advertised properties of the glass disks. No measurements in soil samples were reported. Seemingly soil anisotropy would be strongly displayed by the use of this technique in samples of oriented soil taken in different directions.

Application of pore anisotropy as a fabric parameter may be implemented by two approaches. The permeability  $k_H$  may be evaluated and empirically correlated to grain orientation functions by assumption of the shape factors  $C_s$  for the soil in question. This approach may be useful after a significant backlog of data is established. No

published relations between permeability ratio and grain orientation ratio were discovered during the literature survey. Alternatively, combined permeability and conductivity measurements may be used to determine the effective hydraulic radius  $R_H$  in various directions, and a more direct correlation made to fabric parameters. It is possible that sounding apparatus may be devised to permit in-situ measurements.

### 2.5.3 ELECTRICAL CONDUCTIVITY

Specific values of the resistivity of soil cannot be tabulated to identify soil types. According to Moore (1961), most clays will display low resistivities ranging from several to several tens of ohm-meters. Clean sand and gravel may range up to 10,000 ohm-m. Dense sand or rock such as granite may have resistivities of 10,000 to 40,000 ohm-m, whereas hard volcanic rock formations may be as low as 50 ohm-m.

Electrical conductivity has been employed as a tool for the evaluation of soil microstructure by several investigators. Mitchell and Arulanandan (1968) evaluated the soil properties that influence electrical dispersion. The soil was modeled as a parallel R-C circuit, and the parameters  $\epsilon'$  (real portion of dielectric constant),  $\epsilon''$  (imaginary portion of dielectric constant) and  $\sigma$  (conductivity in mhos/m) were plotted as a function of frequency (Figure 2-53). Anisotropy was found to influence  $\Delta\epsilon_0$ ,  $f_0$ , and  $\alpha$ .

The value  $\Delta\epsilon_0'$  reflects the magnitude of polarization developed at low-frequencies, and thus is a measure of mechanisms requiring relatively long times, such as the displacement of double-layer charges adjacent to particle surfaces.

The characteristic frequency,  $f_0$ , is a measure of the average time for a particular polarization process. This reflects the distance and ease with which charges may move, and charge size. The more easily charges can follow the electric field, the higher will be  $f_0$ .

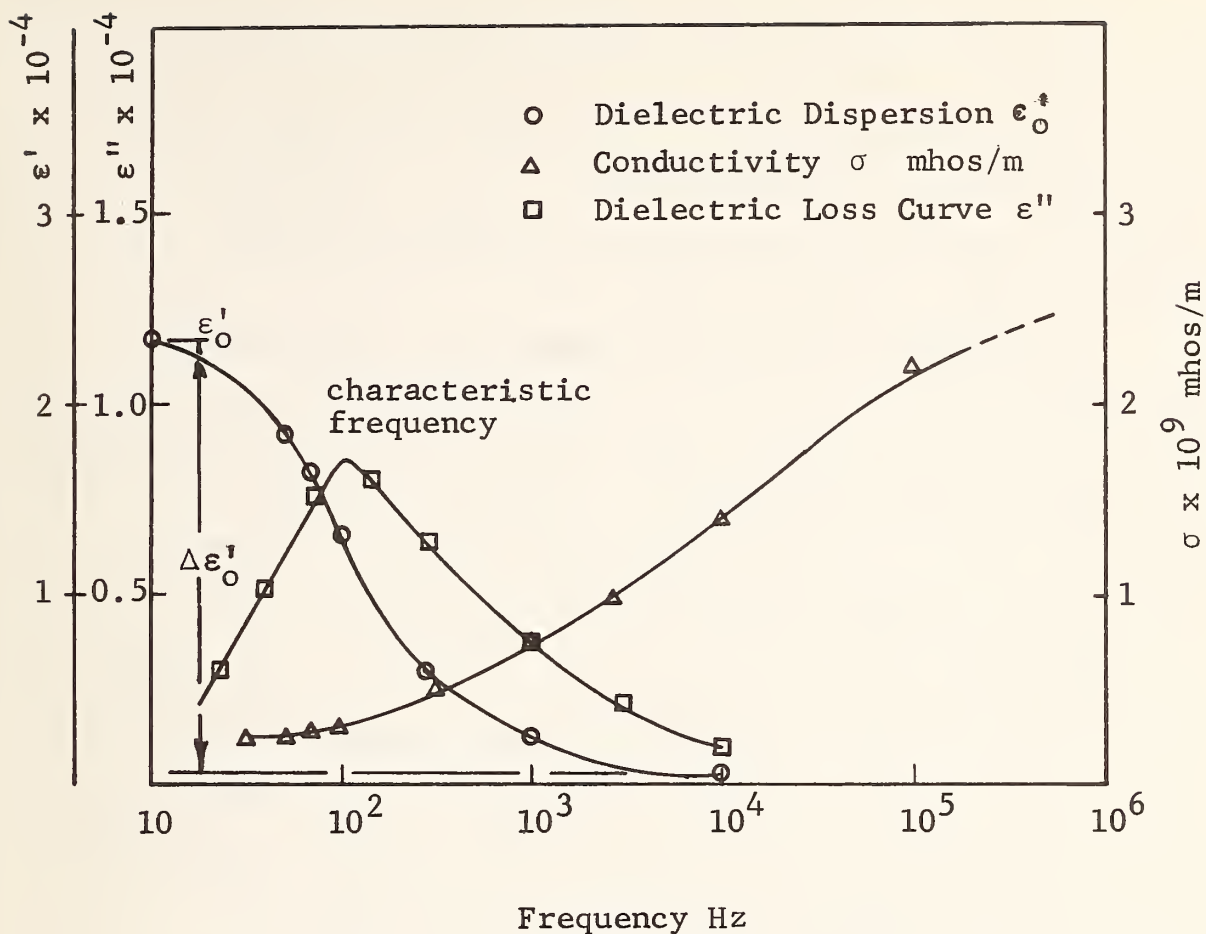


Figure 2.53. Conductivity & Dielectric Dispersion Characteristics of Saturated Kaolinite Hydrite R (Mitchell and Arulanandan, 1968)

#### ELECTRICAL PROPERTIES OF SAN FRANCISCO BAY MUD

	$\Delta\epsilon'$ ( $\times 10^{-4}$ )	$f_o$ (Hz)	$\alpha$ (deg)	$\frac{\sigma_{DC}}{\sigma_{AC}}$	$\sigma_{DC}$ mhos/m
Bay Mud parallel	100	300	18	0.96	19.2
Bay Mud remolded	116	200	14	0.97	10.6
Bay Mud perpendicular	82	500	5	0.93	9.5

(Moisture Content = 90%)

(Pore Fluid Electrolyte Concentration = 0.3 N)

(Mitchell and Arulanandan, 1968)

The DC conductivity,  $\sigma_{DC}$ , measures the amount of free charge and the ease with which it passes through the soil. Thus  $\sigma_{DC}$  may reflect void ratio, flow path tortuosity and pore fluid conductivity. An increase in conductivity with frequency is represented by  $\sigma_{AC} - \sigma_{DC}$ . The major portion of  $\sigma_{AC}$  is ascribed to electrokinetic coupling between current and fluid flow.

If several polarization mechanisms are operative, polarization will occur over a larger frequency range; if a single uniform mechanism exists, polarization will be confined to a narrow band of frequencies. This distribution of relaxation times is measured by the parameter  $\alpha$ , generated by a Cole-Cole plot of  $\epsilon''$  versus  $\epsilon'$ . The wider is the distribution of relaxation times, the larger will be  $\alpha$ .

The parameters  $\alpha$  and  $\sigma_{DC}$  showed consistent trends, whereas remolding may have disrupted cation and absorbed water layers, significantly affecting  $\Delta\epsilon'$  and  $f_o$ . The apparatus used to make resistance and capacitance measurements required manual null-balancing of a physical R-C circuit, and it is likely that development of the method will result in specialized electronics that are much easier to employ.

The difficulty of employing null-balance methods was cited by Ramiah and Purushothamaraj (1971) as the reason for measuring only  $\sigma_{DC}$  in their application of the method to direct shear testing. Direct-current dispersion characteristics were employed as a fabric parameter in a series of direct shear-reversal tests directed at the evaluation of initial structure on residual strength. In this study the DC conductivity was measured in a direct shear box along a path crossing the shear plane at an angle of nearly zero. The conductivity normal to the shear plane was not measured. These data indicate that conductivity decreases with increasing alignment of soil particles to the current flow, counter to the results in Bay Mud. A rough correlation between stress ratio and conductivity ratio

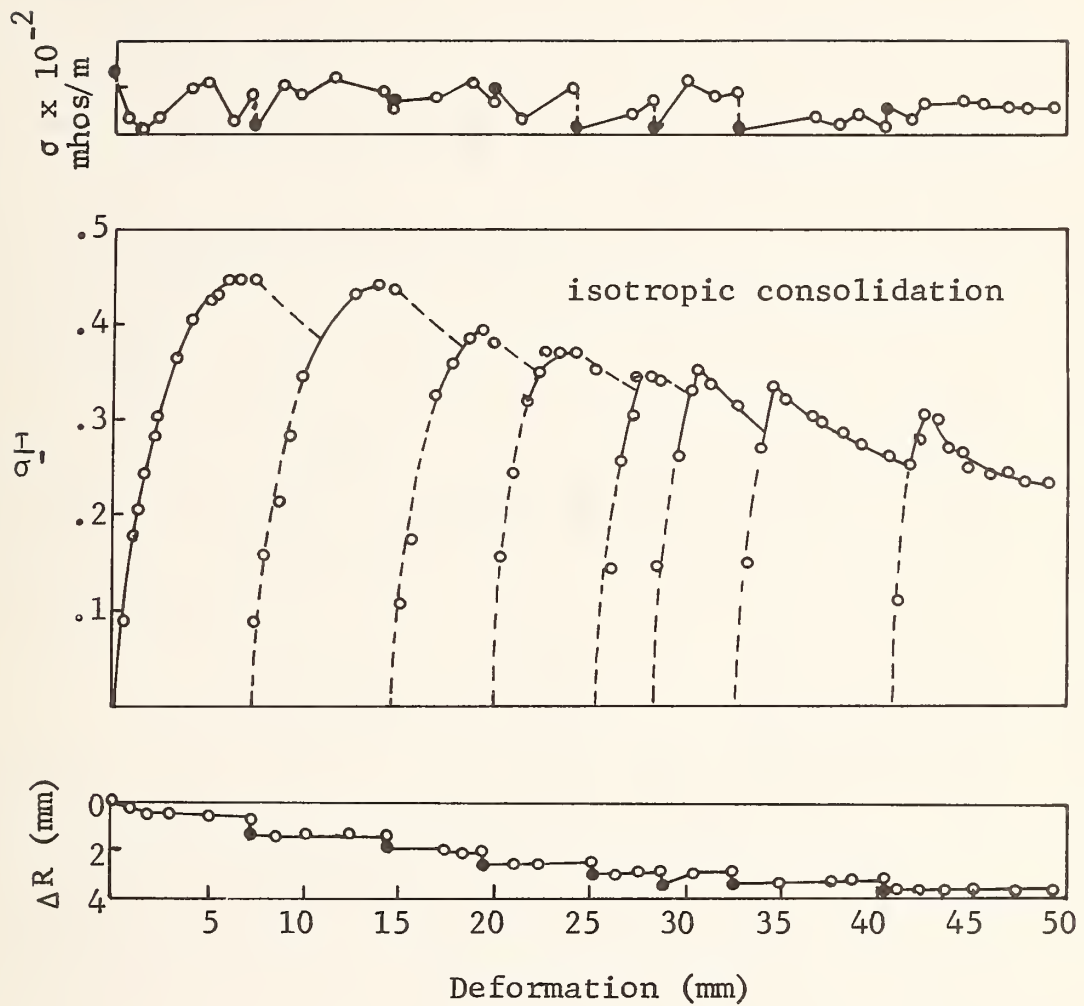


Figure 2-54. Typical Stress-Deformation Curve  
(Ramiah & Purushothamaraj 1971)



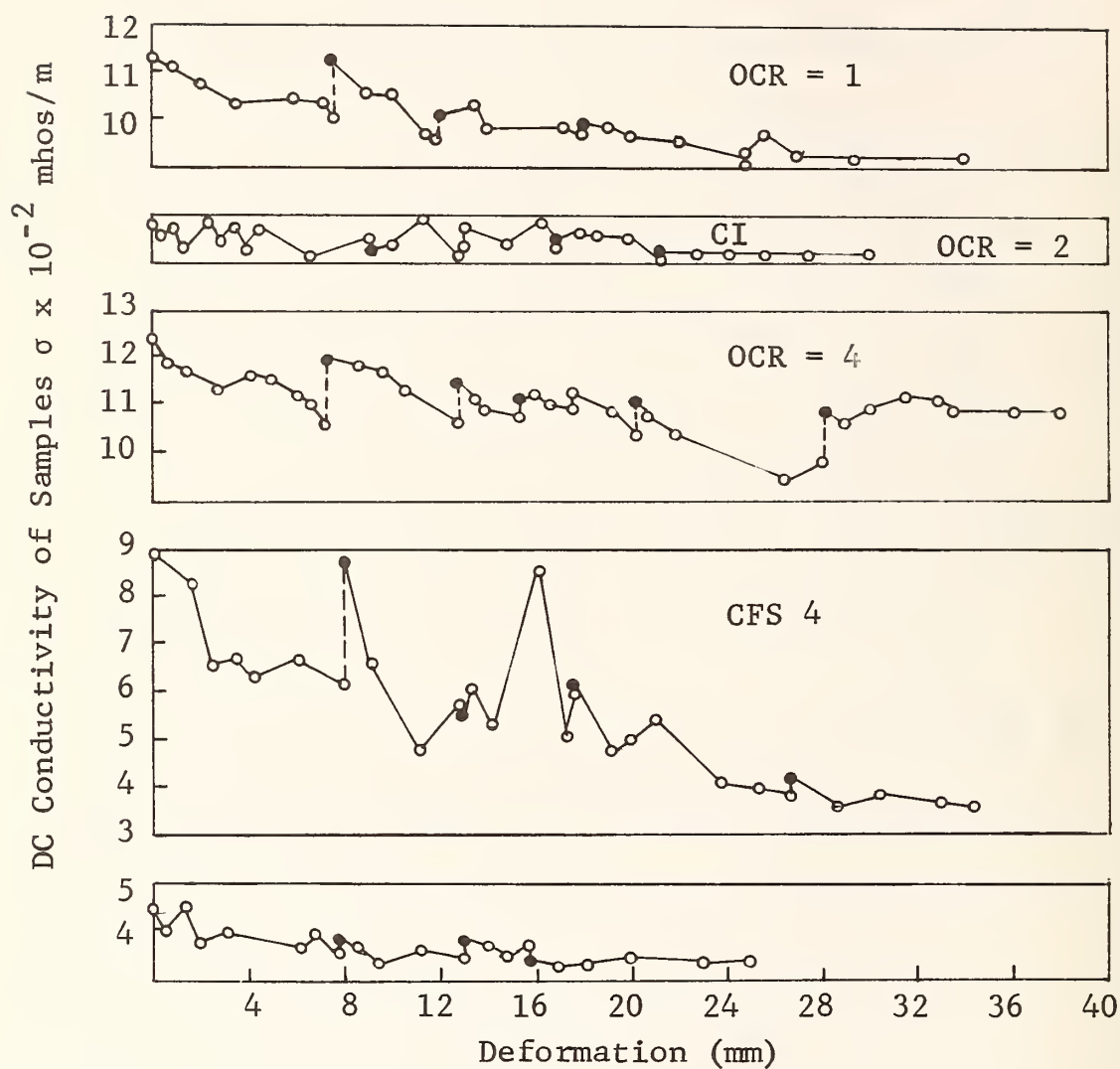


Figure 2-55. DC Conductivity vs Deformation  
(Ramiah & Purushothamara, 1971)



was also found. Portions of these data are shown in Figures 2-54 and 2-55. The decrease in conductivity is attributed to electrostatic shielding resulting from the parallel alignment of clay particles in the shear zone, so that charge carriers housed outside that zone require greater transit times. Many factors influence the response of a clay-water-electrolyte system, e.g., the soil fabric, amount and type of electrolyte, moisture content, the nature of the clay surface and temperature. The change in conductivity as soil fabric changes depend upon the relative importance of mechanisms that increase or decrease charge carrier flow in the particular case.

Electromagnetic techniques are not limited to DC or low frequency methods. The literature survey included the entire electromagnetic spectrum from DC to electron frequencies. Later discussion will include the use of higher frequencies.

#### 2.5.4 ELECTRON MICROSCOPY

The electron microscope must be considered to be a tool for use in fabric analysis. Many excellent micrographs of kaolin are available in the literature, but montmorillonite and illite micrographs are rare. The scanning electron microscope produces excellent representations of kaolinite. These may be viewed directly, or grain orientation may be quantified by measuring grain angles or spacing. This is frequently done manually, but computer scanning techniques could be applied. Various optical conditioning methods are also available, e.g., the optical diffraction and convolution square techniques of Tovey (1971).

We will consider microscopy only as a fabric analysis tool. Geotechnical microscopy may be classed as dealing with structure or as corroborating the results of other techniques, as the use of x-ray diffraction in quantitative analysis. Discussions of microstructure given by Morgenstern and

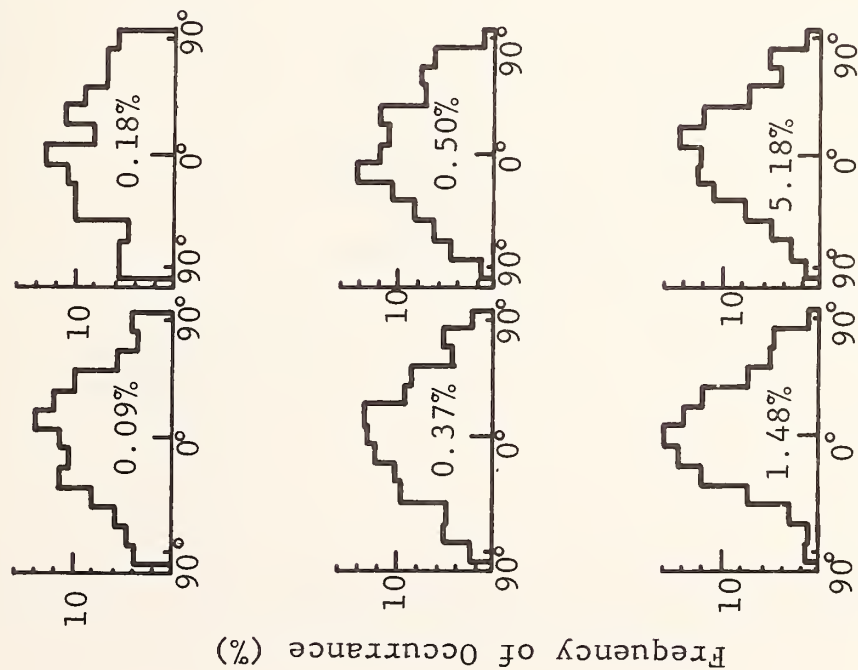
Tchalenko (1967); Lafeber and Kurbanovic (1965); Barden, Sides and Karunaratne (1970), Barden (1962); and Kirkpatrick and Rennie (1972) deal more with the factors that result in anisotropy of soil fabric. Microscopy is used as a tool to corroborate x-ray diffraction studies by Comer (1960, 1962), and Ormsby and Shartsis (1960).

Full utilization of the scanning electron microscope requires that some quantitative parameter representing the soil fabric be commonly employed. The literature indicates that this is not presently the case. It is clear that changes in soil fabric occur under stress, but different parameters are measured by various investigators.

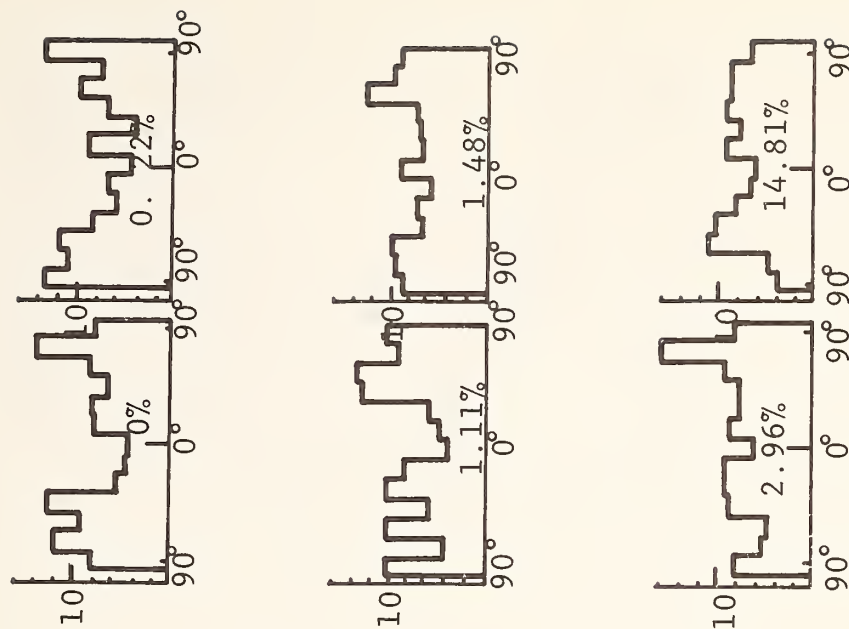
Investigating the deformation fabric of sand, Oda (1972) measured grain orientation distribution and the ratio of grain-grain contact areas projected on the vertical and horizontal planes. The angle  $\theta$  between the long axis of the grains for two degrees of initial orientation are shown in Figure 2-56. In Figure 2-56(a), the sand is initially oriented horizontally, and the preference for this direction becomes stronger with increasing stress ratio. This preference decreases slightly at large axial strains. In Figure 2-56(b), the initially vertically oriented sand also tends toward a horizontal orientation with increasing axial strain, with the result that the initially oriented structure is destroyed.

The projected contact area ratio  $S_z/S_x$ , in (Figure 2-57(a)) was found to change with stress ratio as shown in Figure 2-57(b). An important fact is that the parameter changes continuously with stress ratio and does not display changes in behavior associated with peak stress. Murayama and Matsouka (1973) and Matsouka (1973) argue that the important parameter is not the projected area ratio  $S_z/S_x$ , but the distribution of the contact normal directions. In fact, Oda assumes a mean contact area and his ratio  $S_z/S_x$  appears to be a function of the contact directions only. Murayama and Matsouka conducted direct shear tests on rod

axial strains as noted

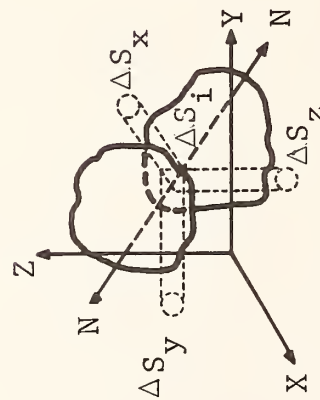


a) Specimens Compacted by Tapping



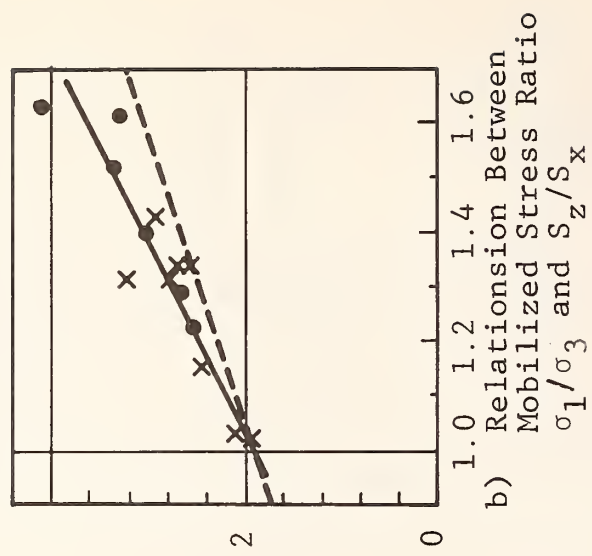
b) Specimens Compacted by Plunging

Figure 2-56 Effect of Triaxial Tests on Orientation Distribution of Long Sand Grain Axis (Oda 1972)



N = vector normal to contact area

a) Determination of Fabric Index  $S_z/S_x$  of Granular Sand



o Compacted by tapping  
x Compacted by plunging

Figure 2-57 Stress Ratio vs Orientation Parameter  $S_z/S_x$  (Oda 1972)

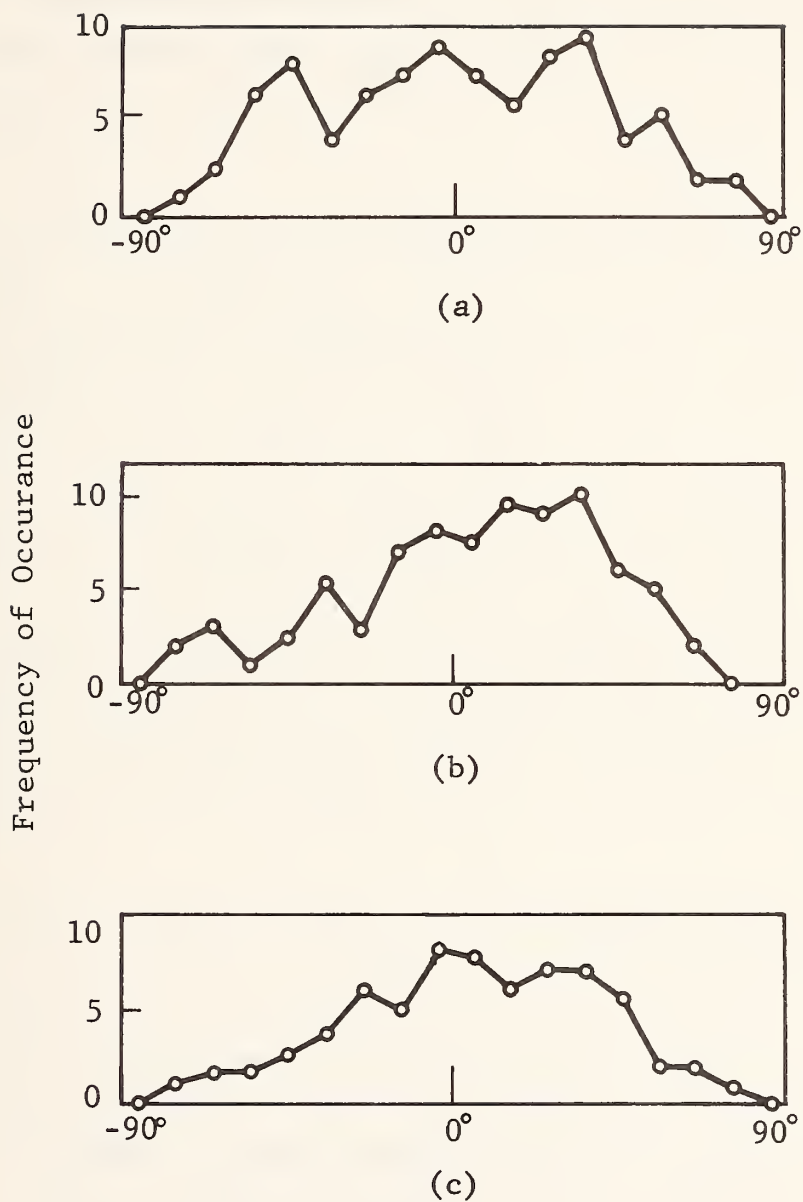


Figure 2-58. Frequency Distribution of  $\theta$  Alunimun Rod Mass  
 (a) Before Shear (b) At the Peak Strength  
 (c) At the Residual Strength



masses and found a nonsymmetric distribution of contact normal directions as shown in Figure 2-58. The different behavior reported in these two papers may be a result of the different forms of symmetry associated with triaxial tests as opposed to direct shear tests. It is clear, however, that fabric changes associated with changes in stress may be observed microscopically, but that additional study will be necessary before the scanning electron microscope can be confidently used to measure stress-dependent parameters.

#### 2.5.5 INFRARED

The use of infrared on soils has been limited primarily to quantitative analysis to determine the amount of various minerals present under various conditions, e.g., MacKenzie (1969). It would appear, however, that IR has some application in fabric analysis. The use of infrared techniques is attractive because wavelengths in this portion of the spectrum are of the same length as clay size particles. Thus, optical techniques employing IR radiation may be quite effective in soils. A wide variety of laser sources is now available so that illumination with wavelengths between 0.3 to 10.6 microns may be employed. Two major alternatives exist: direct detection techniques, such as probing an area with beam of polarized light, and pattern analysis based on IR images.

Detection techniques may be based either on the principle of diffraction or polarization. If the soil matrix is considered to be a diffraction grating, the diffraction depends on the ratio of grain spacing to wavelength. In a highly oriented soil, the grain spacing is much smaller when the plate-like grains are viewed edge-on. Thus, qualitative evaluation of the degree of grain orientation and its direction should be immediately available from the intensity and spacing of the diffraction pattern. A similar direct approach may use a reflection polariscope or ellipsometer to measure the net refractive index on specimen surfaces in various directions.



It is likely that extraction of quantitative data with direct detection techniques will be difficult and that optical or electronic image processing may be necessary. This is the second major alternative of image analysis. Much previous work in the application of fabric analysis has suffered from the lack of rapid and exact techniques for measuring the soil fabric. When actual measurements are made on soil fabric photographs, they are frequently made manually at what must be a relatively high cost for the amount of information returned. If optical or computer image conditioning techniques are to be employed, the advantages of IR techniques relative to visible light are decreased. The additional difficulties associated with IR technology would outweigh any advantages of increased information (i.e., over that obtained by optical diffraction using visible light).

A potential use of IR is in the evaluation of the extent of diagenetic bonding in particular soil specimens. The use of transmission infrared in the determination of the clay content of soils would involve the use of the Si-O absorption band in the 9 to 11 $\mu$  region. This band is of strong intensity and could possibly serve in both qualitative and quantitative roles. However, this portion of the spectrum is a general group frequency range where many oxygenated species other than silicates also absorb and consequently would interfere. The presence of such anions as borates, phosphates, sulfites, sulfates and chlorates would limit the use of this band. Accordingly, the use of transmission infrared spectroscopy would be subject to the presence or absence of a large number of inorganic constituents which may be present in a particular soil sample.

#### 2.5.6 GAMMA RADIATION

Gamma rays are commonly used in the determination of density and moisture content in soils and rock. A number of available nuclear gage configurations use transmission

and/or backscatter techniques for cased or uncased boreholes, ground level or special applications. These include permeability measurements using tagged fluid, determination of the average atomic number of the soil media, and its elemental composition. No techniques by which the soil stresses can be easily determined are available, however.

#### 2.5.7 X-RAYS

X-rays are used to monitor the motion of x-opaque markers placed in a soil sample under test and to determine the orientation of crystal planes by diffraction. The use of x-rays to monitor internal deflections does not appear to be of great usefulness in an in-situ stress measurement system. This is, however, a useful technique in laboratory studies of anisotropic soil properties and is mentioned by Wroth and Hughes (1972,1973), Gerrard and Morgan (1972), Arthur and Shamash (1970), Arthur and Menzies (1972), and others.

X-ray diffraction may be employed to evaluate the mineralogy of soil specimens and its use is especially common in the ceramics literature 'e.g., Friedman, 1973; Bishop, 1958; Kirkpatrick and Rennie, 1972; Comer, 1960; Clark, 1970; Dudley, 1970; Meade, 1964; Ormsby, et al., 1962; and Ormsby and Shartsis, 1960 .

The most useful form of x-ray diffraction is the evaluation of preferred orientation ratios. There are several forms of preferred orientation ratio (POR), each a quantitative measurement of clay particle orientation which may be a most useful fabric analysis parameter. Because x-ray diffraction is a fabric analysis tool, its use in the context depends on the development of fabric analysis. The characteristics of x-ray diffraction include the ability to make quantitative POR determinations. Sample preparation is somewhat simpler than is required for optical methods because the x-rays respond to a layer of soil up to 50 $\mu$ m. Sophisticated apparatus and techniques are required.

Meade (1961) suggests that the ratio of the diffraction pattern at the 001 and 020 peaks be compared on vertical and horizontal sections to obtain a quantitative orientation ratio. That is, the orientation ratio is given by

$$\text{OR} = \frac{\frac{001_z}{020_z}}{\frac{001_x + 001_y}{020_x + 020_y}}$$

in which  $001_z$  is the 001 diffraction peak on a section cut normal to the z-axis and

$020_z$  is the 020 diffraction peak on the same section.

The procedure is indicated in Figure 2-59.

Martin (1966) employed a diffractometer equipped with a pole figure device in his study of kaolinite. He defined a peak ratio, PR, as the ratio of the 002 and 020 reflections as shown in Figure 2-60. Clark (1969) modified Martin's PR ratio by taking the ratio of PR on orthogonal faces, obtaining a preferred orientation ratio POR. This was correlated to strain as indicated for various test conditions (Figure 2-61).

Clearly x-ray diffraction can be used to quantitatively describe the degree of anisotropy in clay minerals. The direction of the principal stresses may be identified within several degrees, but additional effort will be required before quantitative statements regarding the magnitude of the principal stresses can be made.

#### 2.5.8 ELECTRON BEAM TECHNIQUES

Electron beam techniques are summarized in a review article by Tufts (1969). All of these techniques are influenced by the short range of the electrons (10 to 15 mg/cm<sup>2</sup> for electrons with 100 keV energy). As a result,

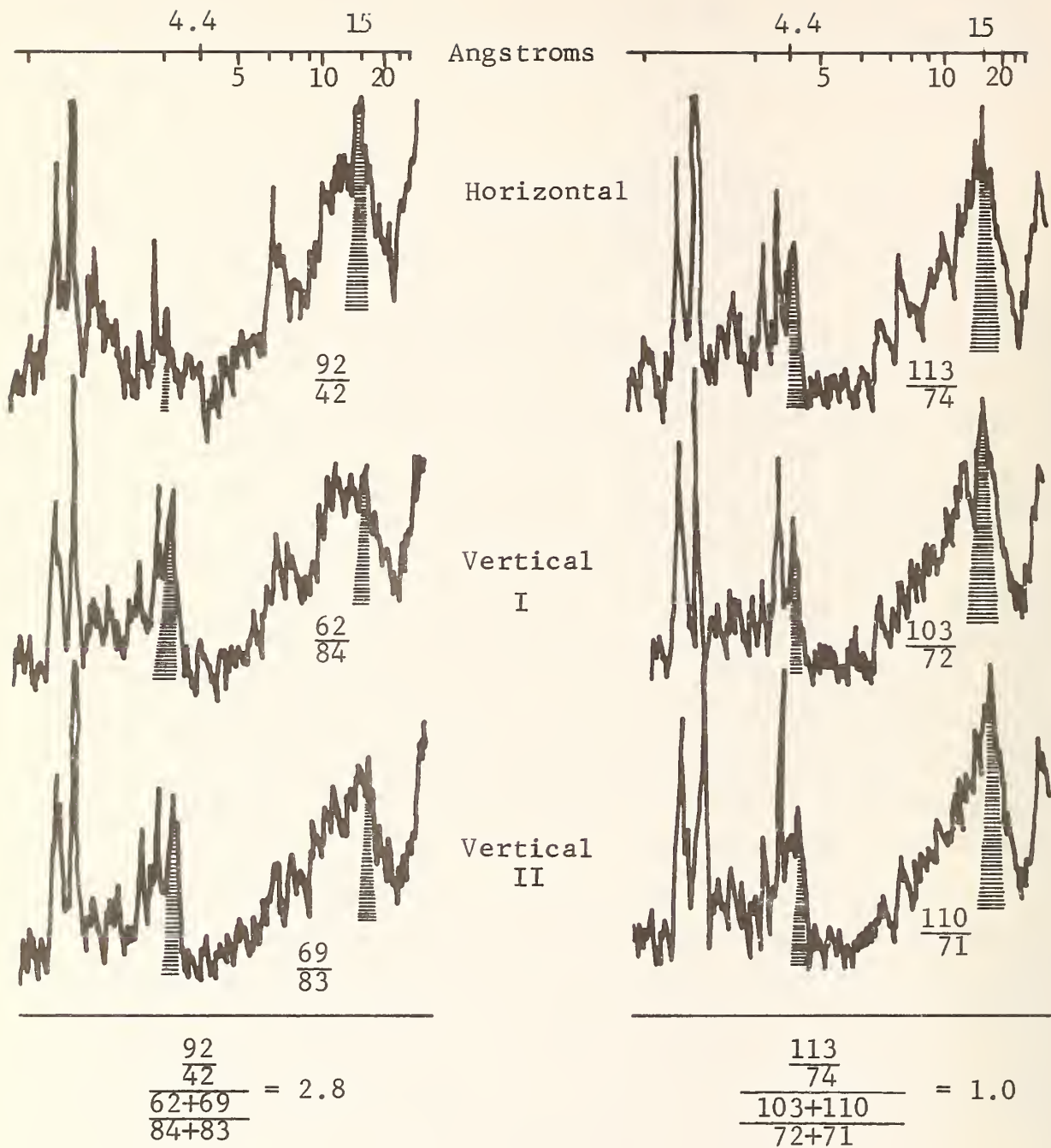


Figure 2-59. Measurement of Horizontal Preferred Orientation By Comparison of X-ray Diffraction Peak Heights (Meade, 1961)



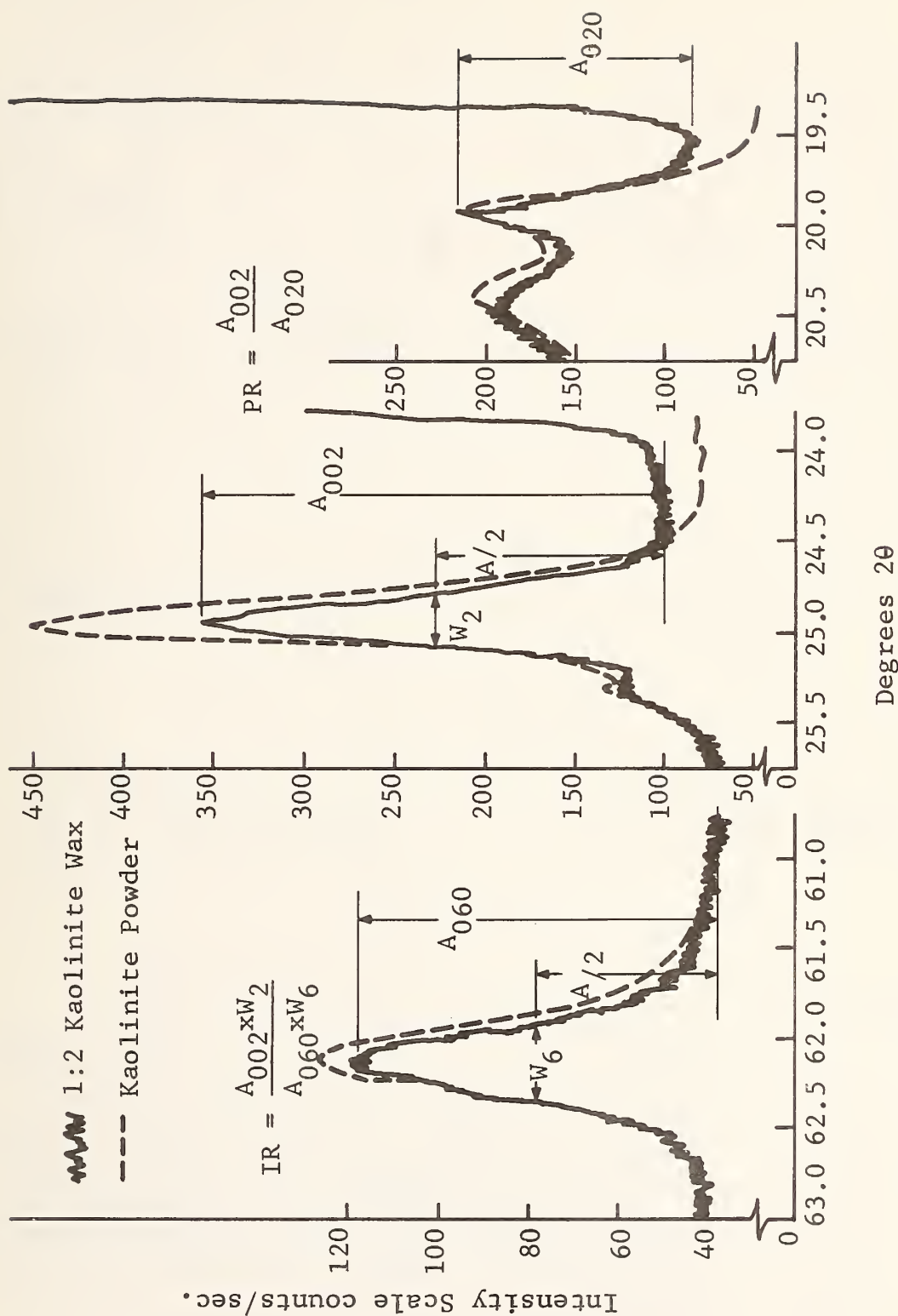


Figure 2-60. Diffraction Trace for the  $2\theta$  Ranges Used in Fabric Measurements (Martin, 1966)

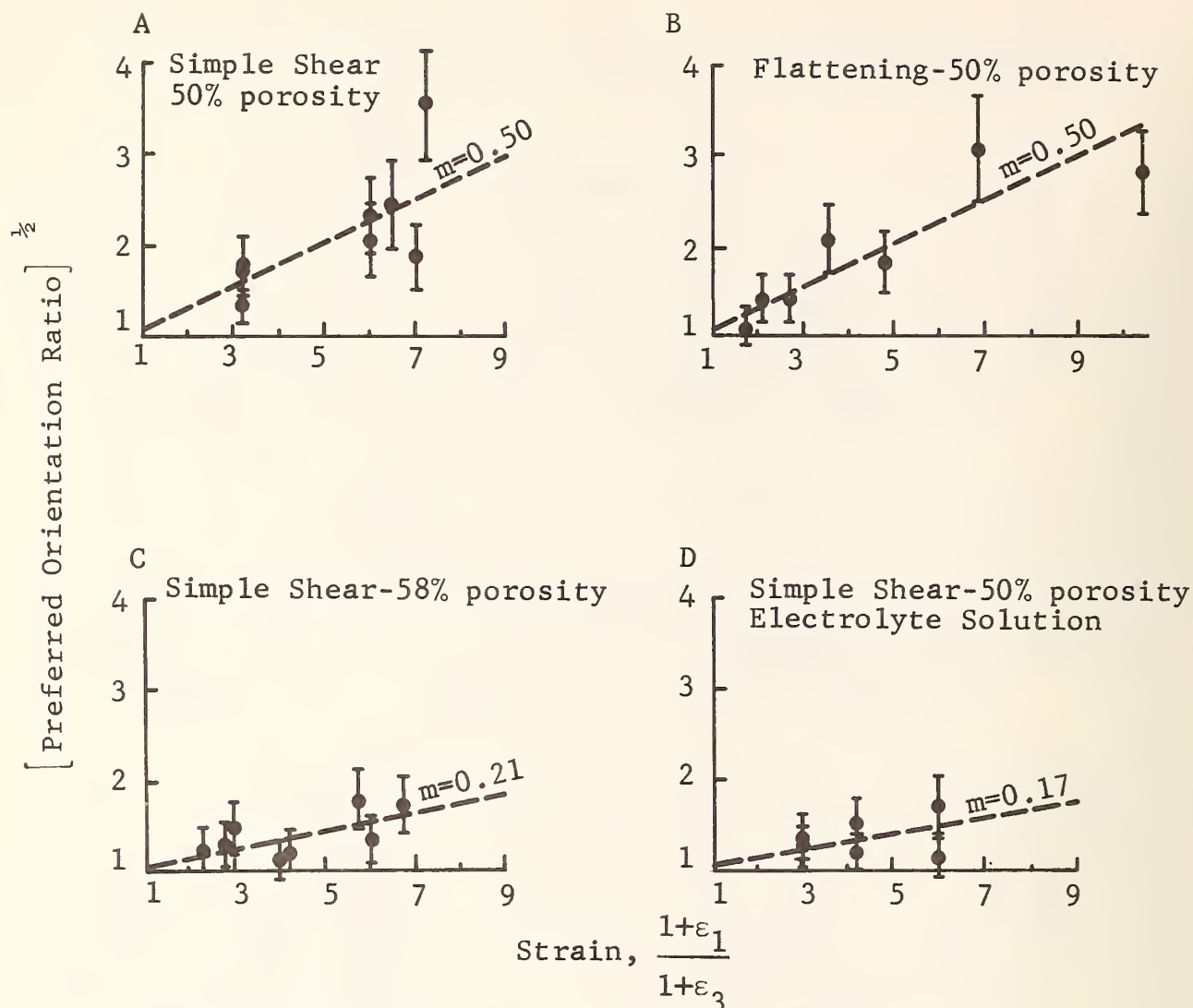


Figure 2-61. Preferred Orientations from Distortion Experiments, Plotted as a Function of Total Strain  $1 + \epsilon_1 / 1 + \epsilon_3$ .  $m$  = approximate slope of straight line fitted by hand to data points. A. Simple shear experiments, saturated samples, 50 percent porosity. B. Flattening experiments, saturated, 50 percent porosity. C. Simple shear experiments, saturated, 58 percent porosity. D. Simple shear experiments, saturated with 1 m NaCl solution, 50 percent porosity. (Clark, 1969)



the beam is either interacting with a surface layer or passing through a very thin (1.500  $\mu\text{m}$ ) sample. Because thin-wafer samples of this size are not practical for soil core samples, surface techniques are the only reasonable possibility. Surface preparation is, of course, critical if bulk characteristics are to be represented.

The closest analogous situation in conventional testing of metals is as follows: a test bar is fractured, producing a very rough irregular surface. What is the preferred orientation and crystal size in the exposed surface? Electron and x-ray diffraction can provide such information. The primary difference between electron and x-ray diffraction in such an application is the depth of the surface layer contributing to the response. X-ray penetration is generally greater than electron penetration. For metal fracture it is important to restrict the measurement to the top most surface layer, i.e., use electrons, in order to correlate the fracture with the local structure. For a soil core sample, this would not be necessary since one is interested in bulk properties. The ability of electron beam techniques to emphasize surface characteristics is, in fact, a disadvantage and, as a result, primary emphasis should be placed on x-ray diffraction procedures (such as texture analysis, pole figure analysis) which are generally easier to implement.

#### 2.5.9 SUMMARY OF ANISOTROPIC PROPERTIES MEASUREMENTS

Laboratory tools that can be used to measure the orientation parameters of soil fabric include x-ray diffraction and scanning electron microscopy. Careful sample preparation is required, especially for the SEM. Field techniques include permeability and electrical conductivity. Some capability is available in IR, gamma-rays and the electron beam but in general these techniques are more difficult to apply and return less information. Quantitative measurements of soil fabric may be made by these techniques as a connecting link between measurements of quantities

(e.g., pore size distribution or preferred orientation ratio), and the state of stress that induced the anisotropy is established.

### 3. FABRIC ANALYSIS

#### 3.1 INTRODUCTION

Fabric analysis is the analysis, usually but not necessarily quantitative, of the spatial data for the interior of the material (e.g., the soil sample) under consideration. Results depend on the methodology used and the materials to which the fabric analysis is applied. Fabric analysis has so far been largely a strain analysis tool in rock mechanics. Although activity in stress analysis has increased in recent years, fabric analysis in soil mechanics has not advanced as far as in rock mechanics.

The treatment of fabric analysis in this section is more applied than theoretical. We present an overview of relevant aspects of fabric analysis, and proceed to a development of the problems and possibilities in the use of fabric analysis to study the state of stress in soils. These include:

- o Expectations of fabric analysis
- o Statistical methods
- o Anticipated behavior of soil types
- o Orientation of measuring devices with respect to soil fabric
- o Experimental work
- o Plans for mapping and analyzing soil fabric
- o Field sampling

#### 3.2 EXPECTATIONS OF FABRIC ANALYSIS

Fabric analysis applied to undeformed materials provides a datum to which analyses of deformed materials can be compared. From such analyses of undeformed materials one can obtain primary or initial fabrics (most commonly exemplified by depositional and diagenetic fabrics) which provide insights into the mode of formation of the materials. Primary fabrics may also permit prediction of the orientation

of mechanical anisotropy under subsequent loading and, under some circumstances the relative degree of mechanical anisotropy. Figures 3-1 and 3-2 indicate relations between fabric and deformation that were developed in rock mechanics but presumably are applicable to soil mechanics.

Kinematic fabric analysis is essentially a geometric or strain analysis approach to deformation, based on the premise that the symmetry of the fabric reflects the symmetry of movement responsible for the fabric. This does not lead directly to the determination of the state of stress in the material, although it may lead to useful inferences regarding the orientation of one or more principal stress axes. In rocks, kinematic analysis has been practical only where deformation has been intense; it is likely that at least some soils develop useful deformation fabrics with considerably less intense deformation. Figure 3-3 illustrates four basic types of fabric symmetry determined from geometric considerations. Kinematic analysis has also been used to restore fabrics to an earlier configuration by unrolling and leveling operations and may be useful in delineating an inferred primary fabric and in determining if more than one stage of deformation has taken place.

Dynamic fabric analysis is essentially a stress analysis approach, via the study of fabrics, based on the premise that specimens deformed in the laboratory can be used to determine the orientation and relative magnitudes of the principal stresses at the time of deformation in their presumably comparable, natural counterparts. Absolute magnitudes of the principal stresses in nature cannot be estimated with confidence from the types of laboratory experiments carried out so far. Relative magnitudes or ranges of magnitudes may sometimes be estimated using physical-chemical principles. Intense deformation is not a necessary condition for application of dynamic fabric analysis in rocks, and this might also apply to some soils. The resolution of

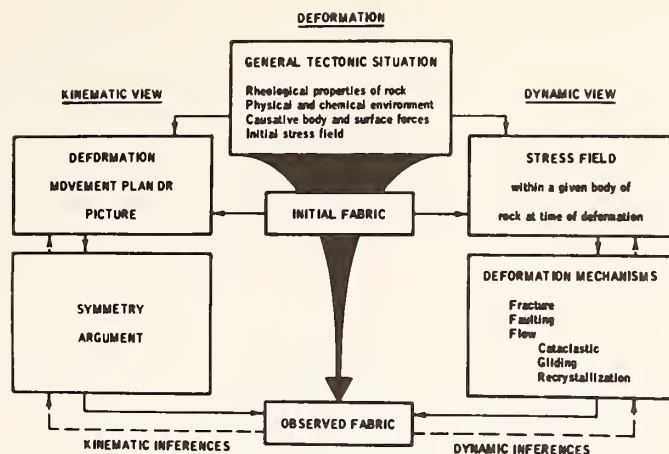


Figure 3-1. Kinematic and dynamic petrofabrics applied to geologic deformation. Both descriptive and interpretive phases of fabric analysis are indicated (Friedman, 1964).

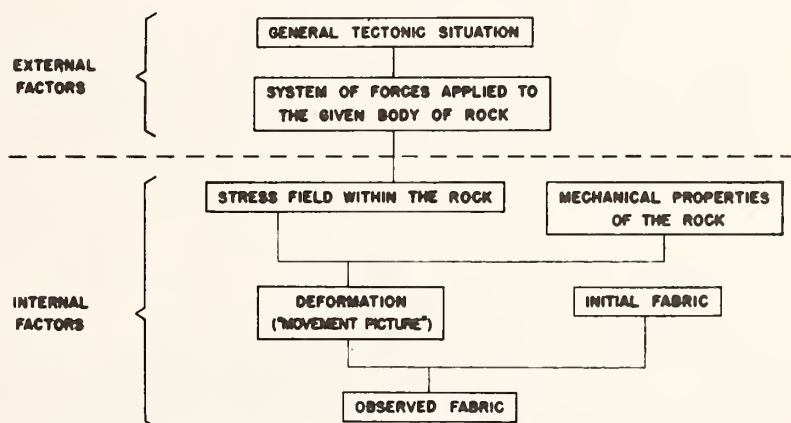


Figure 3-2. External and internal factors concerned in deformation of a body. Relation of initial and observed fabric to deformation is indicated (Pater'son and Weiss, 1961).



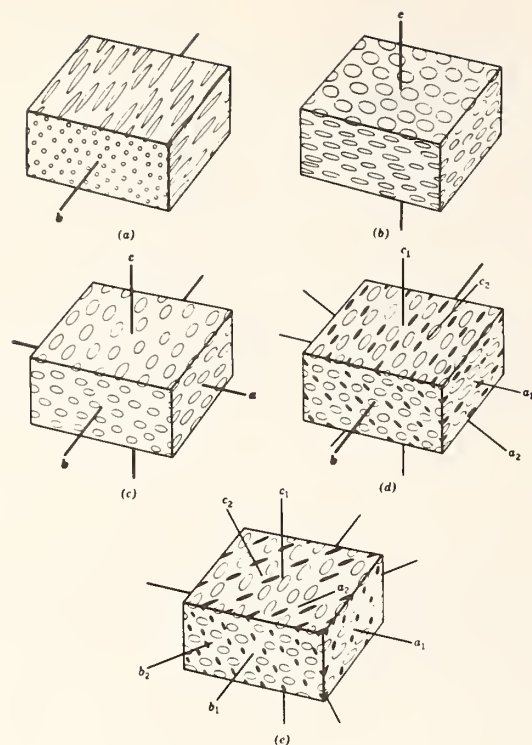


Figure 3-3. Types of fabric symmetry (Turner and Weiss, 1963).

(a) and (b) axial fabrics (symmetry of an ellipsoid of rotation)

(c) orthorhombic fabric (symmetry of the triaxial ellipsoid)

(d) monoclinic fabric (single plane of symmetry)

(e) triclinic fabric (no planes of symmetry)

(Spherical fabric, viz., no preferred orientation, not illustrated. The above fabric terms are not equivalent to crystallographic terminology.)

two or more stress systems by dynamic fabric analysis is at best formidable and usually not feasible. The deformation mechanisms of importance here are fracture, faulting and flow (cataclastic, gliding, recrystallization).

Under very favorable circumstances, it should be feasible to estimate orientations of principal stress axes from soil fabric analysis, to within say 10 degrees. Under favorable circumstances, estimates to within 30 degrees might reasonably be expected. With additional study and refinement, the 30 degree figure might be reduced significantly. The biggest advances in terms of orientation analysis should come in terms of getting useful results in situations that are currently not tractable to such analysis, e.g., 1) multiple deformations in which the principal axes of stress have changed orientation by 45 degrees or more from one episode of deformation to the next; 2) where principal axes of stress have acted obliquely with respect to an initial anisotropy, the orientation of which cannot be recovered unambiguously; 3) where heterogeneous, anisotropic material has been acted on nonuniformly over the region of study. At this time, there does not appear to be justification for estimating stress magnitudes from fabric analysis of soils to any better than one order of magnitude. With additional work, it should be feasible to improve this to a half or quarter order of magnitude for relatively uncomplicated situations.

To work out the stress and strain history of soil from fabric analysis requires that both the directional and magnitude estimates described be feasible and that relative ages of multiple episodes of deformation be established. That such histories can be derived with confidence in some cases is very likely; it is just as likely that it will not be feasible to derive such histories in other cases, at least in the foreseeable future. Studies

following the initial inquiries presented in this report should be concerned with arriving at precise statements of the conditions and combinations of conditions that will permit the derivation of reliable stress and strain histories, and those conditions and combinations of conditions that necessarily preclude the derivation of such histories. Follow-up studies should also estimate the proportions of tractable, doubtful, and intractable situations, in addition to advancing the state-of-the-art.

Relative scales of heterogeneities in the earth materials, of fabric elements being studied and of the sample size are of considerable importance in arriving at valid interpretations of fabric (Figures 3-4 and 3-5). Absolute scales are of considerably less significance in fabric analysis, per se, although they may be crucial in a practical design problem that requires fabric analysis.

Statistical analysis is used in both kinematic and dynamic approaches. The kind of outcome to be expected depends in part on the statistical methods used. Descriptive statistics yield descriptive results; probability statements result from procedures such as hypothesis-testing. Probability statements may be very important in interpreting poorly defined fabrics, fabrics resulting from the superposition of one fabric on another, and suites of apparently genetically related fabrics. The kind of interpretation that can be made will also vary depending on whether one is using parametric or nonparametric methods, Gaussian or von Mises probability, continuous or discrete probability density functions, small-sample or large-sample theory. Although

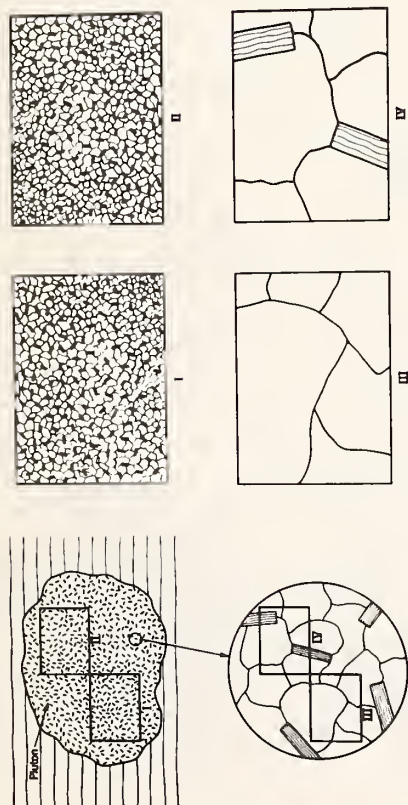


Figure 3-4. Relation between homogeneity and scale (Turner and Weiss, 1963).

Samples I and II are statistically equivalent; at this scale the material is statistically homogeneous.

Samples III and IV, which are smaller than I and II, are not statistically equivalent; at this scale the material is statistically heterogeneous.

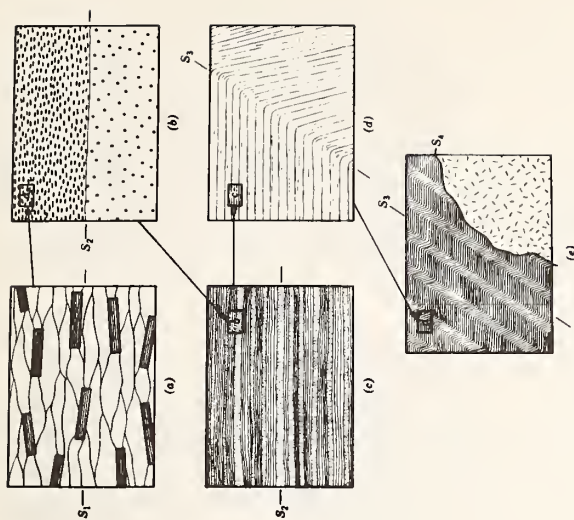


Figure 3-5. Discontinuities (S) in the same body at five different scales (Turner and Weiss, 1963).



the statistical armamentarium is reassuringly formidable, simple descriptive statements that can be rendered quantitatively may be quite adequate for determining what one needs to know about the stress field.

The type of earth materials being studied can have considerable impact upon the type of fabric analysis performed and its relative usefulness. Figures 3-6 and 3-7 illustrate some of the variety of planar (surface) and linear fabrics that may be encountered.

A highly oriented depositional fabric may be quite insensitive to a stress field oriented with maximum compression normal to depositional surfaces; a loosely compacted sand consisting of well-rounded, spheroidal particles may yield very few clues, through fabric analysis, of its deformation history; homogeneous plasmic material may reveal preferred orientation patterns only through x-ray methods, with little or no noncrystallographic fabric data in support. Further, a material in which two or more subfabrics do not agree in symmetry (heterotactic fabric) may present insurmountable interpretative problems.

Either kinematic or dynamic fabric analysis may yield results consistent with an independently evaluated in-situ stress field; then again there might be no clear relationship. Should such consistency be demonstrable in a particular situation, then additional fabric studies might be useful in interpolating or perhaps cautiously extrapolating from sites of verified results. In-situ studies, including such techniques as x-ray, acoustic and photoelastic coatings, might be adapted from studies of rocks in the laboratory and in the field. The study of crack generation and propagation in stress-relieved soils in-situ might yield



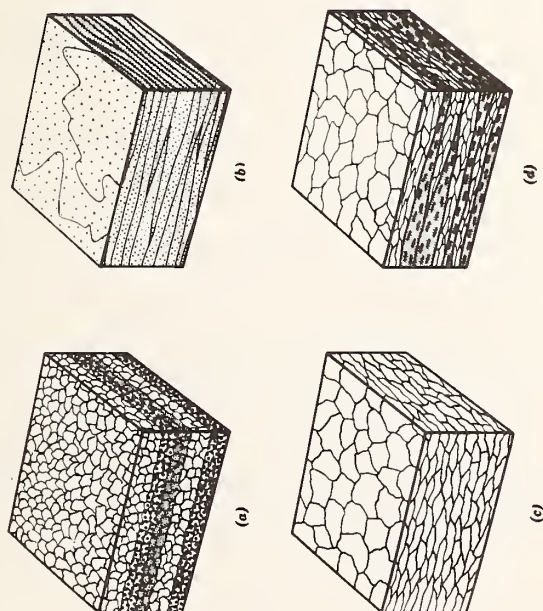


Figure 3-6. Physical features defining foliations (Turner and Weiss, 1963).

- a) Lithologic layering
- b) Discrete fractures or other surface discontinuities
- c) Preferred orientation of grain boundaries
- d) Combination of a), b), and c).

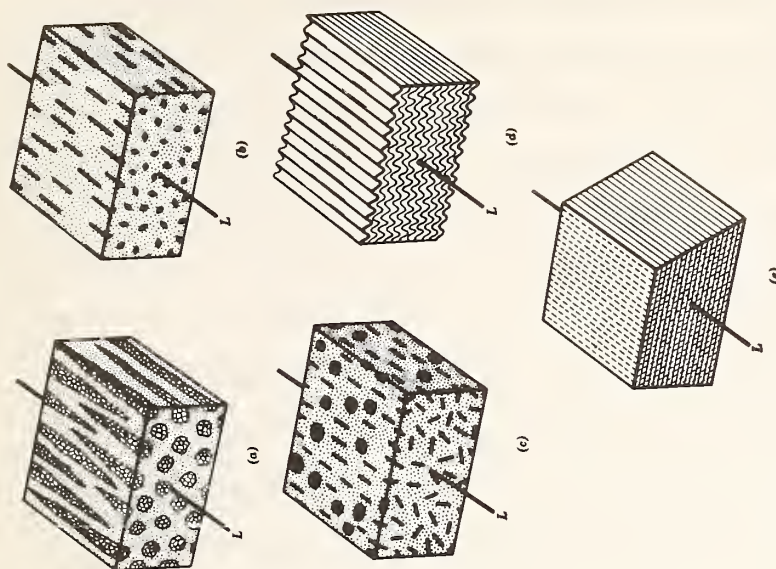


Figure 3-7. Physical features defining lineations L (Turner and Weiss, 1963).

- a) Preferred orientation of elongated domains of equidimensional grains
- b) Preferred orientation of prismatic grains
- c) Linear preferred orientation of platy grains
- d) Small crenulations of surfaces of discontinuity
- e) Intersections of surfaces.

very useful results if suitable precautions are taken to deal with anomalies introduced by drying and excavation.

Some of the uncertainties expressed or implied in the foregoing statements can very likely be dispelled through experimentation with soils. That is, it should be feasible to determine whether or not some of the capabilities described as possibilities can in fact be achieved in a practical way.

### 3.3 STATISTICAL METHODS

As in any investigation, the appropriateness and efficiency of statistical analysis depend in part on identification of the variables to be treated and the understanding of their properties. The particular tools chosen will depend on whether a variable is, for example, continuous or discrete, linear or angular, infinite or finite. The design of the data-collection program and the selection of analytical methods cannot be independent of these variables and their statistical properties. Both kinematic and dynamic fabric analyses are served by such statistical analyses. The variables of interest in relating soil fabrics to strain and stress history and state of stress can be divided into categories such as direction, spacing, and pattern.

Direction applies to entities such as orientation of long axes of peds, grains and voids, of twin lamellae and fractures, and of laminations and other planar or linear expressions of composites. Such variables are angular or cyclic. Degree of preferred orientation (concentration of direction) and direction of preferred orientation (mean direction) may be determined. Tests to ascertain whether there is a preferred orientation may be applied.

Spacing applies to entities such as size of grains, peds, clods, glaebules, fragments, and voids, and width of fracture openings and tabular fabric elements. Spatial frequency (density of fractures and other discontinuities), size distributions, and elongation ratios (long:short dimension) may be determined from spacing data. Tests to ascertain if there is a concentration of spacings (or their inverse, spatial frequencies) may be applied.

Pattern applies to the distribution of fabric elements and combinations of fabric elements into features such as laminations, bands, or layering, smears, clusters, and tertiary structure of secondary peds. In turn, spatial frequency, size, and orientation of such composite features may be the subject of study. Spacing and direction of constituent fabric elements (subfabrics) may be determined in relation to each other within and between composite features.

The kinds of directional data described are examples of vectorial fabric. The kinds of spacing data described are examples of scalar fabric; under the heading of scalar fabric come also such diverse attributes as size of fabric domains, porosity, and composition. Pattern may include both vectorial and scalar fabric.

In treating vectorial data, the von Mises probability density functions are preferable to the Gaussian where the range of the data occupy a substantial portion of the period of the variable. Many orientation variables in the earth sciences are characterized by such large dispersions.

The density function of the circular normal (von Mises) distribution is given by

$$\Psi(\alpha; \alpha_g, \kappa) = \frac{e^{\kappa \cos(\alpha - \alpha_g)}}{2\pi I_0(\kappa)}$$

where

$\alpha$  = angle variate

$\alpha_g$  = angle coordinate of center of gravity of distribution.

$\bar{\alpha}$  = angle coordinate of center of gravity of sample taken as maximum likelihood estimate of  $\alpha_g$ .  $\bar{\alpha}$  is calculated from

$$\tan \bar{\alpha} = \frac{(\sum_{i=1}^n \sin \alpha_i)}{(\sum_{i=1}^n \cos \alpha_i)}$$

$I_0(\kappa)$  = a Bessel function of the first kind of pure imaginary argument.

$\kappa$  = a measure of concentration about the mean; determined uniquely from  $\bar{a}$ , the vector strength.  $\bar{a}$  is calculated from

$\bar{a} = R/n$  for  $n$  measurements, where

$$R^2 = \left( \sum_{i=1}^n \sin \alpha_i \right)^2 + \left( \sum_{i=1}^n \cos \alpha_i \right)^2$$

The density function of the semicircular normal distribution is given by

$$\Psi(\alpha; \alpha_g, \kappa) = \frac{e^{\kappa \cos 2(\alpha - \alpha_g)}}{4\pi I_0(\kappa)}$$

A physical model of the circular normal distribution would be a tilted roulette wheel. The circular normal function applies to variables ranging through 360 degrees, such as azimuth; the semicircular normal function applies to variables ranging through 180 degrees, such as strike or any compass orientation with direction but without sense.



The density function of the spherical normal distribution is given by

$$\Psi(\theta, \alpha, \theta_g, \alpha_g, \kappa) = \frac{\kappa}{4\pi \sinh \kappa} \exp \left[ \kappa [\cos \theta \cos \theta_g + \sin \theta \sin \theta_g \cos(\alpha - \alpha_g)] \right]$$

where  $\hat{\kappa}$  satisfies  $\bar{a} = -1/\hat{\kappa} + \coth \hat{\kappa}$ .

The density function of the hemispherical normal distribution is given by

$$\Psi(\theta, \alpha; \theta_g, \alpha_g, \kappa) = \frac{\kappa}{4\pi(e^{\hat{\kappa}} - 1)} \exp \left[ \kappa [\cos \theta \cos \theta_g + \sin \theta \sin \theta_g \cos(\alpha - \alpha_g)] \right]$$

where  $\hat{\kappa}$  satisfies  $\bar{a} = 1/\hat{\kappa} \left[ \frac{\hat{\kappa} e^{\hat{\kappa}}}{e^{\hat{\kappa}} - 1} - 1 \right]$   
 ( $\theta$  and  $\alpha$  are orientation angles)

$\theta$  = angle between unit vector and z-axis

$\alpha$  = angle between projection of unit vector in xy-plane and x axis.

$\theta_g, \alpha_g$  = angle coordinates of center of gravity of distribution

$\bar{a}$  = vector strength

Maximum likelihood estimates of parameters are denoted by carets.

The orientation of planes and lines in the earth sciences is commonly depicted with reference to a hemisphere (dip and strike of planes; plunge and bearing of lines); accordingly, the hemispherical function above is



of particular interest. A review of the four functions and simplified probability tables for their use are presented in Pincus (1953).

A variety of tests for preferred orientation (or non-uniformity) is available, for example, including those in which the alternative to uniformity is characterized by a specified density function and those in which the alternative's characteristics are not specified. Both two- and three-dimensional treatments are available; two-dimensional treatments in mutually perpendicular planes may be used to approximate three-dimensional treatments under some conditions and where inherent, directionally-dependent sampling biases are manageable. In studying vectorial soil fabrics, particularly in-situ, two-dimensional treatments (both singly and multiply) are likely to be considerably more practical than three-dimensional treatments.

The statistical treatment of spacings is essentially the same as that applying to sizes. Logarithmic scales or transformations often help to normalize the data so that Gaussian and other commonly used probability operations can be undertaken quite easily. In dealing with elongations, the statistics of ratios comes into play, and here extreme caution is necessary. The need for this caution is compounded when ratios of elongations are considered, as for example in studying relative changes in elongation of fabric elements, such as grains, peds, or voids, between materials having been subjected to different loads.

The density function of the ratio  $z$  of two independent and normally distributed variates  $x$  and  $y$  ( $z = y/x$ ) is given by

$$f(z) = (1/\pi) \left[ 1/(1 + z^2) \right]$$

which has neither a mean nor a variance.

The statistical treatment of patterns is usually a composite of vector and scalar treatments, the exact nature of the treatment depending on the features involved. A soil consisting of micaceous layers alternating with granular quartzose material could involve vectorial analysis of the orientation of the mica flakes, scalar analysis of the size distributions of the quartz grains and lamination thicknesses, and vectorial analysis of intra-, inter- and trans-lamina fracture orientations.

Standardized graphical procedures for analysis of fabric data have been available for many years. Figure 3-8 shows the generation of the most commonly used projections for displaying and graphically processing fabric data. Figures 3-9 and 3-10 show graphical treatment of such data. Figures 3-11 and 3-12 display specimen plots of fabric data illustrating the four classes of symmetry presented earlier in Figure 3-3.

The fact that many earth-science data are both multimodal and "noisy" (erratically dispersed) places great obstacles in the way of using many conventional efficient statistical methods. [Compare Figure 3-12(c) which is multimodal and noisy to Figure 3-11(b)]. Sometimes one must settle for the less persuasive results of non-parametric methods. Attempts to mitigate these undesirable qualities by increasing sample size might not improve the data and, in fact, might introduce even more complications by including part of yet another population. Generally speaking, whenever the data have more than one mode and are noisy, the simpler the statistical method chosen (such as picking modes instead of using significance tests to select "concentrations"), the more easily can one use the results, particularly in communicating with the non-statistically-minded user.

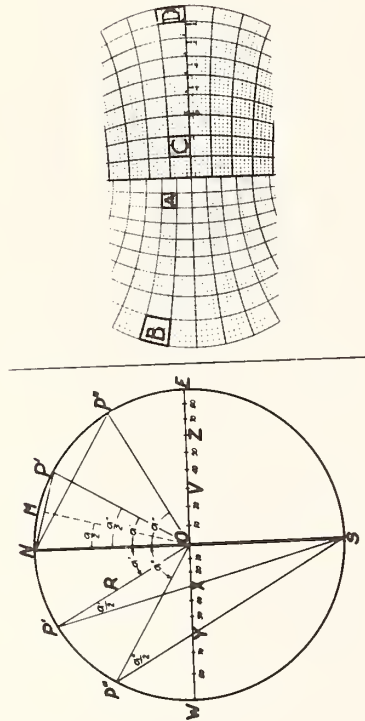


Figure 3-8. Left: Vertical section of a sphere showing generation of stereographic projection (left half) and Lambert equal-area projection (right half). Right: Stereographic projection (left half) and equal-area projection (right half). The former is angle-true but not area-true (Fairbairn, 1949).

(Most fabric diagrams use the equal-area projection. The stereographic projection is used more for solving orientation problems in three dimensions.)

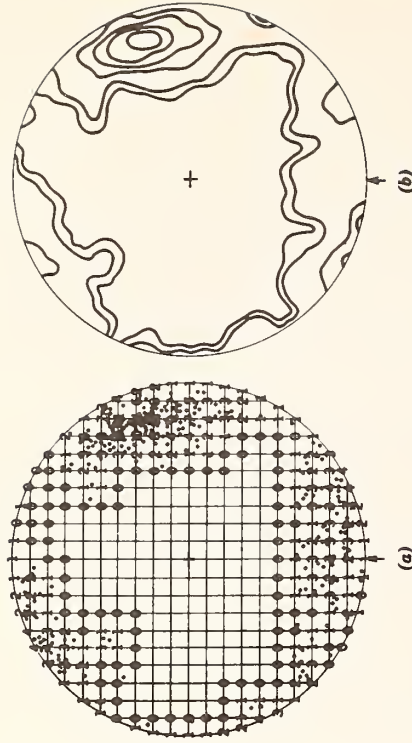


Figure 3-9. Contouring of point diagram (Schmidt method) (Turner and Weiss, 1963).

Points are counted in circular area moved over the diagram on a square counting grid. The circular counting area is 1% of the area of the projection. Grid spacing equals radius of counting circle. Numbers plotted at grid are then contoured.

- a) Diagram of 300 points that have been counted out
- b) Contours drawn on data in a).

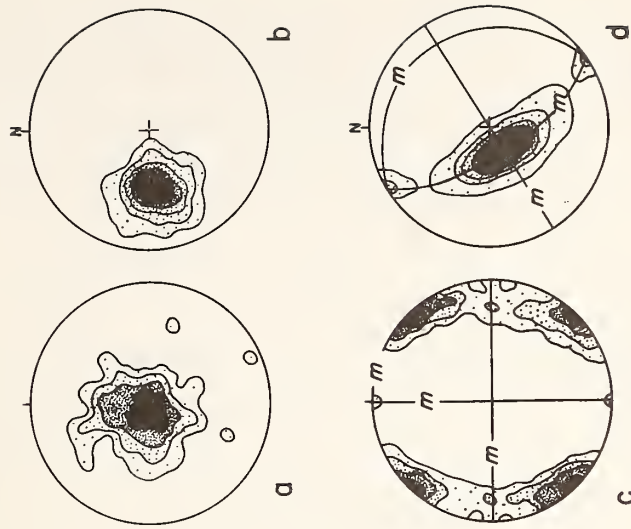


Figure 3-11. Contoured equal-area projections illustrating axial subfabrics (a and b) and orthorhombic subfabrics (c and d);  $m$  = planes of symmetry (Paterson and Weiss, 1961).

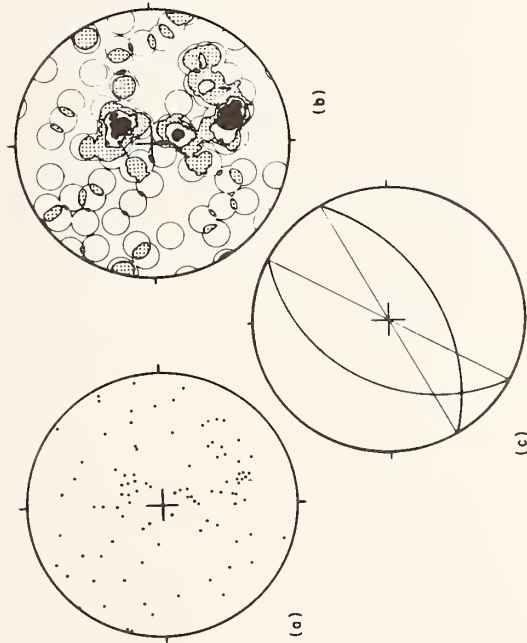


Figure 3-10. Three types of fabric diagrams  
a) Orientation of 100 axes or normals to planar features  
b) Contoured diagram of the points in a)  
c) Two intersecting planes (Friedman, 1964).



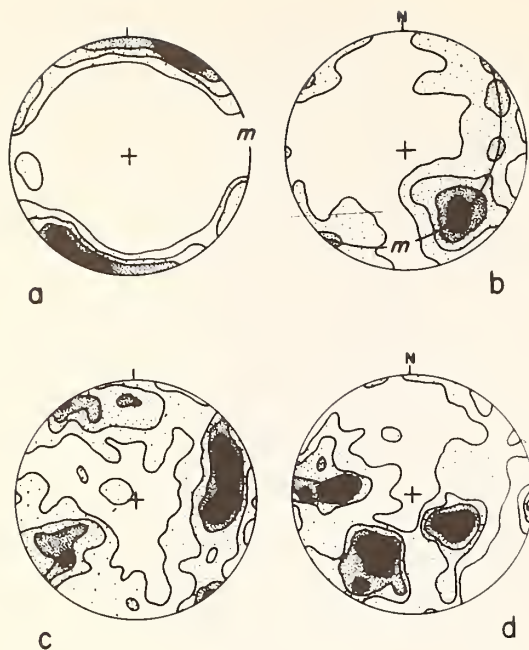


Figure 3-12. Contoured equal area projections illustrating monoclinic subfabrics (a and b) and triclinic fabrics (c and d); m = planes of symmetry (Paterson and Weiss, 1961). (Compare to Figure 3-3, d and e)

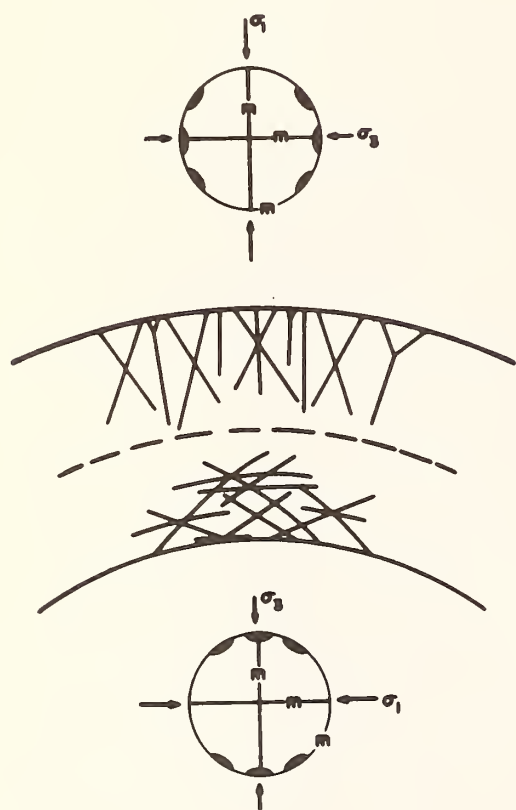


Figure 3-13. Idealized shear and extension fractures above and below neutral surface at the crest of a fold, and above and below their fabric diagram; m = planes of symmetry (Friedman and Sowers, 1970). Fabric diagrams show orientations of normals to fractures. Diagrams show parallel orthorhombic symmetry above and below neutral surface, but state of stress is different in each domain.



Of course, what appears to be multimodal might, on closer examination, turn out to be two, noncoincident unimodal subfabrics, e.g., two nonparallel sets of extension fractures (say one from loading and another from unloading), or a combination of generally related modes (Figure 3-13). A multimodal fabric may be replaceable by a unimodal fabric by virtue of a presumably valid physical relation, e.g., substitution of the acute bisectrix (axis of maximum compression) for conjugate shear pairs. The point here is that the data may be simplified via nonstatistical considerations and, in fact, they should be simplified as much as possible on physical premises prior to statistical treatment.

A straightforward analog method for handling vectorial and scalar data simultaneously is through spatial Fourier analysis by optical diffraction. Figures 3-14 to 3-24 illustrate the basic procedures and lay-outs in optical diffraction analysis that have been applied successfully to fabric studies in rock mechanics. Both orientation and spacing data are transformed directly into a polar coordinate diagram (diffraction pattern or two-dimensional Fourier transform) from the input, which is a transparent replica (usually reduced) of the surface of the earth material.

The two-dimensional Fourier transform is given by

$$F(u,v) = \iint f(x,y) \exp \left[ -2\pi i(ux + vy) / \lambda f \right] dx dy$$

where  $f(x,y)$  = input function as a function of position coordinates  $x,y$  in the object plane (front focal plane)

$F(u,v)$  = complex amplitude as a function of position coordinates  $u,v$  in the transform plane (back focal plane)

$f$  = focal length of lens

$\lambda$  = wavelength of incident light

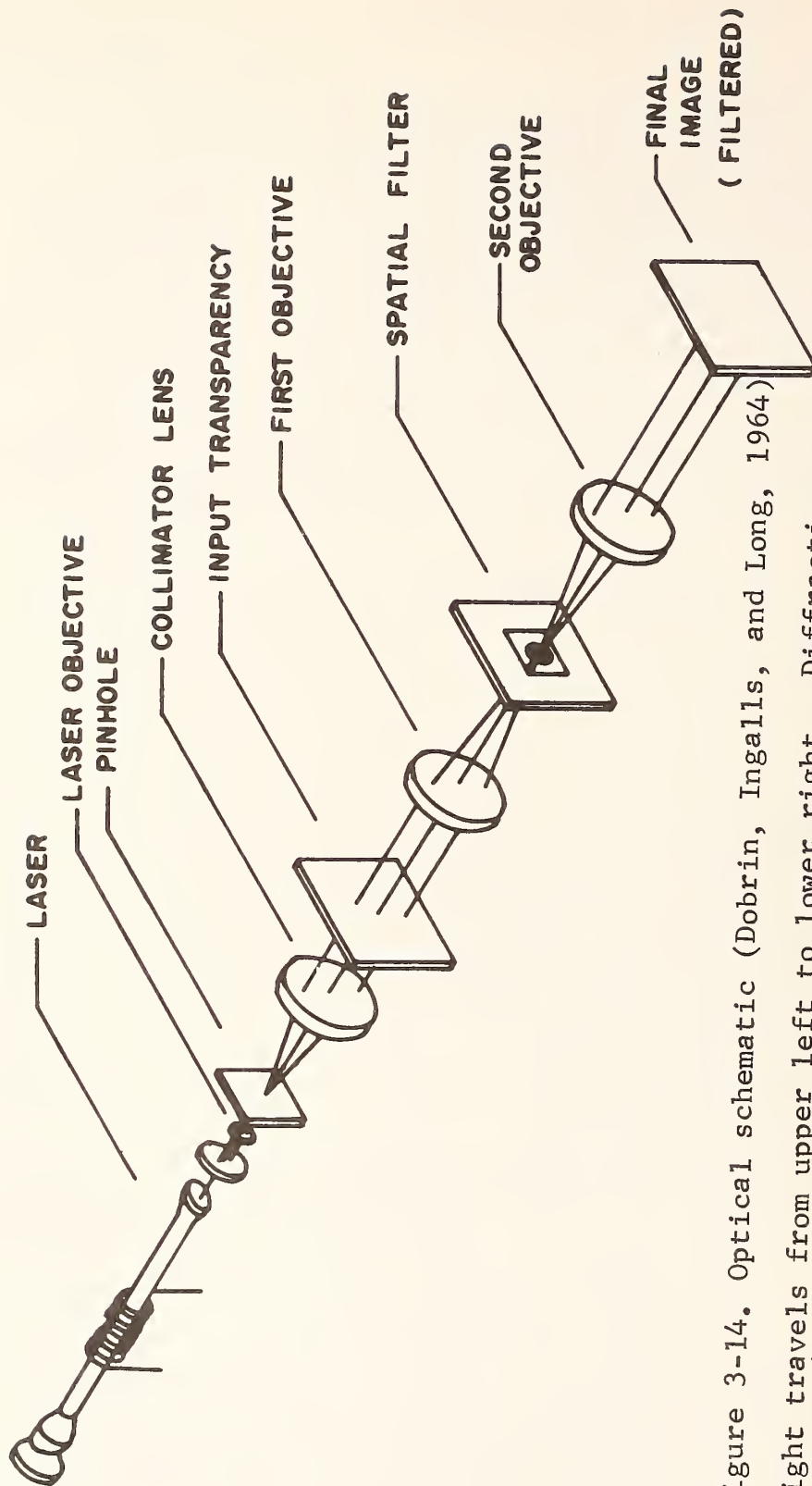


Figure 3-14. Optical schematic (Dobrin, Ingalls, and Long, 1964)  
 Light travels from upper left to lower right. Diffraction pattern (transform) appears in the plane of the spatial filter, where it may be photographed or mapped. Spatial filter is inserted when it is desired to produce a filtered image at lower right.

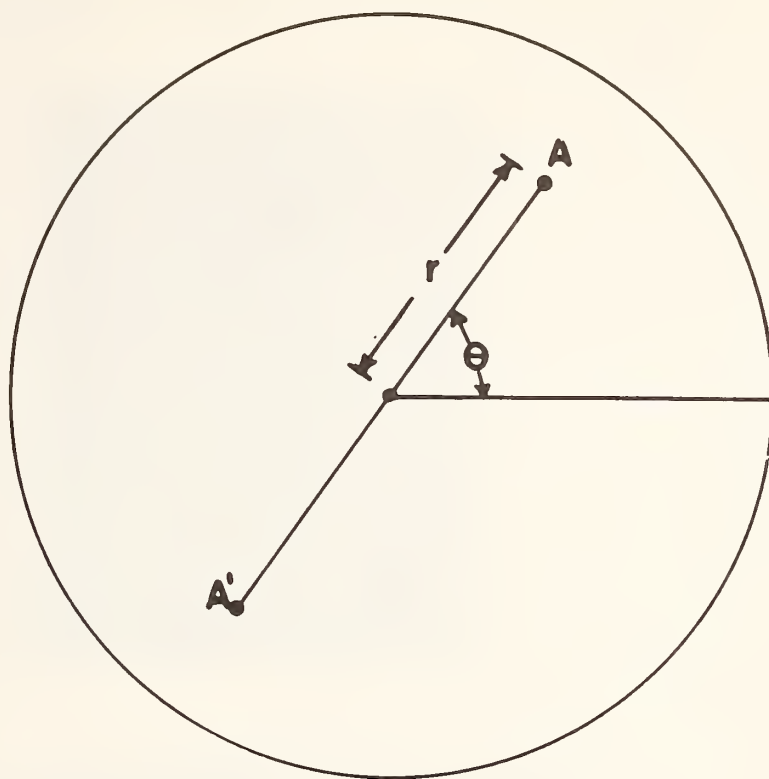


Figure 3-15. Relation of diffraction pattern to distribution parameters (Dobrin, et al, 1964).

$r$  is proportional to spatial frequency

$\theta$  is direction normal to the lineation giving rise to diffraction pattern  $AA'$

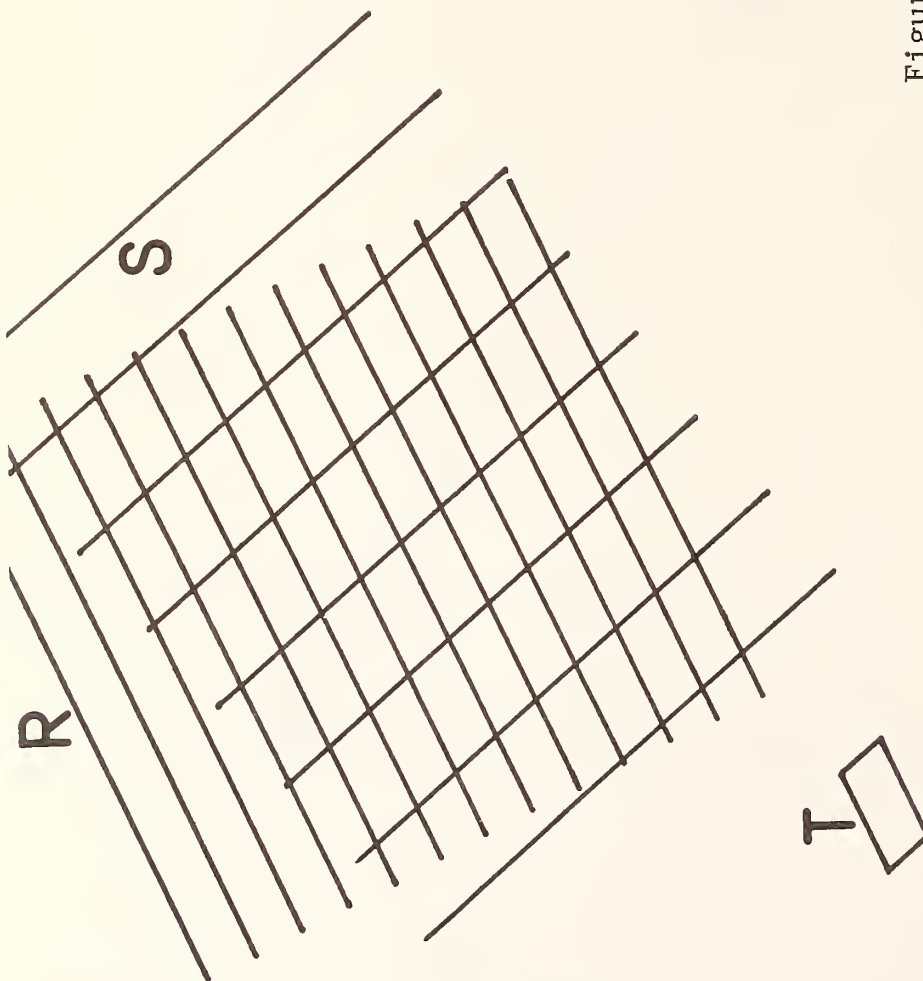


Figure 3-16a. Idealized input: two sets of intersecting lines, R and S. T is the unit figure generated by intersections.

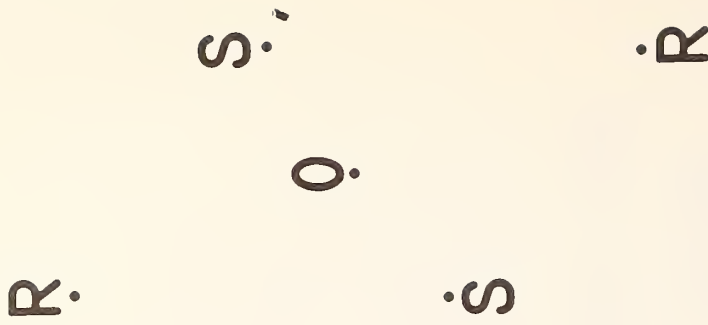


Figure 3-16b. Idealized output: diffraction pattern of sets R and S. 0 marks the center of the pattern. Pairs of dots R and S are first-order diffraction patterns. OR and OS are linear measures of the relative spatial frequencies of input sets R and S, respectively. OR and OS are perpendicular to R and S, respectively. Spatial frequency at 0 is zero or "D.C." (Pincus, 1969a).

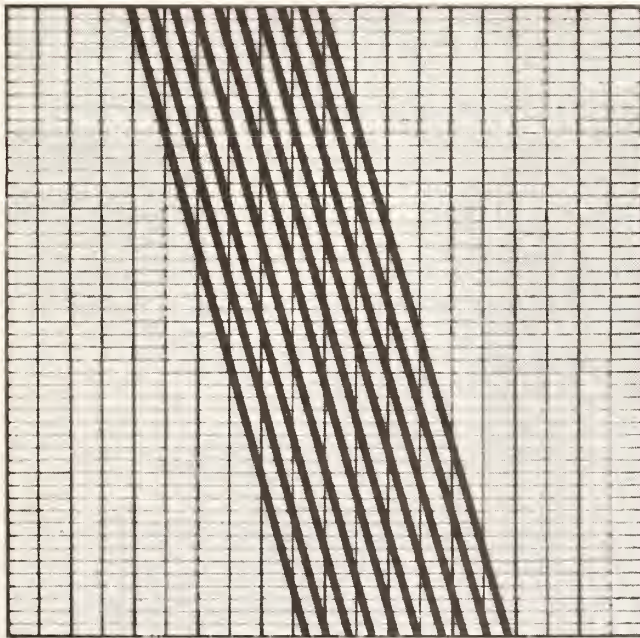


Figure 3-17. Real input and output (Dobrin, Ingalls, and Long, 1964).  
Note that the transform is the superposition of the transforms of each of the three sets of lines; this illustrates the additive property of the transforms.



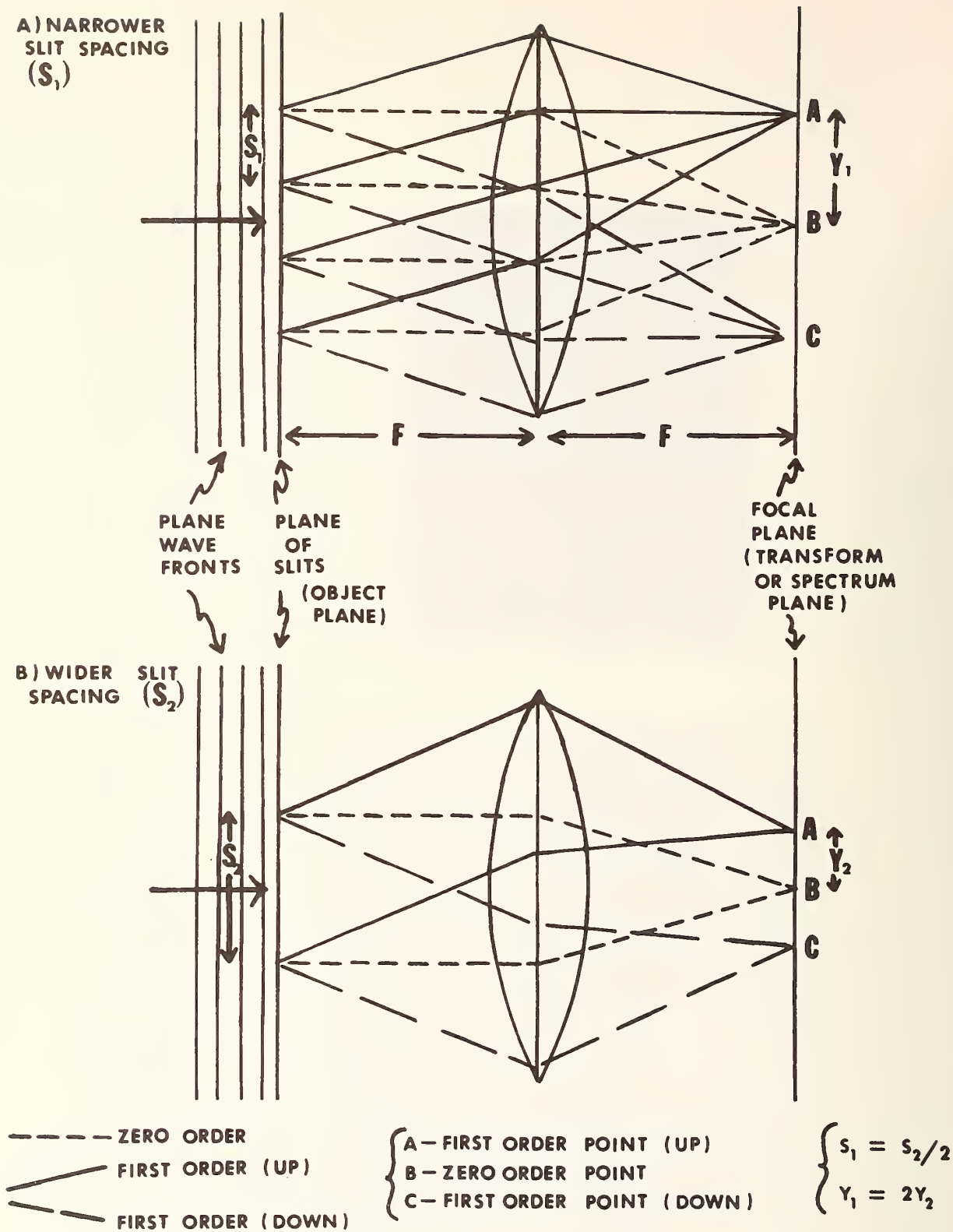
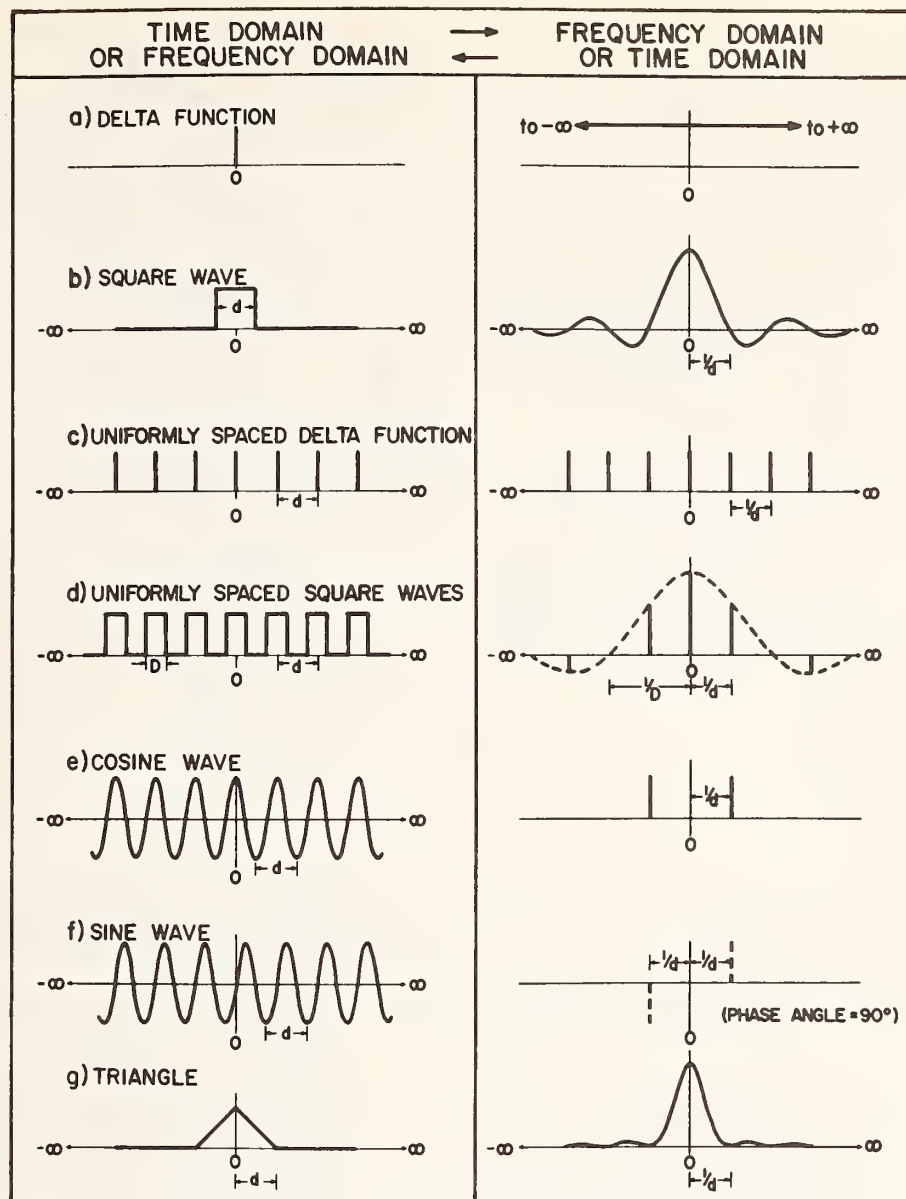


Figure 3-18. Spatial frequency analysis by diffraction via lens (After Shulman, 1970).



## FOURIER TRANSFORM PAIRS FOR TYPICAL SIGNALS

Figure 3-19 Fourier Transforms of simple functions  
(Peterson and Dobrin, 1966)

The functions in each column are the transforms of the corresponding functions in the adjoining column.

A white line on a black background would be represented by b), the square wave.

The diffraction pattern that is seen, photographed, or mapped is actually the square of the transform function, so all negative values in the transform are rendered positive.

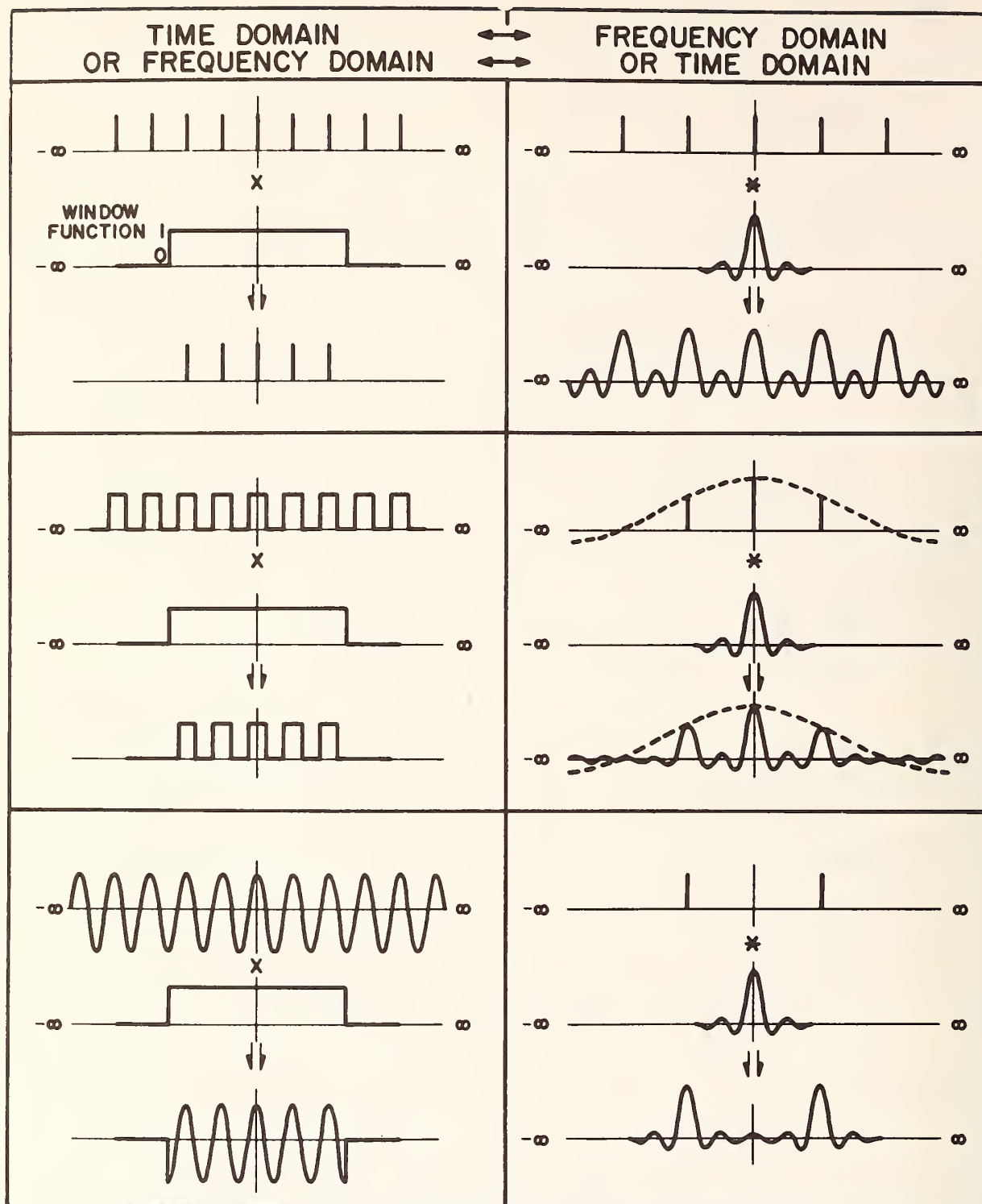


Figure 3-20. Fourier Transforms of truncated functions (Peterson and Dobrin, 1966).

Functions such as those in 3-19 are truncated with a window function. The convolution process, denoted by \*, explains the derivation of the transform of the truncated function from the infinite function and the window function.



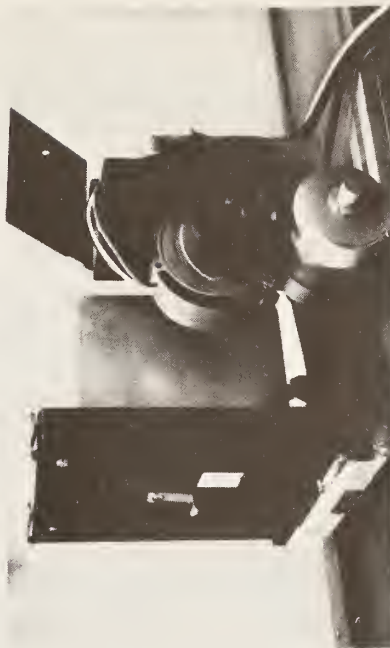
a) Optical bench configuration for photographing the transforms. Laser is at left and camera is at right



c) Set-up used for producing an intensity profile of the transform. The output of the scanning photomultiplier (shown in detail in d)) is recorded on the strip chart at the right, second shelf from the top.



b) Optical bench configuration for real-time production of reconstructed filtered images. Laser is at lower left and TV camera is at upper right. TV monitor screen is shown on top shelf in c) on this page.

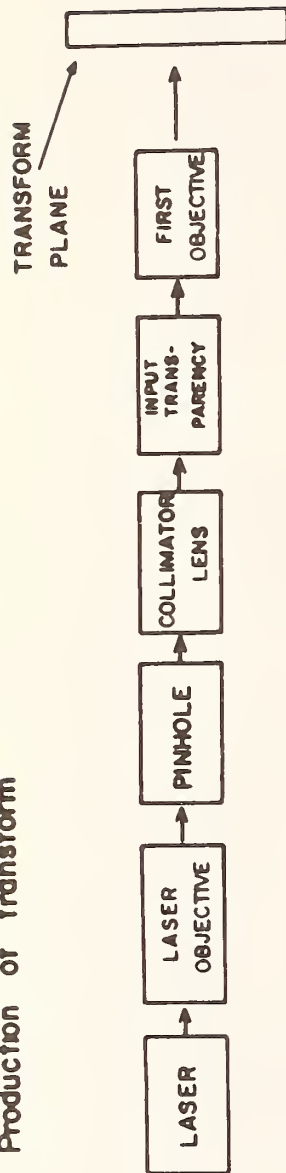


d) Detail of the optical scanner used for mapping transforms. Pin-hole is just below the J-shaped bracket on the black face-plate.

Figure 3-21 Basic optical diffraction analysis; lay-out of equipment (Pincus, 1973).



a) Production of transform



b) Production of filtered image

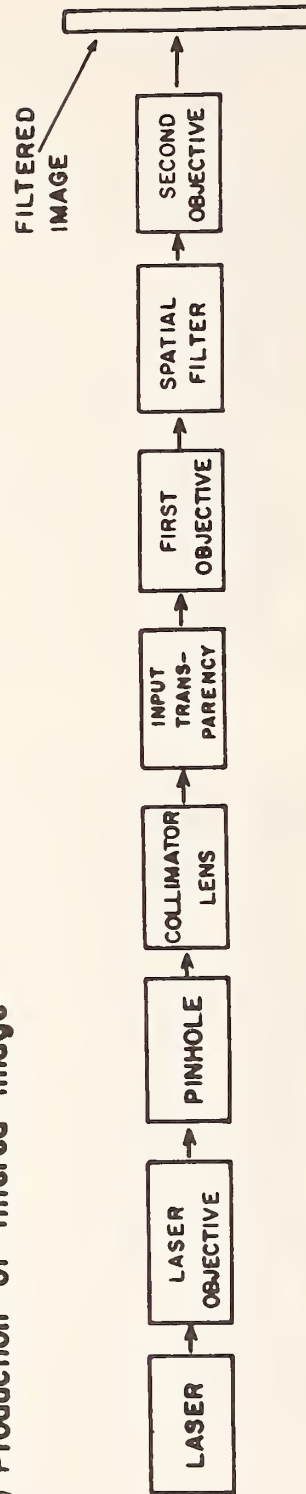


Figure 3-22 Flow charts for production of transform and filtered images (Pincus, 1969b). Spatial filter is inserted in the transform plane.



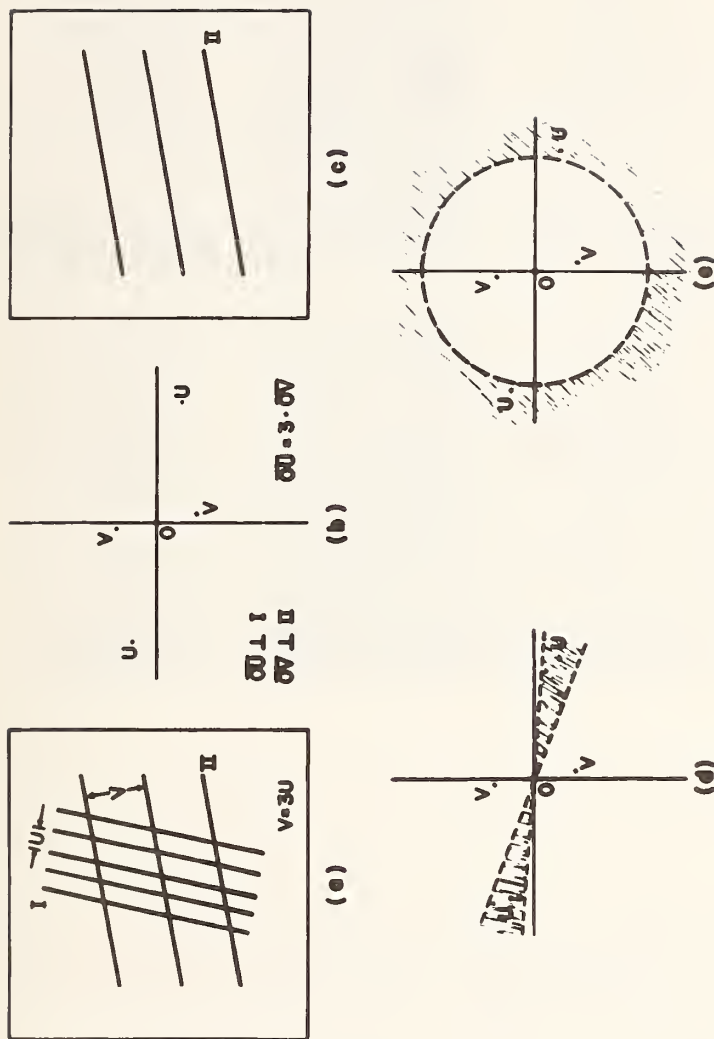


Figure 3-23 Idealized input and outputs (Pincus, 1969b).

- a) Input: Spatial frequency (inverse of spacing) of Set I is 3X that of Set II.
- b) Transform of a) Diffraction dots "U" and "V" are produced from Sets I and II, respectively.
- c) Filtered output: Set I has been removed by filtering, as in (d) or (e).
- d) Directional filtering: Rays forming dots "U" are blocked by wedges (shaded).
- e) Frequency filtering: Rays forming dots "U" are blocked by high-cut filter (shaded).

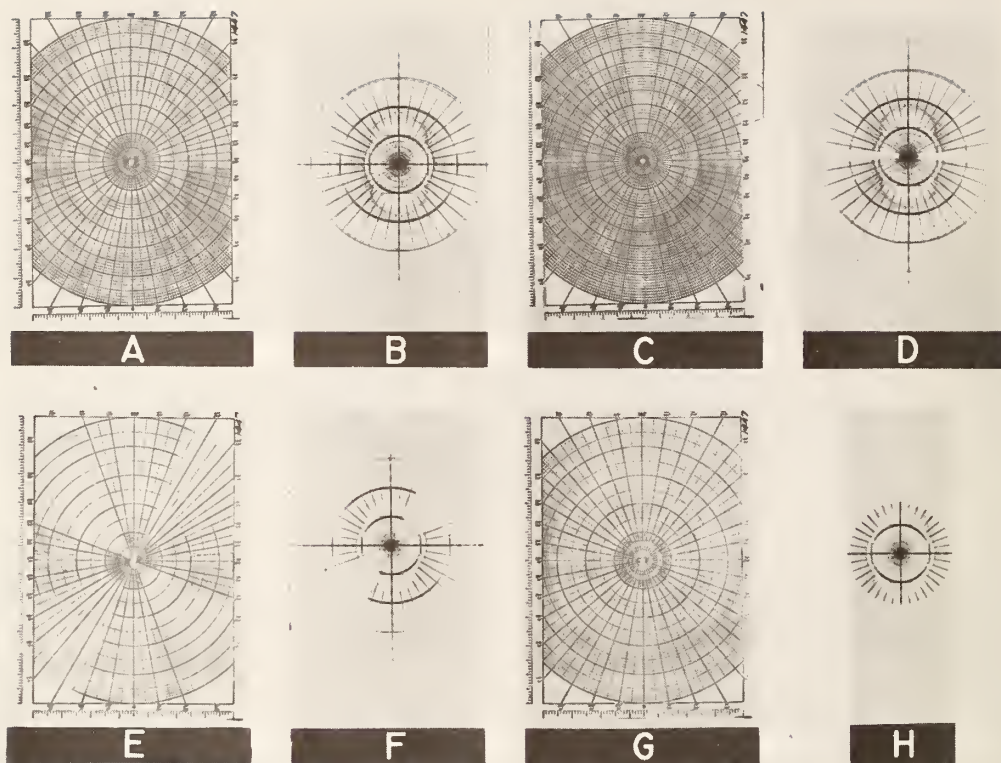


Figure 3-24 Filtering of input of polar coordinate paper  
Inputs and outputs are negative photographs.  
(Pincus, 1969a).

- A - Unfiltered input ( $0^\circ$  reference at 6 o'clock)
- B - Transform of A
- C - Directionally filtered image ( $10^\circ$  wedge)
- D - Filtering for C (filter centered at  $90^\circ$  and  $270^\circ$ )
- E - Directionally filtered image ( $40^\circ$  wedge)
- F - Filtering for E (filter centered at  $135^\circ$  and  $315^\circ$ )
- G - High cut filtered image
- H - Filtering for G (circular filter)

This equation expresses the relation between the spatial distribution of light passing through the input image in the focal plane and the distribution in the back focal plane where the diffraction pattern (Fourier transform) is formed.

Spatial filtering is rendered practical by the fact that the Fourier transform of the Fourier transform is the input function, i.e., the output function is the reconstructed image of the input image. Such filtering is accomplished, in its simplest form, by placing filters (masks) in the transform plane and an additional transform lens (reconstruction lens) one focal length beyond the transform plane.

Through directional and frequency filtering, some features can be suppressed or eliminated in the reconstructed image (spatially filtered image) so that less prominent details of the fabric can be studied more easily.

The optical diffraction method has been used to study changes in fabric of rocks under load, and has equally great promise for study of soils. Both the overall style of fabric and changes or contrasts in fabric can be quantified by this method. Features of fabric at widely different scales can be studied making it feasible, for example, to compare soil fabric viewed by the scanning electron microscope with that viewed by the light microscope, in hand specimens and in-situ (in the excavation).

Optical diffraction analysis is further illustrated and applied later in the section titled Application of Optical Diffraction Analysis to Soil Fabrics. Here, transform (diffraction pattern) analysis is illustrated; spatial filtering of soil fabric data is not illustrated in the current report.

Results equivalent to those of optical diffraction analysis can also be obtained digitally, but less conveniently and with less versatility in varying data-processing parameters. Digital processing can be very helpful, however, in

preparing and analyzing equal-area diagrams obtained from universal-stage work and field measurements.

The analysis of x-ray data obtained from soils can yield useful information on crystallographic orientations. In a sense, such data are already processed statistically by the very nature of the procedures used to obtain the x-ray data.

### 3.4 ANTICIPATED BEHAVIOR OF VARIOUS SOIL TYPES

The change in fabric associated with a particular loading history depends on factors such as the direction, intensity, and rate of loading and the constitution of the material that has been loaded. Included in these constitutional factors are scalar and vector fabrics, as well as (or overlapping with) the usual compositional expressions of soil mechanics.

Here it is important that the primary fabric of the soil, i.e., the fabric developed during formation of the soil and prior to subsequent deformation, be known or accurately inferred in order to characterize the deformation in some useful way. Whether the soil initially has, for example, single-grained, honeycombed, or flocculent structure will determine, in part, what kinds of interpretations can be made following deformation.

In soils with single-grained structure, i.e., cohesionless soils such as sands and gravels, individual grains may be displaced or rotated to save space in the direction of maximum compression, grains may be crushed thereby increasing the dispersion of particle sizes and providing a means for packing intergranular voids with fine material, and individual grains may be deformed elastically, plastically, or by fracture. Elastic deformation of individual grains or aggregates of grains might be determined in-situ by photoelastic or x-ray methods adapted



for this purpose; plastic deformation might be detected by studies of grain elongation or twin-gliding. The deformation of intergranular voids in soils with single-grained structure requires essentially the same treatment as in the study of changes in grain shape and size.

In soils with honeycombed structure, viz. fine enough for cohesion to be significant such as in fine silts and clays, the undisturbed honeycomb structure itself could provide a datum against which to measure deformation. Of course, a pervasive destruction of the honeycombs might leave no evidence of the initial structure. Individual grains might undergo the same changes as considered for grains in single-grained structure. With cohesion, structural units of higher organization such as peds and clods can provide yet another scale at which deformation may be characterized.

In soils with flocculent structure, viz., those consisting of colloidal-size particles, measures of deformation may be based on changes in grains, flocs (honeycombs of grains) and honeycombs of flocs (second-order honeycombs). In such fine-grained material, the practical approach may be to study changes in larger-scale features such as peds, fractures, and bands.

Soils of mixed structures provide a larger variety of features with which to attempt kinematic and dynamic fabric analysis, but this also makes interpretation much more difficult. The presence of more than one type of structure, unless the structures are homogeneously distributed through the material, creates interpretation problems of as great difficulty as those arising from a history of more than one episode of deformation.

The presence of water (or its absence) certainly affects the course of deformation and consequently the fabric associated with deformation. For example, the total absence of water in granular noncohesive soils is likely



to yield obviously cataclastic features with deformation. The role of water is increasingly dramatic with decreasing particle size; in fact it can be asserted that the same fine-grained soil, wet and dry, is in fact not the same material under these two sets of conditions, even with no changes in soil mineralogy. Despite all these contrasts, it is not likely that the presence or absence of water will enhance or reduce the usefulness of fabric analysis. And, experiments to determine unambiguously the role of water in fabric change should be limited, at least initially, to those ranges of saturation most likely to be found in the major soil types.

Table 3.1 shows possible deformation indicators that could be used for soil types recognized in the Unified Soil Classification Systems. Table 3.2 shows a comparable breakdown by type of fabric component in soils as recognized in pedology (Brewer, 1964). Both the Unified Soil Classification System and Brewer's breakdown of soil components appear to lend themselves to useful associations with deformation indicators.

An important step in follow-up studies will be to relate, where feasible, features of soil fabric to basic soil mechanics properties such as sensitivity and Atterberg limits, and to contrasts in properties such as those between remolded and unremolded soil. Microfabric features, such as average space between particles (pore fabric), might explain transitional points such as liquid limits in rational, useful terms. Figure 3-25 indicates some interesting possibilities.

### 3.5 ORIENTATION OF MEASURING DEVICES WITH RESPECT TO SOIL FABRIC

The design of instrumentational configurations for measuring stress or strain in earth materials is usually rendered difficult by the materials' anisotropy and

Table 3.1

DEFORMATION INDICATORS RELATED TO SOIL TYPES

Outline of Unified Soil Classification      Possible Deformation Indicators

Major Divisions		Symbols	Orientation	Spacing	Pattern	Remarks
Coarse-Grained Soils	Gravels and gravelly soils	GW	X	Size Elong. X		same for voids
		GC	X	X	X	
		GP	X	X	X	
		GF	X	X	X	
	Sands and sandy soils	SW	X	X		same for voids
		SC	X	X	X	
		SP	X	X	X	
		SF	X	X	X	
Fine-Grained Soils	Low to medium compressibility	ML	X	X	X	
		CL			X	
		OL			X	
	High compressibility	MH	X	X	X	
Highly Organic Soils	Very high to high compressibility	CH			X	
		OH			X	
		Pt			X	

Table 3.2

## DEFORMATION INDICATORS RELATED TO FABRIC COMPONENTS

Components	Fabric Orientation	Characteristics		Pattern	Remarks
		Size	Spacing Elongation		
Skeleton grains	X	X	X	X	Intracrystalline twinning, etc.
Peds	X	X	X	X	S-matrix component (grains, plasma, voids) treated separately
Clods	X	X	X	X	
Fragments	X	X	X	X	
Plasma				X	Visible plasmic grains treated like skeleton grains
Pedological Features					
Cutans	X			X	
Pedotubules	X		X	X	
Glaebules	X		X	X	
Crystallaria	X		X	X	
Subcutanic Features				X	
Fecal Pellets	X		X	X	
Voids					
Packing voids	X	X	X	X	
Vughs	X	X	X	X	
Vesicles	X	X	X	X	
Channels	X	X	X	X	
Chambers	X		X	X	
Planes (Surfaces)					
Joint	X			X	May be filled
Skew	X			X	
Craze	X			X	

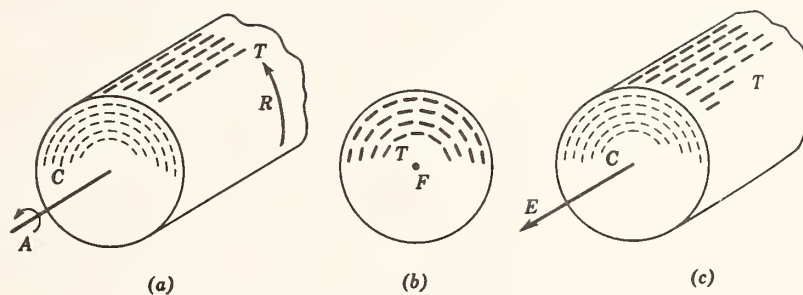


Figure 3-25. Alignment of grains in experimentally deformed clays (Turner and Weiss, 1963).

- a) Rolling in direction and sense R about axis A
- b) Flattening of a sphere to a disk normal to axis F
- c) Extrusion of a cylinder parallel to axis E.

heterogeneity, the presence of discontinuities (both natural and man-made), the perturbations in behavior of the earth materials induced by the instrumentation itself, the frequent nonparallelism between principal stress and principal directions of mechanical anisotropy, and departures from ideal elastic and plastic behavior of many earth materials even where intact, homogeneous, and approximately isotropic materials are involved. Interpretations of the results of such measurements are rendered difficult by the same factors.

Generally these difficulties are encountered whether one is measuring (a) stress or strain resulting from a known external load or (b) stress or strain associated with residual stress. The latter measurements are more subject to error than are the former. Strain measurements are typically more reliable than stress measurements (at least some of which are not really measurements of stress) and the strain field can probably be more easily related to fabric anisotropy.

As mechanical anisotropy increases, these difficulties in design and interpretation may be accentuated. Where fabric anisotropy is related to mechanical anisotropy in some direct, systematic way, fabric analysis can be of help in anticipating design and interpretation problems. In addition, fabric analysis might help directly in specifying orientation of some components of the measuring device and in calculating meaningful results. For example, if fabric analysis reveals a single, strong, preferred orientation with axial symmetry (Figures 3-3a and 3-11a), (e.g., parallel channel-voids), which is probably associated with a strong, similarly oriented mechanical anisotropy, then one could orient one of the measuring axes parallel to this direction in order to increase the sensitivity of the entire measuring system.



On the other hand, should fabric analysis reveal that the fabric is heterotactic, i.e., the symmetries of the constituent subfabrics do not coincide, then the most practical strategy might be to ignore the fabric in orienting the instrumentation but to recall the details of the fabric in interpreting the results.

All of the foregoing remarks apply as well to time-dependent and location-dependent measurements.

Considering the complexities outlined in the first paragraph of this section, it seems wise to investigate possibilities for making measurements initially in many or all directions in a given plane, to do this in three mutually perpendicular directions, and to use fabric analysis to help explain the results. From this might come sufficient understanding to use fabric data to specify orientations of measuring devices. Photoelastic borehole inclusions, photoelastic coatings, brittle lacquer coatings, and Moire coatings should all be considered for this purpose. The coating and its adhesive medium should be selected and applied so as not to result in a significant reinforcing effect. Coatings with thicknesses less than several times that of fabric elements such as grains may respond to grain-by-grain strain gradients; accordingly the thickness must be considered as part of the instrument design. Photoelastic borehole inclusions can be fabricated from a variety of materials that can be used to achieve desired matches or mismatches between mechanical properties of the inclusion and the surrounding earth materials.

Despite the importance of fabric anisotropy in all of these considerations, it seems likely that the local vertical will usually be one of the directions of great interest, and at least one direction in the horizontal will be of at least secondary interest. (In fact, both local

vertical and some direction or directions in the horizontal are likely to be important fabric directions in some and perhaps many cases). Where the fabric is unknown or diverse (e.g., heterotactic), vertical and horizontal orientations may be included in the measuring program. Where there are also conspicuous discontinuities of moderate dip, such as joint sets (Figure 3-13) or layering, a third (or fourth) orientation could be taken perpendicular to these surfaces.

The design of the instrumental configuration should include provision for measuring as many variables as would be required in the worst case possible in the situation being studied. As additional information about anisotropy and loading at the locality are obtained, the number of measurements required may be decreased from the original theoretical maximum. With increasing experience, additional reductions may be effected.

### 3.6 EXPERIMENTAL WORK TO INVESTIGATE RELATIONS AMONG CHANGES IN FABRIC, STRESS HISTORY, AND INITIAL FABRIC AND COMPOSITION

A principal objective of experimental work should be to determine under what conditions and with which soil types dynamic fabric analysis is feasible, the combinations of conditions and materials permitting useful kinematic fabric analysis, and the combinations of conditions and materials that will not permit effective use of any kind of fabric analysis.

Materials selected should represent, at the very least, single-grained, honeycombed and flocculent initial structures. Preferably, the selection should give representation to perhaps half to two-thirds of the 15 categories in the Unified Soil Classification. Beyond this, specimens should also be selected to show effects on larger-scale features such as peds and clusters, and to oriented

features such as elongated grains, layering and smears. As noted elsewhere (Section 3.4 ANTICIPATED BEHAVIOR OF VARIOUS SOIL TYPES), variations in saturation should be limited to ranges to be anticipated in-situ in the particular type of soil being studied. Grossly heterogeneous materials should be avoided, at least initially and perhaps entirely.

Variables in loading to be included in an experimental program should be magnitude, rate, ratio of principal stresses, orientation of principal stresses with respect to orientation of directional fabric elements, and pore pressure. Both normal and shear loading, in relatively simple configurations, should be used. Dynamic testing, if undertaken at all, should come in the latter stages of an experimental testing program.

Another objective of experimental work should be to help lay the groundwork for in-situ tests that could be later adapted for routine use by the field practitioner. It seems advisable to begin the experimental program very simply, with a small number of pilot experiments designed to indicate which categories of experiments are likely to be most productive and should be explored in the later phases of experimentation.

Samples of well-graded and poorly graded sands (SW and SP), saturated and dry, tested in compression and in shear, should have their fabrics recorded before and after deformation. Loads should be carried incrementally to progressively higher values, for sets of like specimens. The fabrics may be recorded on photographs or acetate peels. The analysis of the fabrics may then consist of conventional microcounting and micromeasuring techniques, opto-electronic counting and digital processing, or optical diffraction analysis. Associated with whichever of these techniques may be selected should always be old-fashioned "eyeball" evaluation overall of the fabric.

Samples of inorganic silts and clays of low and high liquid limit and from slight to high plasticity (ML, CL, MH, CH) tested in compression uniaxially and triaxially and in shear, should have their fabrics recorded before and after deformation as in the treatment of the sands above.

Samples of organic silts and clays and highly organic soils (OL, OH,  $P_t$ ) should also be treated this way. As the grain size decreases and the organic content increases there are likely to be practical problems in using acetate peels to record the fabrics and there may also be problems in macro and microscale photography. Here it might be necessary to turn to scanning electron microscopy to obtain useful fabric data.

In the early stages of experimentation, samples without obvious stratification, large discontinuities and other conspicuous heterogeneities should be selected. In addition to studying effects of loading on fabric, early experimentation should also provide for evaluation, adaptation, and development of a variety of experimental techniques. For example, strain-birefringence effects in quartz grains, lattice-strain determined by x-ray diffraction, and stereological techniques such as grain intercept-area ratios, should be considered and perhaps attempted. Partially indurated soils, in which natural chemical cements or ice serve as the indurating medium, should also be studied in an intermediate phase of experimentation. The percentage induration and its spatial distribution would be of interest, particularly in frozen soils.

We have investigated the possibility of applying optical diffraction analysis to soil fabrics of different types.

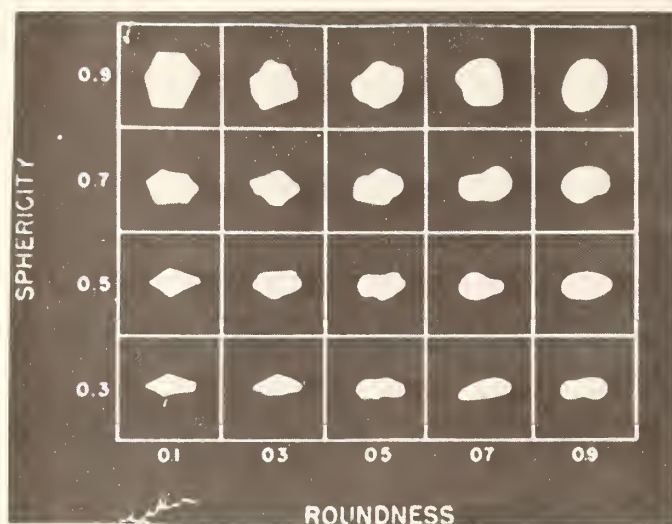


As inputs, 14 photographs from Brewer (1964), reduced four times, have been used to generate diffraction patterns. The results are presented in Figures 3-32 through 3-45. The same technique can be applied to single examples at progressively higher loads or to comparable specimens loaded in different modes (uniaxial, triaxial, direct shear).

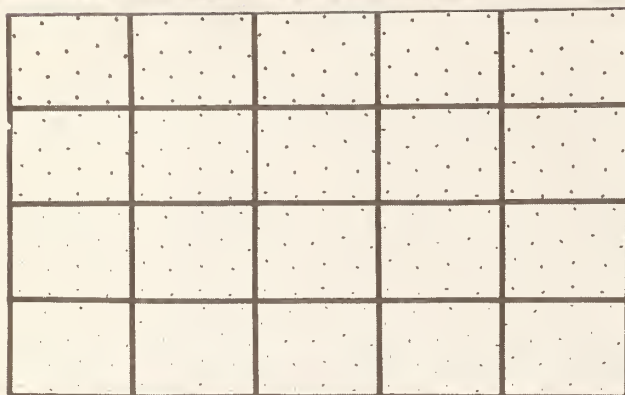
Details of optical diffraction analysis and interpretation are covered elsewhere in references such as Pincus and Dobrin (1966), Pincus (1966, 1969(a), 1973), and Pincus, Power, and Woodzick (1973). Results of spatial filtering and holographic subtraction as applied to soil fabrics are not presented here, but will likely prove to be powerful tools in subsequent work.

In studying inputs and their transforms or diffraction patterns, the evaluation of scaling factors is necessary if the transform is to be used as a measuring device. Typically, a small piece of rectangular coordinate paper is photographed with the input, and is then used to generate a calibration transform. Lines intersecting in a rectangular grid, like the vertical and horizontal lines in the input of Figure 3-17, generate series of dots (along horizontal and vertical lines as in the Figure 3-17 transform) also distributed in a rectangular network. The spacing between the dots varies linearly with the spatial frequency of the input lines. Figure 3-31 is the calibration transform for Figures 3-32 to 3-45; calibration transforms also appear in Figure 3-27(b), 3-49(b) and 3-50(b); profiles of calibration transforms are shown in Figures 3-51(a) and 3-52 (upper left). Table 3.3 summarizes scaling relationships for inputs and outputs in this work.

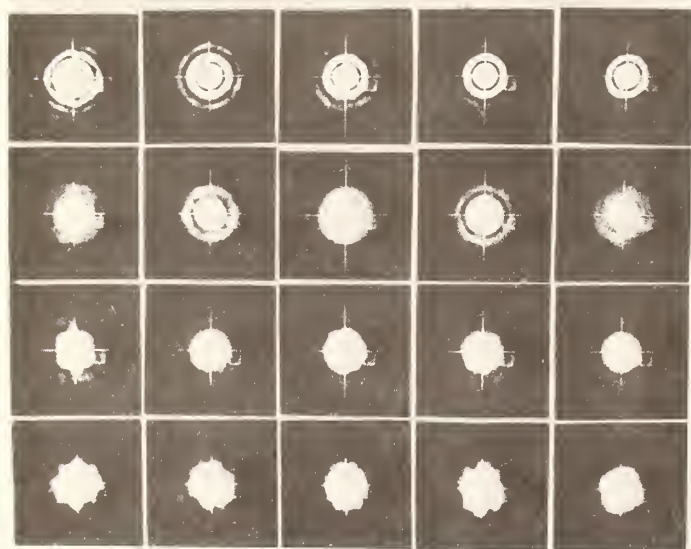




a) Sphericity and roundness chart



b) Assemblages of particles such as those in a).



c) Transforms of b).

Figure 3-26. Idealized particulate shapes and their transforms (Larson, 1973).

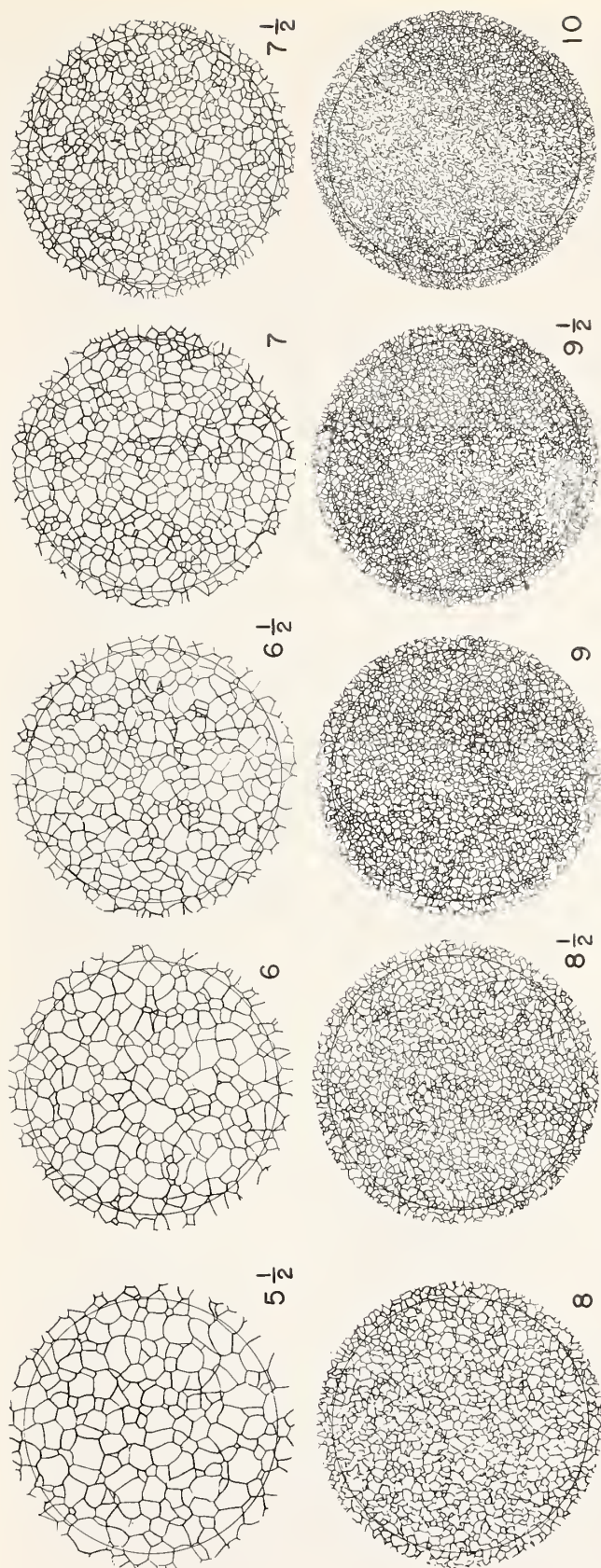


Figure 3-27a. Grain-size chart, line drawings, from ASTM Plate I, E-112-63, size numbers 5-1/2 to 10. Each input has 9 cm (3.5 in.) in diameter in the standard, published at 100X magnification (Pincus, 1969a).

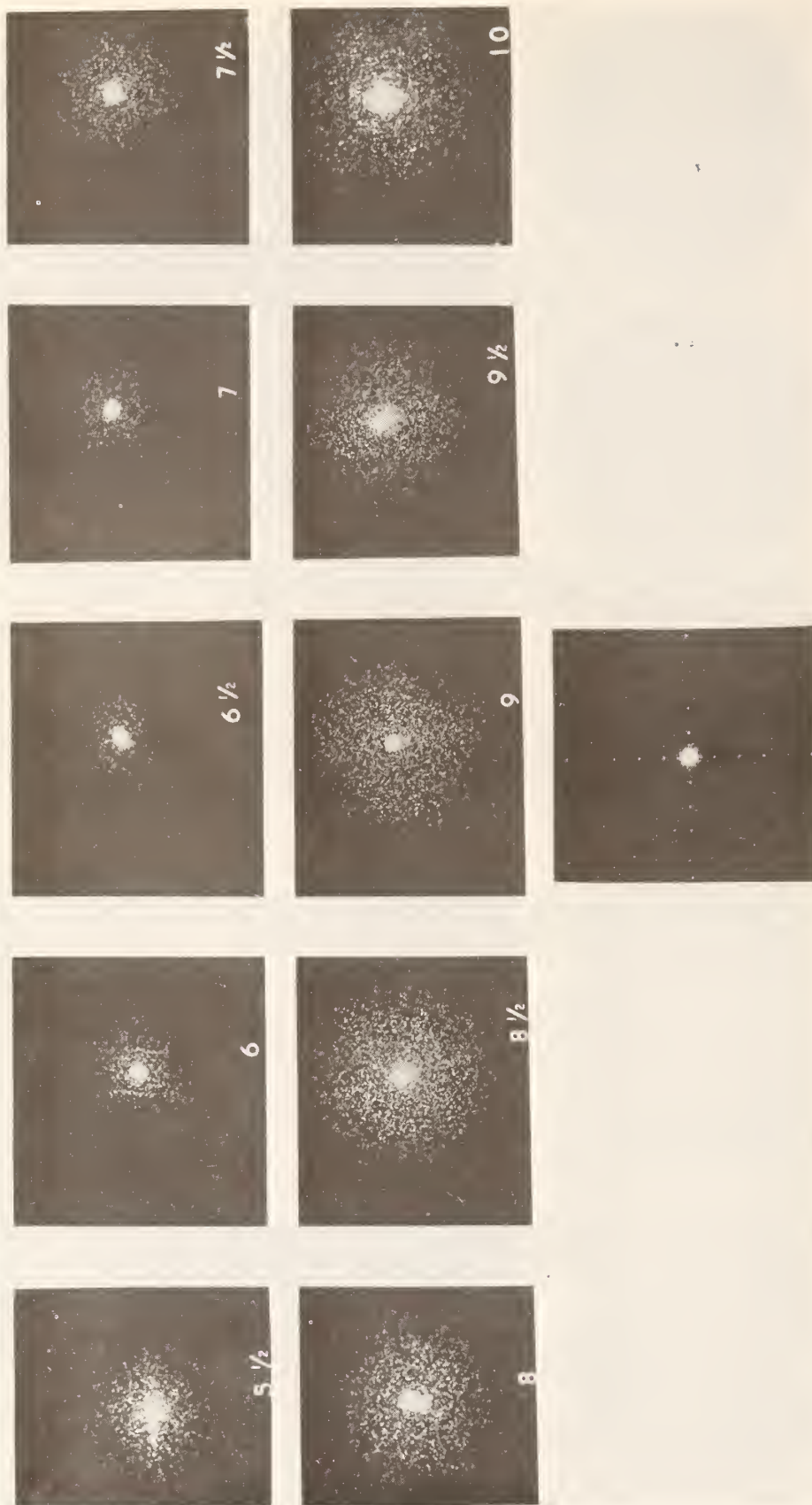


Figure 3-27b. Transforms of grain-size line drawings, sizes 5-1/2 to 10 (Pincus, 1969a).

(Calibration transform at bottom)



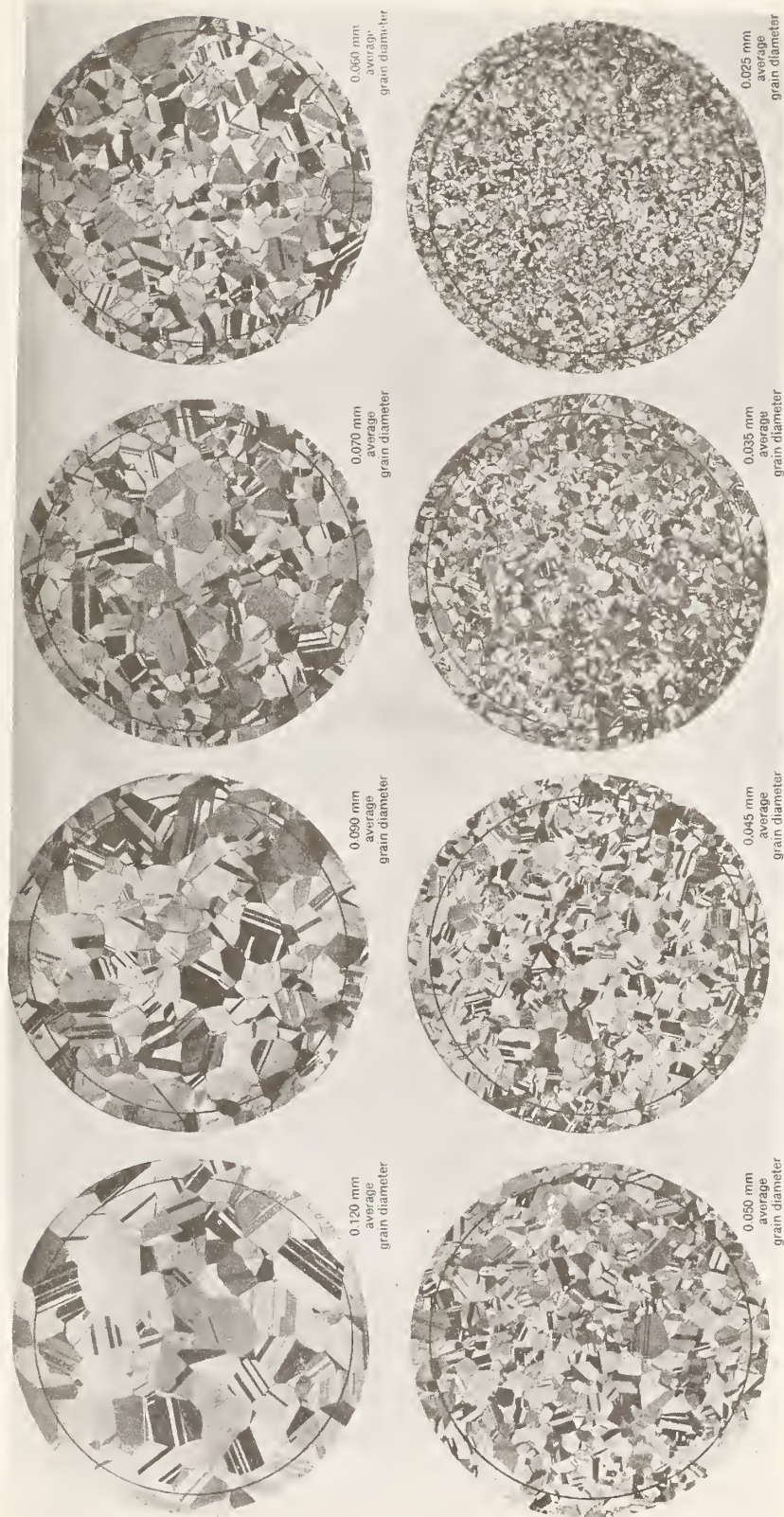


Figure 3-28a. Grain-size chart, half-tones, from ASTM Plate III, E-112-63, sizes .120-.025 mm (.005-.0001 in.). Each input has 9 cm (3.5 in.) diameter in the standard, published at 75X magnification (Pincus, 1969a).

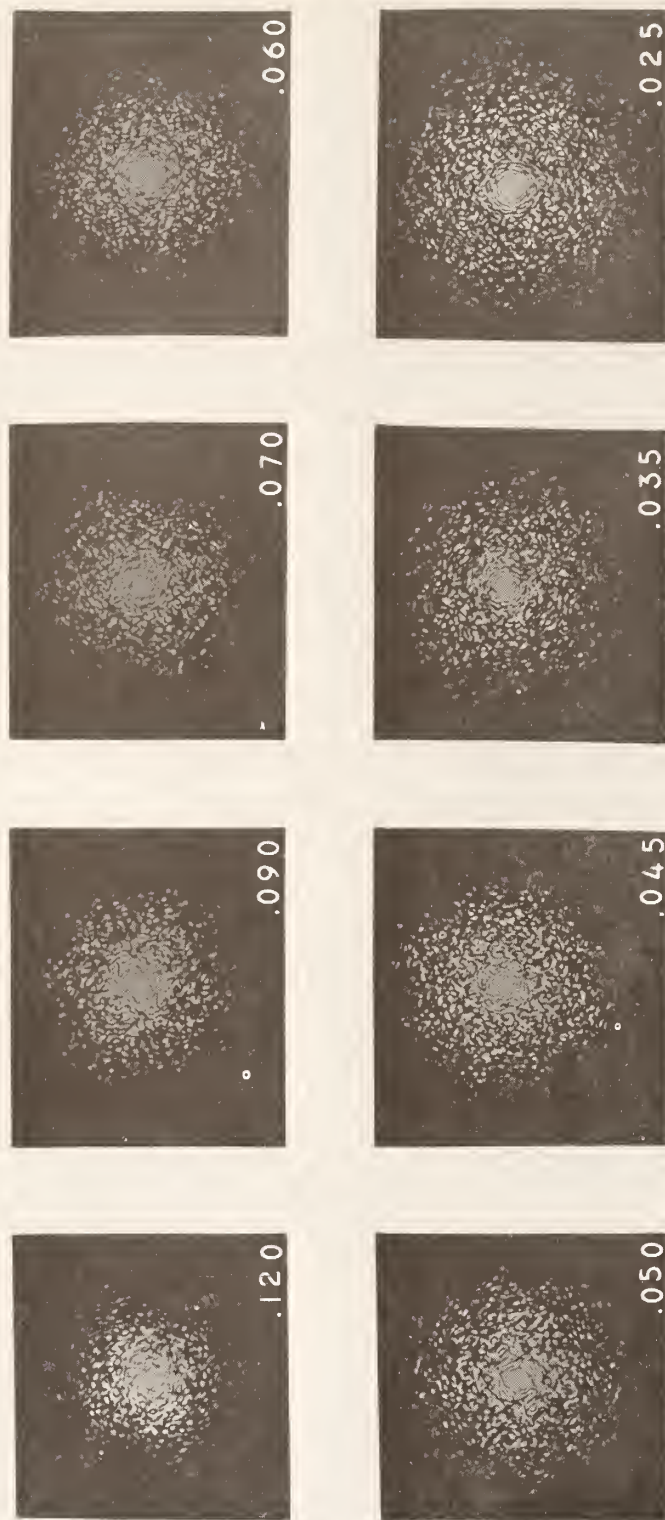


Figure 3-28b. Transforms of grain-size halftones, sizes .120-.025mm (.005-.0001 in.) (Pincus, 1969a).



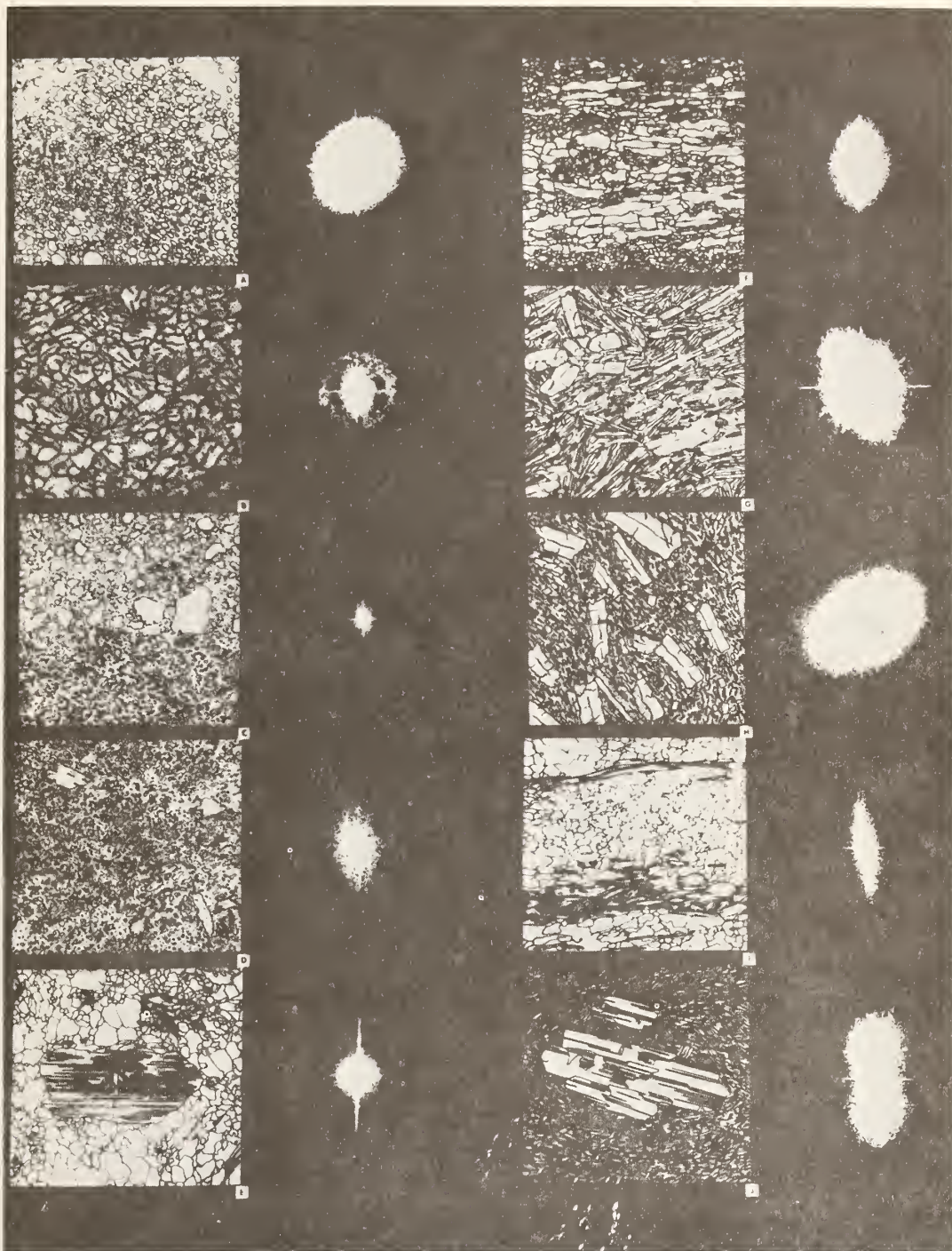


Figure 3-29 Some reference inputs (line drawings) and their respective transforms (Pincus, 1973). (Inputs from Jung, 1969).

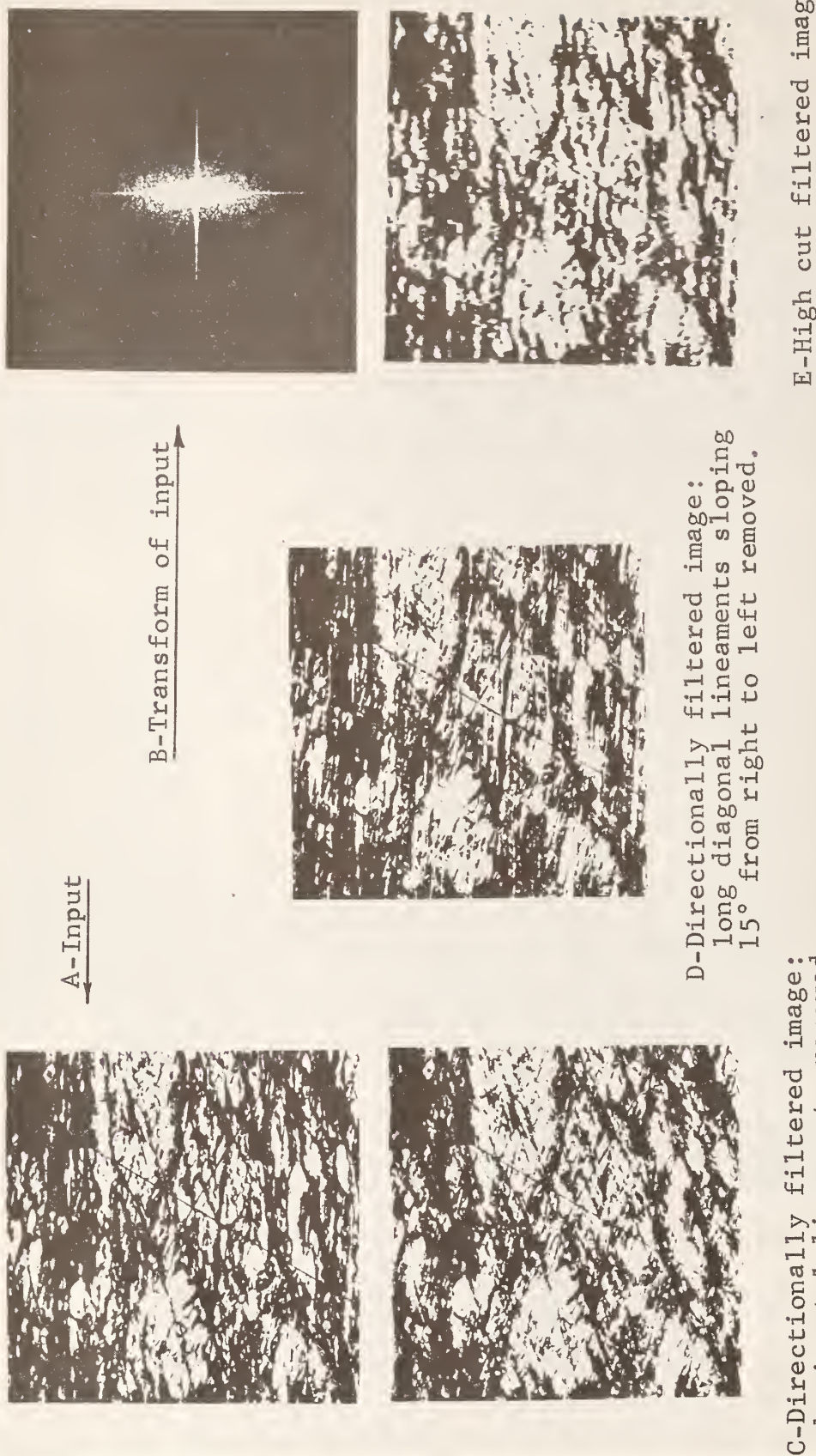


Figure 3-30. Filtering of photomicrograph of quartzite. Side of photo about 20 mm in specimen (Pincus and Dobrin, 1966).



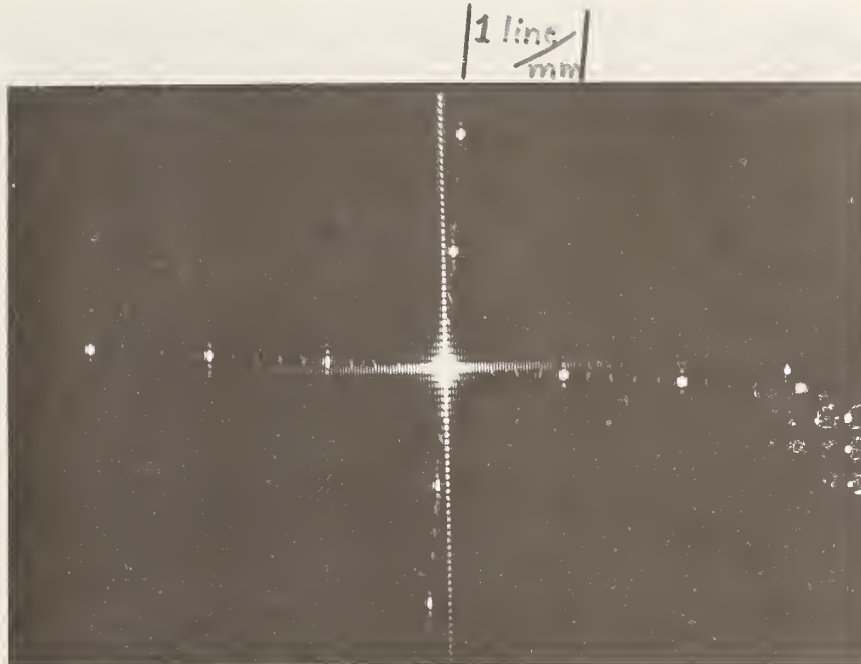
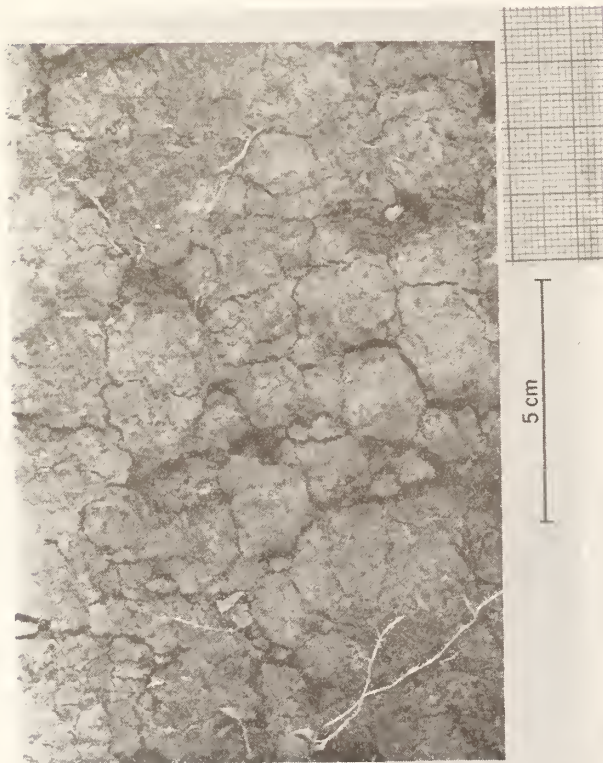


Figure 3-31. Calibration Transform

The central bright cross is generated by the rectangular aperture used to illuminate the input transparency.

The slightly rotated cross composed most conspicuously of bright, circular dots is the calibration transform, generated by the millimeter coordinate paper visible in the lower right corner of the inputs that follow. This millimeter paper provided the scale for the photographs; the scale for the specimens, per se, can be obtained from the scale bar in the bottom center of the picture.

The upper margin of the transform shows the interval corresponding to a spatial frequency of 1 line/mm in the photograph (1mm spacing). Twice this interval represents 2 lines/mm (0.5mm spacing) in the photograph, and so forth.



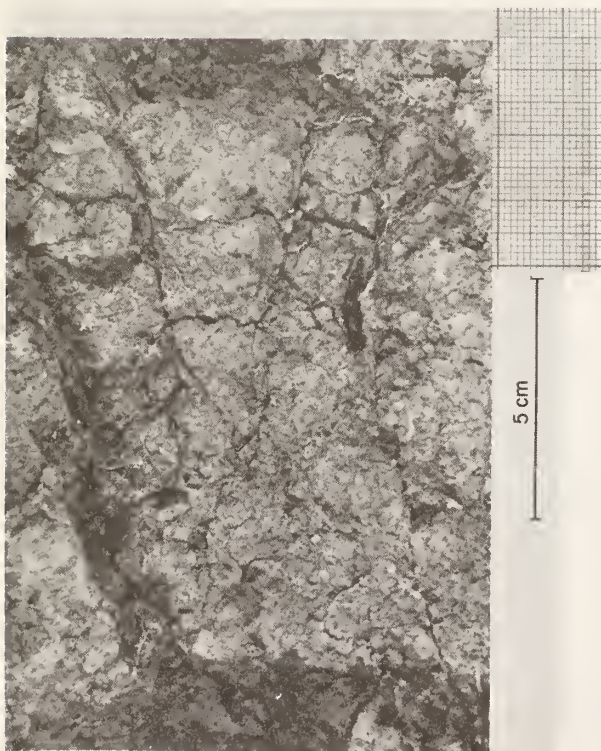
Input 1499-(Brewer-Figure 13) Macropeds of similar size and shape with offset packing.

Figure 3-32a. Input



Outer limits of the transform mark the spatial frequencies of the interpedal voids. Relative abundance of vertical, roughly planar joints with a range of widths, accounts for horizontal elongation of transform.

Figure 3-32b. Transform



Input 1500-(Brewer-Figure 15) Cuneate macropeds of dissimilar size separated by inclined sets of joint planes.

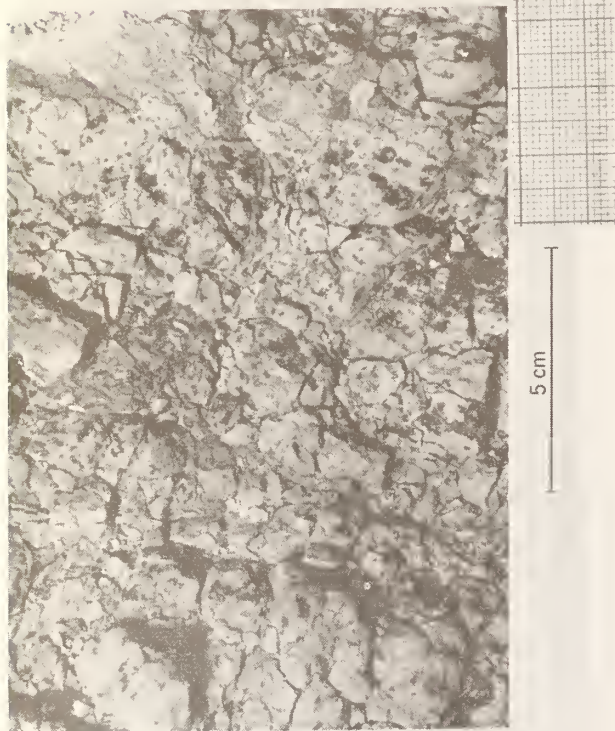
Figure 3-33a. Input



Overall shape of transform is circular. Superimposed on this pattern are two faint bands lying a few degrees on each side of the vertical axis; these are generated by the gently inclined joint sets.

Figure 3-33b. Transform





Input 1501-(Brewer Figure 16) Macropeds of very dissimilar size and shape separated by craze planes.



The transform shows more strength in the medium frequency range than either of the two preceding transforms. A stubby band, nearly vertical and from upper right to lower left is generated by gently inclined joints. Approximately perpendicular to it (nearly horizontal) is a band generated by irregular joints approximately perpendicular to the gently inclined joints.

Figure 3-34a. Input

Figure 3-34b. Transform



Input 1502-(Brewer-Figure 17) Apedal soil material with a set of joint planes.

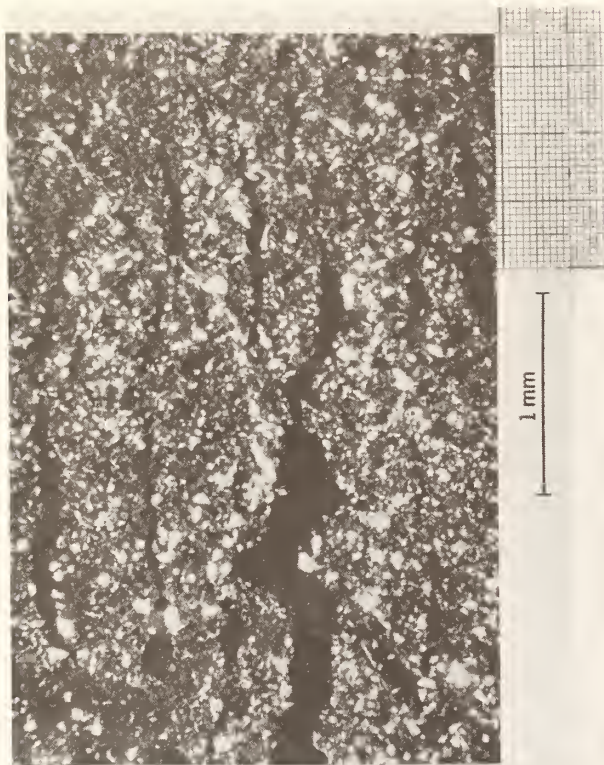


Aside from the D.C. spot and the aperture cross, the most prominent features are two faint, orthogonal lines generated by relatively faint joints, one set of which is identified in the input caption.

Figure 3-35a. Input

Figure 3-35b. Transform





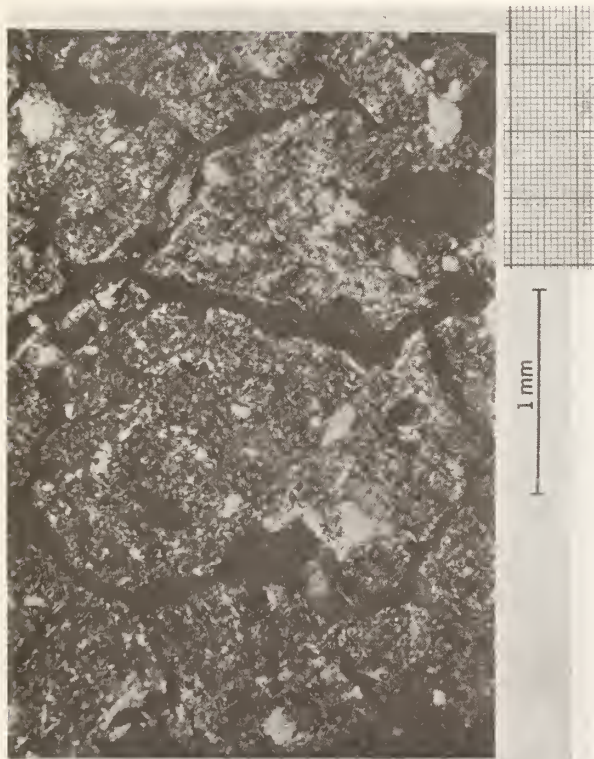
Input 1503-(Brewer-Figure 40) Irregular ortho-joint planes. Thin section under crossed polarizers. The planes have a banded distribution pattern parallel to the surface of the soil.

Figure 3-36a. Input



Overall shape of the transform is circular, although the low-frequency (very bright) region shows a slight vertical elongation generated by the horizontal joints.

Figure 3-36b. Transform



Input 1504-(Brewer-Figure 42) Craze planes. Thin section under crossed polarizers.



Transform shows high low-frequency content. Oblique low-frequency bands have been generated by diagonal craze surfaces in the input.

Figure 3-37a. Input

Figure 3-37b. Transform



Input 1505-(Brewer-Figure 43) Simple free grain argillans with strong continuous orientation. Thin section under crossed polarizers. The thin white borders to the skeleton grains are the argillans. Most of the black areas are simple packing voids since all the plasma occurs as argillans.

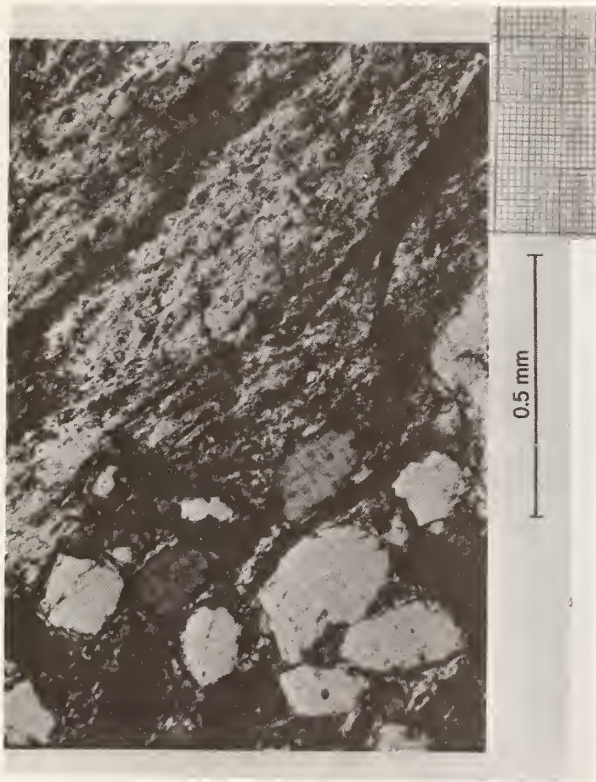
Figure 3-38a. Input



Transform shows little high-frequency content other than in the two conspicuous diagonal bands generated by the thin white argillans in the input.

Figure 3-38b. Transform





Input 1506-(Brewer-Figure 55) Simple skew-plane argillan with striated orientation. Thin section under crossed polarizers. Note the lack of distinct extinction lines in the argillan.

Figure 3-39a. Input



The elongation of the transform from upper right to lower left results from the oriented striations in the input. These are seen to range from low to high spatial frequencies.

Figure 3-39b. Transform



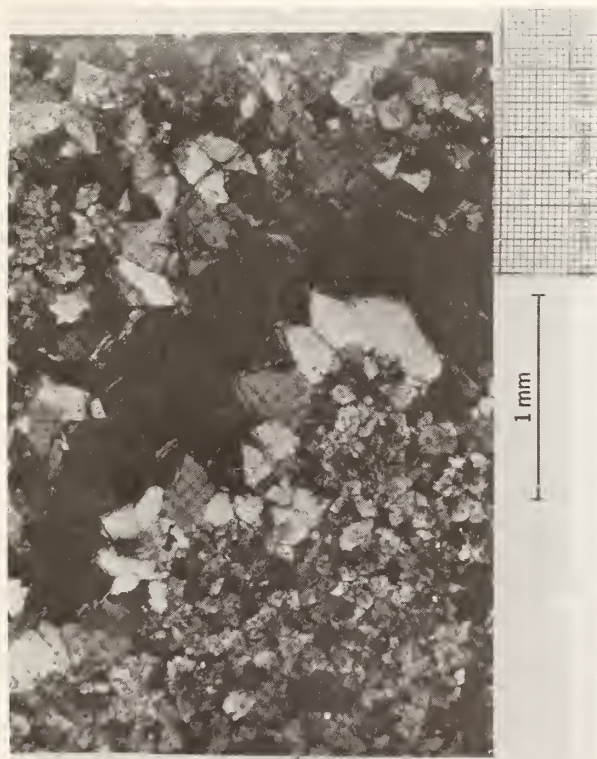
Input 1507-(Brewer-Figure 59) Section through a thick complex zone (Z) of vugh and plane argillans and chalcidans. Thin section under crossed polarizers. M is the s-matrix.

Figure 3-40a. Input



The sharp line from upper left to lower right results from the ZZ line in the input and is therefore superfluous. The band from upper right to lower left is clearly related to the orientations of vughs and cutans in the input.

Figure 3-40b. Transform



Input 1508-(Brewer-Figure 90) Compound crystal chamber. Thin section under crossed polarizers. The black central area is a void around which the calcite crystals are much larger than those away from the void. The thin white border to the void is an argillan with strong continuous orientation.



A preferred orientation, especially among the higher spatial frequencies, is not evident. The lowest spatial frequency region seems to have a polygonal boundary, almost diamond-shaped, resulting from calcite crystal boundaries.

Figure 3-41a. Input

Figure 3-41b. Transform



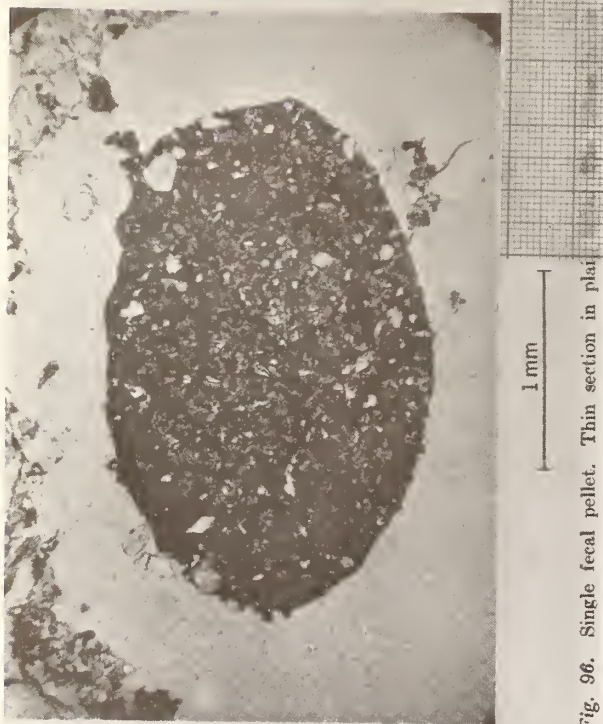


Fig. 96. Single fecal pellet. Thin section in plain light.

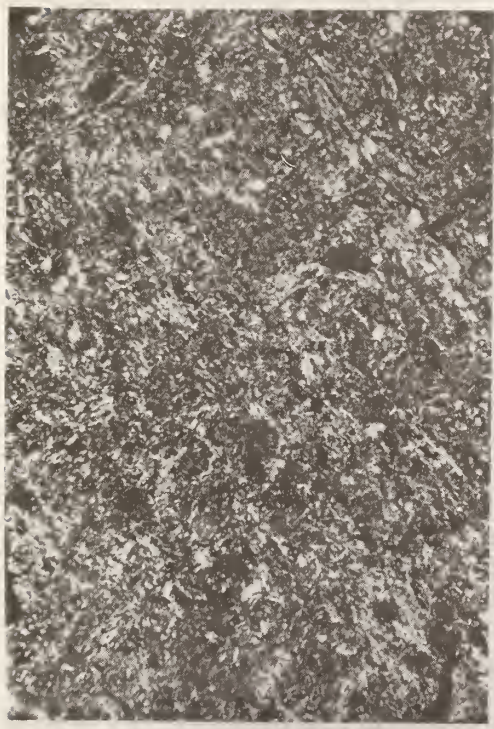
Input 1509-(Brewer-Figure 96) Single fecal pellet. Thin section in plain light. The diffuse darker border constitutes a neoorganon.



Transform shows a medium-frequency concentration from upper right to lower left, and a low-frequency concentration from upper left to lower right. These concentrations are generated by scattered white elongated grains.

Figure 3-42a. Input

Figure 3-42b. Transform



Input 1510-(Brewer-Figure 102) Mosepic  
 plasmic fabric. Thin section under  
 crossed polarizers. Plasma separations  
 occur as numerous patches.

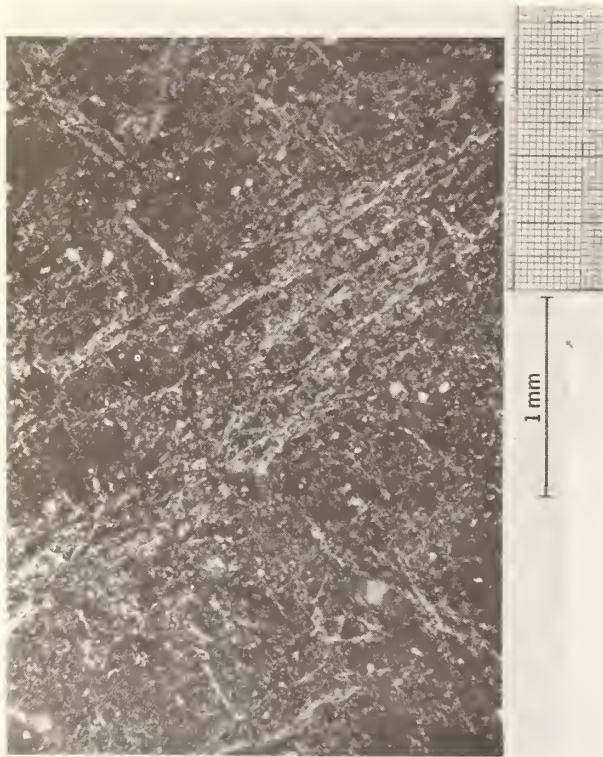
Figure 3-43a. Input



Transform shows faint suggestion of  
 preferred orientation, like from that in  
 the lower right corner of the input  
 However, the many orientations in the  
 input yield an overall pattern showing  
 very little directional banding.  
 Transform cloud drops off in intensity  
 fairly sharply at the outer edges,  
 reflecting discontinuity in distribution  
 of sizes.

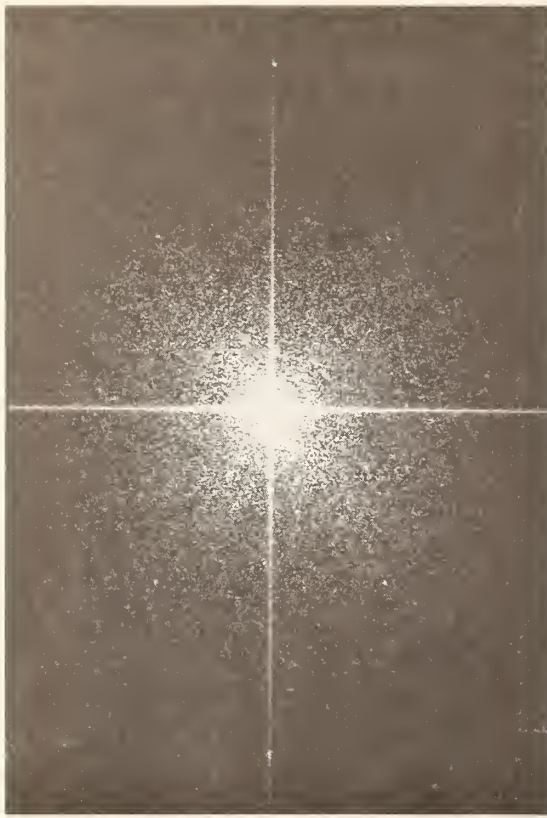
Figure 3-43b. Transform





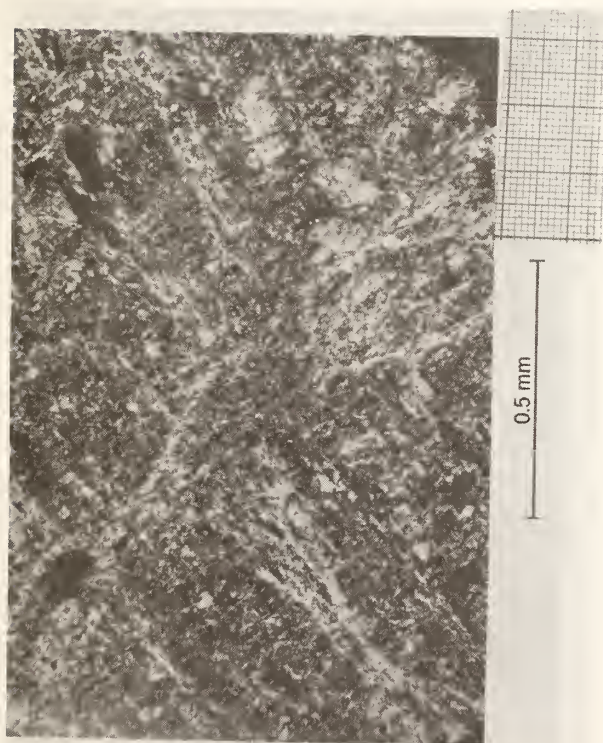
Clino-bimasepic plasmic fabric. Thin section under crossed polarizers. Note the broad plasma separation with a striated orientation pattern within the s-matrix and the narrow, less well-developed plasma separations at approximately 60 degrees to it.

Figure 3-44a. Input



Transform shows evidence of both inclined zones in the input, the more prominent band from upper left to lower right in the input generating the band in the transform from upper right to lower left.

Figure 3-44b. Transform



Input 1512-(Brewer-Figure 110) Omnisepic plasmic fabric. Thin section under crossed polarizers. Essentially an extreme development of bimasepic plasmic fabric.



Although the input is described first as having omnisepic fabric, the later characterization as bimasepic is shown by the transform's two oblique bands to be more appropriate.

Figure 3-45a. Input

Figure 3-45b. Transform

Table 3.3

REDUCTION, ENLARGEMENT, AND SCALING RELATIONSHIPS  
VIA MEASUREMENTS ON INPUTS AND OUTPUTS  
(Pincus, 1973)

Corresponding distances, intervals.		Reduction (enlargement)	Scale	Remarks
Original (Ground distance, distance on peel, micro-slide, etc.)	$x_0$			Same scale as input for direct processing of thin section or 1:1 photocopy of acetate peel.
Photo, map, line drawing of original. ("Record") (Calibration grid included at this stage)	$x_i$	$\frac{x_0}{x_i}$	$\frac{x_i}{x_0}$	Often the display "of record," in publication, etc. Work back from calibration grid to original as well as forward to outputs.
Input (reduced transparency)	$x_t$	$\frac{x_0}{x_t} = \frac{x_0}{x_i} \cdot \frac{x_i}{x_t}$ ----- $\frac{x_i}{x_t}$ (from preceding step)	$\frac{x_t}{x_0}$	This is the "original" in direct processing of thin section ( $x = x_0$ ); for contact of 1:1 copy of acetate peel, $x_t$ also = $x_0$ .
Transform generated by input	$r_1$		$K \left( \frac{1}{x_t} \right)$ $K' x_t$	$K = x_t^2 K'$
Photo, map or profile of transform; TV	$r_1'$	$e_1 r_1 = \frac{e_1 K_1}{x_t} = e_1 K_1 x_t$ =enlargement of print or TV display of transform	$\frac{r_1'}{r_1} = e_1$	$\frac{r_1'}{x_f'} = \frac{e_1}{e_2} \cdot K_2'$

(Continued)



REDUCTION, ENLARGEMENT, AND SCALING RELATIONSHIPS  
VIA MEASUREMENTS ON INPUTS AND OUTPUTS  
(Pincus, 1973)

173

Figures 3-26 to 3-30 demonstrate some results from earlier studies that indicate some possibilities for analysis of soil fabrics. Particle shapes (Figure 3-26) and shapes, sizes, and arrangements of grains (Figures 3-27 to 3-29) are all amenable to this type of analysis. Spatial filtering of a "real" input is illustrated in Figure 3-30. Figure 3-29 is taken from a reference collection of inputs and their transforms, used for quick comparisons in fabric studies of rocks.

Figures 3-32 to 3-35 are a preliminary sampling, with inputs from Brewer (1964), to show relationships between a variety of soil fabric elements and types of fabrics on the one hand, and their transforms, (diffraction patterns) on the other. Input captions are quoted from Brewer.

Input transparencies prepared from the input photographs were prepared on 35 mm film at a reduction of 4X. The first six input transparencies were negatives and the remaining eight were positives. The prints of the transforms of the first four inputs were given twice as much exposure as their 10 counterparts in order to bring out useful details.

### 3.7 PLANS FOR MAPPING AND ANALYZING SOIL FABRICS

Plans for mapping and analyzing soil fabrics must always take into account, implicitly if not explicitly, that the ultimate general objectives are to determine the orientation of principal stress directions and the magnitudes of principal stresses associated with the fabric, and the stress and strain history of the soil.

Where some features of soil fabric that appear to bear upon any of these objectives can be perceived quickly, the type and layout of mapping can be tentatively specified to optimize utilization of these features. For example,



the type and layout of mapping will not be the same in one area with a single dominant joint direction as in another area with three mutually perpendicular joint directions. Nor will the mapping and analysis procedures be the same in an area in which the most conspicuous feature is a single set of joints as in another area showing a single set of joints and squeezed-out peds, indicating compression parallel to the direction of tension inferred from the joint orientations alone. Work on cross-cutting relations might establish the relative ages of two episodes of stressing represented by the joints and the elongation of the peds.

The selection of type of mapping of soil fabrics, and the type of analysis associated with such mapping, depends on (a) the purpose of the fabric analysis (and the investigation of which it is a necessary but not unique component) (b) the type of soil material being studied, (c) the form and size of the body composed of the soil material (such as a mappable unit on an engineering soil map), (d) the spatial distribution of anisotropies in the soil body, (e) the directional distribution of anisotropies in the soil body, (f) the type, form and requirements of the engineering structure to be designed and constructed, (g) the range of possible orientation relations between the engineering structure and soil anisotropies, (h) the range of possible size relations among the engineering structure, boundaries of soil body, and soil heterogeneities, (i) the scale or scales at which fabric is to be mapped, and (k) the resources available for such mapping. All of the foregoing factors are mutually interdependent; none can be considered effectively in isolation.

Mapping techniques may range from conventional, infrared, radar, and multispectral photography, down to scanning electron microscopy and x-ray diffraction. It is

desirable that soil fabrics be studied at more than one scale in any soil, say at the scales of grains and of peds, laminations and large joints, grains and laminations, and so forth.

At the scale of photographs of large surface exposures, the recorded differential responses of different soils to incident radiation may yield only scalar fabric data; although vector fabric data on soils may be recovered at this scale, they are less likely to be as available as in studies of comparable rock surfaces. Multi-spectral photography of large surface exposures should yield additional useful information in those studies, as it has in so many remote sensing investigations.

At the scale of small surface exposures, say those visible in test pits, shafts, and tunnels, some fabric elements such as layering, jointing and oriented pebbles, can be recorded quite satisfactorily by careful sketching; such fabrics can be recorded more precisely by good-quality photography of the type routinely done in field work by earth scientists and engineers or by macrophotography. Figure 3-46 illustrates some of the types of features that should be recorded.

Color photography is not universally essential; in fact it is usually easier to establish standard sets of mutually comparable black-and-white photographs than to attempt this with color. Photography in 35 mm and 120 formats is probably the most practical in this work. Voids in the exposed surface can be highlighted by impregnation with fluorescent material and illumination with ultraviolet radiation, and then photographed on black-and-white film. A variety of impregnating materials for both dry and wet soils is available for stabilization as well as for fluorescence although this might be more difficult in-situ than in the

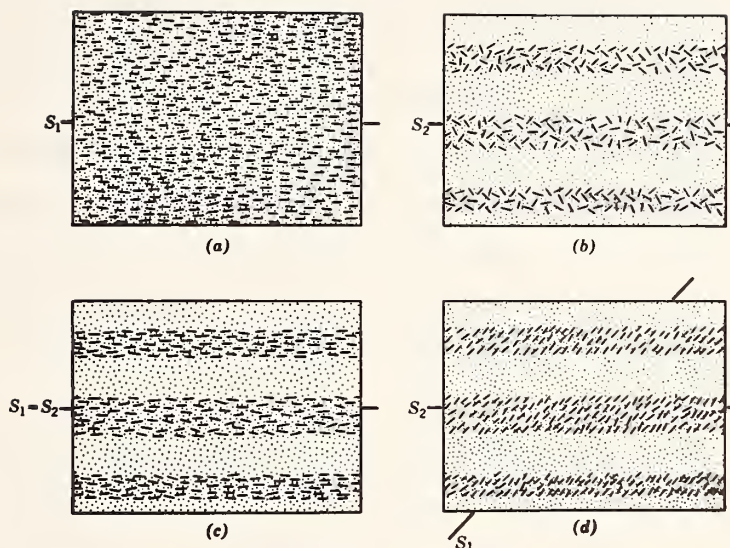


Figure 3-46. Surfaces of discontinuity or heterogeneity defined by preferred orientation and preferred location of fabric elements (Turner and Weiss, 1963).

- a) Preferred orientation alone
- b) Preferred location alone
- c) Combination of a) and b)
- d) Combination of a) and b) defines two surfaces oblique to each other.

laboratory. Recording of fabrics in-situ with acetate peels might be very effective; whether or not prior stabilization by impregnation will commonly be necessary is not known at this time.

The scale of small surface exposures grades into that of samples, such as the pedographer's soil monolith (.67m x .15m x .10m); (26in. x 5.9in. x 3.9 in.) and so-called undisturbed core samples, and the techniques for mapping the fabric are much like those to accomplish microscopic work in the laboratory, where conditions for recording the fabric can be more carefully controlled and the use of high-resolution photographic equipment is more feasible. Inherent in working with samples is the hazard of destroying fabric elements, particularly of the vectorial type, in sampling and subsequent processing of samples.

Samples used for microscopic and x-ray analyses may yield valuable information at the intragranular scale. Some features studied at this scale (fractures, dislocations, etc.) can be handled much the way they are in larger samples, but some of the techniques used (optical and x-ray diffraction) yield aggregated data directly. The preparation of thin sections of soils can be accomplished routinely, but it is not known to what extent the preparation of thin sections will diminish the ability to resolve slight differences in vectorial fabrics.

All plans for mapping fabrics exposed in surfaces, other than at aerial scales, should provide the opportunity to map fabrics on three mutually perpendicular surfaces bounding presumably homogeneous materials. This might not be practical to achieve in test pits, shafts, and tunnels, but it should be relatively easy to achieve down to the scale of the thin section. As the specimens become smaller and approach a size only a few times larger than the elements of a subfabric, the specimens become, effectively, less



homogeneous; this could present some problems in optical and scanning electron microscopy. Conventions for collecting and marking oriented rock specimens are shown in Figures 3-47 and 3-48.

If samples can be withdrawn from boreholes without damaging the soil fabric, some consideration should be given to recording the fabric through 360 degrees using acetate peels; this could be done on the surface of the core, or better, on the surface inside the hole.

Fabrics should also be studied from the bottom of a section to the top, particularly in sections where some consolidation has taken place. This could demonstrate, in a practical way, the sensitivity of fabric analysis to important changes in material properties.

The data analysis can follow at least some of the techniques already applied successfully in conventional studies of rock fabrics, e.g., deformation or preferred orientation, if any, of elongated grains and of fractures. In addition, some of the newer techniques used in studying rock fabrics, such as optical diffraction analysis, can be used to characterize preferred orientations, elongations, and concentrations of spatial frequencies (Figure 3-49 and Table 3.4; Figure 3-50). With optical diffraction analysis, it is quite a simple matter to compare fabrics over the whole range of scales mentioned earlier. Much of the photography mentioned can directly provide the input transparencies used in optical diffraction analysis.

Quantitative methods are available for characterizing the information in the transforms, and to compare them with each other. For example, as shown in Figure 3-51, transforms of progressively deformed material can be compared; changes in the width of crack openings and the initiation of fracturing at higher load levels leave their marks on these profiles.



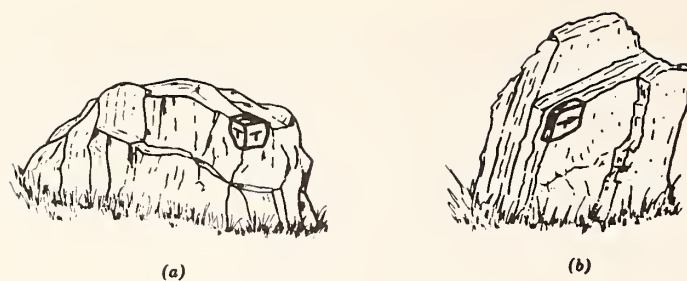


Figure 3-47. Methods of marking oriented hand specimens (Turner and Weiss, 1963).

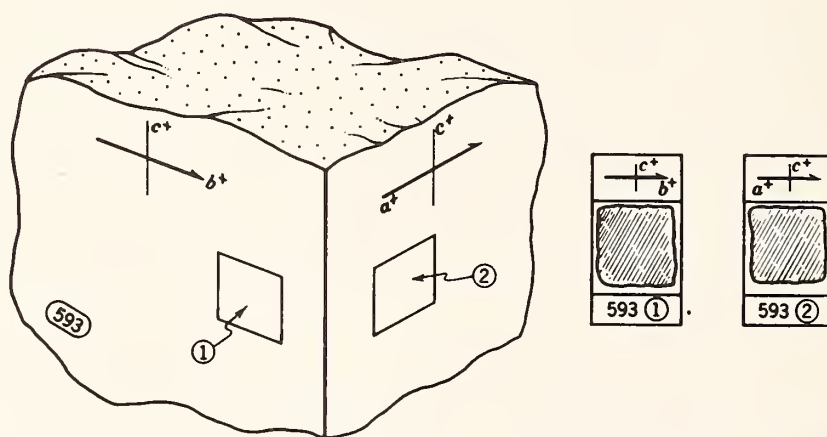
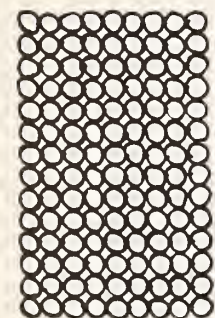
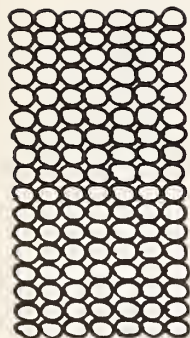


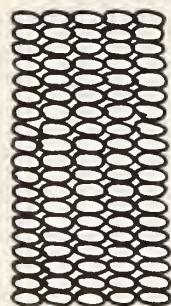
Figure 3-48. Orientation and marking of hand specimen and thin sections (Turner and Weiss, 1963).



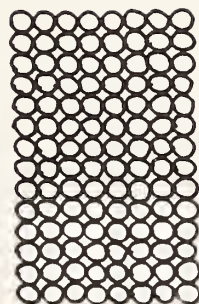
1.0



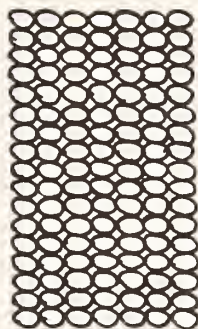
1.3



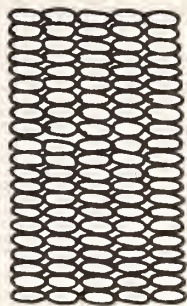
2.0



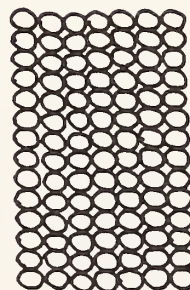
1.1



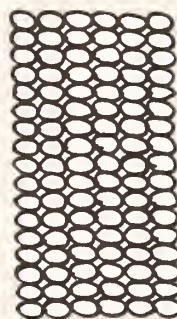
1.4



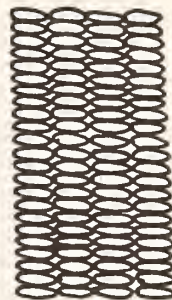
2.5



1.2



1.5



3.0

Figure 3-49a Rectangularly stacked ovals with varying axial ratios (Pincus, 1969a).  
Vertical to horizontal axial ratios (elongations) are shown below  
each stack.

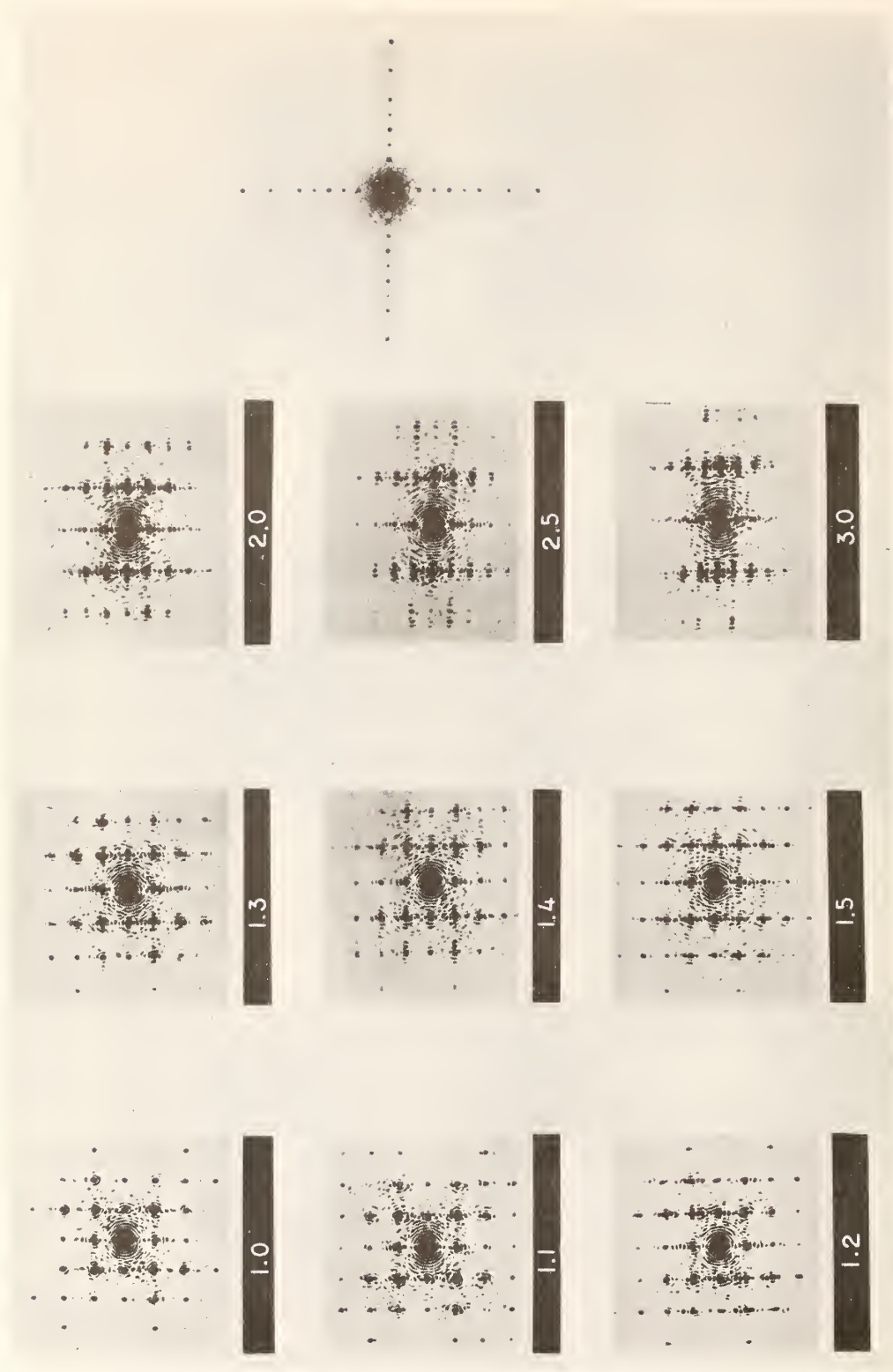
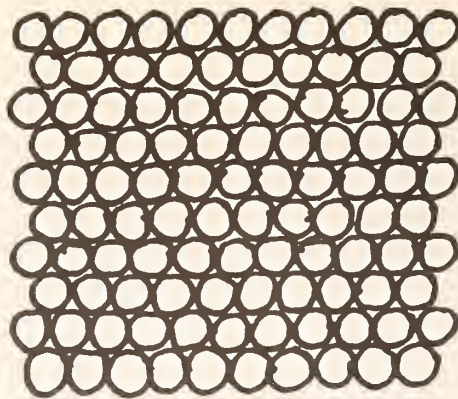


Figure 3-49b Negatives of transforms generated by rectangularly stacked ovals (Pincus, 1969a). (Calibration transform at right)

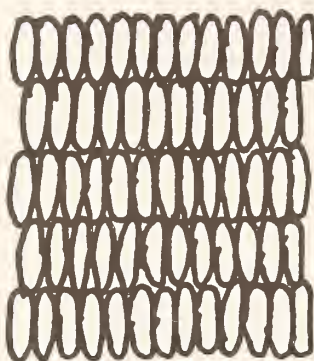
TABLE 3.4

ELONGATIONS OF RECTANGULARLY  
STACKED OVALS (Pincus, 1969a)

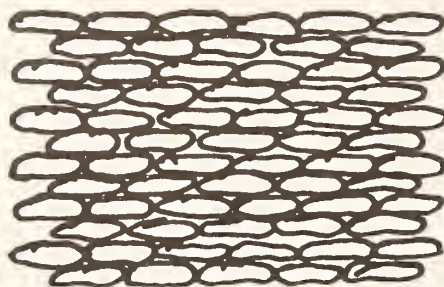
Input ratio	Transform ratio
1.0	0.99
1.1	1.08
1.2	1.23
1.3	1.30
1.4	1.40
1.5	1.49
2.0	1.92
2.5	2.50
3.0	3.05



a) Elongation = 1



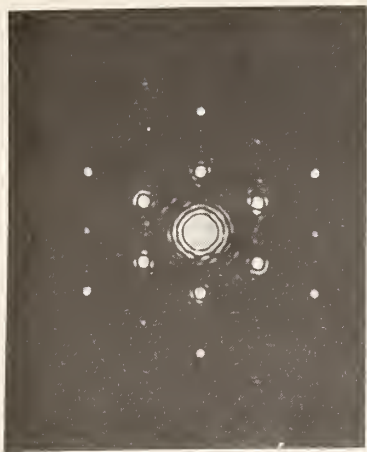
b) Elongation = 3



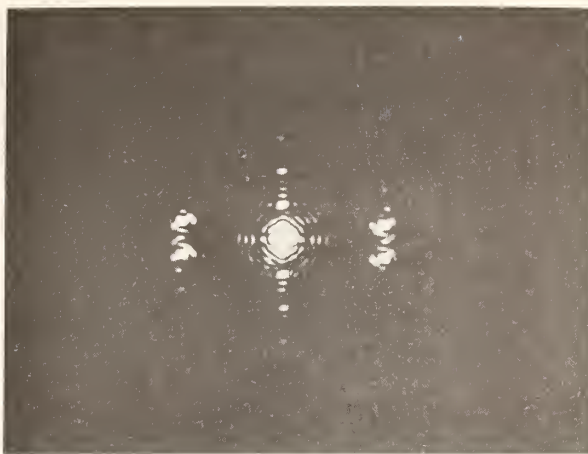
c) Elongation = 3

Figure 3-50a. Rhombic Stacking of ovals: Inputs.

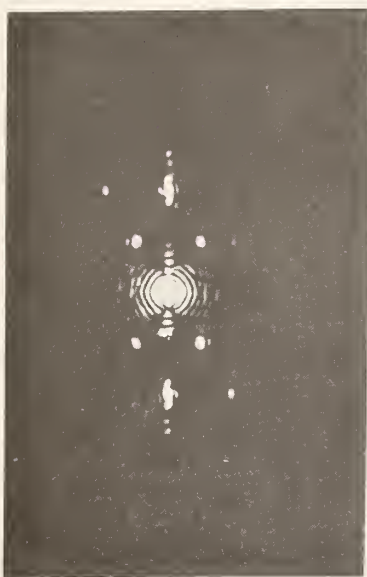




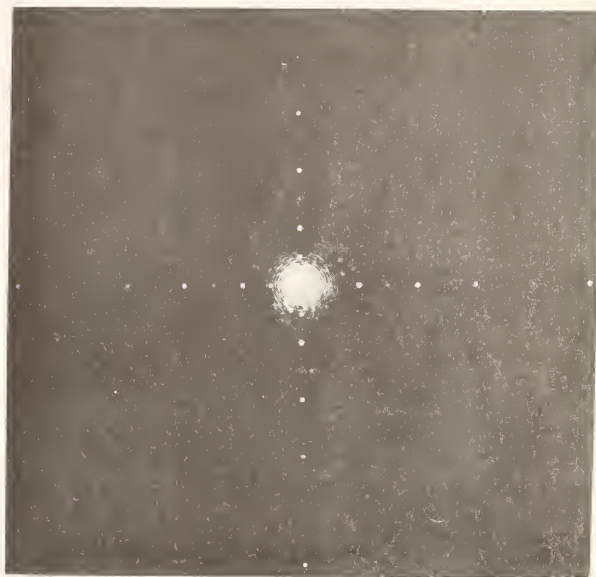
a) Elongation = 1



b) Elongation = 3

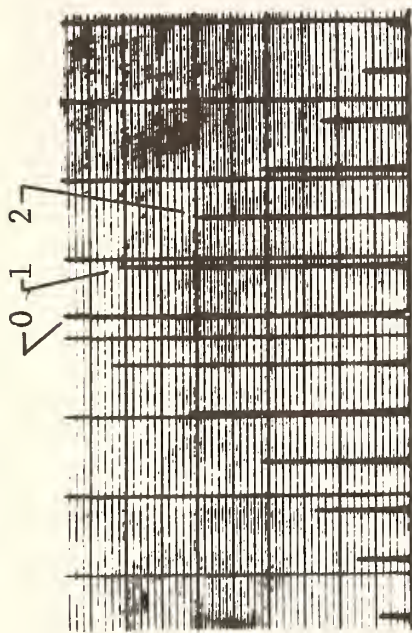


c) Elongation = 3

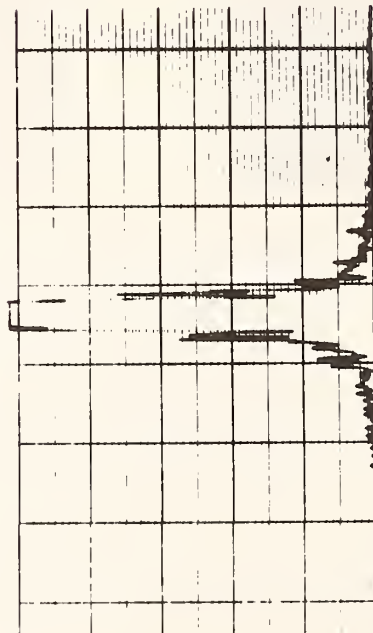


d) Calibration Transform

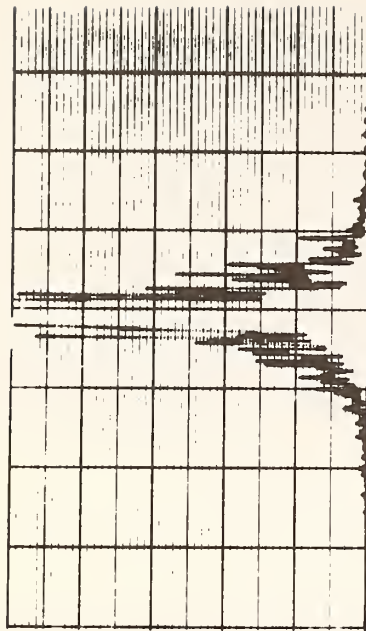
Figure 3-50b. Rhombic Stacking of ovals: Transforms.



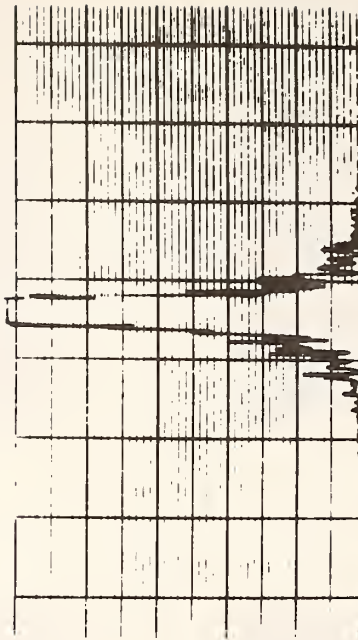
a) Calibration transform;  
0-1 interval is 2.5 lines/mm



c) Transform, load of 7220 psi  
(49.78 MN/m<sup>2</sup>)



b) No load transform



d) Transform, load of 13540 psi  
(93.36 MN/m<sup>2</sup>)

Figure 3-51. Profiles of transforms of deformation experiment, uniaxial compression of Tennessee marble cylinder (Pincus, 1973).

A particularly useful region of the profiles is between the two second-order diffraction spikes, and within that range, the region between the first and second-order spikes is most useful. This corresponds to spacings of 0.40-0.20 mm (or spatial frequencies of 2.5-5 lines/mm) in the inputs. Note that as the specimen goes from no-load to the first-loaded state (b) to (c), the profile becomes smoother and the profile level in the region of the first order spike diminishes. Going from the first- to the second-loaded state (c) to (d), the profile level remains about the same, but the curve becomes rougher. These changes are consistent with the closing up of cracks under initial loading and the onset of new fractures with increasing loading. Profiles (b), (c), and (d) are oriented parallel to the axis of the cylinder, which is also the direction of compression.

To proceed further along the quantitative route, we have devised procedures (Pincus, 1973), which must be clearly understood to be subject to further refinement. Figure 3-52 represents the graphical aspects of this approach.

First note the similarity between Figure 3-52(a) and Figure 3-51, and recall the discussion of Figure 3-51. In Figure 3-52 a), we have smoothed the profile in the region of the first and second-order diffraction spikes. The a-curve is the straight line connecting the ordinates of the smoothed curve at the positions of the first and second-order diffraction spikes, for the transform at load a. The b-curve serves the same purpose for the transform at load b.

Figure 3-52(b) shows the change from an a-curve to a b-curve where the area beneath each from zero-frequency to the x-intercept is a constant; this conservation of area (actually total spatial frequency in this interval) is not required for what follows, but it is useful analytically to determine whether this area is indeed conserved, say in a

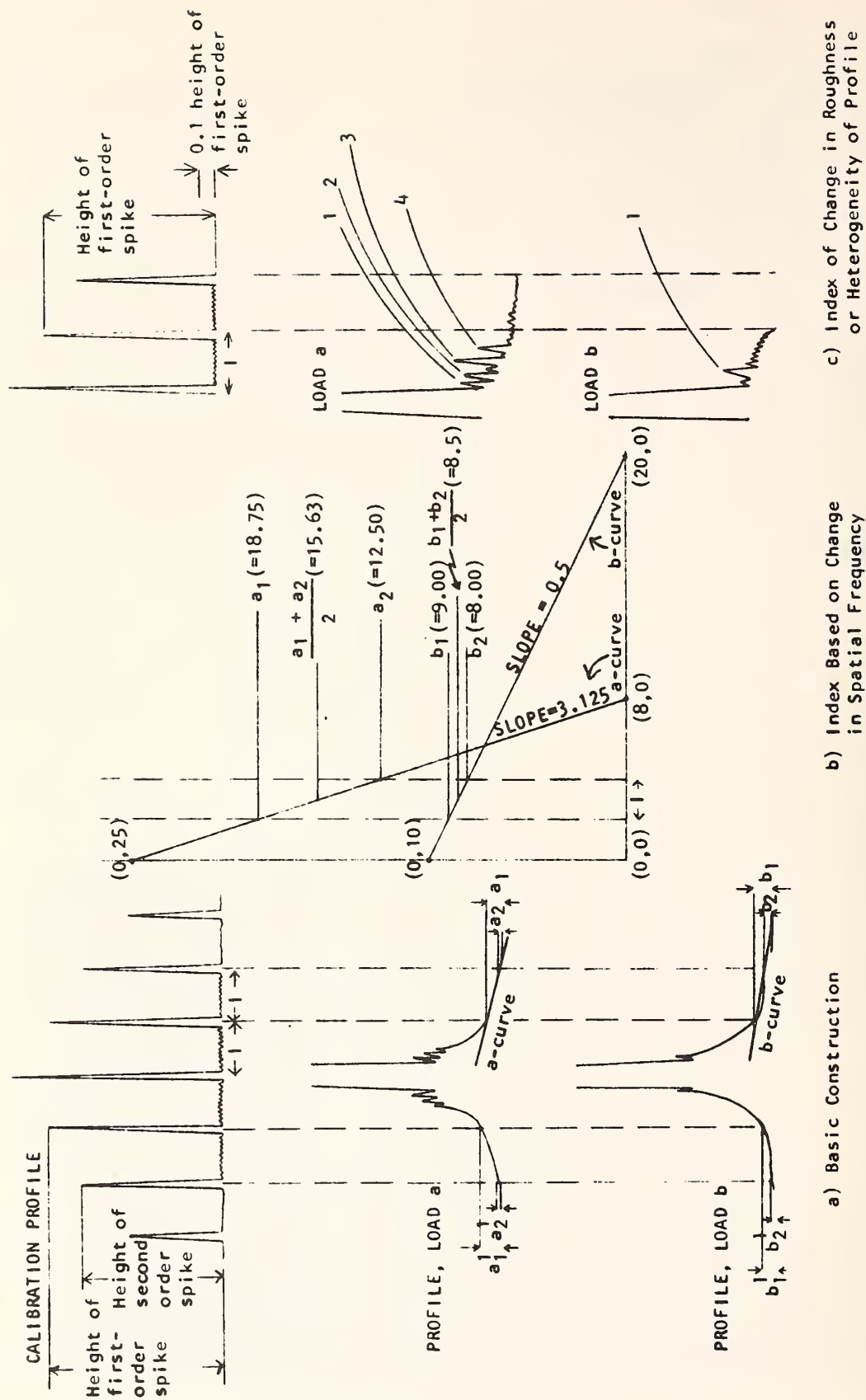


Figure 3-52 Graphical analysis of transform profiles (Pincus, 1973).



deformation series. (The area would not be conserved, for example, where twinning or cleavage develops in calcite grains as observed in our experiments with Tennessee marble; this adds a high frequency component to spatial frequencies already present.)

We then proceed to construct some indexes based on the profile in the interval (I) between the first and second order diffraction spikes.

The relative change in area from the a-curve to the b-curve over the interval I is:

$$\overline{\Delta A} = \frac{1/2 (\bar{a}_1 + \bar{a}_2) / (I) - 1/2 (\bar{b}_1 + \bar{b}_2) / (I)}{1/2 (\bar{a}_1 + \bar{a}_2) / (I)}$$

$$\text{or } \overline{\Delta A} = 1 - (\bar{b}_1 + \bar{b}_2) / (\bar{a}_1 + \bar{a}_2)$$

where  $\bar{a}_1 = 1/2 (a_1 + a'_1)$ ,  $\bar{b}_1 = 1/2 (b_1 + b'_1)$ , etc.

Reading errors for small values of b or a can be minimized by extending the b and a curves, reading the intercepts on the x and y axes, and calculating the b and a values at the first and second order spikes.

When  $\bar{b}_1 \gg \bar{b}_2$  and  $\bar{a}_1 \gg \bar{a}_2$

$$\overline{\Delta A} \approx 1 - (\bar{b}_1) / (\bar{a}_1)$$

When  $\overline{\Delta A} > 0$ , there is a decrease in area over I

$\overline{\Delta A} = 0$ , there is no change in area over I

$\overline{\Delta A} < 0$ , there is an increase in area over I

In Figure 3-52b),  $\overline{\Delta A} = +0.46$ . In this example, areas are conserved. The shift in spatial frequencies is toward higher values (+).

The relative change in slope from the a-curve to the b-curve is



$$\overline{\Delta S} = \left[ \frac{(\bar{a}_1 - \bar{a}_2)/I}{(\bar{a}_1 - \bar{a}_2)/I} \right] - \left[ \frac{(\bar{b}_1 - \bar{b}_2)/I}{(\bar{a}_1 - \bar{a}_2)/I} \right]$$

or 
$$\overline{\Delta S} = 1 - (\bar{b}_1 - \bar{b}_2)/(\bar{a}_1 - \bar{a}_2)$$

when  $\bar{b}_1 \gg \bar{b}_2$  and  $\bar{a}_1 \gg \bar{a}_2$ ,

$$\overline{\Delta S} \approx 1 - (\bar{b}_1)/(\bar{a}_1), \text{ which is also the approximate}$$

value  $\overline{\Delta A}$  under the same conditions. We introduce the notation

$$\overline{\Delta M} = 1 - (\bar{b}_1)/(\bar{a}_1)$$

to identify this expression.

In Figure 3-52(b),  $\overline{\Delta S} = 0.84$  and  $\overline{\Delta M} = +0.52$ .

When  $\overline{\Delta S} > 0$ , there is a decrease in slope over I

$\overline{\Delta S} = 0$ , there is no change in slope over I

$\overline{\Delta S} < 0$ , there is an increase in slope over I

A positive value of  $\overline{\Delta M}$  means a decrease in the first-order coordinate; a negative value of  $\overline{\Delta M}$  means an increase in the first-order coordinate.

Finally, Figure 3-52 (c) presents the basis for an index based on change in roughness or heterogeneity of transform profiles. Here, we work in the interval between the DC spike (zero frequency) and the first-order spike. The index is defined as

$$\overline{\Delta R} = (\bar{r}_a - \bar{r}_b)/(\bar{r}_a) \text{ or } \overline{\Delta R} = 1 - (\bar{r}_b/\bar{r}_a)$$

where  $r_a$  = number of spikes between DC (zero frequency) and the first-order spike with height  $\geq$  some constant, specified fraction of the height of the first-order spike, for load a.

$r_b$  = same as for  $r_a$  , for load b.

$\bar{r}_a$  = mean value of  $r_a$  for both sides of the profile.

$\bar{r}_b$  = mean value of  $r_b$  for both sides of the profile.

In Figure 3-52(c), the constant fractional value of the first-order spike is taken at 0.1, and  $\bar{\Delta R} = +0.75$ .

In our work in rock mechanics, the constant fractional value actually used is  $10^{-5}$ , because several scale changes are necessary to chart spike amplitudes for the very intense calibration transform profile and the transform profiles of the rock fabrics studied. All of the transforms of rock fabrics are run with identical instrumental and optical settings.

When  $\bar{\Delta R} > 0$ , there is a transition to a smoother profile.

$\bar{\Delta R} = 0$ , there is no change in roughness.

$\bar{\Delta R} < 0$ , there is a transition to a rougher profile.

Changes in magnitude but not sign of any of these indexes are easily interpreted. For example, suppose that in a deformation series we calculate a  $\bar{\Delta R}$  for the first loading point with respect to zero load and find it to be positive. Then suppose that we calculate the  $\bar{\Delta R}$  for the second loading point with respect to zero load and find it also to be positive but smaller than the first  $\bar{\Delta R}$ . This means that the transform profile becomes smoother from zero load to first load and less smooth from the first load to the second. All of the foregoing operations can be digitized, thereby increasing the volume of the data that can be handled. Experiments like the one shown in Figure 3-53 can be treated in this way. (Note that even without profiling, the transforms in Figure 3-53(b) clearly show changes in spatial frequency and, at some levels of loading, evidence for preferred orientation).

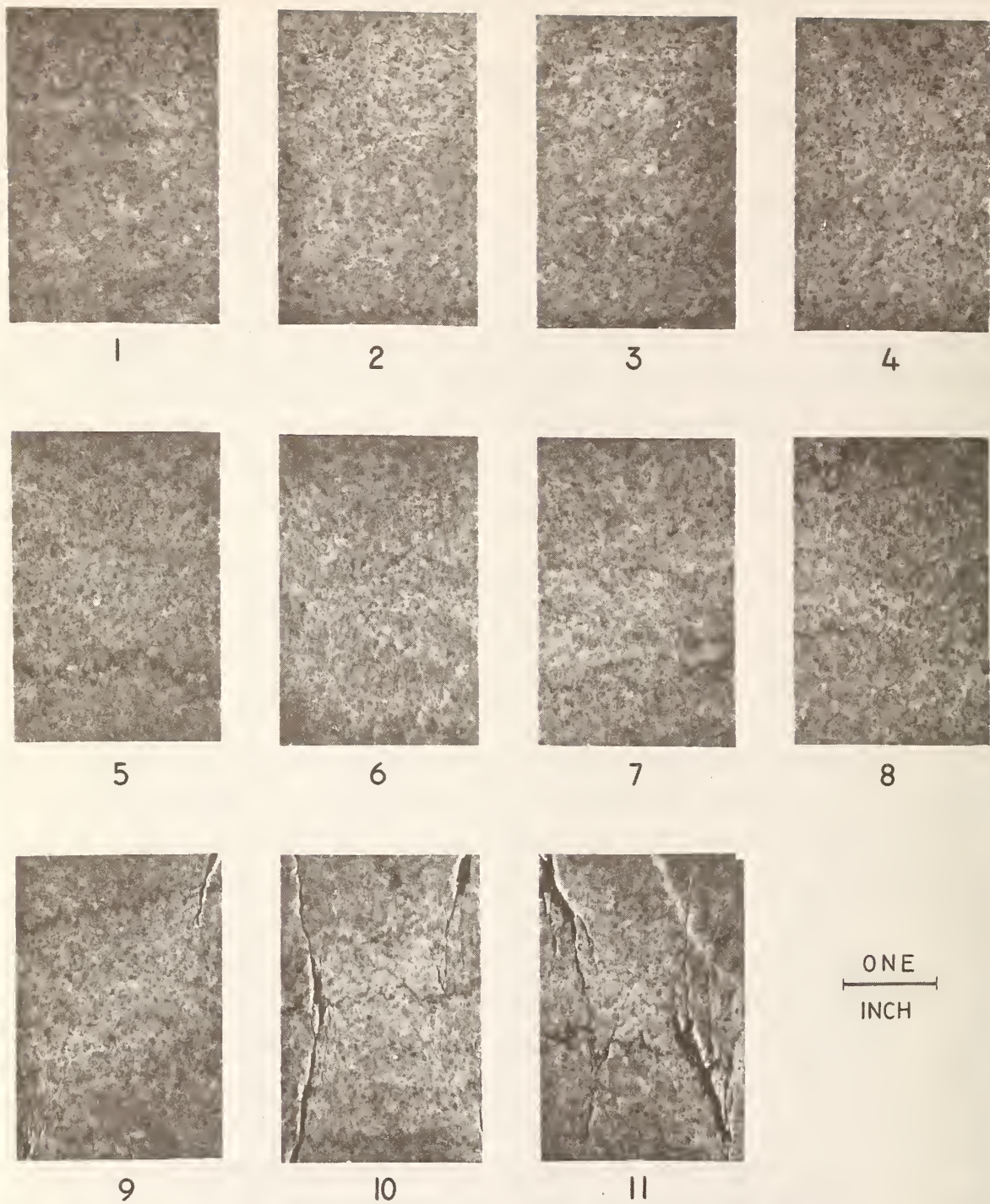


Figure 3-53a. Negative photographs of series of uniaxially loaded specimens of Tennessee marble. Strain increases from 1-11 (Wawersik, 1968), (Pincus, 1969a).





Figure 3-53b Transforms of uniaxially loaded specimens 1-11 of Tennessee marble. #12 is calibration transform. Transforms have been rotated 90° (Pincus, 1969a).

Finally, Figure 3-54 shows that the specimen surface need not be planar to achieve useful results. In this case, we are looking at the surface of a cylinder. Cylindrical soil samples could be processed in the same way. To avoid propagation of projection errors in calculating indexes such as  $\overline{\Delta A}$  or  $\overline{\Delta S}$ , it is advisable to generate the transform from that part of the image of the cylinder in which the photographed surface departs no more than moderately from perpendicularity with the line of sight.

### 3.8 FIELD SAMPLING

Any sampling scheme should be designed to optimize the information/cost ratio with respect to the collection of samples and the collection of data from in-situ surfaces.

The same principles that apply to location, recovery, and logging procedures in collecting samples as a part of an engineering soil exploration program also apply here, in general. The considerations governing location and spacing of say, inforatory, main, and supplementary borings, and of test pits, shafts, and tunnels, are appropriate here. These considerations can be thought of as being generally necessary, but they will usually not be sufficient.

In sampling for fabric studies, orientation considerations are quite important. Thus, completely oriented samples should be collected; and accordingly it might be necessary to get as many as three mutually perpendicular oriented cores at a site where conventional exploration would require only one unoriented sample. It might be advisable where a test pit is dug to collect data from in-situ surfaces, to put additional effort into maintaining planar faces and in trying to cut these to be as nearly mutually perpendicular as is practical. Where fabric is clearly directional, the long axis of a test pit or the axis of a test tunnel might better be oriented perpendicular to the dominant megascopic fabric than in some random or "convenient" direction.



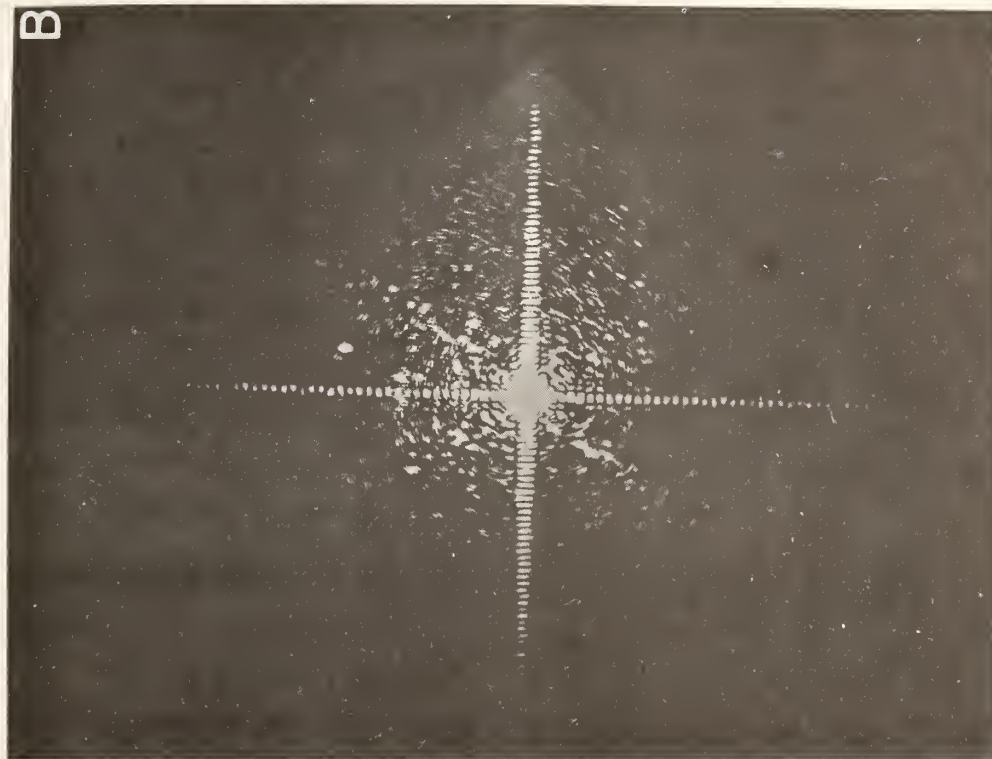
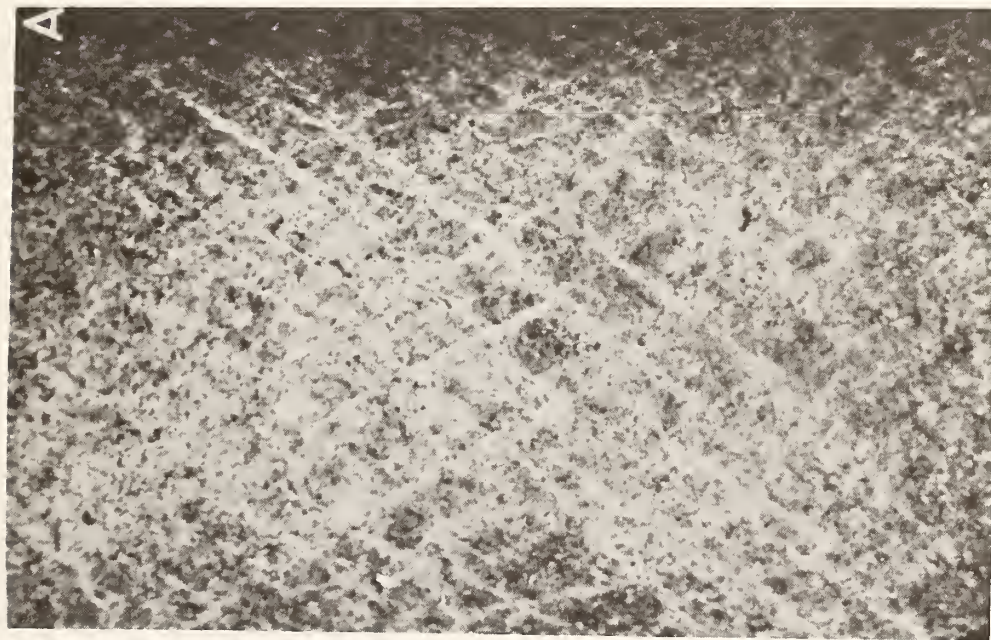


Figure 3-54 Surface of triaxially loaded cylindrical specimen of Tennessee marble, and its transform, rotated 90° (Pincus, 1969a; input from Wawersik, 1968).

The collection of the rectangular soil monoliths used by pedographers might turn out to be much more efficient for fabric studies than are the "undisturbed" core borings of engineering. The soil fabrics are less likely to be disturbed by monolith sampling and the mutually perpendicular planar faces of both the monolith and the matching in-situ faces are both amenable to replication and interpretation. The size, shape, and orientation of the monoliths are also more readily varied than are the corresponding attributes of conventional undisturbed soil samples. Typical monolith dimensions, 1 to 2 ft x 6 in. x 4 in. (.30 to .60 m x .15 m x .10 m) can be varied to say, cubes of the same volume, that is, 8.3 in. (.21 m) or 6.6 in. (.17 m) on each side, where nothing is known about orientation of fabric or mechanical anisotropy. Elongated monoliths could be cut with their long axes perpendicular to the dominant megascopic fabric or to prominent planar heterogeneities, or in some direction (such as vertical) that might have some special significance for soil mechanics property testing or for purely design or construction requirements.

In determining the size of any surface studied, whether this be in samples or on in-situ faces, it appears wise to adopt a requirement that is an adaptation of ASTM practices regarding sample sizes of soil and rock specimens prepared for mechanical testing. That is, the minimum dimension or span of any surface studied should be at least 10 times the maximum dimension of the largest fabric element in any subfabric of interest in the study.

Further, the size of surface to be studied as a unit sample of fabric should not be extended to include materials that will render the sample heterogeneous, unless the purpose of extension is to contrast fabrics (Figures 3-4 and 3-5). This puts a maximum limit on the permitted surface dimensions.

Spacing or density and pattern of samples and of in-situ surfaces studied will depend on purposes of the investigation and characteristics of the soil, particularly on its heterogeneity and anisotropy. Both the physical collection of samples and the collection of fabric data from in-situ surfaces must be regarded as the sampling of fabric data, and accordingly must be coordinated.

A soil with planar banding (Figure 3-6), for example, should have smaller spacings perpendicular to the banding than parallel to the banding, if banding is deemed to be a legitimate object of concern. A soil with curvilinear banding may require a curvilinear sampling grid.

The sampling scheme should be designed three-dimensionally to sample from the entire volume of materials likely to influence the design and performance of the engineering structure. Ordinarily, sampling density should vary directly with heterogeneity gradient, but many exceptions to this guideline, chiefly for practical reasons, will arise. The sampling scheme should also provide for sequential alteration of the sampling grid to optimize the information return without vitiating the basic sampling design and without increasing the cost of the sampling operation; the most important ingredient here is commonsense field judgement.

Collection of soil samples can serve the dual purposes of fabric analysis and mechanical property testing in the laboratory. Collection of fabric data from in-situ surfaces has the advantage of providing data from material less likely to be disturbed; also, much data can be coordinated with data from in-situ property tests and with data on residual stress.



### 3.9 RECOMMENDATIONS

Expectations for determining principal stress directions and magnitudes and stress and strain history have been discussed in 3.2. At this time it appears that progress in refining determination of principal stress directions is likely to be greater than determination of absolute stress magnitudes. Determination of relative magnitudes of principal stresses involves about the same level of difficulty and is in fact part of the same problem as determining principal orientations.

It is very likely that some situations will not yield any success with regard to any of the three major objectives (directions, magnitudes, history). It should be feasible, with additional study, to spell out quite explicitly the conditions that will permit successful determination of any of the three, to specified accuracies.

Some experimental work that might superficially appear to be quite academic could have very important practical payoffs. For example, fabric studies in conjunction with in-situ vane shear tests would be very helpful in evaluating quantitatively the strain history along a variety of shear surfaces and zones.

In contemplating the task components outlined in Table 3.5, each listing can be shown to be actually or potentially useful. It is most unlikely that every technique investigated will turn out to be practical in terms of cost-effectiveness and some techniques, if not discarded, will have to be modified to be practical. Those techniques that do prove practical should be classified, in the final stages of the work, according to relative reliability, cost in dollars and time, and genetic relationship to standard soil mechanics tests and properties. We anticipate that we can shed light on the basis in microfabrics, for example, for the values of Atterberg limits and the like.

Table 3.5

## OUTLINE, RECOMMENDED FABRIC ANALYSIS

TASK I - Laboratory and Experimental Work		Task I	P.I.*	<u>Man-Years</u> A.I. R.A.	
<u>Materials</u>					
Cohesive Noncohesive Wet Dry Frozen Soil-rock transitions Homogeneous vs. Heterogeneous Isotropic vs. anisotropic Variety of primary fabrics	<u>Loading</u>				
	Uniaxial	Yr. 1	1/2	1/4	(2 x 1/2) = 1
	Triaxial (Polyaxial?)				
	Static				
	Dynamic				
	Unremolded and remolded	Yr. 2	1/4	1/8	1/2
	Atterberg limits				
	Vane shear				
	Superposition of 2 or more loading episodes				
TASK II - In-Situ		Task II	P.I.	A.I.	R.A.
<u>Materials</u>					
See I, above	<u>Loading</u>	Yr. 2	1/4	1/8	1/2
	Simulated Natural				
	Unloading Simulated structures	Yr. 3	1/4	1/8	1/2
TASK III - (I + II) and		Task III	P.I.	A.I.	R.A.
Increase resolution Increase effectiveness Approach real operating conditions		Yr. 3	1/4	1/8	1/2
		Yr. 4	1/2	1/4	(2 x 1/2) = 1
		Yr. 5	1/2	1/2	1/2

\* P.I. - Principal Investigator  
A.I. - Associate Investigator  
R.A. - Research Assistant



Table 3.5 (Cont'd.)  
MAN - YEAR SUMMARY RECOMMENDED  
FABRIC ANALYSIS STUDIES

	<u>P.I.</u>	<u>A.I.</u>	<u>R.A.</u>	<u>Total</u>
Yr. 1	1/2	1/4	1	1 3/4
Yr. 2	1/2	1/4	1	1 3/4
Yr. 3	1/2	1/4	1	1 3/4
Yr. 4	1/2	1/4	1	1 3/4
Yr. 5	1/2		1/2	1
Totals	2 1/2	1	4 1/2	<u>8 *</u>

Additional hourly help (technical and clerical support),  
an average 1/4 - 3/8 man-year per year, will also be required.

Tasks, objectives, milestones, and estimated net results are outlined in Table 3.6. The first two-year unit (Task I) will concentrate on experimental work in the laboratory, with some minor initial field work. Task II, the second two-year unit, will overlap the first unit by one year, and will move the experimental work into the field. Task III, the first year of which will overlap the second year of Task II, will last two to three years; in addition to moving the work directly into the realm of practical operations, Task III will also concern itself with increasing resolution and decreasing data acquisition costs in terms of time and money. Task III should be coordinated closely with operations in the nonfabric components of the program, although some such coordination should prevail at a meaningful level throughout the project's life.

Of course, sufficient flexibility should be built into the program to allow for shifting emphasis and for accommodation to exploit breakthroughs in both fabric and nonfabric components of the program and to utilize advances developed outside the program. Year 5 is, as is to be expected, the most uncertain. This could range from 0 to 2 man-years, depending on what happens in years 1-4.

Table 3.6

## OBJECTIVES, MILESTONES, AND RESULTS

TASK	OBJECTIVE	EXAMPLES (Not Inclusive)	MILESTONES (Not Inclusive)	ESTIMATE OF NET RESULTS	REMARKS
I - Laboratory and Experimental work	Under close control of state of stress and initial soil properties, search for demonstrable relationships between stress parameters (magnitude, direction, and time-variation or history) and responsive fabric parameters.	<p>a) Relationships between magnitude of load and grain orientation, starting with material with no preferred grain orientation; plot degree or preferred orientation vs. load magnitude. Then repeat, varying time-rate of loading.-----</p> <p>Replicate all of above for dry and saturated material, coarse and fine material, cohesive and non-cohesive material, etc.-----</p> <p>Then use materials with initial preferred grain orientation and replicate the above, varying in addition the orientation of the load with respect to fabric orientation.-----</p> <p>Replicate above for other fabric elements and parameters (void orientation and elongation, crack orientation and spacing, etc.)</p>	<p>1) Statistically significant correlation between degree of preferred orientation and load magnitude and loading rate.</p> <p>2) Estimate of confidence for predicting direction of maximum load to within 30° from direction of preferred orientation of fabric; ditto above to within 10°</p> <p>3) Establish relative sensitivity rankings for fabric elements and fabric parameters</p> <p>4) Rank soils in unified soil classification according to suitability for estimating magnitude and direction of stress field, as inferred from experimental work.</p>	<p>A) Orientation of maximum load estimated with confidence to within 30° and possibly to within 10°, for some materials. (Results will vary with material, load magnitude, loading rate, etc.).</p> <p>B) Estimation of load (or stress) magnitudes likely to be more difficult, and probably not practical in many cases. (Ditto for loading rates)</p> <p>C) Major events in stress history not likely to be completely identified, unless different fabric elements have been affected in each event, and direction of maximum loading varies from one event to the next.</p>	<p>Replications cited in the "examples" column will not necessarily require separate experiments. For example, more than one fabric element can be studied during a single loading experiment.</p>

Table 3.6 (Cont'd.)

OBJECTIVES, MILESTONES, AND RESULTS

TASK	OBJECTIVE	EXAMPLES (Not Inclusive)	MILESTONES (Not Inclusive)	ESTIMATE OF NET RESULTS	REMARKS
I-(continued)		b) Relationships between changes in fabric and Atterberg limits, for a range of soil types.	1) Identify fabric elements and fabric parameters most sensitive to soil consistency variations. 2) Identify initial fabric elements and parameters that are reliable predictions of consistency indexes and conversely, index values that are reliable predictions of fabric.	A) An explanation in terms of microfabric changes, of variation in soil behavior as manifested in evaluating atterberg limits. B) As a consequence of A), a better understanding of when atterberg limits are likely to be of real usefulness.	Much the same approach can be used with other property tests, such as vane-shear, etc., in Task II below.
II Work In-Situ	Under moderate control of state of stress, and using selected sites to provide satisfactory materials, search for same relationships as under I above; range of variables will be limited by design (From knowledge gained from I above) and by field constraints.	a) Same as a) above, with more restricted range of variables, using field loading experiments.	3) Relate milestones associated with b) to those related with a) above. Same as 1)-3) above, associated with Task I, example a), with qualifications imposed by field relations and field conditions.	Same as A)-C) above associated with Task I, example a), but with smaller likelihood of success in B) and C)	"Loading," as used in this task includes also unloading, where appropriate and feasible. ----- Model studies might also be included.



Table 3.6 (Cont'd.)

OBJECTIVES, MILESTONES, AND RESULTS

TASK	OBJECTIVE	EXAMPLES (Not Inclusive)	MILESTONES (Not Inclusive)	ESTIMATE OF NET RESULTS	REMARKS
III - Combination and reconciliation of I and II and testing under real or almost-real operating conditions.	Using results of I and II, and incorporating refinements based on prior evaluations, apply the most effective approaches in real or almost-real operating conditions, and arrive at final identification of critical parameters and evaluation of resolution and effectiveness of "best methods."	In areas with known loading or unloading histories (either from man-made structures or from geological processes) investigate some of the same relationships as in Task I, example a) and Task II, example b) above. Time-dependence can be investigated in some excavations.	Same as for Task II, plus final review and evaluation.	Same as for Task II, plus final review and evaluation.	Coordinate results with IITRI developments in Tasks I-III, but especially in Task III.

## 4. ELECTROMAGNETIC RESONANCE

### 4.1 INTRODUCTION

As used in this study, electromagnetic resonance (EMR) is defined as any technique that exploits the absorption of electromagnetic energy by resonating centers. A variety of resonant centers are available in soil; all absorb energy at characteristic frequencies. Examples of such centers include polar molecules such as water, nuclear magnetic moment, nuclear quadrupole, and electron spin. The frequency at which a particular center resonates depends on its type and environment. The environment of a resonant center may include crystal lattice distortion, the distance separating resonant centers, the strains imposed on molecular bonds and other considerations that reflect gross mechanical stress or grain orientation. Electromagnetic resonance is separated into the three major branches: Nuclear Magnetic Resonance (NMR), Electroparamagnetic Resonance (EPR or ESR) and Nuclear Quadrupole Resonance (NQR).

### 4.2 NUCLEAR MAGNETIC RESONANCE

Nuclear magnetic resonance is for the investigation of atoms having a nonzero nuclear magnetic moment. The technique measures the rate at which the magnetic moment precesses about an external magnetic field. Approximately 175 different isotopes of the elements have the necessary nonzero magnetic moment and, in theory, are observable by NMR spectroscopy. Many of the elements that are found in soil samples (Table 4.1) theoretically provide suitable species for NMR study. There are, however, many factors that must be considered in deciding the suitability of an isotope for NMR investigation.

The important parameters used in determining if an NMR study of a particular isotope is feasible are natural abundance of the isotope and relative sensitivity. If the values for these two parameters (Table 4.1) are

Table 4.1  
NMR-ACTIVE ISOTOPES<sup>a</sup>  
FOUND IN SOIL SAMPLES

Isotope	NMR <sup>b</sup> Frequency (MHz)	Natural Abundance (%)	Relative Sensitivity	Magnetic <sup>c</sup> Moment	Nuclear Spin
<sup>1</sup> H	42.5759	99.9844	1.0000	2.79268	1/2
<sup>13</sup> C	10.705	1.108	1.59 x 10 <sup>-2</sup>	0.70220	1/2
<sup>14</sup> N	3.076	99.635	1.01 x 10 <sup>-3</sup>	0.40358	1
<sup>17</sup> O	5.772	3.7 x 10 <sup>-2</sup>	2.91 x 10 <sup>-3</sup>	-1.8930	5/2
<sup>27</sup> Al	11.094	100.	0.206	3.6385	5/2
<sup>29</sup> Si	8.458	4.70	7.84 x 10 <sup>-3</sup>	-0.55477	1/2
<sup>25</sup> Mg	2.606	10.05	2.68 x 10 <sup>-3</sup>	-0.85471	5/2
<sup>43</sup> Ca	2.865	0.13	6.40 x 10 <sup>-2</sup>	-1.3153	7/2

<sup>a</sup>After NMR Table by Varian Associates 5th Edition (1965)

<sup>b</sup>At a field strength of 10,000 Gauss

<sup>c</sup>In units of Bohr magnetons (Bohr magneton =  $eh/4\pi Mc$ )

multiplied any isotope with a combined value of less than 0.1 are considered very difficult to detect with current instrumentation, excluding fast Fourier transform and computer averaging techniques. With computer averaging and FFT, isotopes with a combined value of less than  $10^{-3}$  become undetectable.

A second consideration is the sample and sampling techniques. Commonly NMR is done in the liquid phase to improve the homogeneity of the magnetic field and also to decrease the magnetic interaction between isotopes which are near each other. IITRI is currently engaged in perfecting a high resolution NMR technique for studying solid samples by NMR. This is an attempt to extend the work of E. R. Andrews (1971), who has done extensive work on the technique. The successful completion of this work may make it very attractive for the study of species found in soil and the interaction of these species under stress. At present, the broad lines one observes in the solid state limit the amount of information that can be obtained from the sample.

It would be desirable to be able to investigate stresses and the preferential orientation into planes of the crystallites. The resulting effect on the nuclei is to

- (1) distort the environment in which the nuclei occurs and
- (2) to move the nuclei relative to one another.

The first will have little effect on an NMR spectrum characterized by broad lines. Much higher resolution will be necessary to observe the result of small perturbations in the field of the nucleus by distortion of the crystal lattice. The necessary preliminary work on such a high resolution technique is being done at IITRI.

The second change is also not usually observed in most isotopes other than  $^1\text{H}$  and  $^{19}\text{F}$ . Cook (1972) reports that the line width "second moment" is often proportional to  $r^{-3}$ , the inverse cube of the distance separating the



resonating protons. Since this distance changes under mechanical stress, NMR may be used, at least in principal, to measure stress.

The largest drawback to the use of NMR, especially for in-situ studies, is the need for a large stable magnetic field. The sensitivity of an NMR spectrometer is directly related to the strength of the magnetic field (i.e., the flux measured in Gauss). This is dictated by the theory of Boltzmann distributions and the conditions for observing NMR resonance transitions. Suggestions have been made that the earth's magnetic field could be used, however, with a field strength of less than 1 Gauss as compared to that of the average NMR spectrometer (14,000 Gauss), it is easy to see that the sensitivity would be exceedingly low and that detection would require a more complex electronics package than is now feasible.

#### 4.3 NUCLEAR QUADRUPOLE RESONANCE

The nuclei of certain atoms behave as if their charge were distributed over a spheroid instead of a sphere. This charge distribution, which behaves like an electric quadrupole, will experience a torque in an electric field gradient. Such gradients are produced by the atoms' electron cloud and by charged particles near by in the crystal lattice. These provide a natural field about which the quadrupole precesses at a characteristic Larmor frequency. Because the electric field gradient is sensitive to the distance of the charges in adjacent atoms, NQR should be sensitive to volume changes, hence the mechanical stress in the crystal. Nuclear quadrupole resonance is similar to NMR, except that no external magnetic field is required.

Cook reports that the resonant frequency in crystals usually increases with pressure and notes that changes reported in the literature are on the order of 1 Hz/psi.

The bulk of this work has been done on optically clear gem-quality semiprecious stones or relatively rare minerals. Some success has been found with powdered samples if sophisticated techniques are employed. It appears that NQR is a promising tool provided techniques applicable to soils can be developed.

Therefore, NMR may be appropriate for future use in studying stresses in soil for model systems. Continued efforts in the field of high resolution solid NMR is imperative and may possibly yield results which will allow for the development of an in-situ method.

#### 4.4 ELECTRON PARAMAGNETIC RESONANCE

Of the three main branches of magnetic resonance, EPR is unique in that it detects or observes the electrons of an atom, and unlike NMR or NQR, can directly investigate the effect produced by changes in the environment of electrons, the actual participants in molecular bonding. This property will be useful in evaluating the strains imposed on selected molecular bonds. It is expected that empirical relationships can be found between the soil effective stresses and the response of those unpaired electrons associated with some molecular bonds. The soil effective stresses contribute to forces on individual soil grains, resulting in distortion in molecular bonds. This distortion of resonant centers provides a potential mechanism by which EPR may be employed to measure soil stresses if appropriate centers can be found or created. There are reproducible differences between tetrahedral  $\text{SiO}_4$  in quartz tubing and in kaolin clay. These differences are associated with the differing environments in which the paramagnetic species is situated. The line width is a measure of the degree of crystallinity. The quartz, being a highly crystalline form of silica, has the narrowest line widths. The silica in kaolin clay is probably distorted from pure tetrahedral by being included in a crystallite

with alumina. The presence of the alumina also causes the crystal to be more anisotropic, an effect which produces a broader EPR resonance.

The differences between various forms of soil-related compounds such as calcium carbonate are even more pronounced. Many similarly related forms of calcium carbonate exist. X-ray powder patterns cannot distinguish between them, however, the EPR spectrum of  $\text{Mn}^{++}$ , which substitutes for the  $\text{Ca}^{++}$  ions, can easily identify the various forms. In addition, EPR is not limited to one phase. Solid samples are as easily investigated as liquids and gases. Very small quantities ( $10^{-12}$  mole) or larger samples (0.1 percent in 20 grams of material) can be investigated.

The limitation to the use of EPR in in-situ experiments is, as with NMR, the need for a high-strength magnetic field. However, most transition metal ions produce spectra in the absence of a magnetic field and many examples of "zero-field EPR" are reported in the literature.

Two indirect methods also exist which lend themselves to model studies of stresses in soils and to possible use in in-situ measurements. The first is the use of ionizing radiation to create paramagnetic centers. This method could be applied to the development of an in-situ technique utilizing a  $\gamma$ -source in the field to create paramagnetic centers. A core sample would be removed and, since the molecules were irradiated under a stressed condition, their EPR spectrum might be indicative of the stresses under which the soil was subjected and would be different than for soil similarly irradiated in the absence of stress.

The second technique is more applicable to montmorillonite soils. A paramagnetic ion such as  $\text{Cu}^{++}$  can be exchanged with all exchangeable ions in the soil sample. The  $\text{Cu}^{++}$  ion is then investigated by EPR and the



difference between stressed and unstressed soils would be indicated by differences in the EPR spectrum of the  $\text{Cu}^{++}$  ions.

Of the three tools, EPR affords the best sensitivity to the kinds of differences expected for stressed and unstressed soils. Experimental studies have shown that the potential for developing a successful method of determining stresses in model systems is high. The subsequent utilization of the technique for in-situ measurements depends on the success of the research on model systems.

#### 4.5 EXPERIMENTAL RESULTS

In an attempt to establish that electron paramagnetic resonance (EPR) spectroscopy can be used to investigate resonances arising from defects in soil samples, some preliminary studies were conducted on  $\gamma$ -irradiated kaolin clay. The EPR of kaolin clay (98 percent pure) was investigated at room temperature and at approximately 77 degrees K in its unirradiated state. No EPR resonances were found, indicating that no naturally occurring paramagnetic centers associated with the kaolin crystallites were present. The lack of EPR resonances in the unirradiated state also indicated the lack of paramagnetic impurities existing substitutionally in the kaolin crystallites. Since most soil deposits are not 98 percent pure, it would be expected that actual soil samples would contain many paramagnetic impurities such as  $\text{Mn}^{++}$ ,  $\text{Fe}^{++}$ ,  $\text{Co}^{++}$ ,  $\text{Ni}^{++}$ , and  $\text{Cu}^{++}$  either in interstitial or substitutional positions in the crystal lattice of the various clays and inorganic matter (such as calcium carbonate) from which the soil was composed.

The kaolin clay was  $\gamma$ -irradiated by two  $^{60}\text{Co}$  sources for 2-1/2 hours at a flux of 7500 rads/hour for each source. The total dose was 37,500 rads. Ionizing radiation, such as that produced by  $^{60}\text{Co}$  when done at liquid nitrogen temperatures (77 degrees K) and in a vacuum (50  $\mu$  of Hg



pressure), produces paramagnetic ions which can be observed by EPR spectroscopy. An example of the spectrum obtained for kaolin clay is shown in Figure 4.1. The single asymmetric resonance at  $g = 2.0064$  can be identified with a species occurring in the silica portion of the kaolin lattice. A similar EPR resonance in  $\gamma$ -irradiated quartz glass has been observed in previous experiments at IITRI. The  $g$ -values and line widths vary with the kind of quartz and degree of crystallinity. Both the quartz and kaolin clay contain silicon and oxygen atoms in a tetrahedral arrangement, thus the similarity of the EPR spectra is not surprising.

#### 4.6 RECOMMENDATIONS

Electron paramagnetic resonance holds potential for investigating the environments of specific entities (ions, electron bonds, nuclei) within the soil. Little is known of the EPR response of soil except that it is influenced by stress state. Considerable basic research is required to quantify soil EPR under stress. Baseline soils data, which are not now available, must be acquired by laboratory experimental work. This should be a relatively low-level long-range program. A high level of effort is not justified because of the lack of suitable electronics. Current hardware is bulky and unsuited for use downhole but this drawback will be overcome as electronics packages become smaller and EPR techniques more sophisticated. The general plan should be to first identify paramagnetic centers in several soil types, such as has been done for silica and the  $\gamma$ -irradiated kaolin. Once identified, the response of these centers to such macroscopic conditions as stress, orientation, and moisture can be evaluated. It is anticipated that approximately one man-year of effort will be required for the initial phase and that subsequent work will depend upon the results obtained.

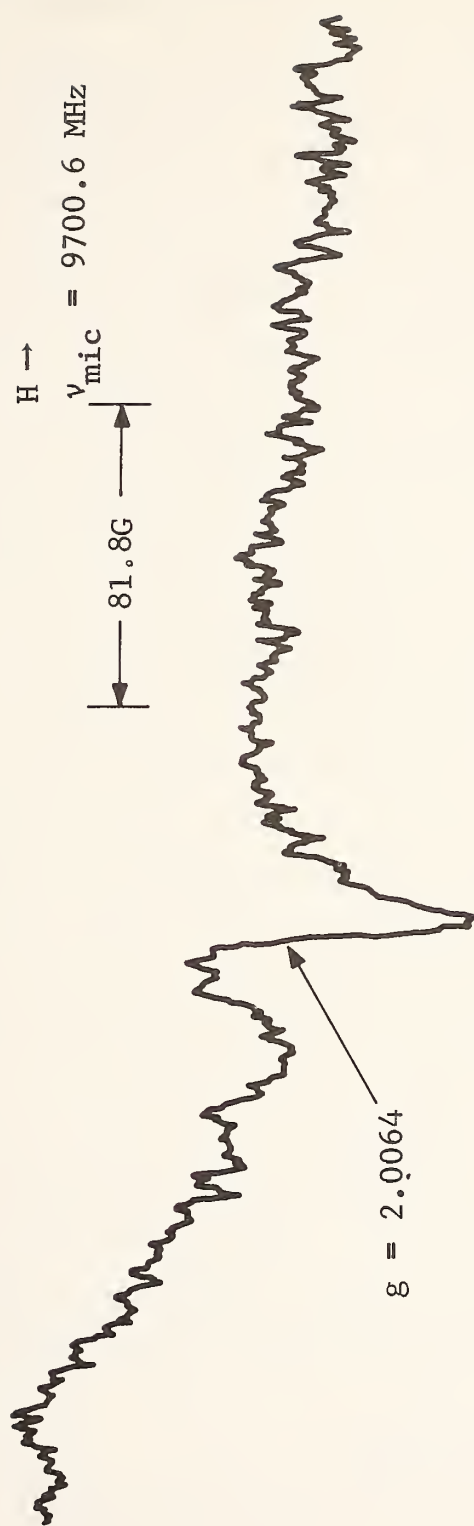


Figure 4.1. EPR Spectrum Obtained from Gamma-Irradiated Edgar Plastic Kaolin

## 5. RECOMMENDED IN-SITU STRESS GAGE DEVELOPMENT

There exists immediate need for hardware capable of measuring the full stress tensor in soil. There currently are no instruments that are capable of making rapid determinations of more than a single component of the in-situ stress tensor. The only instruments known to attempt measurements of multiple stress components are self-boring stress probes currently under development in England and France. These devices employ high modulus interface stress gages in place of pressuremeter bladders. They are otherwise similar to the self-boring pressuremeters previously discussed in Section 2.4.2. The use of high modulus gages results in stress relaxation times of hours, as was previously shown in Figure 2-39. A production rate of one or two tests per day may be acceptable in a research tool, but is inappropriate for a production testing device. Under some conditions a self-boring pressuremeter is a rapid stress measuring tool, but it will be shown that it can not be used if the lateral in-situ stresses are not equal. What is required is a measurement system capable of obtaining the in-situ stress tensor rapidly for a wide range of soil types and stress conditions. Speed of testing means that significant pore-pressure changes should be eliminated, both during placement and operation of the instrument. A rapid drained test results from operating at vanishingly small strains, using low modulus transducers to avoid lengthy stress relaxation delays. The operating parameters during insertion must be simple in theory and operation. Sophisticated development is required to identify, remove or automate those system elements that are operator sensitive, while maintaining an acceptable total system cost.

### 5.1 CRITERIA AND CAPABILITIES

Criteria for such an in-situ stress gage are as follows:

- o Capability for measuring the full stress tensor  $\sigma_1 \neq \sigma_2 \neq \sigma_3$
- o No inherent limitations to operating depth
- o Applicability to a wide range of soil types
- o Measurement accuracy and precision
- o Relatively inexpensive in terms of both time and costs
- o Highly skilled operators not required

These criteria and the state-of-the-art suggest that a method employing direct measurement in-situ should be developed. Regardless of the care with which an "undisturbed" specimen is taken, the in-situ stresses are released when it is removed from its location, and stress measurement must then depend on secondary effects, as in the methods of Skempton and of Poulos and Davis. The disturbance involved in placing a probe in-situ should be reviewed so that the measurements can be made directly on the in-situ stress field.

In addition to the development of new hardware, the precision of the anisotropic vane shear should be evaluated. The simplicity and low cost of this technique are very attractive, so that the small effort required to determine its operating limitations will be well rewarded.

## 5.2 ANALYSIS OF INSERTION DISTURBANCE

### 5.2.1 ANALYSIS METHODS AND ASSUMPTIONS

To support the feasibility of the recommended development effort, preliminary analyses were conducted to evaluate the disturbance associated with probe insertion and operation. While low disturbance devices have been developed and tested by other investigators, (Baguelin and Jezequel, Kenney, and Wroth and Hughes), none was specifically designed for use in a full triaxial stress field, and several were intended to



measure soil stiffness as well as in-situ stress. These devices indicate that probes can be inserted with insignificant disturbance in fine grained soils under  $K_0$  stress conditions.

Six quantities must be measured to fully determine the full stress tensor. Because of the difficulty in making a measurement of in-situ shear stress--recognizing that shear failure occurs on the transducer surface during insertion--the recommended hardware must operate by measuring the normal stress in different directions. Specifically, the stress ellipse in the plane normal to the axis of the probe was selected for measurement. The full stress tensor may be determined by three measurements made with the probe axis in three noncoplaner orientations.

The two dimensional state of stress in a plane is given by the stress tensor

$$\sigma_{\alpha\beta} = \begin{vmatrix} \sigma_{\alpha\alpha} & \sigma_{\alpha\beta} \\ \sigma_{\beta\alpha} & \sigma_{\beta\beta} \end{vmatrix}$$

which requires the measurement of three independent quantities. This tensor contains in-plane principal stresses  $\sigma_{\alpha\alpha}$  and  $\sigma_{\beta\beta}$  regardless of the orientation of the plane. In general, the in-plane two dimensional principal stresses  $\sigma_{\alpha\alpha}, \sigma_{\beta\beta}$  are not equal to any of the three-dimensional principal stresses  $\sigma_{aa}$  unless the plane happens to be normal to a principal direction. The full stress tensor may be obtained from measuring  $\sigma_{\alpha\beta}$  in three directions and solving the simultaneous equations given by the tensor transform  $\sigma_{mn} = a_{im} a_{jn} \sigma_{ij}$ .

For many cases, the vertical may be taken as a principal direction and the vertical stress as  $\sigma_{zz} = \gamma z$ . For these conditions, which are basic to the design of all existing low-disturbance probes, the full stress tensor is

determined by determination of the two dimensional stress tensor  $\sigma_{\alpha\beta}$  in the horizontal plane.

Our analysis is based on the assumption that the hardware will be self-boring, with the features typical of this class of devices (Figure 5-1).

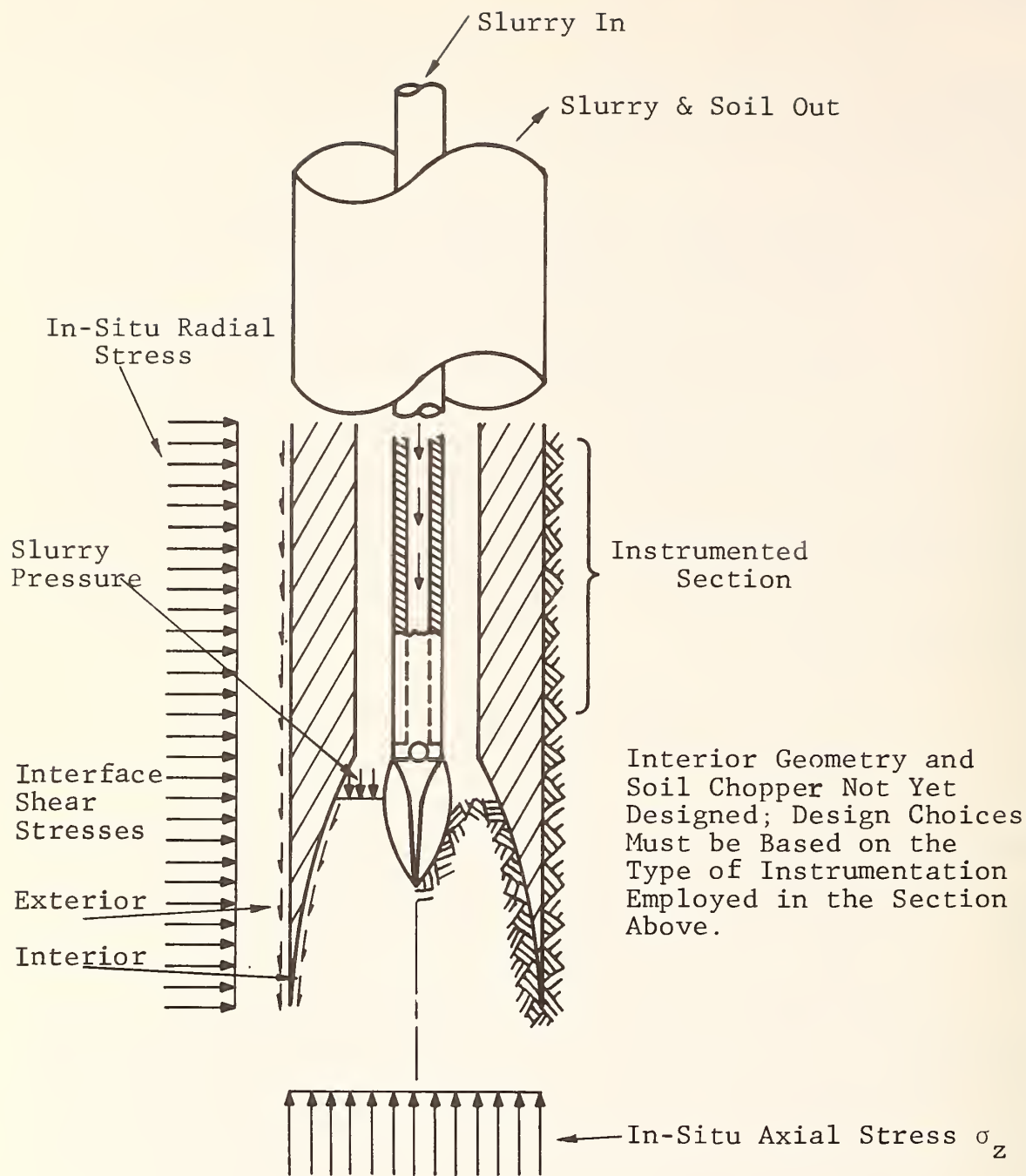
These include:

- o smooth outer surface with no projections
- o soil removal through the interior by slurry fed through a soil chopper
- o in-situ stress ahead of the probe maintained by friction on the interior probe walls or by slurry pressure

Much of the analysis to follow was conducted using the finite element method. This is a departure from previous investigations of the expanding cavity problem (e.g., Vesic, 1972; Gibson and Anderson, 1961) in which closed form analytic solutions were obtained. The FEM was used for the following reasons:

- o noncircular geometry may be investigated,
- o general loading conditions are easily applied,
- o soil constitutive laws can be changed, and
- o stress and strains are available for the entire mesh, whereas closed-form solutions are usually solved for the response at some selected point.

An elastic-plastic finite element program was employed, but the plasticity option was suppressed for these preliminary analyses. This allowed a considerably greater number of runs and is justified if only small stresses and strains are considered. Because the intention is to analyze a low disturbance device, large stress changes are to be avoided. Should the disturbance become significant with respect to the in-situ stresses, design modifications or special operational procedures would be modeled in an effort to reduce disturbance. The object is not to predict large changes in stress accurately, but to avoid them.



Note: In the general case, the radial in-situ stress will vary with  $\theta$ , and in-situ shear stresses may be present in  $\sigma_z$ ,  $\sigma_r$  and  $\sigma_\theta$

Figure 5-1. Components Typical of Self Boring Devices

The finite element mesh employed for much of the analysis is shown in Figure 5-2. A comparison of radial deflections made with the closed form solution for the case  $\sigma_y = 100$  psi ( $6.9 \times 10^5$  N/m<sup>2</sup>),  $\sigma_x = P_I = 50$  psi ( $3.4 \times 10^5$  N/m<sup>2</sup>) shown close agreement between the two solutions. Contours of maximum shear stress in the vicinity of the hole were obtained from the FEM solution as shown in Figure 5-4. Displays such as this are helpful in visualizing the stress field, but are not easily obtained from closed-form solutions.

### 5.2.2 VERTICAL STRESS BELOW PROBE

The soil immediately in advance of the probe must not experience a change in stress. A pressure equal to the in-situ normal stress in the axial direction must be supplied by the axial thrust of the probe. Depending upon the design details, this may be supplied either by interface shear resistance acting on the interior surface of the probe, or by the pressure of slurry acting on the top of an intact soil column within the probe mouth. By varying these parameters, the soil may be made to displace either inward into the probe or outward away from the probe. The three groups of investigators cited have shown that it is possible to operate a low disturbance probe in such a fashion that zero radial movement occurs in advance of the probe. With this assurance, detailed design of the probe interior and operation procedure was not investigated. This analysis should be conducted during the development phase so that an optimum geometry may be produced that will be effective over a full range of soil types. It is anticipated that a transducer will be required to measure the axial thrust directly so that it may be continuously controlled. This may take the form of a slurry pressure gage or a load cell to monitor



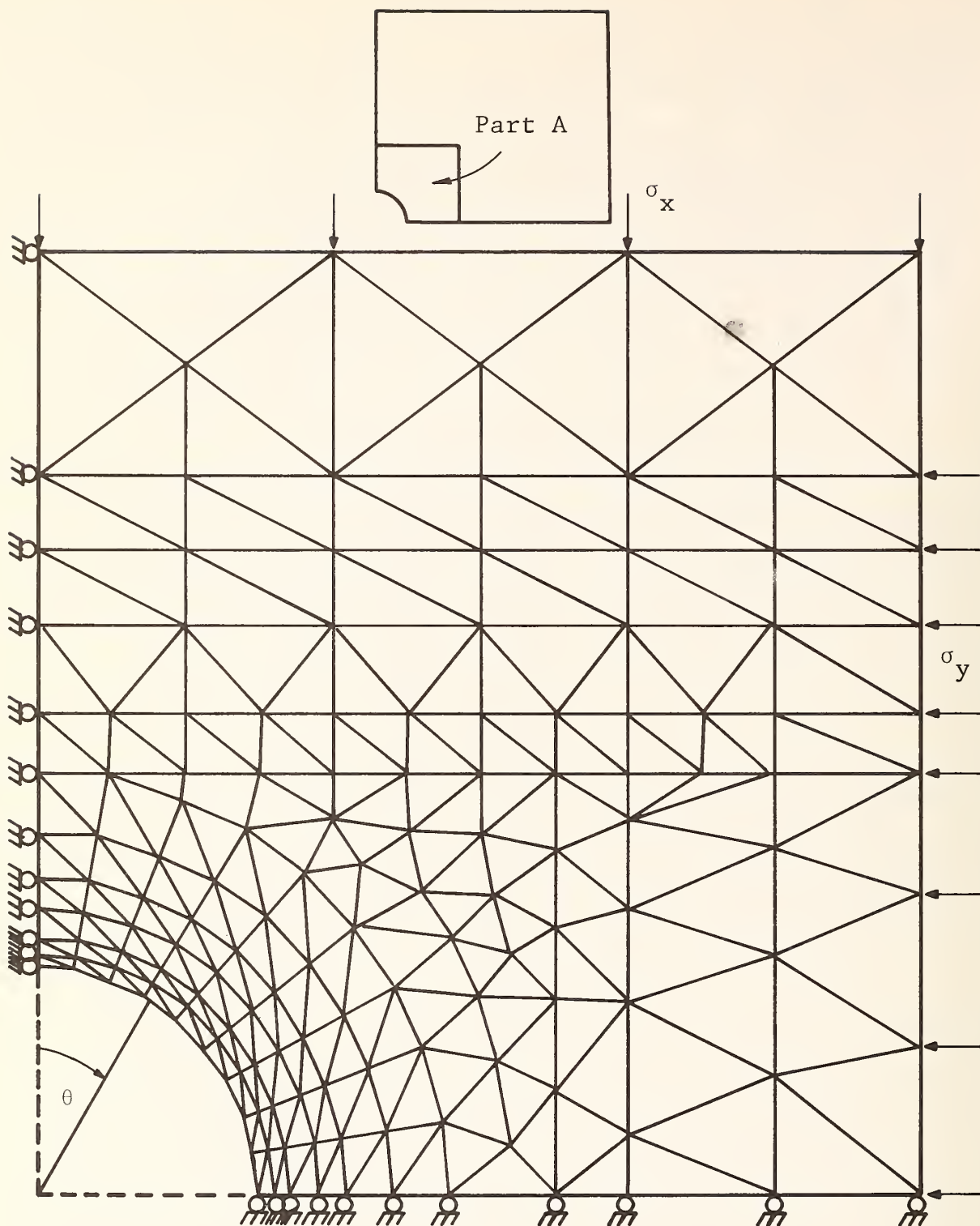


Figure 5-2. Finite Element Idealization of a Part (Part A) of a Cylindrical Cavity in Any Infinite Soil Mass

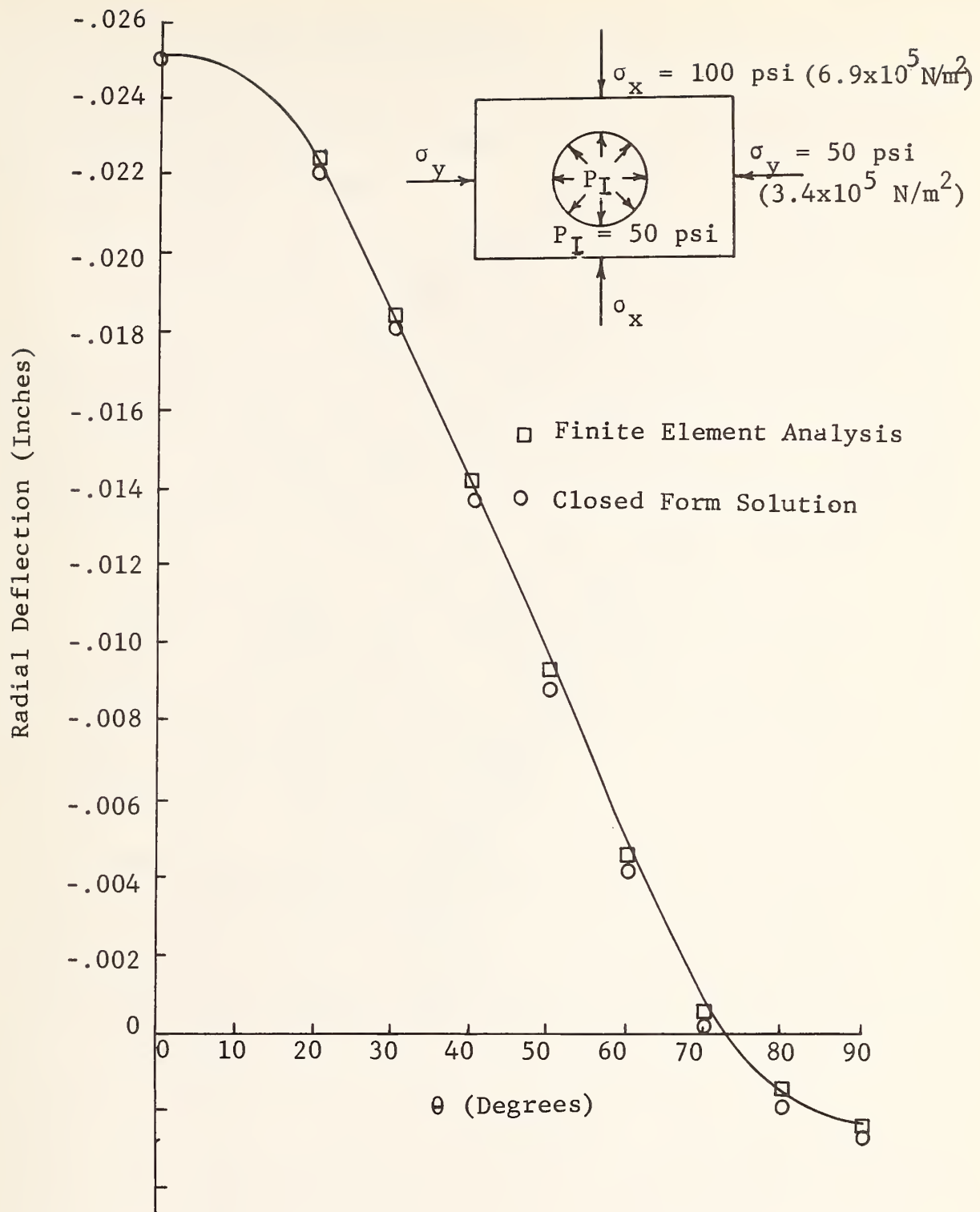


Figure 5-3. A Comparison of Elastic Radial Displacement At Hole Boundary Obtained by Finite Element Analysis and Closed Form Solution

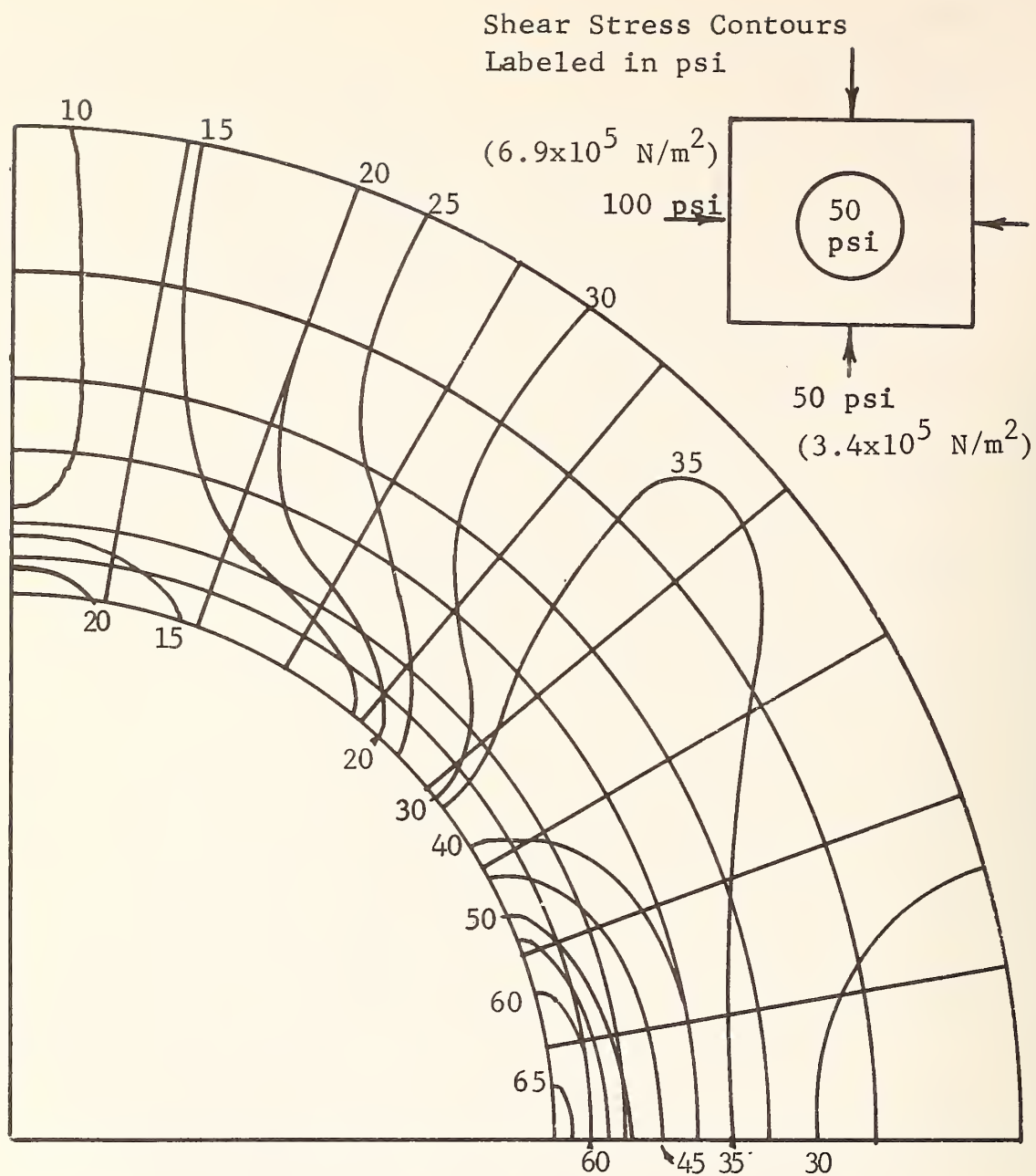


Figure 5-4. Maximum Shear Stress Contours Around a Cylindrical Hole Subjected to Uniform Internal Pressure

axial thrust on the probe interior. Detailed FEM analysis may suggest measurement locations on the probe exterior to monitor anomalous stress concentrations resulting from improper operating parameters. This would provide a direct control on the disturbance effects.

### 5.2.3 DRIVING SHEAR STRESS

During insertion, interface shear failure conditions exist on the outer surface of the probe. Basic research on soil/interface shear resistance (Leonards, 1965; Potyondy, 1961) is reviewed by Huck et al., (1973). The results are summarized in Table 5-1. Using Potyondy's data we can express the interface shear resistance  $\tau_I$  as

$$\tau_I = cf_c + \sigma \tan (\delta f_\phi)$$

Table 5-1 shows that the angle of interface shear resistance  $\delta$  can be as high as  $0.8 \phi$  for polished steel. The data of Leonards indicate that the interface shear resistance may be reduced by a graphite coating, but a teflon coating is ineffective for granular materials.

The effect of the interface shear stress induced on the exterior of the probe is shown in Figure 5-5 for a normally consolidated soil having  $K_o = 0.5$  and interface shear resistance  $\mu = 0.5$ . This is a conservative example in that it is equivalent to the effect of  $\mu = 0.25$  in an overconsolidated soil with  $K_o = 1$ . As shown in Figure 5-5(a) the lateral normal stress  $\sigma_x$  is unchanged, but a shear stress  $\tau_{xz} = \sigma_x/2$  is superimposed. The principal stress directions rotate  $22\frac{1}{2}$  degrees and the minor principal stress is reduced from  $\sigma_x$  to  $0.71 \sigma_x$ . In a real soil displaying dilatational behavior, the lateral stress  $\sigma_x$  will change in response to volume changes accompanying shear.



Table 5-1  
INTERFACE SHEAR RESISTANCE

Interface Conditions Steel on	$\delta$	$f = \frac{\delta}{\phi}$	$\mu = \tan \delta$	Adhesion $C_a$ ( $C_a \text{ max}$ )	$f = \frac{C_a}{C}$ ( $f_{\text{max}}$ )
Dry Dense Sand $\phi = 44\frac{1}{2}^\circ$	$24^\circ$	0.54	0.45		
Sat Dense Sand $\phi = 39^\circ$	$25^\circ$	0.64	0.46		
Clay $\phi = 16\frac{1}{2}^\circ$ $c = 750 \text{ psf}$ $C_{\text{max}} = 1175$	$9^\circ$	0.55	0.16	200 (600)	.27 (.51)
Clay $\phi = 11\frac{1}{2}^\circ$ $c = 460 \text{ psf}$ $C_{\text{max}} = 675$	$6\frac{1}{2}^\circ$	0.56	0.11	140 (360)	.30 (.53)
Cohesive Granular Soil					
$\phi = 13^\circ$ $C = 385$	$7\frac{1}{2}^\circ$	0.58	0.13	10	0.03
$\phi = 19^\circ$ $C = 520$	$8\frac{1}{2}^\circ$	0.44	0.15	55	0.11
$\phi = 22^\circ$ $C = 920$	$10^\circ$	0.45	0.17	105	0.11
Dry Dense Silt $\phi = 40^\circ$	$31\frac{1}{2}^\circ$	0.79	0.61		
Sat Dense Silt $\phi = 30 \text{ (} 32\frac{1}{2}^\circ \text{)}$	$20^\circ \text{ (} 24\frac{1}{2}^\circ \text{)}$	0.68 (0.75)	0.36 (0.45)		
20-30 Sand $\phi = 40^\circ$	$\delta$	$f = \frac{\delta}{\phi}$	$\mu = \tan \delta$		
polished steel	$19^\circ$	0.47	0.34		
teflon coated steel	$18^\circ$	0.46	0.33		
graphite coated steel	$12^\circ$	0.31	0.22		
60-80 Sand $\phi = 48^\circ$					
polished steel	$27^\circ$	0.56	0.51		
teflon coated steel	$33^\circ$	0.70	0.66		
graphite coated steel	$21^\circ$	0.44	0.39		

+Potyondy (1961)

+Leonards (1965)

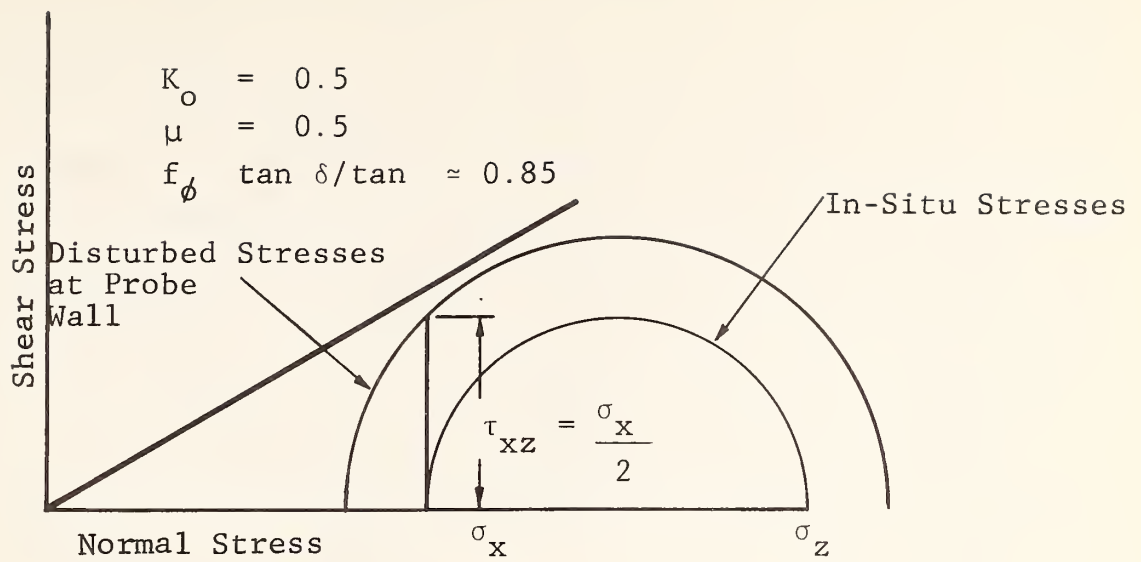


Figure 5-5A. Rotation of Principal Stresses Resulting From Driving Shear Stress Induced on Probe Surface

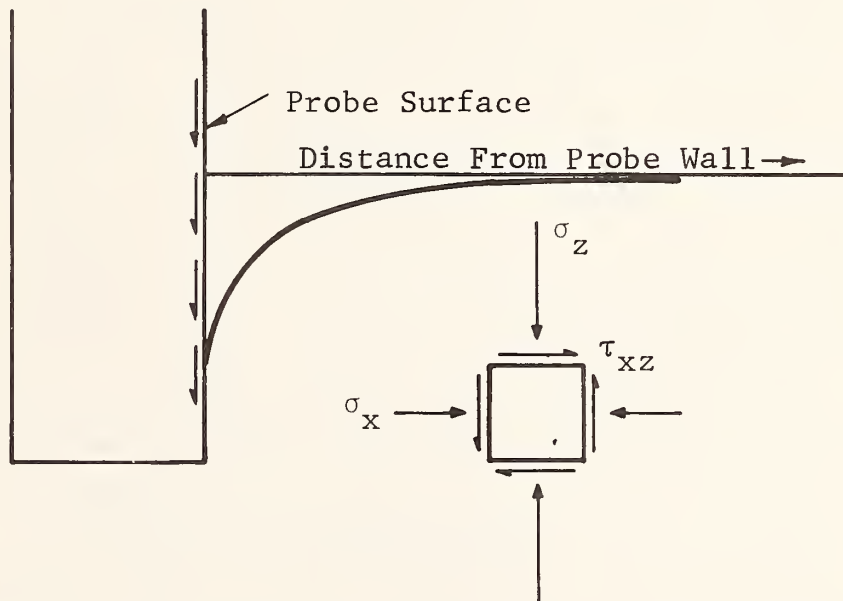


Figure 5-5B. Distribution of Induced Wall Shear Stress

The magnitude of this change depends upon the soil behavior and the volume of soil affected. The soil dilatational behavior may cause increase or decrease in volume, depending on void ratio and other properties. The amount of soil affected is known, since the shear stress decays with the inverse radius, as shown in Figure 5-5(b). It is desirable that the influence of the induced wall shears be reduced or eliminated. This may be accomplished by materials selection, reducing  $\mu = \tan \delta$ . The results of reducing  $\mu$  are shown in Figure 5-6. For a value of  $\mu = 0.2$ , the minor principal stress is reduced by 4% with an accompanying rotation of 11 degrees, if  $K_0 = 0.5$ . For  $K_0 = 1$ ,  $\mu$  must be reduced to 0.1 to achieve equal benefits.

#### 5.2.4 LATERAL PERTUBATIONS WHILE DRIVING

It is expected that the insertion process will be accompanied by a certain amount of vibration and accidental lateral displacements. To evaluate this effect, a finite element model was assembled to determine the effect of a 0.001-inch ( $2.5 \times 10^{-5}$  m) lateral displacement of a rigid circular inclusion, as shown in Figure 5-7. In this run, the node at  $\theta = 0$ , at the top of the circular inclusion, was permitted to move freely in the y-direction because slippage might be expected at this location. All other nodes on the inclusion boundary were deflected an equal amount,  $\Delta$ , in the y-direction. The slippage allowed the single node induced stress concentrations in the adjacent nodes. In an actual soil these would be distributed. The stresses on the boundary are shown in Figure 5-7(b). For the conditions indicated, the radial stress change produced by a 0.001 in. ( $2.5 \times 10^{-5}$  m) deflection is on the order of 1.75 psi ( $12 \times 10^3$  N/m<sup>2</sup>). The lateral force required to produce this displacement is 112 lb (488N) on an 18-inch long by 3-inch diam. (.46m x .076m)

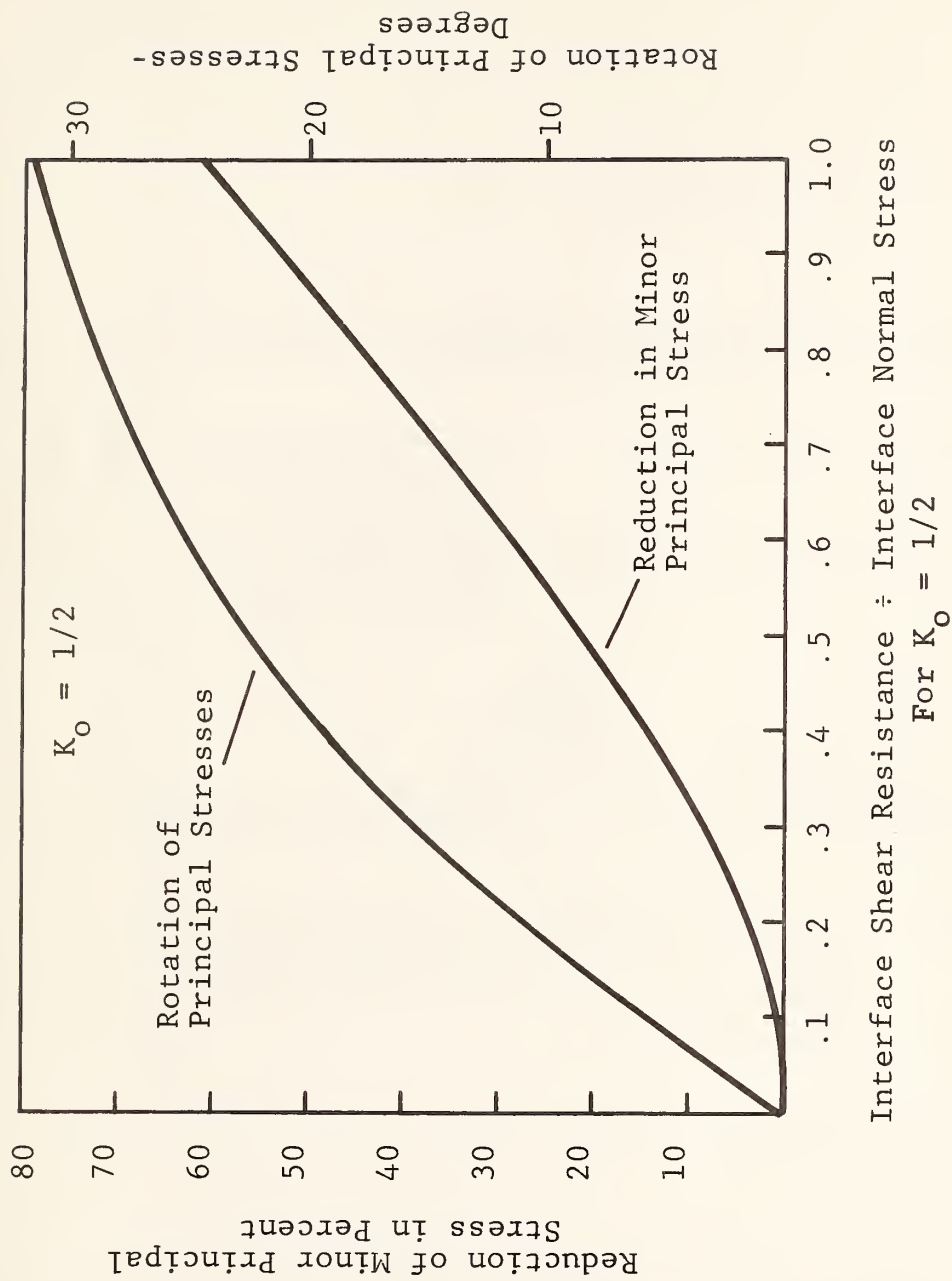
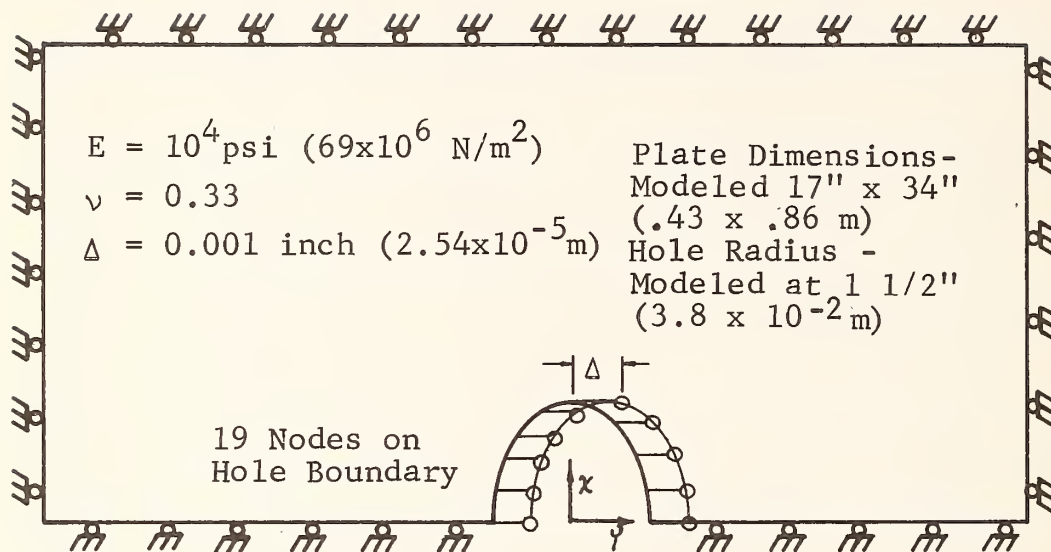


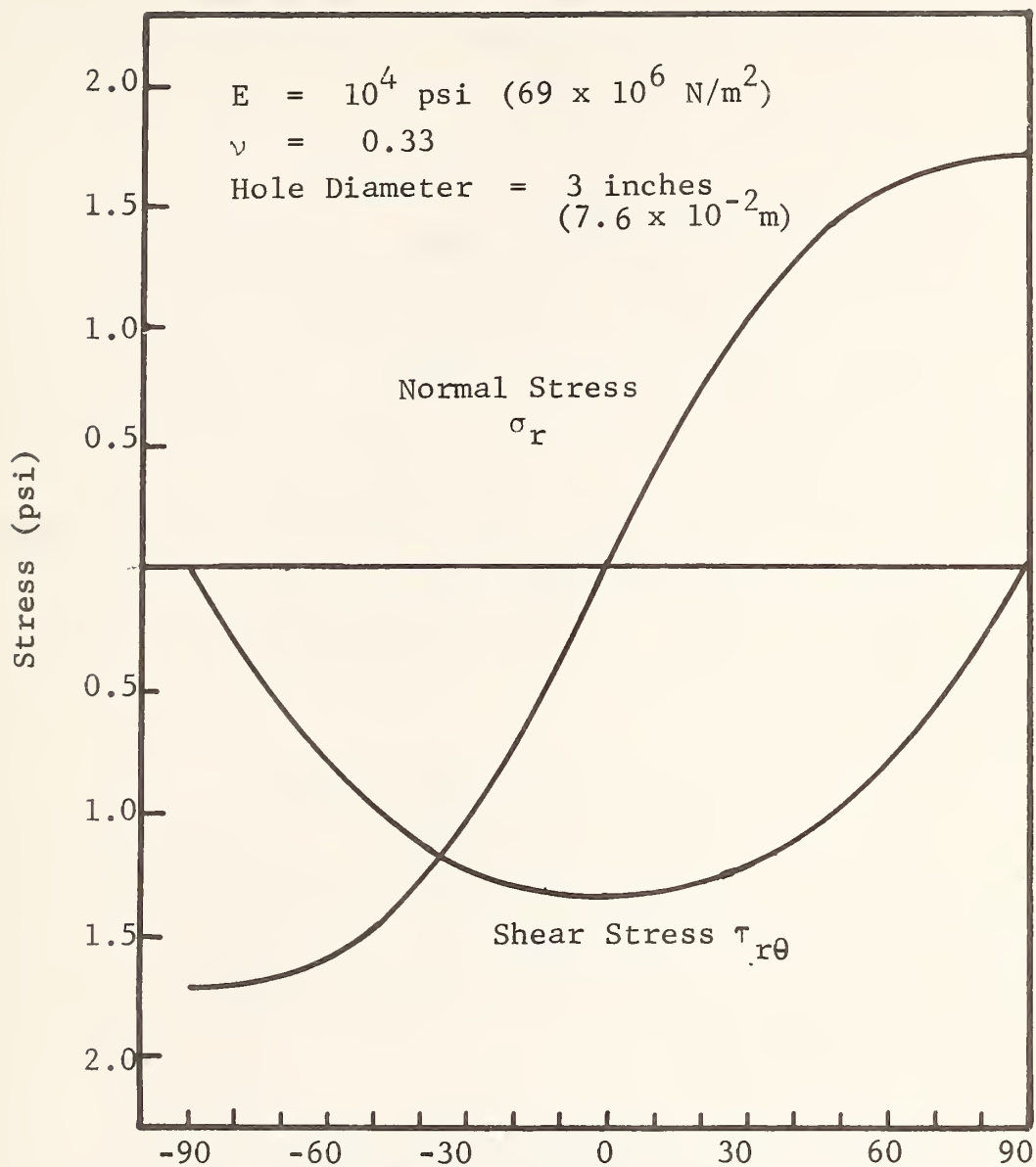
Figure 5-6. Effect of Interface Driving Shear Stress - Example for Normal In-Situ Stress =  $1/2$  Axial In-Situ Stress





Note: Top node on hole boundary allowed to slip. All other hole boundary nodes displaced 0.001 inch ( $2.54 \times 10^{-5} \text{ m}$ ) in x direction.

Figure 5-7A. Rigid Body Motion of Hole in Semi-Infinite Plate



Position on Hole Boundary - Degrees From Top Node

Figure 5-7B. Normal and Radial Stresses on Hole Boundary Resulting From Lateral Deflection of 0.001 inch  $(2.54 \times 10^{-5} \text{ m})$

probe. The behavior on rebound depends upon the soil behavior. If the soil unloading modulus is twice the loading modulus, the stresses resulting from a displacement-relaxation cycle would be equal to but opposite in sign to those in Figure 5-7(b) assuming the probe is forced back to its initial position.

This analysis is subject to the assumption that the perturbation stresses are small relative to the existing in-situ stresses. If this is true, then the soil will behave elastically, and the stresses will be everywhere compressive with no debonding from the probe surface. In general, it may be said that lateral perturbing forces on the order of 100 lb (450N) may be acceptable, yet loads on the order of 1000 lb (4500N) will cause 15 psi ( $10^5 \text{ N/m}^2$ ) changes in stress, which will probably not be acceptable except at depths where the in-situ stresses are high. Sustained vibrations may cause problems, depending upon the cyclic loading behavior of the particular soil.

#### 5.2.5 RELEASE OF IN-SITU SHEAR STRESS

A very low interface shear resistance is desirable to avoid significant driving wall shears on the outer surface of the probe. If a completely frictionless cylindrical probe is inserted in a triaxial stress field, the in-situ lateral shear stress  $\tau_{xy}$  will be released at the probe surface. The case  $\sigma_x = 2\sigma_y = \sigma_z = 100 \text{ psi}$  ( $6.90 \times 10^5 \text{ N/m}^2$ ) was evaluated using the quarter plane mesh shown in Figure 5-2. The existing in-situ normal and shear stresses on the probe surface are shown in Figure 5-8(a). Upon full release of the in-situ shear stress  $\tau_{xy}$ , the in-situ normal stresses at the probe surface change as indicated in Figure 5-8(b). The major principal stress increases by 15% and the minor principal stress decreased by 30%.

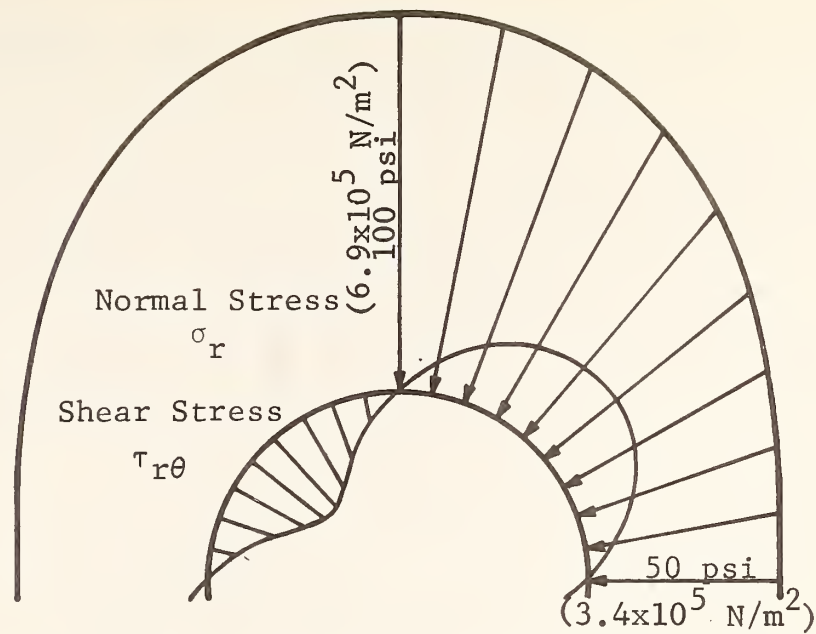


Figure 5-8A. Normal and Shear Stresses on a Circular Locus in a Biaxial Stress Field

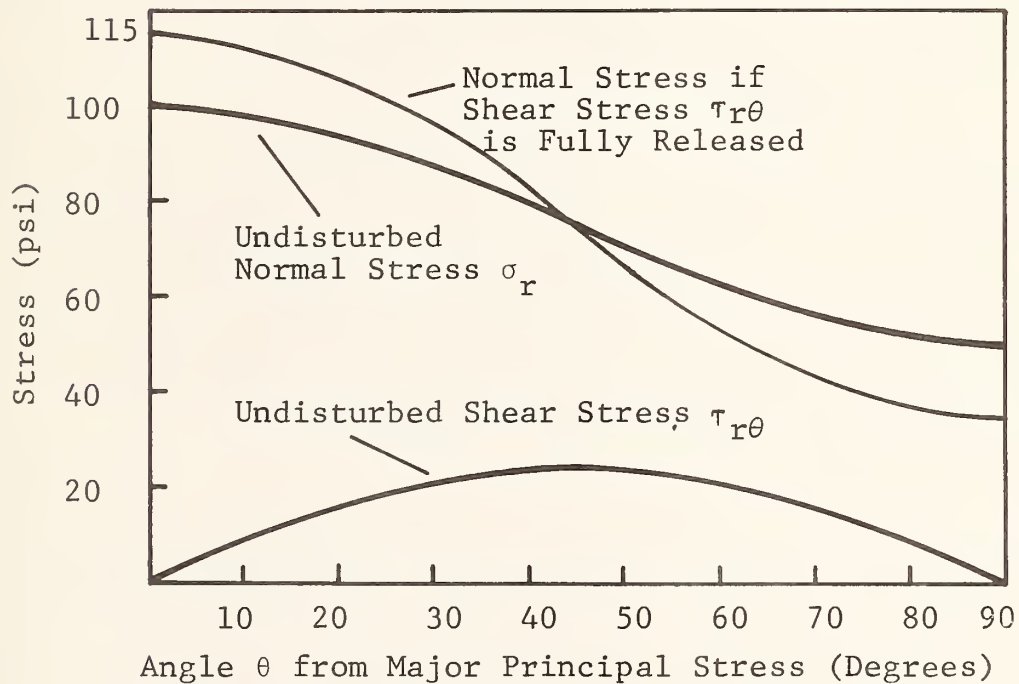


Figure 5-8B. Normal Stress Changes Upon Full Release of Shear Stress on Circular Locus



It is likely that full release of  $\tau_{xy}$  will not occur, but the shear distribution after partial release is not obvious. If the partially released shears are assumed to have a maximum value of  $\mu\sigma_r$  ( $45^\circ$ ), but to be unchanged in distribution, a linear interpolation may be made to approximate the effect of changes in the interface shear resistance ratio  $\mu$ . This is shown in Figure 5-9, together with the effect of  $\mu$  on the driving shear stresses. By the use of this figure, a qualitative choice for an optimum value of  $\mu$  may be made of 0.2. The trends acting in the decision are:

- o For larger values of  $K_o$ , a lower  $\mu$  is desirable, and  $\mu = 0$  improves the problem of driving shears for any stress ratio.
- o For equal lateral stress,  $\mu$  has no effect on the release of in-situ lateral stress  $\tau_{xy}$  which is zero for  $\sigma_x = \sigma_y$ . If the lateral stress ratio  $\sigma_y/\sigma_x = K$  is increased above 1, the effect of shear release is negligible for  $\mu > -\frac{1-K}{1+K}$ .

A range of reasonable choices is provided by the maximum values of the stress ratios  $K_o$  and  $\sigma_x/\sigma_y$ . Additional analysis is required in the developmental program to incorporate the effects of dilatational and nonlinear soil response. This is basically a detailed design and materials selection problem requiring parallel analytic and experimental analysis.

The entire problem of selecting  $\mu$  may be side-stepped if a technique is found to provide  $\mu \approx 0$  in the axial direction

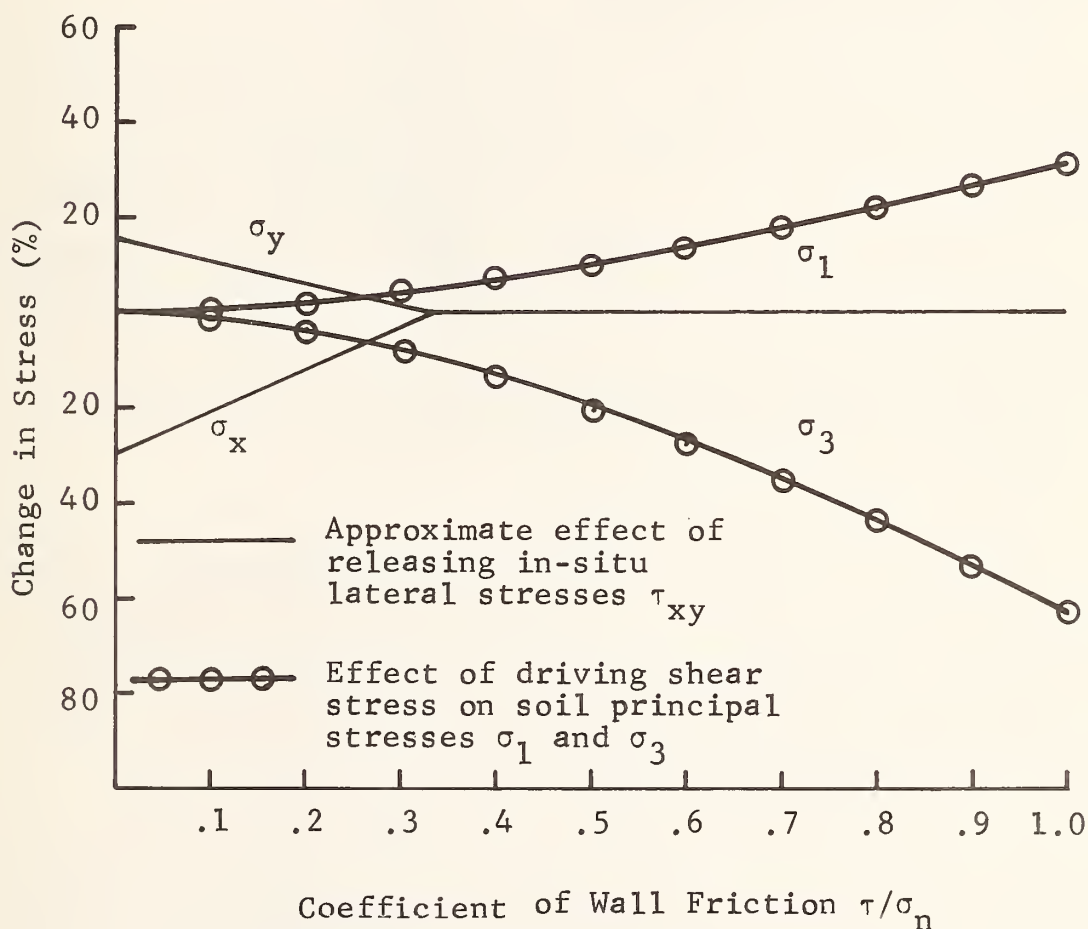
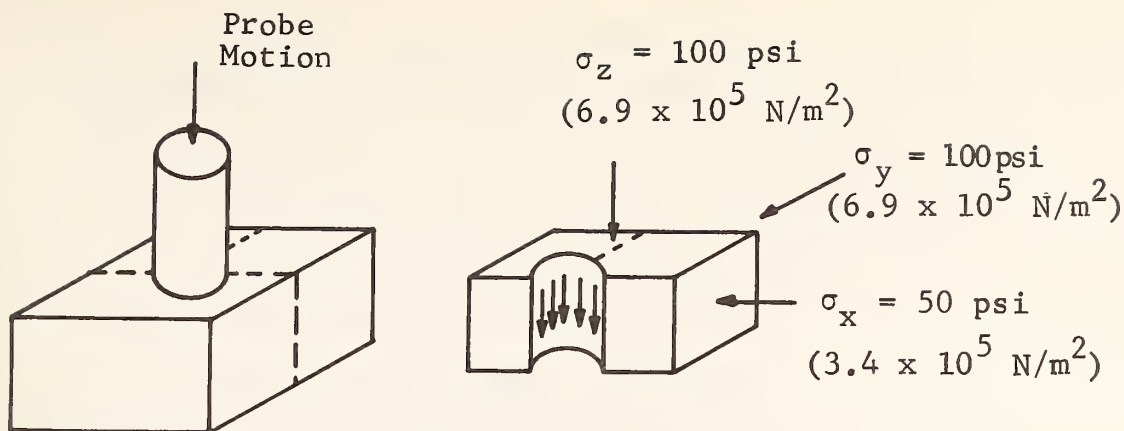


Figure 5-9. Effect of Wall Friction on In-Situ Stresses  
For Assumed Case  $\sigma_z = \sigma_y = 100 \text{ psi}$ , ( $6.9 \times 10^5 \text{ N/m}^2$ )  
 $\sigma_x = 50 \text{ psi}$ , ( $3.4 \times 10^5 \text{ N/m}^2$ ).

and  $\mu > 0.5$  in the circumferential direction. Possible techniques by which this might be accomplished are driving through a lubricated membrane (Figure 5-10) or departure from circular geometry as in Figure 5-11. The inverting lubricated membrane would require a mechanical clamp to release, cut and hold the membrane, and only a limited number of measurements can be made in any given hole until the stored membrane is expended. Both schemes require experimental evaluation to determine their relative advantages.

### 5.3 STRESS MEASUREMENT CONCEPTS

The mechanism by which biaxial stresses may be measured in the plane normal to the axis of the instrument is considered in the following paragraphs. This will be accomplished by analysis of increasingly elaborate techniques, until, at the end of the discussion, the advantages of designing increasingly sophisticated devices will be clearly established. The major concern is how accurately a biaxial lateral stress tensor can be evaluated without knowledge of the detailed constitutive relations of the soil.

#### 5.3.1 MENARD PRESSUREMETER

Early pressuremeter designs required first that a borehole be drilled into which a pressuremeter could be dropped and inflated. The normal stresses on the borehole wall are first reduced to zero, then increased hydrostatically. The resulting radial deflections are plotted in Figure 5-12 as a function of internal pressure. For this particular stress ratio and Poisson's ratio, the initial deflections are everywhere inward when the borehole is opened and the boundary stress drop to zero. Pressurizing the pressuremeter to 50 psi ( $3.4 \times 10^5 \text{ N/m}^2$ ) and 100 psi ( $6.9 \times 10^5 \text{ N/m}^2$ ) results in the curves shown. The linear elastic solution employed indicates large disturbances before the pressuremeter is lowered into the borehole. The use of this device requires detailed knowledge of the constitutive relations of the soil.

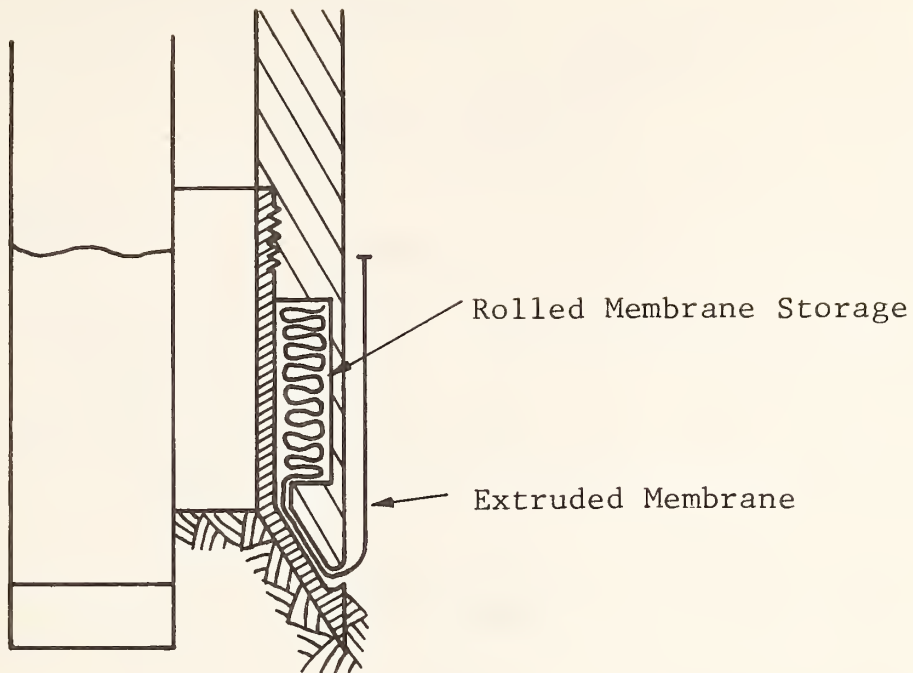
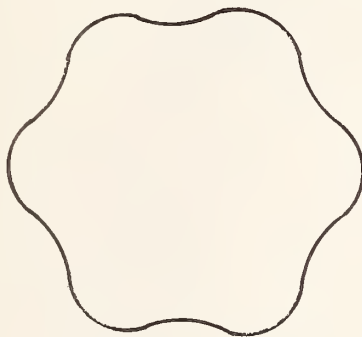


Figure 5-10. Driving Through Extruded Lubricated Membrane Prior to Test



cross section

Corrugation Depth, Height  
and Interface Shear Resistance  
Optimized to Minimize Driving  
Shear Stress and to Maintain  
In-Situ Lateral Shear Stress

Figure 5-11. Non-Circular Geometry to Provide Anisotropic Interface Shear Resistance

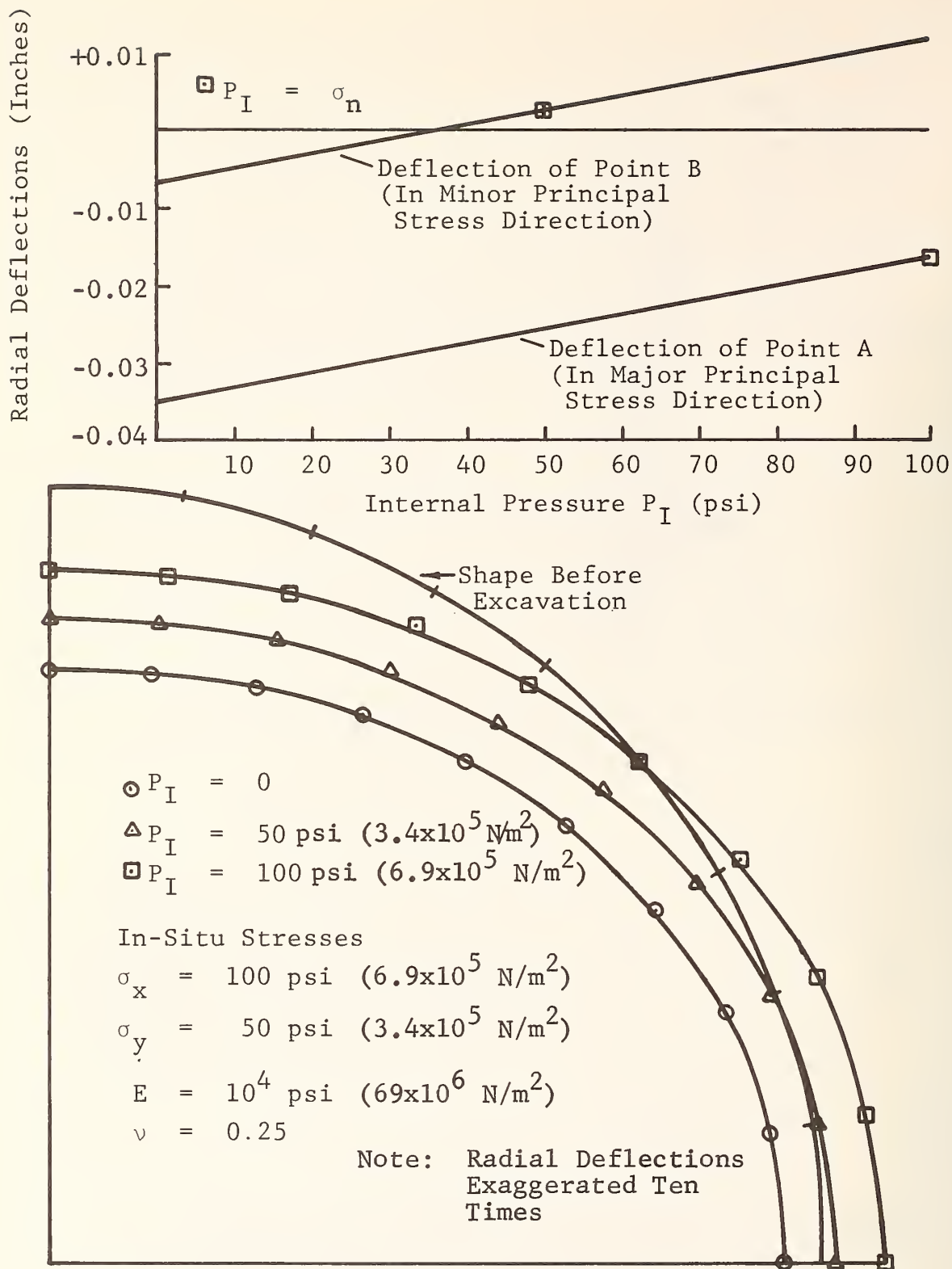


Figure 5-12. Radial Deflections of 1.5 Inch ( $3.81 \times 10^{-2} \text{ m}$ ) Radius Borehole For Various Uniform Internal Pressures.



This device was designed as an analogue to foundation strength and deformation characteristics (Menard, 1957; Smith and Smith, 1968; Baguelin and Jezequel, 1973) and is not desirable for in-situ stress measurements.

### 5.3.2 SELF-BORING PRESSUREMETER

The disturbance associated with opening a borehole is eliminated by the use of a self-boring probe. The stress field about such a device may be somewhat disturbed. We shall consider the response of a self drilling pressuremeter to the stress in which it is immersed, regardless of disturbance. The basic assumptions are that the in-situ lateral shear stress is not released and that inward deflection as large as 0.001 in. ( $2.54 \times 10^{-5}$  m) may occur. These assumptions are not the same as either the French or the English self-boring pressuremeters, but do approximate the response expected of this general class of devices.

As pressure is bled into the device, no deflections occur until the internal pressure exceeds the soil normal stress acting on the membrane at some point. As the internal pressure increases, membrane deflection is initiated in the direction of the smallest normal stress and an expanding zone of hydrostatic pressure develops until the entire membrane is pressurized. The radial deflections of points on the probe boundary are shown as functions of the internal pressure in Figure 5-13. The elastic curves corresponding to internal pressures of 50 psi ( $345 \times 10^3$  N/m<sup>2</sup>), 76 psi ( $525 \times 10^3$  N/m<sup>2</sup>) and 100 psi ( $690 \times 10^3$  N/m<sup>2</sup>) are shown in Figure 5-14. The stress conditions for  $P_I = 50$  psi ( $345 \times 10^3$  N/m<sup>2</sup>) are identical to the existing in-situ stresses and the deflections are everywhere zero. An approximation in the analysis results from the superposition techniques employed in this analysis. The deflections shown in Figures 5-13 and 5-14 result from the wedge-shaped stress diagram shown cross-hatched in Figure 5-13. This is the difference in the hydrostatic internal pressure under the membrane and the existing in-situ stresses, which were supported by the rigid backing of the membrane prior to

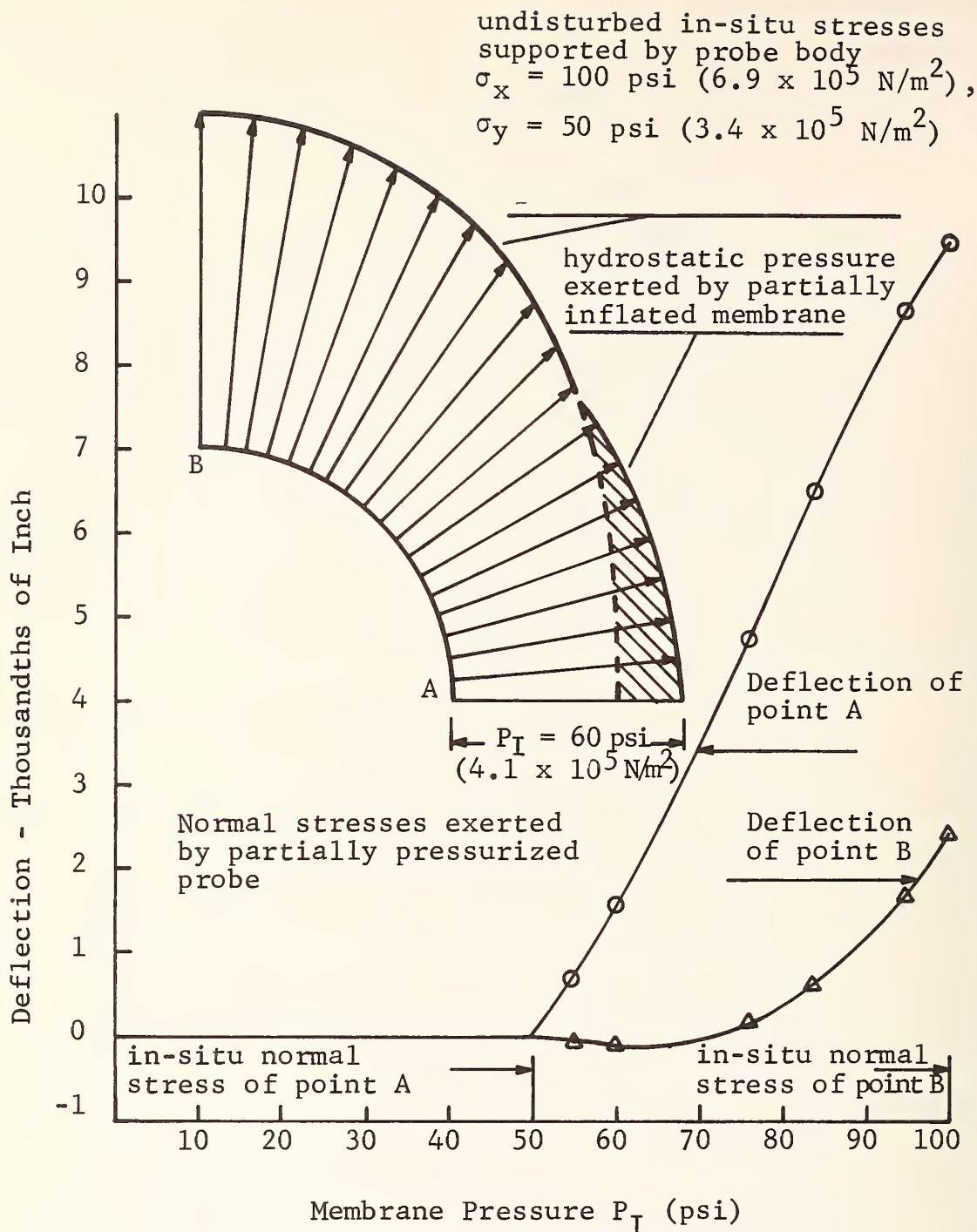
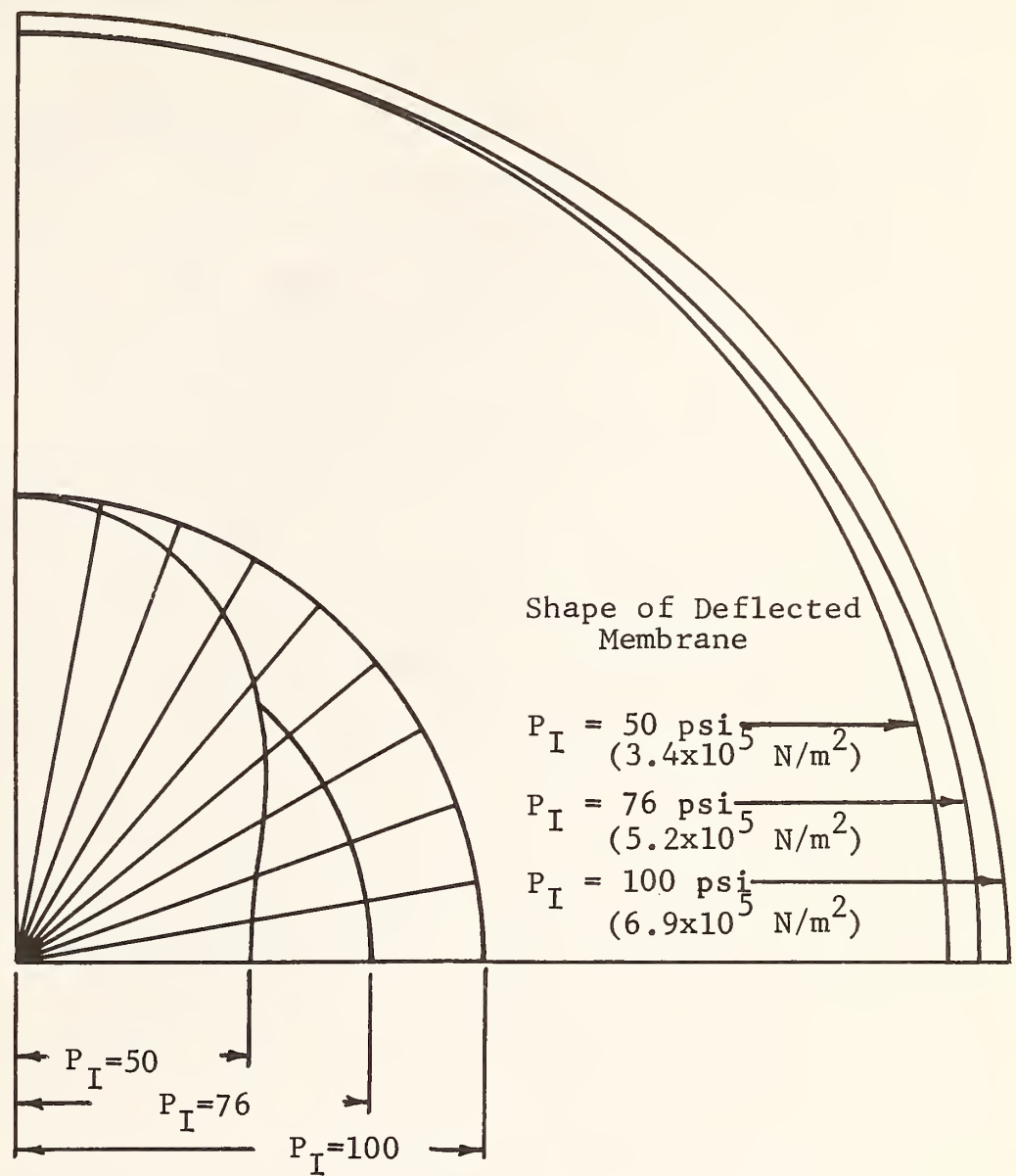


Figure 5-13. Behavior of Rigidly-Supported Membrane Pressuremeter in Biaxial Lateral Stress Field.  $\sigma_x = 100 \text{ psi } (6.9 \times 10^5 \text{ N/m}^2)$ ;  $\sigma_y = 50 \text{ psi } (3.4 \times 10^5 \text{ N/m}^2)$ ;  $E = 10^4 \text{ psi } (69 \times 10^6 \text{ N/m}^2)$



Normal Stress Conditions

5-14. Radial Deflections for Self-Boring Pressuremeter

pressurization. At internal pressures between the values of the maximum and minimum in-situ normal stresses, the normal stresses are slightly decreased outside the pressurized zone as the soil deflects away from the probe body. Normal stresses cannot be reduced to a value less than the fluid pressure under the membrane, which will flow into any region having normal stresses less than  $P_I$ . The deflection curves for  $P_I = 50 \text{ psi}$  ( $345 \times 10^3 \text{ N/m}^2$ ) and  $100 \text{ psi}$  ( $690 \times 10^3 \text{ N/m}^2$ ) are not affected by this approximation, since the membrane is not pressurized at all in the first case and is fully pressurized in the second case.

This type of device ideally indicates the normal stress in any given direction by the level of the internal pressure at the time the membrane initially deflects away from the probe body. The minor lateral principal stress is easily measured, since membrane deflection in this direction (point A, Figure 5-13) begins when the internal pressure is equal to the normal stress. The major lateral principal stress is difficult to measure, since the membrane at point B may begin deflection when the internal pressure is either less than or greater than the normal stress. The deflections at this point are affected by Poisson's ratio effects. This uncertainty, or the converse need to measure Poisson's ratio, may be eliminated by pressurizing only small zones under the membrane.

### 5.3.3 ZONE PRESSURIZATION

If a self drilling probe is placed without disturbance in the ground, the membrane may then be pressurized over a small, randomly selected zone, say 30 degrees or less of the circumference of the probe. If the pressurizing fluid is not allowed to escape from the selected area, only second-order effects will occur outside the zone pressurized. The mechanical details may be arranged in a number of fashions. For our later discussion, we will assume that this is accomplished in the manner shown in Figure 5-15. In this configuration,

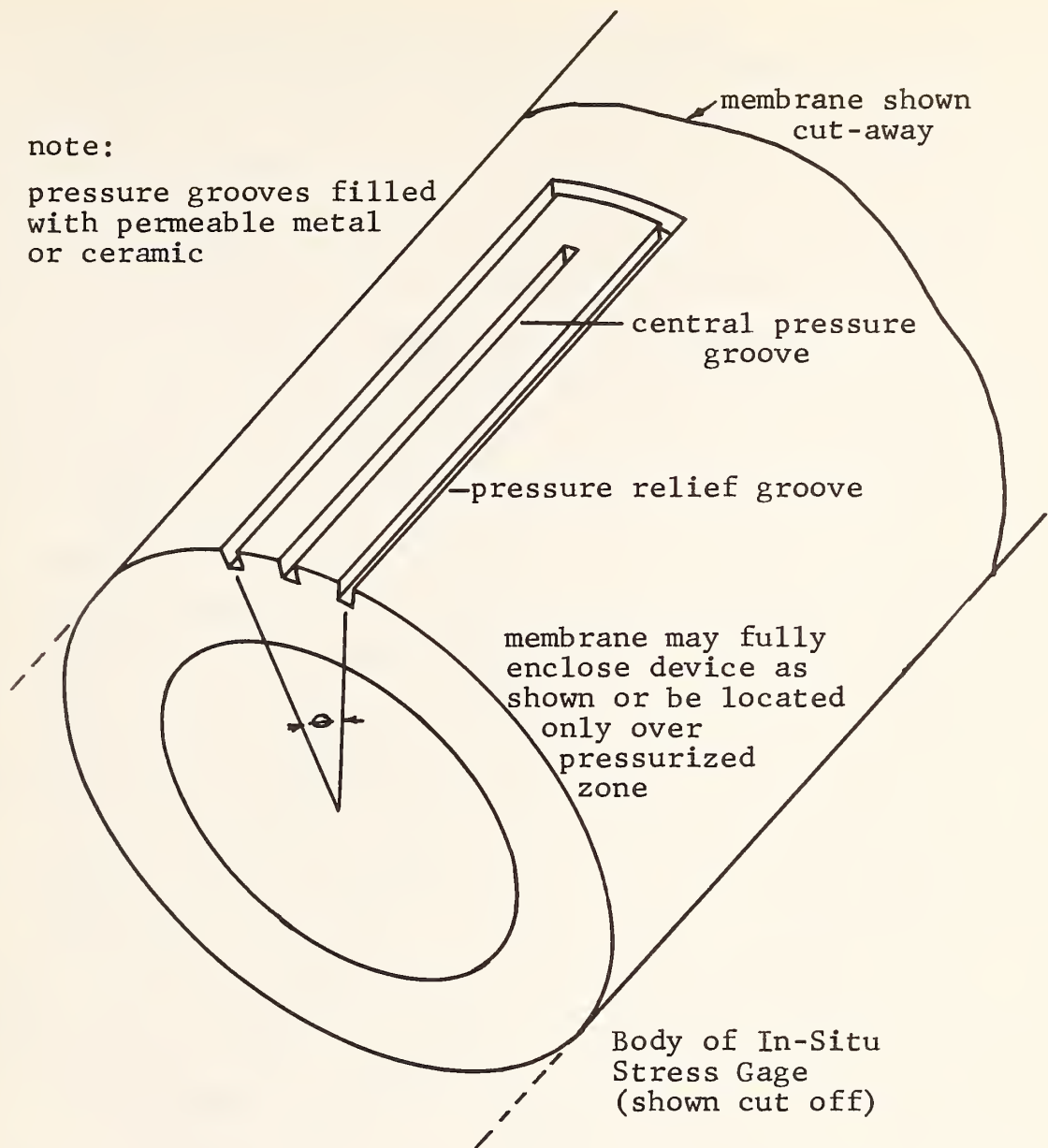


Figure 5-15. Cut-Away View of Hydraulic Zone Pressurization Concept for 30° Pressurized Zone



fluid pressure is introduced into the center groove and drained by the edge grooves, so that a region of locally increased pressure is established in the vicinity of the center groove. If the fluid pressure is increased to a value slightly above the in-situ normal stress at the location of the center groove, the membrane will lift slightly, allowing flow to occur beneath the membrane to the relief grooves at the side. For a pressure 10 psi ( $69 \times 10^3 \text{ N/m}^2$ ) greater than the normal stress in the selected direction and for soil properties  $E = 10^4$  ( $69 \times 10^6 \text{ N/m}^2$ ) and  $\nu = 0.33$ , a deflection of 0.005 in. ( $1.3 \times 10^{-4} \text{ m}$ ) will occur on the pressurized area. Because the area outside the pressurized zone does not deflect, the existing normal stresses are slightly reduced. The stress distribution around an arbitrarily located 30 degree zone pressurized to 20 psi ( $138 \times 10^3 \text{ N/m}^2$ ) above the existing in-situ normal stresses is indicated in Figure 5-16. The solid line represents the existing in-situ stresses around the probe, the dashed line is the distribution with pressure in the zone, and the dotted line shown the stresses after the zone is unpressurized if the unloading modulus is twice the loading modulus. It can be seen that the normal stresses more than 20 degrees away from the pressurized zone are not changed. This procedure may be employed to measure the normal stress at up to seven locations around the probe (Figure 5-17). The seven zones are numbered sequentially in order of pressurization in Figure 5-17(a), the normal stresses at these seven locations define the numbered points on the stress diagram, Figure 5-17(b). From this diagram, the magnitude and orientation of the in-situ stresses are easily found. Note that measuring the average normal stress over a 30-degree arc tends to decrease the radius of the indicated Mohr's circle without shifting its center. This is a geometric error that is easily accounted for by knowing the width of the pressurized zones. It appears that if the membrane deflections can be measured accurately, then the lateral stress tensor may be defined with precision by the zone pressurization technique.

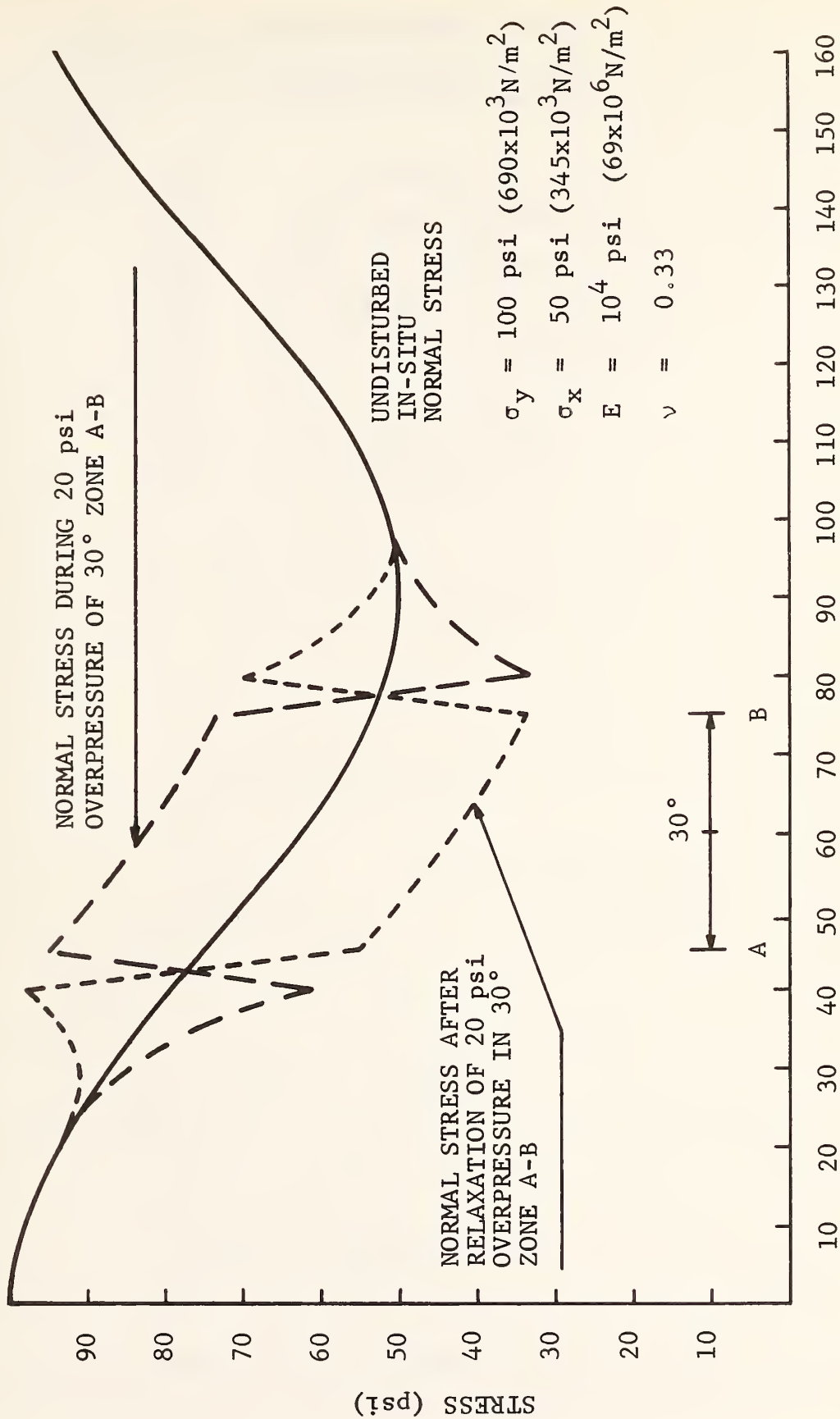
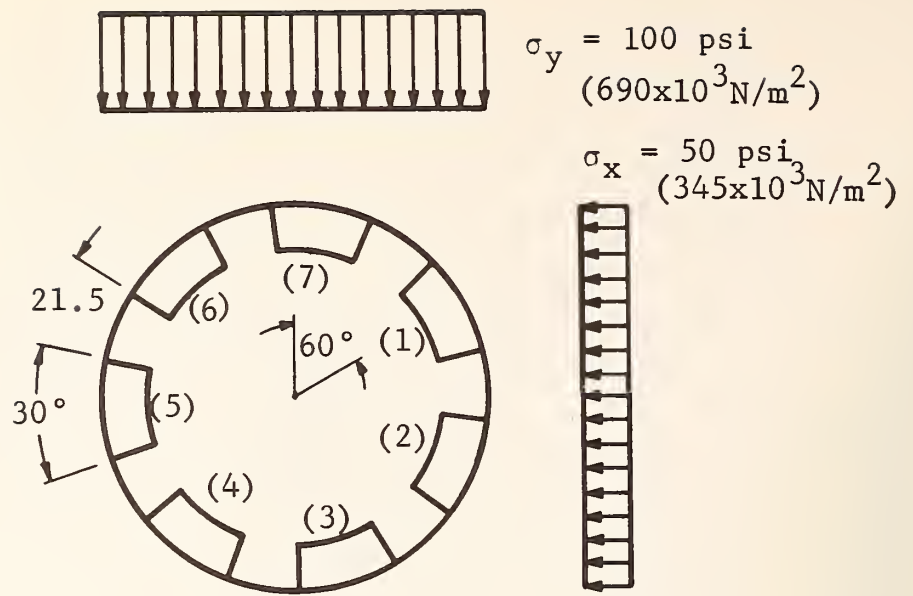
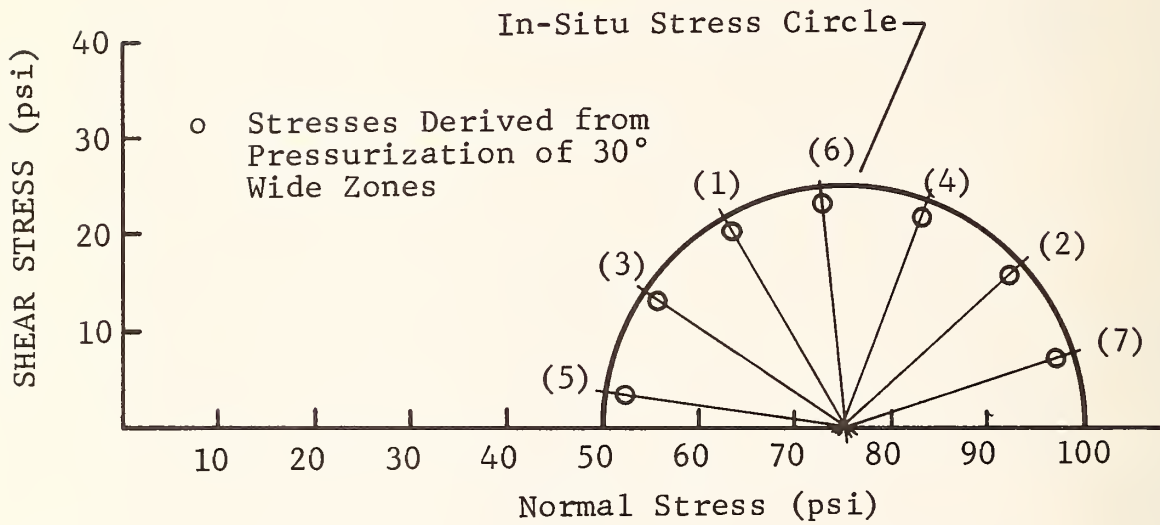


Figure 5-16. Location on Probe - Angle  $\theta$  in Degrees



a) location of 30° pressurized zones



b) average normal stresses in 30° pressurized zones

Figure 5-17. Stress Circle Obtained from Zone Pressurization Concept

The accuracy of membrane deflection techniques can be judged by considering past experience with borehole pressuremeters. The maximum error in the device of Baguelin and Jezequel (1973) is given as  $3.3 \times 10^{-4}$  in. ( $8.5 \times 10^{-6}$  m). The Wroth and Hughes (1972) device employs feeler gages to measure radial deflections on the .039m (1.5 in.) diameter device. The accuracy of the experimental data after differentiation is said to be within 0.5% strain, or  $3.8 \times 10^{-3}$  in. ( $9.5 \times 10^{-5}$  m) on the radius. The raw data appears to measure raw deflections to within  $2 \times 10^{-3}$  in. ( $5 \times 10^{-5}$  m). Bronstein, et al. (1973) suggest that radial deformation should be measured with an accuracy of  $4 \times 10^{-4}$  to  $6 \times 10^{-3}$  in. ( $10^{-5}$  m to  $1.5 \times 10^{-4}$  m). It can be seen that quite precise measurements of radial deflection are possible. In the transducer design mentioned earlier in this section, a transducer similar to a hydraulic earth pressure cell was suggested. The flowrate in such a device increases with the square of the membrane deflection. The response of such a system is shown in Figure 5-18. It is assumed that small pressure levels beneath the membrane cause slight penetration of the membrane into the spaces between the soil grains. If this is taken as arbitrarily equivalent to a uniform separation of 0.001 in. ( $2.5 \times 10^{-5}$  m), a base flow rate of 1.5 in.<sup>3</sup>/min (25 cm<sup>3</sup>/min) is established. When the internal pressure increases above the normal stress, gross membrane deflections take place in the pressurized zone. The flowrate curves that occur at three different locations on the probe depart radically from the base flowrate when the normal stress is exceeded. At 10 psi ( $69 \times 10^3$  N/m<sup>2</sup>) overpressure, the flowrate has more than doubled even though the effective deflection has increased only 50% over the assumed base rate. The pressure-flowrate curve easily indentifies the point at which gross membrane deflections begin. It should be noted that this transducer is not necessarily the best that can be conceived but it is included to indicate that workable designs can be evolved to measure the necessary deflections accurately.

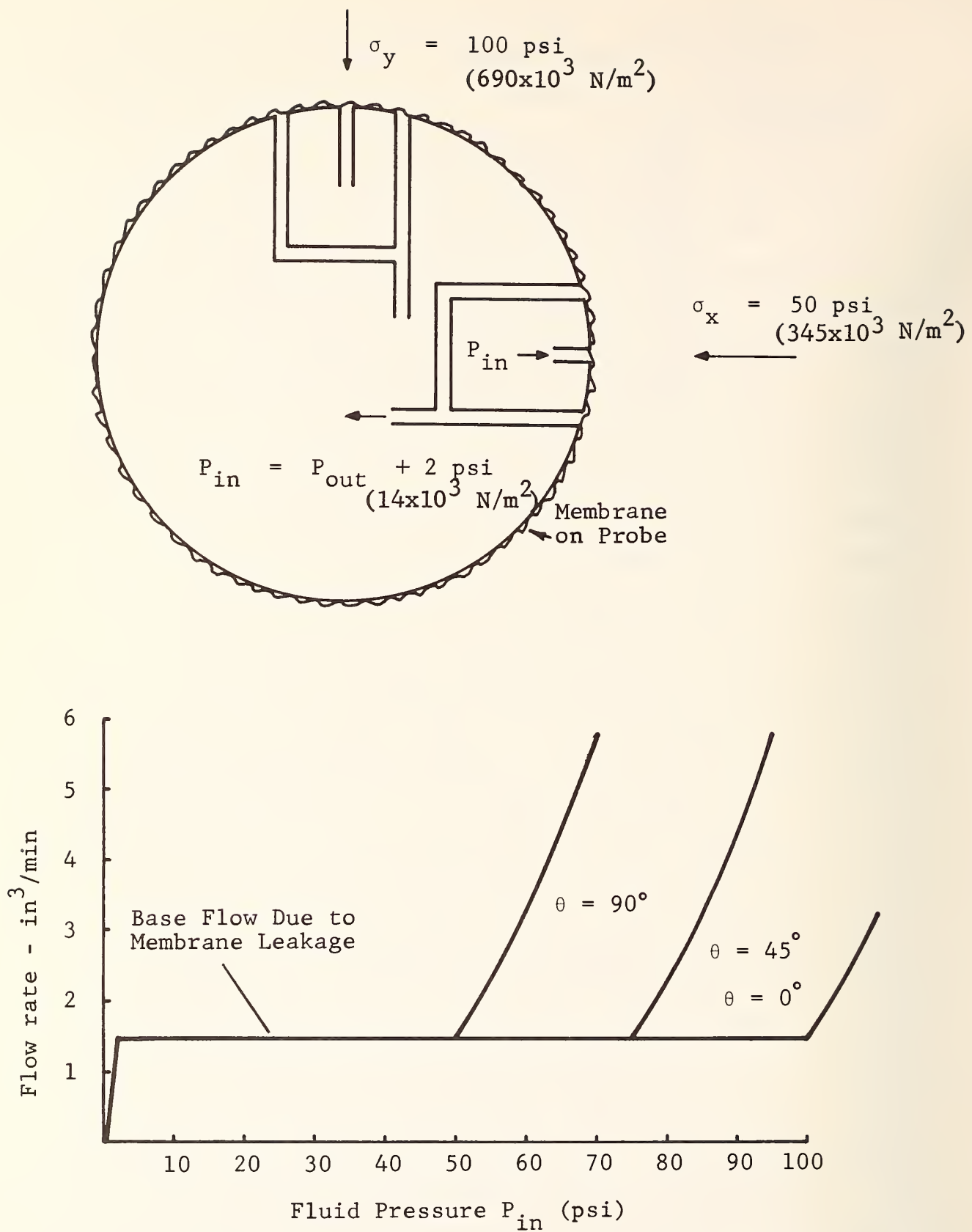


Figure 5-18. Hydraulic Zone Pressurization Gage Response



#### 5.4 PROBE REQUIREMENTS

An in-situ gage for use in a biaxial lateral stress field must be designed to perform accurately and rapidly. The recommended design includes several critical elements:

- o Detailed design of the interior of the probe together with appropriate instrumentation and operational techniques will insure that the axial in-situ stress is not disturbed by the approach of the device.
- o Materials should be selected to produce an interface shear resistance on the outer probe surface of 0.2 times the normal stress or less. If experimental work indicates that grooving or other minor departure from circular geometry will support the in-situ lateral shear stresses, then even lower friction coefficients should be attempted.
- o A technique (e.g., zone pressurization) that will measure in-situ stresses without a knowledge of the soil moduli should be used. If pressuremeter techniques are to be used instead, major corrections must be made to account for the effect of Poisson's ratio in biaxial lateral stress fields.
- o The use of high-modulus stress transducers should be avoided because of the long times needed for stresses to relax. A technique that operates by stress transfer at vanishingly small strains will offer the advantage that measurements can be made very rapidly without troublesome pore pressure effects.

A tentative view of the device emerges from these requirements. It is a heavy-wall self-boring device with the instrumented section located near the bottom. The outer surface is smooth, of a material with lower frictional resistance than polished steel. The outer surface may have shallow grooves to increase the frictional resistance in the circumferential direction, as shown in Figure 5-11. Alternative

treatments of the interface shear resistance problem may involve driving through an inverting membrane, as in Figure 5-10, or extruding a thin film of lubricant in certain soils. This problem can be best evaluated by preliminary experimental work. The pressure transducers will be small zones spaced around the circumference of the device that are individually pressurized. Borehole pressuremeters universally use rubber membranes, but a better choice for the recommended stress gage may well be thin metallic membranes. This choice is permitted because of the small maximum deflections measured, and would have the advantage of low wall friction. This again is a problem for design detail after preliminary laboratory investigation. It may be desirable that the device be useable as both a stress gage and a borehole pressuremeter. This would be possible if zone pressurization and a rubber membrane are used in that the stress circle could first be traced by pressurizing individual zones, then the gross soil stiffness measured by pressurization of the entire membrane in pressure-meter mode.

## 5.5 PROPOSED DEVELOPMENT PLAN FOR IN-SITU STRESS GAGE

The detailed design, fabrication and evaluation efforts should be undertaken with the goal of delivering an operational in-situ stress gage within a period of 18 months. The major emphasis of this effort plus reporting is to deliver proven hardware for operation under general soil and full stress conditions. The recommended program plan is shown in Figure 5-19 .

### Phase IA-Analysis

Phase IA is an intensive theoretical analysis of the proposed in-situ stress gage. The broad design will have been established and it is necessary to evaluate the performance of the device. The following areas should be treated:

- o effect of soil type, using realistic constitutive relations,

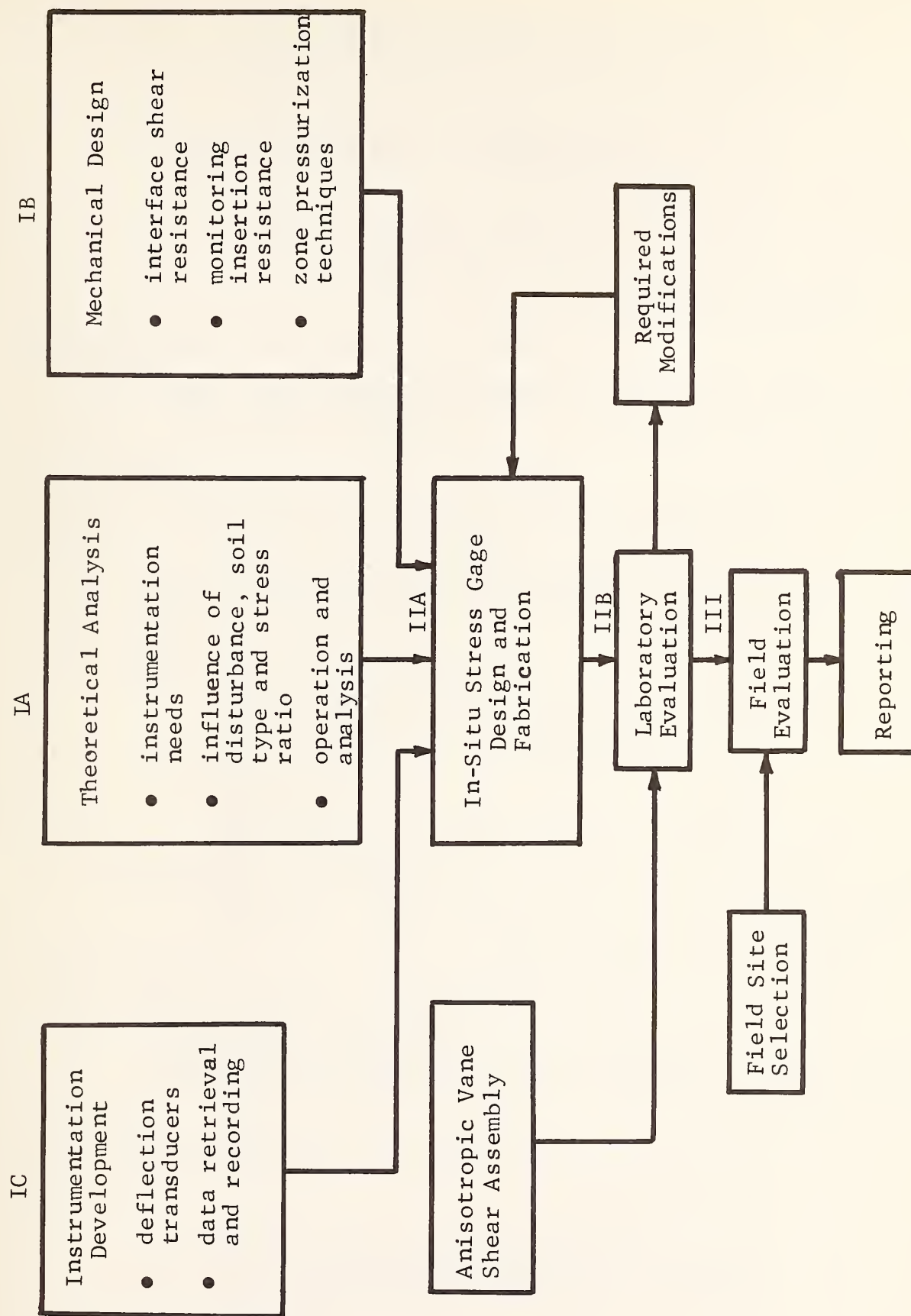


Figure 5-19. Recommended Hardware Development Work Plan

- o effect of lateral stress ratios,
- o permissible degree of soil disturbance,
- o instrumentation requirements,
- o optimum gage geometry - length, diameter, nose and excavator geometry, transducer sensing area and location,
- o insertion operational parameters, and
- o test and data reduction procedures

#### Phase IB-Mechanics

In Phase IB, the mechanical subsystems will be evaluated. Models of the various subsystems will be designed, fabricated and tested in the laboratory. The following areas will require treatment:

- o reduction of shear stress along the outer soil-instrument interface,
- o real time measurement and control of the vertical loading imparted by the interior of the instrument to the underlying soil during insertion,
- o elimination of other disturbance sources such as lateral thrust, vibration or others,
- o driving and instrumentation subsystems coupling the device to the surface hardware and
- o automatic control of testing functions.

Much of Phase IB should consist of experimental feasibility and optimization efforts conducted in the laboratory

#### Phase IC-Instrumentation

In Phase IC, candidate transducer designs will be evaluated and compared with the requirements developed in Phase IA. The following technical and operational areas should be treated:

- o effective transducer modulus, range, accuracy, and precision,
- o data retrieval,
- o simplicity, durability and cost of mechanical, transducer and recording systems,



- o applicability to full circle or zone pressurization, and
- o detailed design of competitive candidate transducer.

#### Phase IIA-Design and Fabrication

The Phase IIA effort is to tie together the three corroboratory Phase I efforts. During the design and fabrication of the in-situ stress gage, the minor hardware required to evaluate the anisotropic vane shear technique will also be fabricated.

#### Phase IIB-Laboratory Evaluation and Modifications

The Phase IIB effort is a major laboratory hardware evaluation of the in-situ stress gage. It is expected that design improvements may be revealed that will require cycling through a modification-reevaluation loop. Testing will include the insertion, measuring and data recording functions under realistic laboratory modeling. These tests will evaluate at least the following parameters:

- o variations in the magnitudes and the ratios of the three principal stresses,
- o operation at arbitrary angles to the principal directions,
- o soil type, including a range of cohesive and cohesionless soils,
- o degree of saturation in fine-grained soils.

These tests will reveal the accuracy of the device, optimum operating parameters, conditions to be avoided and useful software for data reduction and presentation.

While these evaluations of the in-situ stress gage proceed, a parallel but much smaller evaluation of the anisotropic vane shear technique will proceed. This will include:

- o cohesive and cohesionless soils,
- o effect of testing rate, and
- o the possibility of using data at large rotation.



The anisotropic vane shear evaluation is not to constitute a large portion of the testing program.

### Phase III Field Testing

Phase III constitutes the final evaluation of the in-situ stress gage. The field work will include comparative testing of the in-situ stress gage and at least one existing technique. The following areas will be studied:

- o accuracy of in-situ stress measurement.
- o technical operational parameters.
- o economic factors associated with the use of the new instrument.

### Reporting

The theoretical and experimental efforts will be fully documented in a technical report. In addition, operational requirements and limitations in the application of the in-situ stress gage will be delineated to provide the practicing geotechnical engineer with all the information needed to determine when and how to use the instrument. An operator's manual will be carefully prepared and appended to the report. This will include step-by-step operating procedures, recommended data handling schemes, or nomographs and example problem solutions.

The level of effort recommended for each phase is shown in Table 5-2. The total effort is expected to amount to 28 engineer-months and 20 technician-months.

In addition to the tentative level of effort as shown, secretarial time, materials costs including computer time, and rental charges on standard field equipment, should be added.

Table 5.2

RECOMMENDED LEVEL OF EFFORT FOR IN-SITU GAGE  
DEVELOPMENT

<u>Phase</u>	<u>Engineer (Months)</u>	<u>Technician (Months)</u>
IA Stress Analysis	4	1
IB Mechanical Design Modeling	5	1
IC Instrumentation Design	3	1
IIA Design & Fabrication	3	3
IIB Laboratory Testing	7	4
III Field Evaluation	4	4
Reporting	2	
	<hr/>	<hr/>
TOTAL	28	14

## 6. SUMMARY

### 6.1 OVERVIEW

A number of techniques are currently available for use in the partial determination of in-situ stress fields. Existing methods measure a single component of stress. If it may be confidently assumed that a given site has a history of  $K_0$  loading, measurement of the lateral stresses and the assumption that the vertical stress is given by  $\sigma_z = \gamma z$  define the full stress tensor. If the site is not level or has experienced events to modify the lateral stresses, more extensive testing is required. To provide the capability required by the latter conditions, a three-level recommendation is made:

- a) Immediate development of an in-situ stress gage capable of determining the two-dimensional stress tensor in the plane normal to its axis.
- b) Medium-range development of fabric analysis as an effective soil mechanics tool.
- c) Long-range development of methodology using electroparamagnetic resonance as a soil stress determination tool.

### 6.2 CURRENTLY EXISTING TECHNIQUES

Current techniques are classified into (a) laboratory  $K_0$  tests (b) laboratory stress tests and (c) in-situ stress tests. The first classification includes a number of laboratory test methods and devices by which  $K_0$  loading conditions may be imposed on a sample of soil. Use of these methods requires that the stress history at the site be known and that the soil respond to laboratory testing in a fashion similar to the geological behavior in-situ (Section 2.3).

Two examples of test methods by which the actual in-situ stress is estimated by laboratory testing were found. These are the Skempton method, which employs the effect of stress on the pore pressure parameter  $A$ , and the lateral

consolidation test reported by Poulos and Davis. These techniques, both of which are applicable to fine grained soils only, are reviewed in Section 2.3.5.

Five in-situ test methods were discussed in Section 2.4, and compared in Section 2.4.6. The most applicable geotechnical conditions and the quantity measured by each method are as follows:

Table 6.1

CHARACTERISTICS OF VARIOUS IN-SITU TECHNIQUES

<u>test</u>	<u>most applicable geotechnical conditions</u>	<u>quantity measured</u>
sonic velocity (2.4.1)	granular or cohesive soils	stress directions by multiple use; estimate mean stress by single use.
borehole pressuremeter (self drilling) (2.4.2)	best in cohesive soil	mean lateral stress also soil stiffness.
borehole stressprobe (2.4.3)	frictional or cohesive	normal principal stress regardless of orientation.
hydraulic fracturing (2.4.4)	fine-grained $K_0 \leq 1$	minimum principal stress regardless of orientation.
anisotropic vane shear (2.4.5)	best in frictional soil	stress ratio.

The choice of technique must be made on the basic circumstances associated both with the site and the experience and facilities available to the engineer. We cannot include all the various capabilities and limitations of each technique and the table is not a substitute for sound engineering judgment.

### 6.3 RECOMMENDED DEVELOPMENT

In Sections 3, 4 and 5 recommendations were made for additional development of fabric analysis, electroparamagnetic



resonance (EPR), and the in-situ stress gage. The use of EPR as a soil stress gage is a long-range recommendation. The concept shows considerable promise, but very little of the basic data on soil response is known. Because of the uncertainties involved in converting a research tool to a production testing device, a detailed estimate for such a program cannot be reliable.

The development of fabric analysis as a soil stress gage is a medium-range recommendation. This technique may confidently be expected to resolve the principal stress directions and the relative magnitudes of the principal stresses but it is less certain that the absolute magnitudes of the principal stress can be determined with any degree of accuracy. Fabric analysis can currently be used with some success for some simple cases not involving rotation of principal stress directions or other complications.

The development of an in-situ stress gage is the strongest recommendation. This unit will be capable of resolving the two-dimensional stress tensor in the plane normal to its axis in a single operation. This is not possible with existing hardware. For conditions under which the device axis can be oriented along the direction of a known principal stress, as in  $K_0$  conditions, the full three-dimensional stress tensor can be obtained. In the case of no prior knowledge concerning the principal stress magnitudes or directions, three orientations of the axis in oblique planes are required to fully resolve the full stress field in a region. This will require six measurements using existing hardware. In addition to the greater quantity of data provided by the in-situ stress gage, the stress data are expected to be of a high order of accuracy. Disturbances in a full triaxial stress field are given more extensive treatment, and the proposed measurement techniques effectively reduce the effect of soil stiffness by the use of stress transfer methods. Because of the low strain



levels involved, the testing time in saturated soils will be reduced, as little if any pore pressure will require dissipation during the test. The result is a much reduced testing time as compared with pressuremeters, which operate at large strain levels, or stress probes, which require lengthy relaxation times.

The recommended system, by providing economical and accurate in-situ stress data will permit the more confident use of powerful computational tools such as the finite element method.

## APPENDIX A

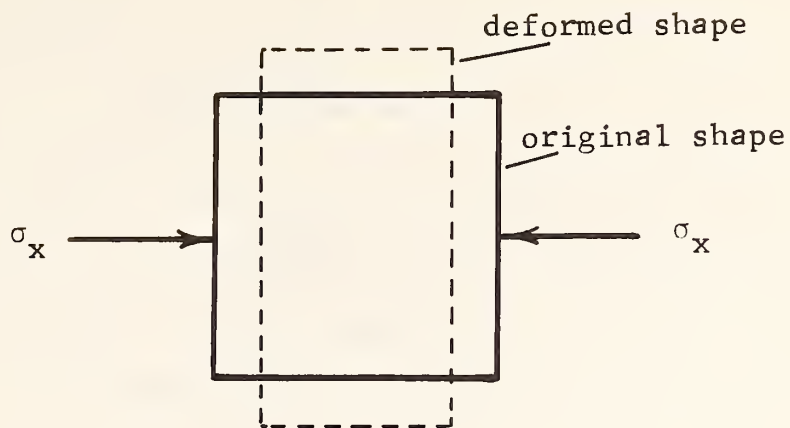
### SOIL STRESSES

#### A.1 STRESS TENSOR

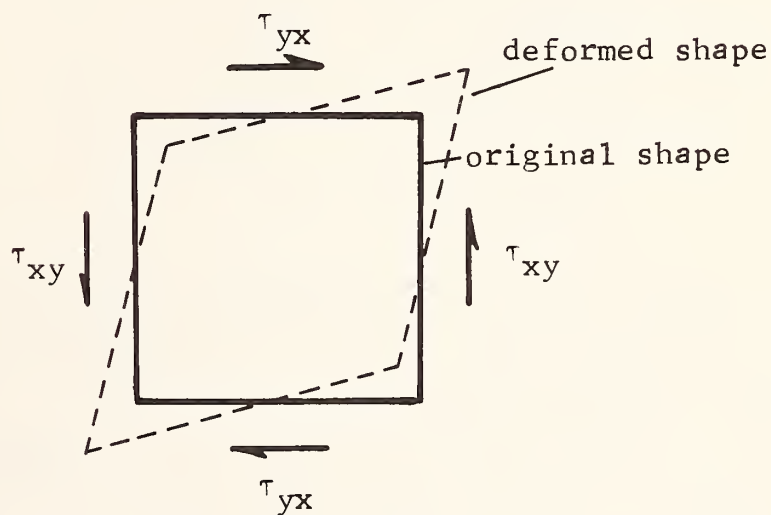
Stress is defined as the quotient of force divided by area, having the units pounds per square inch (psi) or Newtons per square meter ( $\text{N/m}^2$ ). Geotechnical engineers frequently also use the units tons per square foot (TSF) and the dimensionally incorrect units kilograms per square centimeter ( $\text{Kg/cm}^2$ ). This report will deal in psi and  $\text{N/m}^2$ .

Stress notation employs the symbols  $\sigma$  or  $\tau$  to indicate individual stress components. Subscripts are used to indicate the direction in which each particular component acts. Either of two notation systems may be employed to note the normal stress acting perpendicular to the plane of interest and shear stresses that act parallel to the plane. In the second (matrix) notation, repeated subscripts (xx) indicate normal stress and different subscripts (xy) indicate shear stress. The difference in normal and shear stresses is shown in Figure A.1.

Normal Stress Component			Direction of Action		
$\sigma_x$	or	$\sigma_{xx}$	$\perp$	to	yz plane
$\sigma_y$	or	$\sigma_{yy}$	$\perp$	to	xz plane
$\sigma_z$	or	$\sigma_{zz}$	$\perp$	to	xy plane
Shear Stress Component					
$\tau_{xy}$	or	$\sigma_{xy}$	$\parallel$	to	xy plane
$\tau_{xz}$	or	$\sigma_{xz}$	$\parallel$	to	xz plane
$\tau_{yz}$	or	$\sigma_{yz}$	$\parallel$	to	yz plane



Normal Stress  $\perp$  to y-z Plane



Shear Stress  $\parallel$  to x-y Plane

Figure A-1. Normal and Shear Stresses in the x-y Plane

The concept of stress is typically introduced by the consideration of forces acting on an imaginary cube cut from a solid body having an arbitrary shape and external loads as shown in Figure A-2. In the absence of gravitational or other body forces, a system of normal stresses  $\sigma_x$ ,  $\sigma_y$ ,  $\sigma_z$ , and shear stresses  $\tau_{xy}$ ,  $\tau_{xz}$ , and  $\tau_{yz}$  are seen to act on the cube. The magnitude of the normal and shear stresses acting on a surface depends on the orientation of that surface. Three mutually perpendicular planes exist on which the shear stresses vanish and the normal stresses attain a maximum, or "principal" value. The two dimensional case in the x-y plane is represented in Figure A-3.

If matrix calculus is employed, it is convenient to consider stress to be a second order symmetric tensor represented by

$$\sigma_{ij} = \begin{pmatrix} \sigma_{xx} & \sigma_{xy} & \sigma_{xz} \\ \sigma_{yx} & \sigma_{yy} & \sigma_{yz} \\ \sigma_{zx} & \sigma_{zy} & \sigma_{zz} \end{pmatrix}$$

In this notation, the normal stresses are represented by the double indices  $\sigma_{xx}$ ,  $\sigma_{yy}$ , and  $\sigma_{zz}$  corresponding to the previously developed notation  $\sigma_x$ ,  $\sigma_y$ , and  $\sigma_z$ . The shear stresses are represented by  $\sigma_{yx} = \sigma_{xy} = \tau_{xy}$ ,  $\sigma_{xz} = \sigma_{zx} = \tau_{xz}$ , and  $\sigma_{zy} = \sigma_{yz} = \tau_{yz}$ . The matrix is symmetrical across the major diagonal. Finally, the eigenvalue, or principal stresses become

$$\sigma_{ij} = \begin{pmatrix} \sigma_{xx} & 0 & 0 \\ 0 & \sigma_{yy} & 0 \\ 0 & 0 & \sigma_{zz} \end{pmatrix}$$

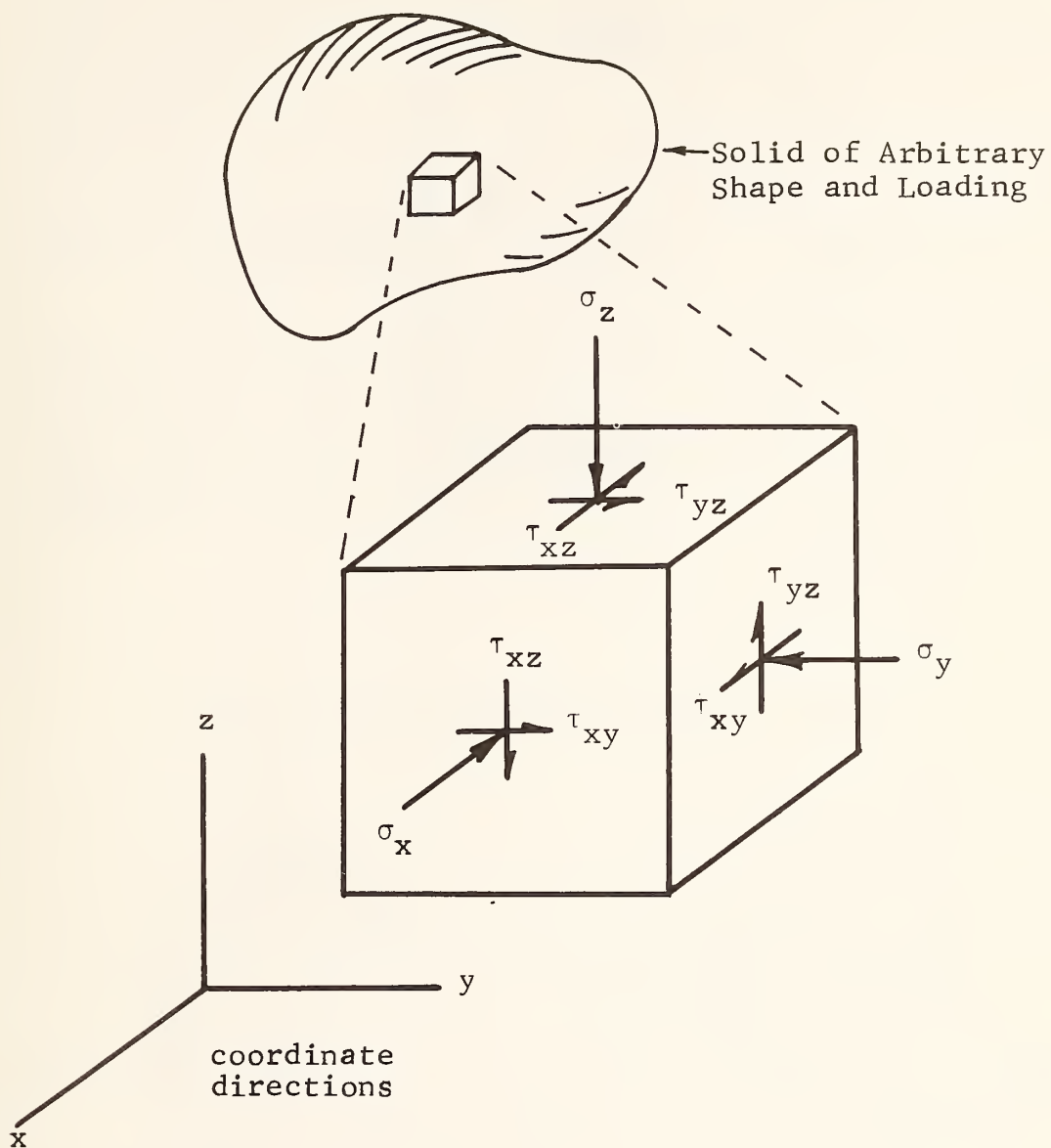
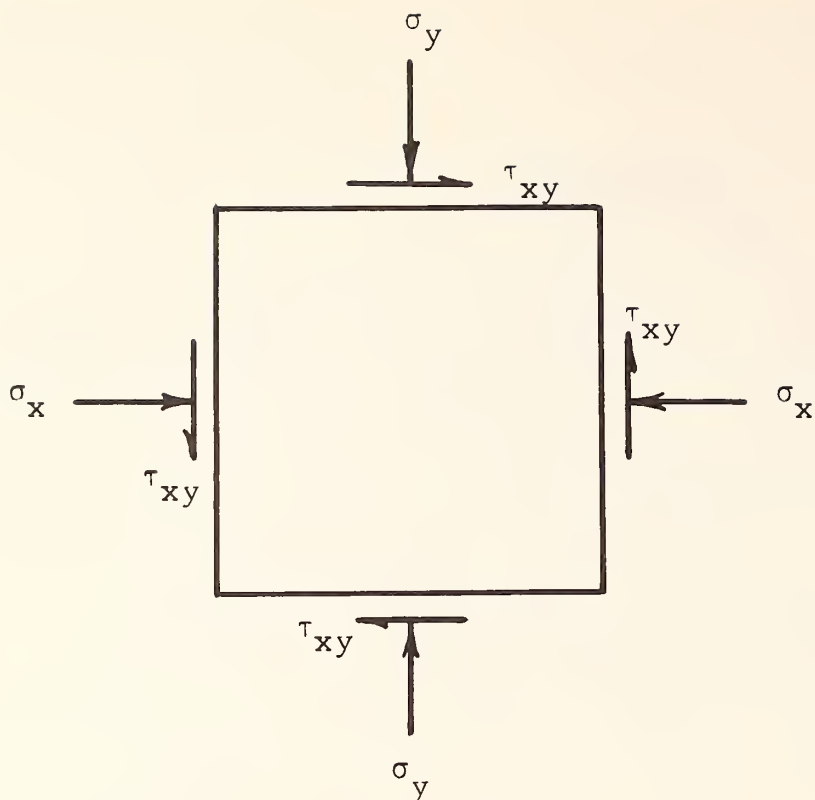
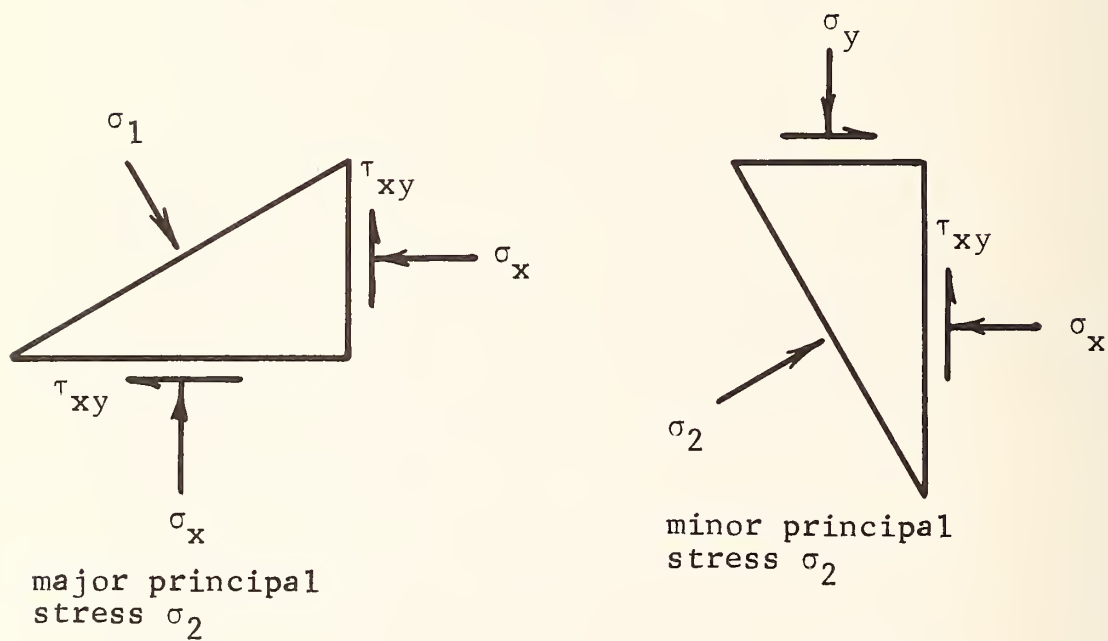


Figure A-2. Development of the Stress Concept





(a) Stresses Acting in the x-y Plane



(b) Principal Stresses in the x-y Plane

Figure A-3. Principal Stresses in a Plane

in as much as the shear stresses vanish in the principal stress directions.

A convenient representation of the shear tensor in two dimensions is the Mohr's circle indicated in Figure A-4. On a plot of shear vs normal stress, the stress tensor is represented by a circle having a center at  $[(\sigma_1 + \sigma_3)/2, 0]$  and radius of  $[(\sigma_1 - \sigma_3)/2]$ . The stresses at any angle  $\alpha$  are represented by the coordinates of points on the circle at angle  $2\alpha$  as indicated in the figure.

Finally, the normal stresses about a point may be represented by an ellipse in normal stress space as shown in Figure A-5. The normal stress components at an inclination  $\alpha$  and  $\alpha \pm 90^\circ$  are represented by the  $\sigma_1$  and  $\sigma_3$  coordinates of the stress ellipse.

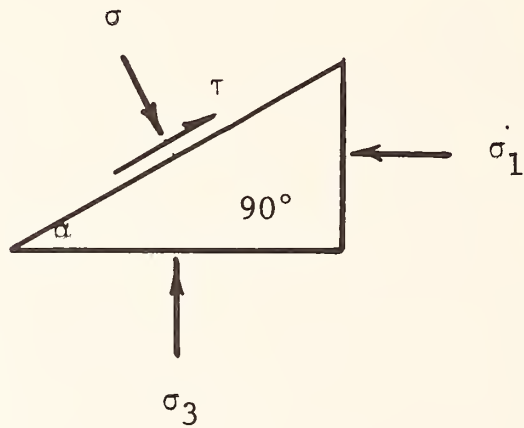
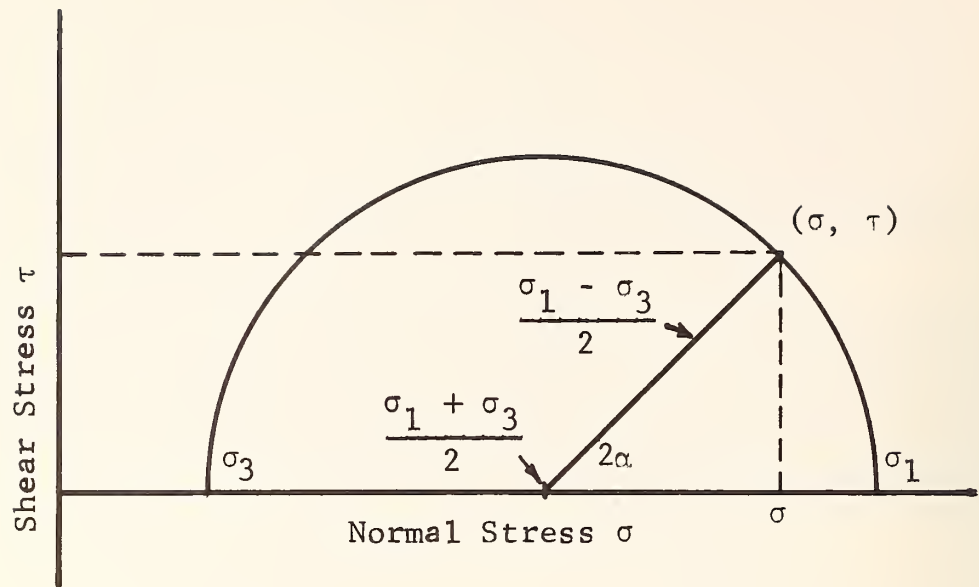


Figure A-4. Mohr's Representation of the Stress Tensor in Two Dimensions

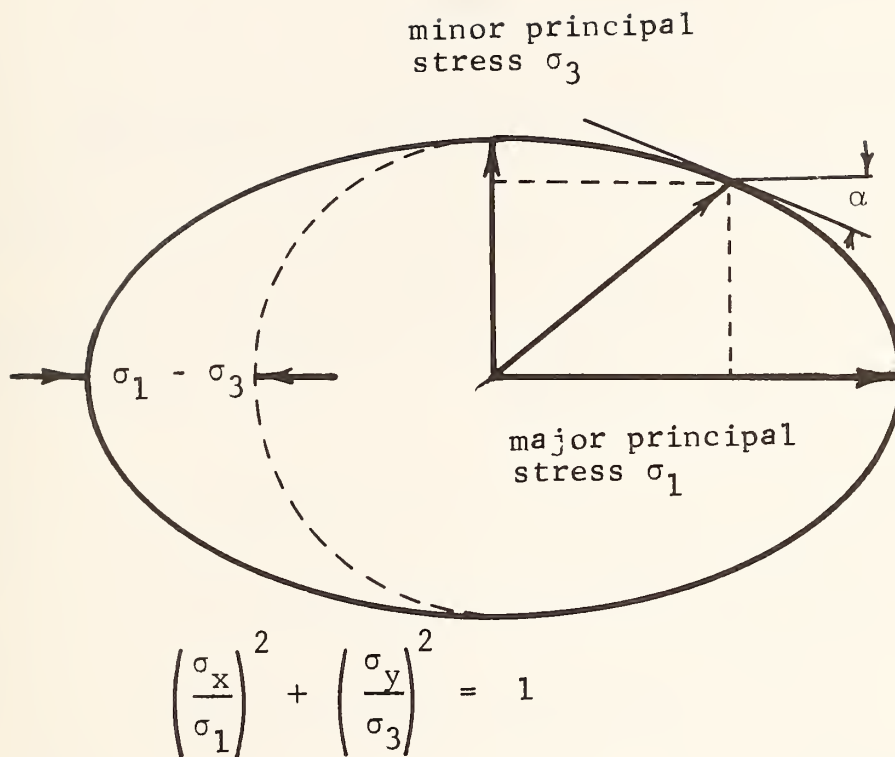


Figure A-5. Stress Ellipse showing Normal Stresses Around a Point

## A-2. EFFECTIVE STRESS CONCEPT

Stress tensors in geotechnical applications are frequently represented as the sum of the effective stress  $\sigma'$  and the pore pressure  $u$  that results from the pressure of fluid within the soil pores. The effective stress is associated with the grain to grain contact forces. The concept of total stress  $\sigma$  is expressed by

$$\sigma = \sigma' + u$$

The effective stress concept is convenient because the Mohr Rupture theory frequently used to express soil shear strength is given by

$$\begin{aligned} S &= c + \sigma' \tan \phi \\ &= c + (\sigma - u) \tan \phi \end{aligned}$$

in which

$S$  = shear strength

$c$  = cohesion

$\phi$  = angle of internal friction

Thus the effective stress concept is used to evaluate the behavior of the soil, while the total stress determines the forces that a structure must resist.

## A.3 STRESS TRANSFORMATION EQUATIONS

To deal with the stresses at an arbitrary orientation, the stress transformation equations may be employed.

In matrix notation

$$\sigma_{mn} = a_{im} a_{jn} \sigma_{ij}$$



where  $\sigma_{mn}$  and  $\sigma_{ij}$  are the stress tensor referred to two coordinate systems having different orientations with direction cosines  $a_{ab}$

Because each coordinate system is composed of three orthogonal axes, the direction cosines are constrained by

$$a_{\alpha\beta} a_{\alpha\gamma} = \delta_{\beta\gamma} \quad \text{Kronecker delta}$$

$$a_{\alpha\beta} a_{\gamma\beta} = \delta_{\alpha\gamma} \quad \text{Kronecker delta}$$

The usual index notation and range conventions apply.

If algebraic notation is employed, the stress transformation equations for coordinate systems  $xyz$  and  $x'y'z'$  became:

$$\begin{aligned} \sigma_{x'x'} &= \sigma_{xx} \cos^2(x',x) + \sigma_{yy} \cos^2(x',y) + \sigma_{zz} \cos^2(x',z) \\ &+ 2\tau_{xy} \cos(x',x) \cos(x',y) + 2\tau_{yz} \cos(x',y) \cos(x',z) \\ &+ 2\tau_{zx} \cos(x',z) \cos(x',x) \end{aligned}$$

$$\begin{aligned} \tau_{x'y'} &= \sigma_{xx} \cos(x',x) \cos(y',x) + \sigma_{yy} \cos(x',y) \cos(y',y) \\ &+ \sigma_{zz} \cos(x',z) \cos(y',z) \\ &+ \tau_{xy} [\cos(x',x) \cos(y',y) + \cos(x',y) \cos(y',x)] \\ &+ \tau_{yz} [\cos(x',y) \cos(y',z) + \cos(x',z) \cos(y',y)] \\ &+ \tau_{zx} [\cos(x',z) \cos(y',x) + \cos(x',x) \cos(y',z)] \end{aligned}$$

where the direction cosines are given by  $\cos(A,B)$ .

Similar forms are used for the remaining four stress components in  $x'y'z'$  coordinate system. The matrix and algebraic equations are, of course, mathematically identical.

For the case in which the stresses are measured on an arbitrary plane  $x'y'$  in a  $\sigma_x \sigma_y \sigma_z$  stress field, the transformation equations give  $\sigma_{x'x'}$ ,  $\sigma_{y'y'}$ ,  $\tau_{x'y'}$  in the plane, and  $\sigma_{z'z'}$ ,  $\tau_{x'z'}$ ,  $\tau_{y'z'}$  acting normal to the plane.

It is convenient to formulate the equations relating the normal stresses,  $\sigma_n$ , in arbitrary directions  $\alpha_1, \alpha_2, \dots \alpha_i$  to the principal stresses  $\sigma_1$  and  $\sigma_3$ , and their orientation  $\beta$ . This may be treated by reference to the stress circle

$$\sigma_n = \frac{\sigma_1 + \sigma_2}{2} + \frac{\sigma_1 - \sigma_2}{2} \cos 2\beta$$

$$\sigma_n = \sigma_m + \Delta\sigma \cos 2\beta$$

where  $\sigma_m$  and  $\Delta\sigma$  are the mean and deviator stresses.

If measurements of  $\sigma_n$  are made at angles  $(\alpha_1 + \beta)$ ,  $(\alpha_2 + \beta)$  ...  $(\alpha_i + \beta)$

$$\sigma_{n1} = \sigma_m + \Delta\sigma \cos 2(\alpha_1 + \beta)$$

$$\sigma_{n2} = \sigma_m + \Delta\sigma \cos 2(\alpha_2 + \beta)$$

$$\sigma_{ni} = \sigma_m + \Delta\sigma \cos 2(\alpha_i + \beta)$$

In this system, the measured  $\sigma_n$  and  $\alpha_i$  are known, the  $\sigma_m$ ,  $\Delta\sigma$  and angle  $\beta$  are found by simultaneous solution of three equations. In the body of this report it is suggested that normal stresses be measured in seven directions. This would permit a least squares fit to be made on the values of  $\sigma_m$ ,  $\Delta\sigma$  and  $\beta$  since up to 35 sets of simultaneous equations could be written if such a thing were desired.

#### A.4 DISCONTINUOUS IN-PLANE STRESSES IN A LAYERED SEMI-INFINITE BODY

Let Figure A.6 represent a layered semi-infinite continuous elastic body, isotropic in each layer, with layer elastic properties  $E_{(i)}$ ,  $\nu_{(i)}$  and layer densities  $\gamma_{(i)}$  where the subscript  $(i)$  identifies the layer in the figure. These properties and densities may vary from layer to layer but are constant within each layer. Let the  $x, y, z$  axes shown in the figure represent a cartesian coordinate system with its origin at the top surface of the first layer and the  $z$ -axis in the direction normal to the layers, with  $z_i$ ,  $i = 0, 1, 2, \dots$ , representing the boundary locations between the layers. Furthermore, let the coordinate system origin be located at an arbitrary point on the top surface and the  $x, y$ -axes have an arbitrary orientation on this surface.

The equations governing the static behavior of this body are as follows.<sup>(1)</sup> The equilibrium Equations (1a,b,c) where  $X, Y, Z$  represent body forces per unit volume. The surface traction boundary conditions, Equations (2a,b,c), where  $\bar{X}, \bar{Y}, \bar{Z}$  represent the surface tractions and  $l, m, n$  are the direction cosines of the external normal to the surface of the body at the point under consideration. Equations (3a,b,c) and (4a,b,c) which represent the stress-strain relations and Equations (5a,b,c), (6a,b,c) which are the conditions of compatibility of strains with the existence of continuous displacements.

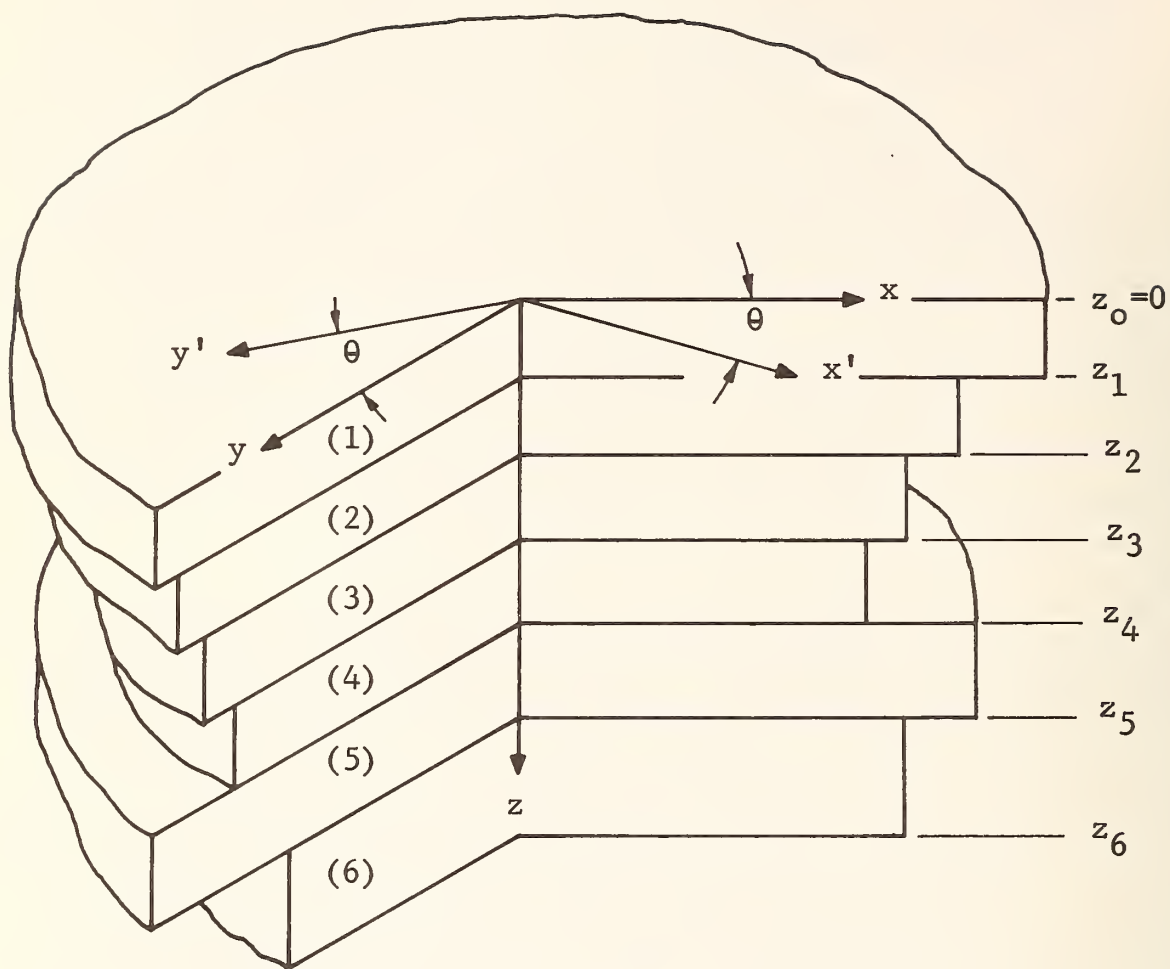


Figure A-6. Layered Semi-Infinite Continuous Elastic Body

$$\begin{aligned}
\frac{\partial \sigma_x}{\partial x} + \frac{\partial \tau_{xy}}{\partial y} + \frac{\partial \tau_{xz}}{\partial z} + X &= 0 \\
\frac{\partial \sigma_y}{\partial y} + \frac{\partial \tau_{xy}}{\partial x} + \frac{\partial \tau_{yz}}{\partial z} + Y &= 0 \\
\frac{\partial \sigma_z}{\partial z} + \frac{\partial \tau_{xz}}{\partial x} + \frac{\partial \tau_{yz}}{\partial y} + Z &= 0
\end{aligned}
\tag{1a,b,c}$$

$$\begin{aligned}
\bar{X} &= \sigma_x l + \tau_{xy} m + \tau_{xz} n \\
\bar{Y} &= \sigma_y m + \tau_{yz} n + \tau_{xy} l \\
\bar{Z} &= \sigma_z n + \tau_{xz} l + \tau_{yz} m
\end{aligned}
\tag{2a,b,c}$$

$$\begin{aligned}
\varepsilon_x &= \frac{1}{E} [\sigma_x - \nu(\sigma_y + \sigma_z)] \\
\varepsilon_y &= \frac{1}{E} [\sigma_y - \nu(\sigma_x + \sigma_z)] \\
\varepsilon_z &= \frac{1}{E} [\sigma_z - \nu(\sigma_x + \sigma_y)]
\end{aligned}
\tag{3a,b,c}$$

$$\begin{aligned}
\gamma_{xy} &= \frac{2(1+\nu)}{E} \tau_{xy} \\
\gamma_{xz} &= \frac{2(1+\nu)}{E} \tau_{xz} \\
\gamma_{yz} &= \frac{2(1+\nu)}{E} \tau_{yz}
\end{aligned}
\tag{4a,b,c}$$

$$\begin{aligned}
\frac{\partial^2 \varepsilon_x}{\partial y^2} + \frac{\partial^2 \varepsilon_y}{\partial x^2} &= \frac{\partial^2 \gamma_{xy}}{\partial x \partial y}, \\
\frac{\partial^2 \varepsilon_y}{\partial z^2} + \frac{\partial^2 \varepsilon_z}{\partial y^2} &= \frac{\partial^2 \gamma_{yz}}{\partial y \partial z}, \\
\frac{\partial^2 \varepsilon_z}{\partial x^2} + \frac{\partial^2 \varepsilon_x}{\partial z^2} &= \frac{\partial^2 \gamma_{xz}}{\partial x \partial z}
\end{aligned}
\tag{5a,b,c}$$

$$\begin{aligned}
\frac{\partial^2 \varepsilon_x}{\partial y \partial z} &= \frac{\partial}{\partial x} \left( -\frac{\partial \gamma_{yz}}{\partial x} + \frac{\partial \gamma_{xz}}{\partial y} + \frac{\partial \gamma_{xy}}{\partial z} \right) \\
\frac{\partial^2 \varepsilon_y}{\partial x \partial z} &= \frac{\partial}{\partial y} \left( \frac{\partial \gamma_{yz}}{\partial x} + \frac{\partial \gamma_{xz}}{\partial y} + \frac{\partial \gamma_{xy}}{\partial z} \right) \\
\frac{\partial^2 \varepsilon_z}{\partial x \partial y} &= \frac{\partial}{\partial z} \left( \frac{\partial \gamma_{yz}}{\partial x} + \frac{\partial \gamma_{xz}}{\partial y} + \frac{\partial \gamma_{xy}}{\partial z} \right)
\end{aligned}
\tag{6a,b,c}$$



It will be shown below that an in-plane state of stress, discontinuous from layer to layer, can exist in the body provided the following sufficient conditions are satisfied:

- a) The in-plane normal strains are uniform for all layers. That is,  $\epsilon_x$ ,  $\epsilon_y$ , are constant, independent of the in-plane orientation of the  $x, y$ -axes and independent of the  $x, y, z$  coordinates. For Fig. 1

$$\epsilon_x = \epsilon_y = \epsilon_{x'} = \epsilon_{y'} = c; z \geq 0 \quad (7)$$

where  $c$  is a constant.

- b) Only one body force is present: that due to gravity.  
' Let that be in the  $z$ -direction. Hence,

$$X = 0; Y = 0; Z = \gamma_{(i)}; z \geq 0 \quad (8)$$

for every layer.

- c) Only one uniform surface traction is present at  $z = 0$ ; that normal to the surface. Hence,

$$\bar{X} = 0; \bar{Y} = 0; \bar{Z} = \bar{Z}_0 \quad (9)$$

where  $\bar{Z}_0$  is a constant.

The stress state resulting from the existence of these conditions is derived as follows. The subtraction of Equation (3b) from (3a) and the substitution of (7) into the result gives

$$\sigma_x = \sigma_y = \sigma; z \geq 0 \quad (10)$$

where  $\sigma$  expresses the commonality of  $\sigma_x$  and  $\sigma_y$ .

Since  $\sigma_z$  does not vary with the orientation of the x,y-axes it follows from (3a,b), (7) and (10) that  $\sigma$  is a principal stress. It follows from orthogonality that  $\sigma_z$  is likewise a principal stress. Hence,

$$\tau_{xy} = \tau_{xz} = \tau_{yz} = 0; \quad z \geq 0 \quad (11)$$

The substitution of (8), (10) and (11) into Equations (1a,b) shows that

$$\sigma = \sigma(z) \quad z \geq 0 \quad (12)$$

where the function  $\sigma(z)$  may be zero, a constant or a suitable function of  $z$  only plus a constant. The substitution of (7) and (12) into (3a) gives

$$\sigma_z = \sigma_z(z) \quad (13)$$

i.e.,  $\sigma_z$  is a function of  $z$  and/or a constant only.

From Equations (1c), (8) and (11) we obtain

$$\frac{\partial \sigma_z}{\partial z} = -\gamma(i) \quad z_{i-1} < z < z_i \quad (14)$$

$$i = 1, 2, 3 \dots$$

Equation (13) is a step function. The function is continuous and single valued within the open interval  $z_{i-1} < z < z_i$ . At the boundary points of a layer,  $z_{i-1}$  and  $z_i$ , it is mathematically undefined. It must therefore be defined from additional considerations beyond the mathematical ones, such as the physical requirements of continuity of displacements and satisfaction of equilibrium. A sufficient definition meeting these requirements is

$$\frac{\partial \sigma_z}{\partial z} = - \gamma_{(1)}; \quad z = z_0 \quad (15a)$$

$$\frac{\partial \sigma_z}{\partial z} = - \gamma_{(i)}; \quad z = z_i \quad (15b)$$

$$i = 1, 2, 3, \dots$$

By combining (15) with (14) we have now a single valued function for  $z \geq 0$  satisfying all the required conditions.

$$\frac{\partial \sigma_z}{\partial z} = - \gamma_{(1)}; \quad z_0 \leq z \leq z_1 \quad (16a)$$

$$\frac{\partial \sigma_z}{\partial z} = - \gamma_{(i)}; \quad z_{i-1} < z \leq z_i \quad (16b)$$

$$i = 2, 3, 4, \dots$$

From integration of Equations (16) and taking into consideration (9) and (13) we get

$$\sigma_z = \bar{z}_0 - \gamma_{(1)} (z - z_0); \quad z_0 \leq z \leq z_1 \quad (17a)$$

$$\sigma_z = \bar{z}_0 - \left[ \sum_{j=1}^{i-1} \gamma_{(j)} (z_j - z_{j-1}) \right] - \gamma_{(i)} (z - z_{i-1}); \quad \left. \begin{array}{l} z_{i-1} < z \leq z_i \\ i = 2, 3, 4, \dots \end{array} \right\} (17b)$$

The substitution of (17), (12), (10) and (7) into (3a) gives

$$\sigma_x = \sigma_y = \frac{E_{(1)}^c - \nu_{(1)} \sigma_z}{1 - \nu_{(1)}}; \quad z_0 \leq z \leq z_1 \quad (18a)$$

$$\sigma_x = \sigma_y = \frac{E_{(i)}^c - \nu_{(i)} \sigma_z}{1 - \nu_{(i)}} ; \quad z_{i-1} < z \leq z_i \quad (18b)$$

$$i = 2, 3, 4, \dots$$

Equation (18b) representing the in-plane normal stresses is a single valued sectionally continuous function. The discontinuities across the boundary points  $z_i$  come about because of the discontinuous elastic properties  $E_{(i)}$ ,  $\nu_{(i)}$  from layer to layer.

It can readily be shown by substitution of the stress functions (18), (17), (11), and (9) into (2) that the boundary condition equations are satisfied. An example of a stress field based on the above formulae is shown in Figure A-7.

The conditions of compatibility (5) and (6) are likewise satisfied as can be seen from the following. The substitution of (17) and (18) into (3c) gives

$$\epsilon_z = \left[ \frac{1 - \nu_{(1)} + 2\nu_{(1)}^2}{1 - \nu_{(1)}} \right] \frac{\sigma_z}{E_{(1)}} - \frac{2\nu_{(1)}^c}{1 - \nu_{(1)}} \quad (19a)$$

$$\epsilon_z = \left[ \frac{1 - \nu_{(i)} + 2\nu_{(i)}^2}{1 - \nu_{(i)}} \right] \frac{\sigma_z}{E_{(i)}} - \frac{2\nu_{(i)}^c}{1 - \nu_{(i)}} \quad (19b)$$

$$z_0 \leq z \leq z_1$$

$$z_{i-1} < z \leq z_i$$

$$i = 2, 3, 4, \dots$$

where the expression for  $\sigma_z$  in (19a) is given by (17a)

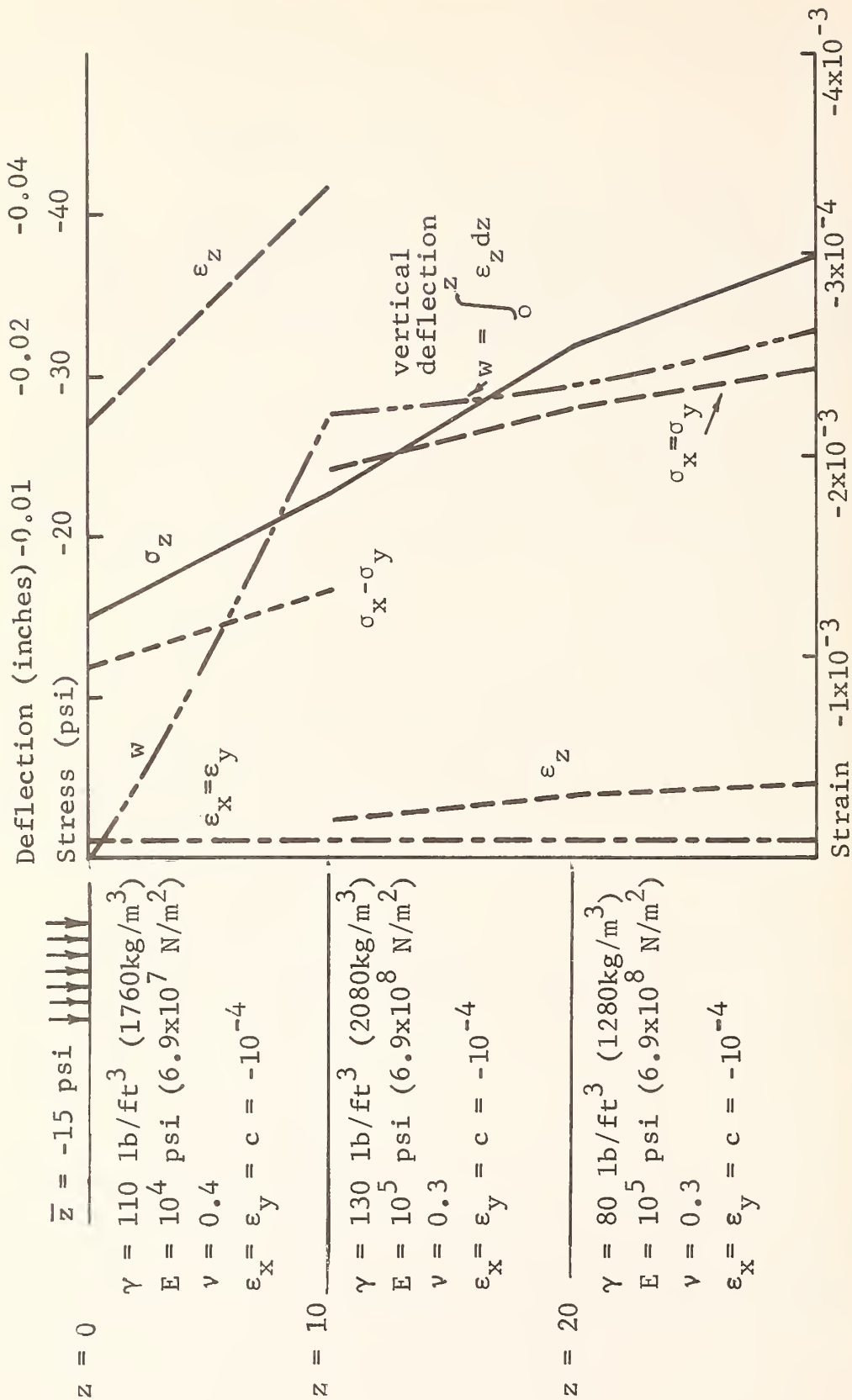


Figure A-7. Example Solution of Stresses, Strains and Vertical Deflection Using Equations 3, 7, 17 and 18 for conditions Indicated



and for (19b) by (17b). From (4) and (11) we have

$$\gamma_{xy} = 0; \quad \gamma_{zx} = 0; \quad \gamma_{yz} = 0; \quad z \geq 0 \quad (20)$$

It then follows readily by differentiation of Equations (7), (19) and (20) and substitution into Equations (5) and (6) that the compatibility conditions are satisfied. Hence it has been shown that an in-plane state of stress, discontinuous from layer to layer, can exist.

The satisfaction of the compatibility conditions insures the existence of a continuous displacement field. That this is the case here, can be readily shown as follows. Let  $u, v, w$  be the displacement in the  $x, y, z$  direction respectively of a point with position  $x, y, z$  in Figure 1. Then :

$$\frac{\partial u}{\partial x} = \epsilon_x, \quad \frac{\partial v}{\partial y} = \epsilon_y, \quad \frac{\partial w}{\partial z} = \epsilon_z \quad (21)$$

$$\frac{\partial u}{\partial y} + \frac{\partial v}{\partial x} = \gamma_{xy}, \quad \frac{\partial u}{\partial z} + \frac{\partial w}{\partial x} = \gamma_{xz}, \quad \frac{\partial v}{\partial z} + \frac{\partial w}{\partial y} = \gamma_{yz} \quad (22)$$

$$\frac{1}{2} \left( \frac{\partial w}{\partial y} - \frac{\partial v}{\partial z} \right) = \omega_x, \quad \frac{1}{2} \left( \frac{\partial u}{\partial z} - \frac{\partial w}{\partial x} \right) = \omega_y, \quad \frac{1}{2} \left( \frac{\partial v}{\partial x} - \frac{\partial u}{\partial y} \right) = \omega_z \quad (23)$$

where  $\omega_x, \omega_y, \omega_z$  are the rotations of the direction of principal strains when moving from point to point in the body. The absence of shear strains, Equation (20), precludes such rotation. Hence

$$\omega_x = 0, \quad \omega_y = 0; \quad \omega_z = 0; \quad z \geq 0 \quad (24)$$

It follows by addition and subtraction between Equations (22), (23) and inclusion of (24) that

$$\begin{aligned}
\frac{\partial u}{\partial y} &= 0; & \frac{\partial u}{\partial z} &= 0; \\
\frac{\partial v}{\partial x} &= 0; & \frac{\partial v}{\partial z} &= 0; \\
\frac{\partial w}{\partial x} &= 0; & \frac{\partial w}{\partial y} &= 0;
\end{aligned} \tag{25}$$

Consequently the displacements are functions of single variables only as follows

$$\begin{aligned}
u &= u(x) \\
v &= v(y) \\
w &= w(z)
\end{aligned} \tag{26a,b,c}$$

Since the body of Figure 1 is semi-infinite we can select an arbitrary point on the body as the point of zero displacement and measure the displacements of all other points relative to it. Let that point be  $x=y=z=0$ . Then

$$\begin{aligned}
u(0) &= 0 \\
v(0) &= 0 \\
w(0) &= 0
\end{aligned} \tag{27a,b,c}$$

In view of Equations (26) and (27) we can use (21), (19), and (7) to obtain  $u, v, w$  by integration

$$u = \int_{x=0}^x \frac{\partial u}{\partial x} dx = \int_{x=0}^x \frac{du}{dx} dx = c \int_{x=0}^x dx; \quad z \geq 0 \tag{28}$$

$$y = \int_{y=0}^y \frac{v}{y} dy = \int_{y=0}^y \frac{dv}{dy} dy = c \int_{y=0}^y dy; \quad z \geq 0 \quad (29)$$

$$w = \int_{z=0}^z \frac{w}{z} dz = \int_{z=0}^z \frac{dw}{dz} dz = \int_{z=0}^z e_z dz \quad z \geq 0 \quad (30)$$

Hence

$$u = cx \quad z \geq 0 \quad (31)$$

$$v = cy \quad z \geq 0 \quad (32)$$

$$w = \left[ \sum_{j=0}^{i-1} \int_{z_j}^{z_{i-1}} e_z dz \right] + \int_{z_{i-1}}^z e_z dz; \quad \left\{ \begin{array}{l} z_{i-1} \leq z \leq z_i \\ i = 1, 2, 3, \dots \end{array} \right. \quad (33)$$

As can be seen from (31), (32), (33)  $u, v, w$  are continuous.

## APPENDIX B

### FABRIC ANALYSIS GLOSSARY

ARRANGEMENT. Arrangement includes distribution and orientation.

basic: arrangement within a group of like individuals.

related: arrangement between groups of unlike individuals.

referred: arrangement of individuals with regard to specific reference feature.

Arrangement of peds at each level includes accommodation (degree to which adjacent faces are molds of each other), packing (regular to random), and inclination (orientation with respect to vertical or horizontal). (Brewer)

BASIC STRUCTURE. The structure of the s-matrix, that is, the size, shape, and arrangement of simple grains (plasma and skeleton grains) and voids in primary peds or apedal soil material, excluding pedological features other than plasma separations. (Brewer)

CLOD. (not a ped) Caused by disturbance, such as plowing or digging, that molds the soil to a transient mass that slakes with repeated wetting and drying. (Brewer)

COLLECTIVITY (of fabric). The number of the arrangements (collectives) into which fall the fabric-elements distinguished. (Sander)

COMPONENTIAL MOVEMENT (related to a mechanical deformation). Any movement of components (in rocks) in consequence of which a rock retains its continuity but acquires a new shape in the period of time considered. (Sander)

CONCRETION. (not a ped) Caused by local concentrations of compounds that irreversibly cement the soil grains together. (Brewer)

CRACK. A partial or incomplete fracture. (AGI Glossary)

CRYSTALLARIA. Single crystals or arrangements of crystals of relatively pure fractions of the plasma that do not enclose the s-matrix of the soil material but form cohesive masses; their morphology (especially shape and internal fabric) is consistent with their formation and present occurrence in original voids in the enclosing soil material. Examples include crystal tubes, crystal chambers, crystal sheets, and intercalary crystals. (Brewer)

CRYSTALLINITY. (a) The degree to which a rock (especially an igneous rock) is crystalline, whether holocrystalline, glassy, or crypto-crystalline. (b) The degree to which the crystalline character of an igneous rock is developed (e.g., macrocrystalline, microcrystalline, or cryptocrystalline) or is apparent (e.g., phaneritic or aphanitic). (AGI Glossary)

CUTAN. A modification of the texture, structure, or fabric at natural surfaces in soil materials due to concentration of particular soil constituents or in-situ modification of the plasma. Cutans can be composed of any of the component substances of the soil material. (Brewer)

DEFORMATION LAMELLA. A type of slipband that is produced especially in quartz by active slip within a mineral grain during tectonic deformation; also, a similar feature produced by shock. (AGI Glossary)

DOMAIN (fabric). A volume defined by boundaries such as structural or compositional discontinuities within which the rock fabric is uniform. (AGI Glossary)

DYNAMIC ANALYSIS (fabric). Dynamic inferences concern the nature of the stresses in the rocks at the time of deformations.

Experimentally deformed specimens are compared with their naturally deformed counterparts to determine statistically the orientation and relative magnitude of the principal stresses in rocks at the time of deformation.

Important deformation processes include fracturing, faulting, gliding flow, rotation, and recrystallization. (Friedman)

ELEMENTARY STRUCTURE. A simplified level of primary structure; it is an integration of a characteristic size, shape, and arrangement of specific pedological features and the basic structure, or structure of the s-matrix. (Brewer)

FABRIC. The spatial data for the interior of the domain under consideration describe its fabric. (Sander)

The physical constitution of a soil material as expressed by the spatial arrangement of the solid particles and associated voids. (Brewer)

Fabric is the element of structure (size, shape and arrangement of solid particles and voids) which deals with arrangements. (Brewer)



Texture-structure and degree of crystallization (crystallinity) of solid particles. (Brewer)

After Turner-petro fabrics is the study of all structural and textural features of a rock as manifested in every recognizable rock element from crystal lattices to large-scale features requiring field investigation. (Friedman)

A fabric, like a crystal structure, is a three-dimensional array of discontinuities or heterogeneities in structure. (Paterson and Weiss)

(struct. petrol.) The sum of all the structural and textural features of a rock. The term incorporates the notion of function or behavior (correlative physical properties) as well as of form (arrangement of structural and textural components). (AGI Glossary)

FABRIC ELEMENTS. Actual or theoretical like parts of the fabric, resembling each other in a particular respect. (Sander)

Deformation examples include crystallographic parameters, deformation lamellae, kink bands, lineations, fold axes, fractures, faults, and other planes of mechanical discontinuity. (Friedman)

A surface or line of structural discontinuity. It may be a crystallographic feature such as a lattice plane, or noncrystallographic, such as foliation. A spatial array of a particular fabric element is called a subfabric. (AGI Glossary)

FAULT. A general term for a dislocation in a crystal.

A surface or zone of rock fracture along which there has been displacement, from a few centimeters to a few kilometers in scale. (AGI Glossary)

FRACTURE. (mineral) The breaking of a mineral other than along planes of cleavage. A mineral can be described in part by its characteristic fracture, e.g. uneven, fibrous, conchoidal.

(struct. geol.) A general term for any break in a rock, whether or not it causes displacement, due to mechanical failure by stress. Fracture includes cracks, joints, and faults

(exper. struct. geol.) Deformation due to a momentary loss of cohesion or loss of resistance to differential stress and a release of stored elastic energy. (AGI Glossary)

FRAGMENT. (not a ped) Caused by rupture of the soil mass across natural surfaces of weakness. (Brewer)

GENEITY (state of). Characterization of the position between homogeneity and heterogeneity. (Sander)

GLAEBULE. A three-dimensional unit within the s-matrix of the soil material, and usually approximately prolate to equant in shape; its morphology (especially size, shape, and/or internal fabric) is incompatible with its present occurrence being within a single void in the present soil material. It is recognized as a unit either because of a greater concentration of some constituent and/or a difference in fabric compared with the enclosing soil material, or because it has a distinct boundary with the enclosing soil material. (Includes nodules, concretions, septaria, and related forms but not the spherulites and other regular crystal growths whose internal fabric suggest formation and present occurrence in a single large void). (Brewer)

HETEROTACTIC FABRICS. Fabrics in which subfabrics do not conform to a common symmetry. (AGI Glossary)

HOMOGENEOUS (mass). Exhibiting essentially the same physical properties at every point throughout the mass. (ASTM-D653-67)

HOMOTACTIC FABRICS. Fabrics in which all subfabrics are conformable in symmetry. (AGI Glossary)

ISOTROPIC (mass). Having the property (or properties) in all directions. (ASTM-D653-67)

JOINT. A surface of actual or potential fracture or parting in rock, without displacement; the surface is usually plane and often occurs with parallel joints to form part of a joint set. (AGI Glossary)

KINEMATIC ANALYSIS (fabrics). Kinematic inferences concern the displacements that have transformed the initial fabric into the observed fabric. It is assumed that the symmetry of the rock fabric reflects the symmetry of the movement responsible for the evolution of that fabric. (Friedman)

MESOSCOPIC. A term introduced by Dennis (1967) to describe a tectonic feature large enough to be observed without the aid of a microscope yet small enough that it can still be observed directly in its entirety. (AGI Glossary)

- MICROSCOPIC. Said of an object or phenomenon or of its characteristics that cannot be observed without the aid of a microscope. (AGI Glossary)
- PED. An individual natural soil aggregate consisting of a cluster of primary particles, and separated from adjoining peds by surfaces of weakness which are recognizable as natural voids or by the occurrence of cutans. (Brewer)
- PEDALITY. The physical constitution of a soil material as expressed by the size, shape, and arrangement of peds. (Brewer)
- PEDOLOGICAL FEATURES. Recognizable units within a soil material which are distinguishable from the enclosing material for any reason, such as origin (deposition as an entity), differences in concentration of some fraction of the plasma, or differences in arrangement of the constituents (fabric) (includes features inherited from the parent rock or formed by the processes of deposition of transported parent material). (Brewer)
- PEDOTUBULE. A pedological feature consisting of soil material (skeleton grains or skeleton grains plus plasma, as distinct from concentrations of fractions of the plasma) and having a tubular external form, either single tubes or branching systems of tubes; its external boundaries are relatively sharp. Tubular form, in this context, means that the feature as a unit, or its impression in the enclosing soil material, has a relatively uniform cross-sectional size and shape, most commonly circular or elliptical; that is, the impression of the pedotubule conforms to the definition of channels. (Brewer)
- PLASMA. That part of soil material which is capable of being or has been moved, reorganized, and/or concentrated by the processes of soil formation. It includes all the material, mineral or organic, of colloidal size and relatively soluble material which is not bound up in the skeleton grains. (Brewer)
- PLASMIC STRUCTURE. The structure of the plasma of the s-matrix, that is, the size, shape, and arrangement of the plasma grains and associated simple packing voids. (Brewer)
- PRIMARY PEDS. The simplest peds occurring in a soil material; they cannot be divided into smaller peds, but they may be packed together to form compound peds of a higher level of organization. (Brewer)



PRIMARY STRUCTURE. The structure within an apedal soil material or within the primary peds in a pedal soil material; it is an integration of the size, shape, and arrangement of all the pedological features enclosed in the s-matrix and the basic structure or structure of the s-matrix. (Brewer)

S-MATRIX. (matrix including skeleton grains) The material within the simplest (primary) peds, or composing apedal soil materials, in which the pedological features occur; it consists of the plasma, skeleton grains, and voids that do not occur in pedological features other than plasma separations. (Brewer)

SCALAR FABRIC DATA (undirected). Examples include individual fabric element considered in isolation; about pairs of fabric elements, e.g. fabric habit of kinds of grain, shape of boundaries between fabric elements reacting with one another, pore volume, percentage of particular species of grain in a given volume, and homogeneity (volume of smallest, statistically homogeneous domain). (Sander)

SECONDARY STRUCTURE. The size, shape, and arrangement of the primary peds, their interpedal voids, and associated interpedal pedological features in a soil material. (Brewer)

SHAPE (particle). The spatial or geometric form of the particles in a sediment or rock; a fundamental property of a particle that determines the relation between its volume and surface area. It depends upon the sphericity and roundness of the particle, although the term is frequently applied to sphericity as distinguished from roundness. Syn.: grain shape. (AGI Glossary)

SKELETON GRAINS. Individual grains which are relatively stable and not readily translocated, concentrated or reorganized by soil-forming processes; they include mineral grains and resistant siliceous and organic bodies larger than colloidal size. (Brewer)

SLIPBAND. One of the parallel lines known as Luders lines or Hartmann lines in the crystalline grains of a material stressed beyond its elastic limit that are visible only under a microscope and are produced by intracrystalline slip. (AGI Glossary)

STRUCTURE (soil). The physical constitution of a soil material as expressed by the size, shape, and arrangement of the solid particles and voids. (Brewer)

SUBCUTANIC FEATURE. A pedological feature (recognized by a difference in texture, structure, or fabric as compared with the enclosing s-matrix) that has a consistent relationship with natural surfaces in the soil material, but does not occur immediately at the surfaces. (Brewer)

SYMMETRY. The presence of any identities in such positions in space that they replace each other as a result of symmetry-operations. (Identities are color, hardness, shape, etc.). (Sander)

TERTIARY STRUCTURE. The size, shape, and arrangement of the secondary peds of a soil material (compound peds resulting from the packing of primary peds), their interpedal voids and associated interpedal pedological features. (Brewer)

TEXTURE (petrology). The general physical appearance or character of a rock, including the geometric aspects of, and the mutual relations among, the component particles or crystals; e.g., the size, shape, and arrangement of the constituent elements of a sedimentary rock, or the crystallinity, granularity, and fabric of the constituent elements of an igneous rock. The term is applied to the smaller (megascopic or microscopic) features as seen on a smooth surface of a homogeneous rock or mineral aggregate. The term structure is generally used for the larger features of a rock. "Texture" should not be used synonymously with "structure" although some textural features such as foliation or flow texture may parallel major structural features of a rock. (AGI Glossary)

The physical constitution of a soil material as expressed by its structure, and by the degree of crystallization (crystallinity) of the solid particles; fabric is a part of structure, which is a part of texture in this context. (Brewer)

TROPY (state of). Characterization of the position between isotropy and anisotropy. (Sander)

VECTORIAL FABRIC DATA (directed). All fabric data which show directional (mostly symmetrical) influences. Examples include preferred orientation according to crystal shape and crystal structure, directionally dependent paths for transport of material, response to stress, etc., and growth fabrics. (Sander)



VOID. Interstice; an opening or space between one thing and another, as an opening in a rock or soil that is not occupied by solid matter. (AGI Glossary)

Space in a soil mass not occupied by solid mineral matter. (ASTM-653)

Packing voids Voids due to random packing.

Vughs Relatively large voids (other than packing), usually irregular and not normally interconnected with other voids of comparable size.

Vesicles Voids that differ from vughs in that their walls consist of smooth, simple curves.

Channels Voids that are significantly larger than those which would result from normal packing of single grains, and have a generally cylindrical shape.

Chambers Voids that differ from vughs in that their walls are regular and smoothed (metavoids) and from both vesicles and vughs in that they are interconnected through channels and usually have a characteristic shape.

Planes Planar voids. (Brewer)

## APPENDIX C

### ELECTRON MICROSCOPY SPECIMEN PREPARATION

A critical factor in the application of electron microscopy is specimen preparation. Because the electron microscopy views the sample surface directly, more careful preparation is required than is the case for other tools that respond to conditions deeper within the surface. Specimens must either be dehydrated or sealed because most microscopy requires that they be exposed to vacuum. Because most soils shrink upon dehydration, special preparation techniques are required.

Barden and Sides (1971) discuss disturbance associated with the following specimen preparation techniques:

- o peeling
- o impregnation
- o partial impregnation
- o grinding
- o microtoming

#### PEELING

The peeling technique requires that water be removed and the dry clay fractured to expose an interior surface, then peeled to remove fracture debris. Water removal may be accomplished by air drying, freeze drying, or critical-point drying. Air drying is fastest and easiest, but may cause shrinkage. Critical-point drying reduces shrinkage due to the lack of liquid-gas meniscus forces at the critical point of water, which is 3200 psi at 706 F. Freeze drying and critical-point drying are discussed by Sridharan, Altschaeffl and Diamond (1971).

Once dry, the specimen is fractured to expose a surface along the desired plane, and the fracture debris is peeled off by 50 to 100 applications of adhesive tape to remove surface debris.

### IMPREGNATION

A number of products have been suggested to impregnate microscope specimens. The intent is to replace (at least partially) the pore water with a substance that will cement the clay grains together. Depending on the permeability of the soil and the viscosity of the cement, a long time may be required for impregnation.

### PARTIAL IMPREGNATION

The partial impregnation procedure attempted by Barden and Sides (1971) involved impregnating only the first 2 or 3 mm of soil below the specimen surface. After hardening, the untreated clay was washed away. However, a zone of partial impregnation was found ahead of the fully impregnated zone, making the technique unreliable in its present form.

### GRINDING, MICROTOMING AND ETCHING

Grinding was used on both impregnated and peeled specimens, but found to cause re-orientation of the surface grains. Microtoming was discarded without trial because of previously reported difficulties and the presence of silt-sized particles in most natural clays. Etching was used with some success, but the open structure of highly flocculated clays may be damaged.

### CONCLUSION

In general, the peeling, impregnation with gelatine, and gelatine impregnation with etching were found satisfactory for optical work. Corbowax impregnation allowed surface damage and was unsatisfactory for the scanning electron microscope. It was adequate for x-ray diffraction which penetrates 30 to 50 microns. A review of Table D.1 indicates that the most

TABLE D-1

USE OF VARIOUS SAMPLE PREPARATION TECHNIQUES  
FOR INVESTIGATIONS OF SOIL MICROSTRUCTURE

		Reference										
		Kirkpatrick and Rennie (1972)										
		Barden and Sides (1971)										
		Arthur and Shamash (1970)										
		Ingles and Lee (1971)										
		Morgenstern and Tchalenko (1967, a&b)										
		Clark (1970)										
		Oda (1972)										
		Windisch and Soulie (1970)										
		Sridharan, Altschaeffl and Diamond (1971)										
		Martin (1966)										
		Meade (1961)										
		Barden, Sides and Karunaratne (1970)										
		Devries and Jugle (1968)										
Air Dry												
Air Dry and Peel	X	X								X		
Freeze						X						
Freeze Dry		X							X			
Impregnate		X	X	X	X	X	X	X	X		X	X
Critical Region Drying									X			

common technique used is impregnation. Since this is a time consuming process, the peeling technique is attractive when air drying shrinkage is not prohibitive.



## BIBLIOGRAPHY

Aas, G., (1965), "A Study of the Effect of Vane Shape and Rate of Strain on the Measured Values of In-Situ Shear Strength of Clays," Proc. Sixth Conf. on Soil Mech. and Found. Engin., Montreal, 1965, vol. I, pp 141-145, publ. Univ. Toronto Press.

Aas, G., (1967), "Vane Tests for Investigation of Anisotropy of Undrained Shear Strength of Clays," Norwegian Geotechnical Institute Publication 76 (reprint for Proc. Geotechnical Conf., Oslo), 1967.

Abbe, Ernst, (1873), "Bertrage zur Theorie des Mikroskops und der mickroskopischen Wahrenehmung: Archiv fur Microskopische Anatomie," vol. 9, pp 413-468.

Afifi, S.S., and Richart, F.E., Jr., (1973), "Stress History Effects on Shear Modulus of Soils," Japanese Society of Soil Mech. and Found. Engin. Soils and Found., vol. 13, no. 1, pp 77-95, March 1973.

Altschaeffl, A.G., and Mishu, L.P., (1970), "Capacitance Techniques for Radial Deformations," Proc. Amer. Soc. Civil Engin. J. Soil Mech. and Found. Engin., vol. 96, no. SM4, pp 1487-1491, July 1970.

Andrawes, K.Z., and El-Shoby, M., (1972), "Discussion-Effect of Mica on  $K_0$  Compressibility of Two Soils," Proc. Amer. Soc. Civil Engin. J. Soil Mech. and Found. Engin., vol. 98, no. SM5, pp 504-507, May 1972.

Andrawes, K.Z., and El-Sohby, M., (1973), "Factors Affecting Coefficient of Earth Pressure  $K_0$ ," Proc. Amer. Soc. Civil Engin. J. Soil Mech. and Found. Engin., vol. 99, no SM7, pp 527-539.

Andrews, E.R., (1971), "Progress in Nuclear Magnetic Resonance," Spectroscopy, vol. 8, no. 1.

Andrews, J.T., and Smith D.I., (1970), "Statistical Analysis of Till Fabric: Methodology, Local and Regional Variability," Q. J. Geol. Soc. London, 125, pp 503-542.

Arthur, J.R.F., and Menzies, B.K., (1972), "Inherent Anisotropy in a Sand," Geotechnique, vol. 22, no. 1, pp 115-128.

Arthur, J.R.F., and Shamash, S.J., (1970), "Sampling of Cohesionless Soils Without Disturbing the Particle Packing," Geotechnique, vol. 20, no. 4, pp 439-440.

## BIBLIOGRAPHY (Cont'd.)

Artsybashev, V.A., and Ivanykovich, G.A., (1971), "Two-Probe System of Gamma-Gamma Well Logging for Studying the Effective Atomic Number and Density of Rock Densities," Geophy. App., no. 46, pp 71-73. In Russian. See Nuclear Science Abstract #26-31028.

Awojobi, A.O., (1973), "Estimation of the Dynamic Surface Modulus of a Generalized Gibson Soil from the Rocking Frequency of Rectangular Foundations," Geotechnique, vol. 23, no. 1, pp 23-31.

Baguelin, F., Goulet, G., and Jezequel, J., (1972), "Etude Experimentale Du Compartement D'un Pieu Sollicite Horizontalement," Proc. Fifth European Conf. on Soil Mech. and Found. Engin., vol. 1, Madrid.

Baguelin, F., and Jezequel, J.F., (1973), Le Pressiometre Autoforeur, annales de l'Institute Technique de Batiment et des Travaux Publics, Supplement au no. 307-308, Juillet-Aout.

Baguelin, F., Jezequel, J.F., Le Mee, E., and Le Mehaute, A., (1972), "Expansion of Cylindrical Probes in Cohesive Soils," Proc. Amer. Soc. Civil Engin., J. of the Soil Mech. and Found. Div., vol. 98, no. SM11, pp 1129-1142, Nov. 1972.

Baguelin, F., Jezequel, J.F., and Le Mehaute, A., (1973), "Study of Pore Pressure Occurring During Pressuremeter Test," Proc. of the Eighth International Conf. on Soil Mech. and Found. Engin., Moscow, pp 19-25.

Baker, D.W., Wenk, A.R., and Christie, J.M., (1969), "X-Ray Analysis of Preferred Orientation in Fine Grained Quartz Aggregates," J. of Geol., vol. 77, pp 144-172.

Baker, W.H., and Krizek, R.J., (1967), "Assessment of Shear Strength Theories for Anisotropic Cohesive Soils," Proc. Symp. on Pore Pressure and Shearing Resistance of Soils, New Delhi, India, pp 75-105.

Bamert, E., Schnitter, G., and Weber, M., (1965), "Tri-axial and Seismic Laboratory Tests for Stress-Strain-Time Studies," Proc. Sixth Conf. on Soil Mech. and Found. Engin., Montreal, 1965, vol. I, pp 151-155, pub. Univ. Toronto Press.

Barden, L., (1971), "Examples of Clay Structure and It's Influence on Engineering Behavior," Proc. Roscoe Memorial Symp. on Stress-Strain Behavior of Soils, Cambridge Univ., pp 195-205.

## BIBLIOGRAPHY (Cont'd.)

- Barden, L., (1972), "The Influence of Structure on Deformation and Failure in Clay Soil," *Geotechnique*, vol. 22, no. 1, pp 159-163.
- Barden, L., and Sides, G.R., (1971), "Sample Disturbance in the Investigation of Clay Structure," *Geotechnique*, vol. 21, no. 3, pp 211-222.
- Barden, L., Sides, G.R., and Karunaratne, J.P., (1970), "A Microscopic Examination of Aspects of Clay Structure," *Proc. Second S.E. Asian Conf. Soil Engin., Singapore*.
- Beckmann, W., (1962), "On the Micromorphometric Investigation of Cavities and Aggregates in Soils," *Z. PflErnabr. Dung., Bodenkunde* 99, pp 129-133.
- Begemann, H.K.S., (1961), "A New Method for Taking Samples of Great Length," *Fifth Int. Conf. Soil Mech. and Found. Engin., Paris*, vol. I, pp 437-440.
- Bishop, A.W., (1958), "Test Requirements for Measuring the Coefficient of Earth Pressure at Rest," *Proc. Conf. Earth Pressure Problems, Brussels*, vol. I, pp 2-14.
- Bishop, A.W., and Henkel, D.J., (1961), The Measurement of Soil Properties in the Triaxial Test, pub. London, Edward Arnold (Publishers) Ltd., 140 pp.
- Bjerrum, L., (1967), "Progressive Failure in Slopes of Overconsolidates Plastic Clay and Clay Shales," *Proc. Amer. Soc. Civil Engin., J. Soil Mech. and Found. Engin.*, vol 93, no. SM5, pp 3-49.
- Bjerrum, L., and Anderson, K.H., (1972), "In-Situ Measurement of Lateral Pressures in Clay," *Norwegian Geotechnical Institute Publication* 90, pp 29-38.
- Bjerrum, L., Nash, J.K.T.L., Kennard, R.M., and Gibson, R.E., (1972), "Hydraulic Fracturing in Field Permeability Testing," *Geotechnique*, vol. 22, no. 2, pp 319-332.
- Blight, G.E., (1971), "Can In-Situ Stress Ratios be Estimated by Means of the Vane Shear Test," *Fifth Regional Conf. for Africa on Soil Mech. and Found. Engin., Luanda, Angola*, Aug. 1971.
- Blight, G.E., Williams, A.A.B., (1971), "Cracks and Fissures by Shrinkage and Swelling," *Fifth Reg. Conf. for Africa on Soil Mech. and Found. Engin., Luanda, Angola*.
- Blight, G.E., (1969), "Foundation Failures of Four Rockfill Slopes," *Proc. Amer. Soc. Civil Engin. J. Soil Mech. and Found. Engin.*, vol. 95, no. SM3, pp 743-767.



## BIBLIOGRAPHY (Cont'd.)

Blumel, F., Janik, V., and Schiller, H., (1969), "The Micromorphology and Colloid Condition of Different Types of Soil," Testchr. Sechsigjahr. Best. Landw-Chem. Bundes. Vers. Anst., Linz, pp 89-120.

Boehler, J.P., and Giroud, J.P., (1971), "Measurements of Soil Anisotropy," Proc. Ninth Ann. Engin. Geol. Soils Engin. Symp., Boise, Idaho, pp 175-187.

Borowicka, H., (1961), "The Mechanical Properties of Soils," Proc. Fifth Intl. Conf. Soil Mech., Paris, vol. I, pp 39-42.

Boulton, G.A., (1968), "Flow Tillis and Related Deposits on Some Vespitsbergen Glaciers," J. Glaciology, vol. 7, no. 51, pp 391-412.

Brace, W.F., and Bombolaskis, E.G., (1963), "A Note on Brittle Crack Growth in Compression," J. Geophys. Res. 68, pp 3709-3713.

Bracewell, R.M., (1965), The Fourier Transform and Its Applications, McGraw-Hill, New York, 381 pp.

Breese, B.F., (1960), "Quartz Overgrowths as Evidence of Silica Deposition in Soils," Aust. J. Sci. 23, p 18.

Brewer, R., (1964), Fabric and Mineral Analysis of Soils, pub. John Wiley and Sons, Inc., 470 pp.

Brewer, R., (1960), "The Petrographic Approach to the Study of Soils," Trans. Seventh Int. Cong. Soil Sci., Madison 1, p 173.

Brewer, R., and Sleeman, J.R., (1960), "Soil Structure and Fabric: Their Definition and Description," J. Soil Sci. 11, pp 172-185.

Briggs, L.I., McCulloch, D.S., and Moser, F., (1962), "The Hydraulic Shape of Sand Particles," J. Sed. Patrol. 32, pp 645-656.

Bromley, K., Monahan, M.A., Bryant, J.F., and Thompson, B.J., (1971), "Holographic Subtraction: Applied Optics," vol. 10, pp 171-180.

Broms, H.B., and Casbarian, A.O., (1965), "Effects of Rotation of the Principal Stress Axes and of the Intermediate Principal Stress on the Shear Strength," Proc. Sixth Conf. on Soil Mech. and Found. Engin., Montreal, 1965, pp 179-183, pub. Univ. of Toronto Press.

## BIBLIOGRAPHY (Cont'd.)

Bronstein, M.I., Mikheev, V.V., Ruppeneit, K.V., Lushnikov, V.V., Shvets, V.B., (1973), "The Pressure-meter Method of Investigating Soil Properties and Its Theoretical Basis, Proc. of the Eighth Int. Conf. on Soil Mech. and Found. Engin., Moscow, pp 79-85.

Brooker, E.W., and Ireland, H.O., (1965), "Earth Pressures at Rest Related to Stress History," Canadian Geotechnical J., vol. II, no. 1, Feb. 1965.

Brown, C.B., (1967), "Pressure Meter Design in Fills with Rock Inclusion," Geotechnique, vol. 17, no. 3, pp 251-260.

Brutsaert, W., (1964), "The Propagation of Elastic Waves in Unconsolidated Unsaturated Granular Mediums," J. of Geophys. Research, vol. 69, no. 2, pp 243-257, Jan. 15, 1964.

Brutsaert, W., and Luthin, James N., (1964), "The Velocity of Sound in Soils Near the Surface as a Function of the Moisture Content," J. of Geophys. Research, vol. 69, no. 4, pp 643-652, Feb. 14, 1964.

Buckman, H.O., and Brady, N.C., (1969), The Nature and Properties of Soils, 7th ed., pub. MacMillan and Co., London, England.

Butler, B.E., (1955), "A System for the Description of Soil Structure and Consistence in the Field," J. Aust. Inst. Agr. Sci. 21, pp 239-249.

Button, D.D., and Lawrence, W.G., (1964), "Effect of Temperature on the Charge on Kaolinite Particles in Water," J. Amer. Ceramic Soc., vol. 47, no. 10, pp 503-509.

Cagnet, L.J., (1960), An Atlas of Optical Phenomena, pub. Prentice-Hall, Englewood Cliffs.

Calladine, C.R., (1971), "A Microstructural View of the Mechanical Properties of Saturated Clay," Geotechnique, vol. 21, no. 4, pp 391-415.

Campbell, D.B., and Hudson, W.R., (1969), The Determination of Soil Properties In-Situ, Univ. Texas - Austin, Center for Highway Research, Research Report 89-7.

Carl, J.D., and Amstutz, G.C., (1958), "Three-Dimensional Liesegang Rings by Diffusion in a Colloidal Matrix and Their Significance for the Interpretation of Geological Phenomena," Bull. Geol. Soc. Amer., vol. 66, p 1467.



Catt, J.A., and Robinson, P.C., (1961), "The Preparation of Thin Sections of Clay," *Geol. Mag.* 98, pp 511-514.

Childs, E.C., (1957), "The Anisotropic Conductivity of Soil," *J. Soil Sci.* 8, pp 42-47.

Clark, B.R., (1970), "Mechanical Formation of Preferred Orientation in Clays," *Amer. J. Sci.*, vol. 269, pp 250-266.

Comer, J.J., (1960), "Electron Microscope Studies of Mullite Development in Fired Kaolinites," *J. Amer. Ceramic Soc.*, vol. 43, no. 7, pp 378-384.

Comer, J.J., (1962), "New Electron-Optical Data on the Kaolinite Mullite Transformation," *J. Amer. Ceramic Soc.*, vol. 44, no. 11, pp 561-563.

Cook, J.C., (1972), *Electronic Measurement of Rock Stress*, Telehyne Geotechnical Report No. 72-10.

Crook, J.M., and Howell, F.T., (1970), "Three New Simple Tests for Measuring and Estimating the Permeability of the Permo-Triassic Sandstones of North-West England," *Geotechnique*, vol. 20, no. 4, pp 446-451.

Davidson, J.M., Biggar, J.W., and Nielsen, D.R., (1963), "Gamma-Radiation Attenuation for Measuring Bulk Density and Transient Water Flow in Porous Materials," *J. Geophys. Res.* 68, pp 4777-4783.

Davis, J.C., (1970), "Optical Processing of Microporous Fabrics," *Data Processing in Biology and Geology*, J.L. Cutbill, ed., pp 69-87.

Deere, D.U., and Cording, E.J., (1970), "Interrelationships of Soil Mechanics, Rock Mechanics, and Engineering Geology," *Proc. Eighth Ann. Engin. Geol. and Soils Engin. Symp.*, Pocatello, Idaho, pp 295-313.

DeVries, R.C., and Jugle, D.B., (1968), "Structure-Property Relation in Flexible Sandstone," *J. Amer. Ceramic Soc.*, vol. 15, no. 7, pp 387-390.

Diamond, S., (1970), "Pore Size Distributions in Clays," *Clay and Clay Minerals*, vol. 18, no. 1, pp 7-23.

DiBiagio, E., and Aas, G., (1967), "The In-Situ Undrained Shear Strength Measured on a Horizontal Failure Plane by Large-Scale Direct Shear Tests in Quick Clay," *Proc. of the Geotechnical Conf. Oslo, 1967*, vol. 1, pp 19-26.

BIBLIOGRAPHY (Cont'd.)

Dobrin, M.B., (1968), "Optical Processing in the Earth Sciences," I.E.E.E. Spectrum, Sept. 1968, pp 59-66.

Dobrin, M.B., Ingalls, A.L., and Long, J.A., (1964), "Velocity and Frequency Filtering of Seismic Data Using Laser Light," Conduction - United Geophys. Corp., p 32, (Pub. in Geophys., vol. 30, pp 1144-1178, 1965).

Donath, F.A., Faill, R.T., and Tobin, D.G., (1971), "Deformational Mode Fields in Experimentally Deformed Rock," Bull. Geol. Soc. Amer., vol. 82, pp 1441-1462.

Dudley, J.H., (1970), "Review of Collapsing Soils," Proc. Amer. Soc. Civil Engin. J. Soil Mech and Found. Engin., vol. 96, no. SM3, pp 925-947.

Dudley, J.H., (1971), "Remote Measurement of Radial Deformations," Proc. Amer. Soc. Civil Engin. J. Soil Mech. and Found. Engin., vol. 97, SM6, pp 965-968, June 1971.

Duncan, J.M., and Dunlop, P., (1969), "Slopes in Stiff-Fissured Clays and Shales," Proc. Amer. Soc. Civil Engin. J. Soil Mech. and Found. Engin., vol. 95, no. SM2, pp 467-492, March 1969.

Duncan, J.M., and Seed, H.B., (1966), "Anisotropy and Stress Reorientation in Clay," Proc. Amer. Soc. Civil Engin. J. Soil Mech. and Found. Engin., vol. 92, no. SM5, pp 21-51.

Dunstan, T., (1972), "The Influence of Grading on the Anisotropic Strength of Sand," Geotechnique, vol. 22, no. 3, pp 529-532.

Elias, H., (1967), "Sterelogy," Proc. 2nd Intl. Cong. on Stereology, Chic, Springer-Verlag, N.M., 336 pp, April 8-13, 1967.

Emerson, W.W., (1959), "The Structure of Soil Crumbs," J. Soil Sci. 10, pp 235-244.

Fairbairn, H.W., (1949), Structural Petrology of Deformed Rocks, pub. Addison-Wesley, 344 pp.

Fookes, P.G., (1969), "Geotechnical Mapping of Soils and Sedimentary Rock for Engineering Purposes with Examples of Practice from the Mangla Dam Project," Geotechnique, vol. 19, no. 1, pp 52-74.

## BIBLIOGRAPHY (Cont'd.)

Fookes, P.G., and Denness, B., (1969), "Observational Studies on Fissure Patterns in Cretaceous Sediments of South-East England," *Geotechnique*, vol. 19, no. 4, pp 453-477.

Friedman, M., (1958), "Determination of Sieve-Size Distribution from Thin-Section Data for Sedimentary Petrological Studies," *J. Geol.* 66, p 394.

Friedman, M., (1962), "On Sorting Coefficients, and the Lognormality of the Grain Size Distribution of Sandstones," *J. Geol.* 70, pp 737-753.

Friedman, M., (1969), "Petrofabric Techniques for the Determination of Principal Stress Directions in Rocks," *Proc. Int. Conf. on State of Stress in the Earth's Crust*, Elsevier, pp 451-552.

Frideman, M., (1973), Investigations of the Relation Between Residual Strains, Fabric, Fracture and Ultrasonic Attenuation and Velocity in Rock, Final Report, Contract H0220062 for ARPA by Texas A and M University.

Friedman, M., and Sowers, G.M., (1970), "Petrofabrics: A critical review," *Can. J. Earth Sci.*, vol. 7, no. 2, pp 477-497.

Friis, J., (1961), "Sand Sampling," *Fifth Int. Conf. Soil Mech. and Found. Engin.*, Paris, vol. 1, pp 451-463.

Fry, W.H., (1933), Petrographic Methods for Soil Laboratories, U.S.D.A. Tech. Bull. 344, 96 pp.

Frydman, S., Domornik, A., and Wiseman, G., (1968), "A Study of In-Situ Testing With the Pressuremeter," *Proc. In-Situ Investigations in Soils & Rocks*, British Geotechnical Soc., London, pp 229-250, May 1968.

Gerrard, C.M., and Morgan, J.R., (1972), "Initial Loading of a Sand Layer Under a Circular Pressure Membrane," *Geotechnique*, vol. 22, no. 4, pp 635-662.

Geyer, R.L., and Myung, J.I., (1970), "The 3-D Velocity Log: A Tool for In-Situ Determination of the Elastic Moduli of Rocks," *Twelfth Rock Symposium*, Soc. of Mining Engin. of AIME, Rolla, Missouri, pp 71-107.

Gibson, R.E., (1970), "An Extension to the Theory of the Constant Head In-Situ Permeability Test," *Geotechnique*, vol. 20, no. 2, pp 193-197.



## BIBLIOGRAPHY (Cont'd.)

- Gibson, R.E., and Anderson, W.F., (1961), "In-Situ Measurement of Soil Properties with the Pressuremeter," Civil Engin. and Public Works Review, vol. 56, no. 658, May 1961.
- Gibson, R.E., England, G.L., and Hussey, M.J.L., (1967), "The Theory of 1-Dimensional Consolidation of Saturated Clays. I. Finite Non-Linear Consolidation of Thin Homogeneous Layers," Geotechnique, vol. 17, no. 3, pp 251-273.
- Gill, W.R., and Vanden Ber, G.E., (1967), Soil Dynamics in Tillage and Traction: Agric. Handbook No. 316, Agric. Res. Svc., U.S. Dept. Agric., 511 pp.
- Gillott, J.E., (1968), Clay in Engineering Geology, Elsevier Publishing Co., New York.
- Gillott, J.E., (1969), "Study of Fabric of Fine Grained Sediments with the Scanning Electron Microscope," J. Sedimentary Petrography, vol. 35, pp 408-414.
- Glossop, R., (1968), "The Rise of Geotechnology and Its Influence on Engineering Practice," Geotechnique, vol. 18, pp 105-150.
- Golder, H.Q., Gould, J.P., Lambe, T.W., Tschebotarioff, G.P., and Wilson, S.D., (1970), "Predicted Performance of Braced Excavation," Proc. Amer. Soc. Civil Engin. J. Soil Mech. and Found. Engin., vol. 96, no. SM3, pp 801-815, May 1970.
- Gravenor, C.P., Meneley, W.A., (1958), "Glacial Flutings in Central and Northern Alberta," Amer. J. Sci., vol. 256, pp 715-728.
- Gresseth, E.W., (1964), Determination of Principal Stress Directions Through an Analysis of Rock Joint and Fracture Orientations, Star Mine, Burke, Idaho, U.S. Bur. Mines Rept. Inv. 6413, 42pp.
- Gresseth, E.W., and Reid, R.R., (1968), A Petrographic Study of Tectonic and Mining-Induced Deformations in a Deep Mine, U.S. Bur. Mines Rept. Inv. 7173, 64pp.
- Haimson, B.C., (1968), Hydraulic Fracturing in Porous and Nonporous Rock and Its Potential for Determining In-Situ Stresses at Great Depth, Ph.D. Thesis, Univ. Minn. Engin. Mechanics.
- Haimson, B.C., (1971), "Static Fracturing of Rock as a Useful Tool in Mining and Rock Mechanics," Symp. Soc. Int. Mecanique des Roches, Nancy, paper II-30.

Haimson, B.C., (1972), Determination of In-Situ Stresses Around Underground Excavations by Means of Hydraulic-Fracturing, Dept. of Metallurgical and Mineral Engin. and the Enng. Expt. Stn. College of Engin., U. of Wisconsin-Madison, Madison, Wisc., ARPA Order No. 1579, Program Code No. 2F10, Contract No. H0220080.

Hansen, and Brinch, (1953), "A General Earth Pressure Theory," Proc. of the Third Int. Conf. on Soil Mech. and Found. Engin., vol. II, Switzerland, pp 170-174, August 1953.

Hardin, B.O., and Richart, F.E., (1963), "Elastic Wave Velocities in Granular Soils," Proc. Amer. Soc. Civil Engin. J. Soil Mech. and Found. Engin., vol. 89, no. SM1, pp 33-65.

Harris, S.A., (1969), The Meaning of Till Fabrics, pp 143-164 in Nelson, J.G. and M.J. Chambers (Eds.), Geomorphology: Selected Readings Methuen, 399 pp.

Harrison, P.W., (1957), "A Clay-Till Fabric: Its Character and Origin," J. of Geol., vol. 65, no. 3, pp 275-308.

Haupt, W.A., (1973), "Discussion-In-Situ Wave Velocity by Cross-Hole Method," Proc. Amer. Soc. Civil Engin. J. of the Soil Mech. and Found. Div., vol. 99, no. SM2, pp 224-228, Feb. 1973.

Henkel, D.J., (1970), "Geotechnical Considerations of Lateral Stresses," Proc. 1970 Specialty Conf. Lateral Stresses and Earth Retaining Structures, Amer. Soc. Civil Engin., pp 1-50.

Higgins, C.M., (1969), "Pressuremeter Correlation Study," Highway Research Record No. 284, pp 51-62.

Holmes, C.D., (1941), "Till Fabric," Geol. Soc. Amer. Bull., vol. 52, pp 1299-1354.

Horne, M.R., (1964), "The Behavior of an Assembly of Rotund, Rigid, Cohesionless Particles - I and II," Proc. Royal Soc. A., vol. 286, pp 62-97.

Howell, F.T., and Woodhead, F.W., (1972), "A Null Method for the Estimation of Irregular Specimens of Permeable Strata," Geotechnique, vol. 22, no. 2, pp 352-355.

Huck, P.J., (1972), The Effect of Specimen Size on Confined Compression Testing of Rock Cores, IITRI Final Report No. D6059, ARPA Contract H0210009, April 1972.



## BIBLIOGRAPHY (Cont'd.)

- Huck, P.J., Liber, T., Chiapetta, R.L., Thomopoulos, N.T., and Singh, M.M., (1973), Dynamic Response of Soil Concrete Interfaces at High Pressure, IITRI Final Report No. AFWL-TR-73-264 for Air Force Weapons Laboratory, Kirtland Air Force Base.
- Hunt, C.B., (1972), Geology of Soils - Their Evolution, Classification, and Uses, Freeman, San Francisco, 344 pp.
- Ingles, O.G., (1969), "Fracture Phenomena in Stabilized Soils," Second Aust. N.Z. Conf. Mech. Struct. Mat., Paper 14, pp 1-14.
- Ingles, O.G., and Frydman, S., (1964), "The Strength of Cement and Lime-Stabilized Fine Natural Minerals and Soils," Proc. of a Colloquium in Mech. of Soil Stabilization, Paper 12, Melbourne: Commonwealth Sci. Industrial Research Org., pp 1-12.
- Ingles, O.G., and Lee, I.K., (1971), "The Influence of Initial Grain Shape and Pore Anisotropy on Strength of Brittle Soils," Geotechnique, vol. 21, no. 2, pp 143-153.
- Ireland, H.O., Moretto, O., and Vargas, M., (1970), "The Dynamic Penetration Test: A Standard That is Not Standardized," Geotechnique, vol. 20, no. 2, pp 185-192.
- Jackson, P.G., (1965), "Analysis of Variable Density Seismograms by Means of Optical Diffraction," Geophysics, vol. 30, pp 5-23.
- Jacot, A.P., (1936), "Soil Structure and Soil Biology," Ecology 17, pp 359.
- Jaeger, J.C., and Cook, N.G.W., (1964), "Theory and Application of Curved Jacks for Measurement of Stresses," Proc. of the Int. Conf. on State of Stress in the Earth's Crust, Santa Monica, Calif., June 1963, pub. American Elsevier Pub. Co. Inc., New York, pp 381-395.
- Jaeger, J.C., and Cook, N.G.W., (1969), Fundamentals of Rock Mechanics, Methuen, London, 513 pp.
- Jaky, J., (1948), "Earth Pressure," Proc. of the Second Int. Conf. on Soil Mech. and Found. Engin., Rotterdam, vol. 1, pp 103-107, June 21-30, 1948.
- Jennison, R.C., (1961), Fourier Transforms and Convolutions for the Experimentalist, pub. Pergamon Press, New York, 120 pp.

- Johnson, W.S., and Nelson, J.S., (1970), "Dynamic Rock Properties from In-Situ Field Seismic Studies - A Case History," Twelfth Symp. on Rock Mech., Soc. of Mining Engin. of AIME, Rolla, Missouri, pp 3-26, Nov. 1970.
- Johnson, W.M., McClelland, J.E., McCaleb, S.A., et al (1960), "Classification and Description of Soil Pores," Soil Sci. 89, pp 319-321.
- Jongerus, A., (1957), "Morphologic Investigations of Soil Structure," Bodemkundige Studies No. 2, Mededelingen van de Stickting voor Bodemkartering, Wageningen.
- Jung, J., (1969), Precis de Petrographie: Roches Sedimentaries, Metamorphiques et Eruptives, 3rd ed., Masson, 332 pp.
- Kallstenius T., and Bergau, W., (1961), "In-Situ Determination of Horizontal Ground Movements," Fifth Int. Conf. on Soil Mech. and Found. Engin., Paris, vol. 1, pp 481-484.
- Katchinski, N.A., (1956), "Soil Structure and Differential Porosity," Rept. Sixth Int. Cong. Soil Sci., Paris, Com. I, pp 35-52.
- Kehle, R.O., (1964), "The Determination of Tectonic Stresses Through Analysis of Hydraulic Well Fracturing," J. of Geophysical Research, vol. 69, no. 2, pp 259-273, Jan. 1964.
- Keller, G.V., (1971), "Natural-Field and Controlled-Source Methods in Electro-Magnetic Exploration," Geoexploration, vol. 9, pp 99-147.
- Kenney, T.C., (1967), "Field Measurements of In-Situ Stresses in Quick Clays," Norwegian Geotechnical Institute, Publication 76 (reprint from Geotechnical Conf., Oslo, 1967).
- Kezdi, Arpad, Private Communication to C. Peter Wroth.
- Kinoshita, N., and Mura, T., (1971), "Elastic Fields of Inclusions in Anisotropic Media," Physica Status Solidi, vol. 5, no. 3, pp 739-767.
- Kirkpatrick, W.M., and Rennie, I.A., (1972), "Directional Properties of Consolidated Kaolin," Geotechnique, vol. 22, no. 1, pp 166-168.
- Koerner, R.M., (1970), "Energy and Surface Characteristics of Quartz Soils," Proc. Eighth Ann. Engin. Geol. and Soils Engin. Symp., Pocatello, Idaho, pp 187-195.

## BIBLIOGRAPHY (Cont'd.)

- Koerner, R.M., (1970), "Effect of Particle Characteristics on Soil Strength," Proc. Amer. Soc. Civil Engin. J. Soil Mech. and Found. Engin., vol. 96, no. SM4, pp 1221-1234.
- Koerner, R.M., and Lord, A.E. Jr., (1972), "Acoustic Emissions in Medium Plasticity Clayey Silt," Proc. Amer. Soc. Civil Engin. J. Soil Mech. and Found. Engin., vol. 98, no. SM1, pp 161-165.
- Komornik, A., and Frydman, S., (1968), "A Study of In-Situ Testing with the Pressuremeter," Proc. In-Situ Investigations in Soils & Rocks, British Geotechnical Soc., London, pp 145-154.
- Krinitzky, E.L., (1970), The Effects of Geological Features on Soil Strength, U.S. Army Engin. W. W. Exp. Stat., Misc. Paper S-70-25, 29 pp.
- Krynine, P.D., (1950), "Microscopic Morphology of Quartz Types, Ann. Second Pan. Amer. Cong. Min. Engin. Geol. 3 (2nd comm.), pp 35-49.
- Kubiena, W.L., (1930), "Micropedological Studies," Wiss. Arch., Pfl., 5, pp 613-648.
- Kubiena, W.L., (1938), Micropedology, (Collegiate Press Inc., Ames, Iowa).
- Kubiena, W.L., Beckman, W. and Geyer E., (1961), "Method of Photogrammetric Analysis of Soil Structure," A. Pfl. Ernabr. Dung., Bodenkunde, 92, pp 116-126.
- Lafeber, D., (1962), "Aspects of Stress-Induced Differential Movements of Fabric Elements in Mineral Soils," Proc. First Conf. Aust. Road Res. Board 1, pp 1059-1067.
- Lafeber, D., (1966), "Soil Structure Concepts," Engin. Geol 1, pp 261-290.
- Lafeber, D., (1967), "The Optical Determination of Spacial Orientation of Platy Clay Minerals in Soil Thin Section," Geotherma, vol. 1, pp 359-369.
- Lafeber, D., (1969), "Micromorphometric Techniques in Engineering Soil Fabrics Analysis," Proc. Third Int. Wkng. Mect. Soil Micromorphology, Wroclaw, Poland.
- Lafeber, D., and Kurbanovic, M., (1965), "Photographic Reproduction of Soil Fabric Patterns," Nature, vol. 208, pp 609-611.



## BIBLIOGRAPHY (Cont'd.)

Lambe, T.W., (1953), "The Structure of Inorganic Soils," J. Soil Mech. and Found. Div., Amer. Soc. of Civil Engin., vol. 79, no. 315, pp 1-49.

Lambe, T.W., (1958), "The Engineering Behavior of Compacted Clay," Proc. Amer. Soc. Civil Engin., vol. 84, no. SM2, p 1655.

Lambe, T.W., Wolfskill, L.A., and Wong, I.H., (1970), "Measured Performance of Braced Excavation," Proc. Amer. Soc. Civil Engin. J. Soil Mech. and Found. Engin., vol 96, no. SM3, pp 817-836, May 1970.

Larson, W.C., (1973), A Study of Particle Parameters to Determine the Fragmentation History of Test Rock and Mineral Samples, M.S. thesis, Univ. of Wis.-Milw., 195 pp.

Laruelle, J., (1956), "Some Aspects of the Microstructure of Soils in the Northeast of the Belgium Congo, Pedologie 6, pp 38-59.

Laruelle, J., (1958), "Micromorphology of the Soils of Belgium," Pedologie 8, pp 79-102.

Leitch, H.C., and Yong R.N., (1967), "The Rate Dependent Mechanism of Shear Failure in Clay Soils," Soil Mech. Series, no. 21, Soil Mechanics Laboratory, McGill Univ. Montreal.

Leonards, G.A., (1965), Experimental Study of Static and Dynamic Friction Between Soil and Typical Construction Materials, pub. Purdue University, Lafayette, Indiana, 65 pp, December 1965.

Lewin, P.I., and Burland, J.B., (1970), "Stress-Probe Experiments on Saturated Normally Consolidated Clay," Geotechnique, vol. 20, no. 1, pp 38-56.

Lin, S.C., Mur, T., Shibata, M., and Mori, T., (1973), "The Work-Hardening Behavior of Anisotropic Media by Non-Deforming Particles or Fibers," Acta Metallurgia, vol. 21, no. 4, pp 505-516.

Lindsay, J.F., (1970), "Clast Fabric of Till and Its Development," J. Sed. Pet., vol. 40, no. 2, pp 629-641.

Lo, K. Y., (1970), "The Operational Strength of Fissured Clays," Geotechnique, vol. 20, no. 1, pp 57-74.

Long, R.P., and Zimmie, T.F., (1973), "Mean Pore Sizes From Flow Measurements," Proc. Amer. Soc. Civil Engin. J. Soil Mech. and Found. Engin., vol. 99, no. SM7, pp 583-587.

## BIBLIOGRAPHY (Cont'd.)

- Low, A.J., (1954), "Study of Soil Structure in the Field and the Laboratory," J. Soil Sci. 5, pp 57-74.
- MacClintock, P., Dreimanis, A., (1964), "Orientation of Till Fabric By Overriding Glacier in the St. Lawrence Valley," Am. J. Sci., vol. 262, pp 133-142.
- MacKenzie, K.J.D., (1969), "Infrared Kinetic Study of High-Temperature Reactions of Synthetic Kaolinite," J. Amer. Ceramic Soc., vol. 52, no. 12, pp 635-637.
- Mardia, K.V., (1972), Statistics of Directional Data, pub. Aca. Press, 357 pp.
- Marshall, C.E., (1935), "The Importance of the Lattice Structure of the Clays for the Study of Soils," J. Soc. Chem. Ind., 54, p 393.
- Martin, R.T., (1965), Quantitative Fabric of Consolidated Kaolinite, Mass. Inst. of Tech., Research Report, Soils Publication, no. 179.
- Martin, R.T., (1966), "Quantitive Fabric of Wet Kaolinite," Clay Mineral Burretex, vol. 14, pp 271-287.
- Matelski, R.P., (1953), "Removal of Coatings from Soil Particles for Petrographic Analysis," Soil Sci. Soc. Amer. Proc. 17, pp 103-106.
- Matsuoka, H., (1973), discussion of "The Mechanism of Fabric Changes During Compressional Deformation of Sand," Japanese Soc. of Soil Mech. and Found. Engin. Soils and Founds., vol. 13, no.1.
- Matulucci, R.V., Shelton, J.W., and Abdel-Hay, M., (1969), "Grain Orientation in Vicksberg Loess," J. Sedim. Petrol. 30, no. 3, pp 969-979.
- McDowell, P.W., (1971), "The Advantages and Limitations of Geoelectrical Methods in the Foundation Investigation of the Tracked Hovercraft Experimental Site in Cambridge-shire," Quarterly J. Engin. Geology, vol. 3, pp 119-126.
- McKyes, E., and Yong, R.N., (1971), "Three Techniques for Fabric Viewing as Applied to Shear Distortion of a Clay," Clay and Clay Mineralials, vol. 19, pp 289-293.
- McMillian, N.S., and Mitchell, J., (1953), "Microscopic Study of Platy and Concretionary Structures in Certain Saskatchewan Soils," Sci. Agr. 33, pp 178-183.
- Meade, R.H., (1960), Compaction and Development of Preferred Orientation in Clayey Sediments, Ph.D. Thesis, Stanford Univ., Dissert. Asts. 21, 3421 pp, 1961.



BIBLIOGRAPHY (Cont'd.)

Meade, R.H., (1961), "X-Ray Diffractometer Method for Measuring Preferred Orientation in Clays," U.S. Geological Survey, Professional Paper 424-B, pp 273-276.

Meigh, A.C., and Greenland, S.W., (1965), "In-Situ Testing of Soft Rocks," Proc. Sixth Int. Conf. Soil Mech. and Found. Engin., Montreal, 1965, vol. I, pp 73-76, pub. Univ. Toronto Press.

Menard, L.F., (1957), An Apparatus for Measuring the Strength of Soils in Place, Ph.D. Thesis, Univ. Illinois, Urbana, 1957.

Milovic, D.M., (1971), "Effect of Sampling on Some Soil Characteristics," ASTM, Spec. Tech. Publ. 483, pp 164-179.

Milovic, D.M., Touzot, G., and Tournier, J.P., (1970), "Stresses and Displacements in an Elastic Layer Due to Inclined and Eccentric Load Over a Rigid Strip," Geotechnique, vol. 20, no. 3, pp 231-252.

Minashina, N.G., (1958), "Optically Oriented Clays in Soils," Soviet Soil Sci., no. 4, pp 424-430.

Mitchell, J.K., (1956), "The Fabric of Natural Clays and Its Relation to Engineering Properties," Proc. of Highway Research Board, vol. 35, pp 693-713.

Mitchell, J.K., and Arulanandan, (1968), "Electrical Dispersion in Relation to Soil Structure," Proc. Amer. Soc. Civil Engin. J. Soil Mech. and Found. Engin., vol. 94, no. SM2, pp 447-471.

Mitchell, J.K., and Houston, W.N., (1969), "Causes of Clay Sensitivity," Proc. Amer. Soc. Civil Engin. J. Soil Mech. and Found. Engin., vol. 95, no. SM3, pp 845-971.

Mitchell, J.K., Singh, A., and Campanella, R.G., (1969), "Bonding, Effective Stresses, and Strength of Soils," Proc. Amer. Soc. Civil Engin. J. Soil Mech. and Found. Engin., vol. 95, no. SM5, pp 1219-1245.

Mitchell, R.J., (1967), Some Applications of the Critical State Theories, Ph.D. Thesis, Cambridge Univ.

Mitchell, R.J., (1972), "Some Deviations from Isotropy in a Lightly Overconsolidated Clay," Geotechnique, vol. 22, no. 3, pp 459-467.

- Moon, A.T., (1970), "A Report in a Study and Analysis of Fractures from Basement of the Aar Massif, Switzerland," B.S. Thesis, Imperial College of Sci. Tech., London.
- Moore, C.A., (1971), "Effect of Mica on  $K_0$  Compressibility of Two Soils," Proc. Amer. Soc. Civil Engin. J. Soil Mech. and Found. Engin., vol. 97, no. SM9, pp 1275-1291, Sept. 1971.
- Moore, P.J., and Spencer, G.K., (1972), "Lateral Pressures from Soft Clay," Proc. Amer. Soc. Civil Engin. J. Soil Mech. and Found. Engin., vol. 98, no. SM11, pp 1225-1244, Nov. 1972.
- Moore, R.W., (1961), "Geophysics Efficient in Exploring the Subsurface," Proc. Amer. Soc. Civil Engin. J. Soil Mech. and Found. Engin., vol. 87, SM3, pp 69-101.
- Morgenstern, N.R., and Eisenstein, Z., (1970), "Methods of Estimating Lateral Loads and Deformations," Proc. 1970 Spec. Conf., Lateral Stresses and Earth Retaining Structures, Amer. Soc. Civil Engin., pp 50-102.
- Morgenstern, N.R., and Tchalenko, J.S., (1967), "The Optical Determination of Preferred Orientation in Clays and Its Application to the Study of Microstructure in Consolidated Kaolin," Part I, Part II, Proc. Royal Soc. London, vol. 300, pp 218-234 and 235-250.
- Morgenstern, N.R. and Tchalenko, J.S., (1967), "Microscopic Structures in Kaolin Subjected to Direct Shear," Geotechnique, vol. 17, no. 4, pp 309-328.
- Moum, J., and I.T. Rosenquist, (1961), "The Mechanical Properties of Montmorillonitic and Illitic Clays Related to the Electrolytes of the Pore Water," Proc. of the Fifth Int. Conf. of Soil Mech. and Found. Engin., Paris, vol. 1, pp 263-267.
- Mura, T. (1971), "A Variational Method for Micro-Mechanics of Composite Materials," Proc of Int. Conf. on Mech. Behavior of Materials, The Soc. of Materials Science, Kyoto, Japan, vol. 2, pp 12-18.
- Murayama, S., and Matsouka, H., (1973), "A Microscopic Study on Shearing Mechanism of Soils," Proc. Eighth Intl. Conf. Soil Mech. and Found. Eng., Moscow, vol. 1.2, pp 293-298.
- Nebergali, W.H., and Schmidt, F.C., General Chemistry, pub. Heath and Co.,

## BIBLIOGRAPHY (Cont'd.)

- Norman, J.W., (1970), "The Photogeological Detection of Unstable Ground," J. Inst. Hwy. Engin. 17, no. 2, pp 19-22.
- Norman, J.W., Price, N.J., and Moon, A.T., (1971), Geotechnique, "Orientation Studies - A Means of Detecting Old Landslides," Geotechnique, vol. 21, no. 2, pp 154-155.
- Obert, L.A. and Duvall, W.I., (1967), Rock Mechanics and the Design of Structures in Rock, pub. Wiley, 650 pp.
- Obert, L., and Duvall, W.I., (1967), In-Situ Measurements, Rock Mechanics and the Design of Structures in Rock, pub. John Wiley & Sons.
- Obrcian, B., (1969), "Determination of Lateral Pressures Associated with Consolidation of Granular Soils," Highway Research Record No. 284, pp 13-25.
- O'Brien, N.R., and Harrison, W., (1969), "Fabric of a Nonfossile Pleistocene Clay," Die Natarwissonchafien, vol. 56, pp 135-136.
- Oda, M., (1972), "The Mechanism of Fabric Changes During Compressional Deformation of Sand," Japanese Soc. of Soil Mech. and Found. Soils and Founds., vol. 12, no. 2.
- Odom, I.E., (1967), "Clay Fabric and Its Relation to Structural Properties in Mid-Continental Pennsylvania Sediments of Sedimentary Petrography," vol. 37, p 610.
- Ormsby, W.C., and Shartsis, J.M., (1960), "Clay Mineral Content of Two Domestic Koalins," J. Amer. Ceramic Soc., vol. 42, no. 7, p 335.
- Ormsby, W.C., Shartsis, J.M., and Woodside, K.H., (1962), "Exchange Behavior of Kaolins of Varying Degrees of Crystallinity," J. Amer. Ceramic Soc., vol. 45, no. 8, pp 361, 366.
- Ozaydin, I.K., (1974), A Micro-Mechanistic Analysis for Creep Response of Kaolin Clay, Ph.D. Thesis, Northwestern Univ., Dept. of Civil Engin., Evanston, Illinois.
- Parrent, G.B., Jr., and Thompson, B.J., (1969), "Physical Optics Notebooks," Soc. of Photo-optical Institute Eng., Redondo Beach, Cal., 63 pp.
- Parry, R.H.G., (1971), "A Simple Driven Piezometer," Geotechnique, vol. 21, no. 2, pp 163-167.



- Paterson, M.A., and Weiss, L.E., (1961), "Symmetry Concepts in the Structural Analysis of Deformed Rocks," *Geol. Soc. Amer. Bull.*, vol. 72, pp 841-882.
- Peck, R.B., (1969), "Advantages and Limitations of the Observational Method in Applied Soil Mechanics," *Geotechnique*, vol. 19, no. 2, pp 171-187.
- Peterson, J.B., (1944), "The Effect of Montmorillonite and Kaolinitic Clays in the Formation of Platy Structures," *Soil Sci. Soc. Amer. Proc.* 9, p 37.
- Peterson, R.A., and Dobrin, M.B. (eds.), (1966), "A Pictorial Digital Atlas," *United Geophys. Corp.*, Pasadena, 53 pp.
- Pettibone, H.C., and Waddell, G.G., (1971), "Stability of an Underground Opening in Frozen Gravel," *Proc. Ninth Ann. Engin. Geol. and Soils Engin. Symp.*, Boise, Idaho, pp 3-30.
- Pickering, D.J., (1970), "Anisotropic Elastic Parameters for Soil," *Geotechnique*, vol. 20, no. 3, pp 271-276.
- Pincus, H.J., (1966), "Optical Data Processing of Vectorial Rock Fabric," *Proc. First Int. Cong. on Rock Mechanics*, vol. 1, pp 173-177.
- Pincus, H.J., (1969a), "Sensitivity of Optical Data Processing to Changes in Fabric: Part I - Geometric Patterns; Part II - Standardized Grain Patterns; Part III - Rock Fabrics," *Int. J. Rock Mech. and Min. Sci.*, vol. 6, pp 259-276.
- Pincus, H.J., (1969b), "The Analysis of Remote Sensing Displays by Optical Diffraction," *Proc. Sixth Int. Symp. on Remote Sensing of Environment*, Ann Arbor, Mich., pp 261-274.
- Pincus, H.J., (1970), "The Analysis of Two-Dimensional Displays by Optical Diffraction With Examples From the Earth Sciences," *Proc. Electro-Optical Systems Design Conf.*, 1969, Industrial and Sci. Conf. Mgmt., pp 625-632.
- Pincus, H.J., (1973), Development of Capabilities of Optical Diffraction Analysis for Quantitatively Comparing and Correlating Rock Fabrics and Fabric Changes, Second Ann. Rept., ARPA-USBM Contract H0220016, Univ. Wis.-Milw., 35pp. + App. A-E and 18 Figures.
- Pincus, H.J., and Ali, S., (1968), "Optical Data Processing of Multispectral Photographs of Sedimentary Structures," *J. of Sedimentary Petrology*, vol. 38, no. 2, pp 457-461.

## BIBLIOGRAPHY (Cont'd.)

- Pincus, H.J., and Dobrin, M.B., (1966), "Optical Processing of Geological Data," J. Geophys. Res., vol. 71, no. 60, pp 4861-4870.
- Pincus, H.J., and Gardner, R.D., (1968), "Fluorescent Dye Penetrants Applied to Rock Fractures," Int. J. Rock Mech. and Min. Sci., vol. 5, no. 2, pp 155-158.
- Pincus, H.J., Power, R.C., Jr., and Woodzick, T., (1973), "The Analysis of Contour Maps by Optical Diffraction," Geoforum, 14/73, Woltsburg, Germany, pp 39-52.
- Potyondy, J.G., (1961), "Skin Friction Between Various Soils and Construction Materials," Geotechnique, XI(4), pp 339-353, Dec. 1961.
- Poulos, H.G., and Davis, E.H., (1970), Laboratory Determination of In-Situ Horizontal Stress in Soil Masses, Research Report No. 156, Univ. of Sydney.
- Poulos, H.G., and Davis, E.H., (1972), "Laboratory Determination of In-Situ Stress in Soil Masses," Geotechnique, vol. 22, no. 1, pp 177-182.
- Power, P.C., (1973), Optical Diffraction Analysis of Petrographic Thin Sections, M.S. Thesis, Univ. Wis.-Milw., 193 pp.
- Preiss, K., and Lahat, A., (1972), "A Gamma-Ray Density Probe Designed for Use in an Uncased Exploration Hole," Geotechnique, vol. 22, no. 4, pp 663-666.
- Preston, F.W., and Davis, J.C., (1972), "Application of Optical Processes to Geological Images," S mp. vol. 13, Inst. of Physics, London, Machine perception of patterns and pictures, Teddington Conf., pp 223-232.
- Ramiah, B.K., and Purushothamaraj, P., (1971), "Effect of Initial Structure on the Residual Strength of Koalinetic Clay," Japanese Soc. of Soil Mech. and Found. Engin. Soils and Founds., vol. 11, no. 4, pp 15-23.
- Raymond, G.P., (1972), "Prediction of Undrained Deformations and Pore Pressures in Weak Clay Under Two Embankments," Geotechnique, vol. 22, no. 3, pp 381-401.
- Richards, B.G., (1965), "Thermistor Hygrometer for Determining the Free Energy of Moisture in Unsaturated Soils," Nature, vol. 20B, pp 608-609.



- Rupert, J.P., (1973), J. Physics Chem., 77, pp 784.
- Saada, A.S., and Zamani, K.K., (1969), "The Mechanical Behavior of Cross Anisotropic Clays," Proc. of the Seventh Int. Conf. of Soil Mech. and Found. Engin., Mexico City, Mexico, vol. 1, pp 351-360.
- Sander, Bruno (1936), "Contributions to the Study of Depositional Fabrics," Amer. Assn. Petrol. Geol., Tulsa (Transl. by E.B. Kuopf, 1951).
- Sander, B., (1970), An Introduction to the Study of Fabrics of Geological Bodies, Transl. by F.C. Phillips and G. Windsor, pub. Pergamon, New York, 641 pp 641.
- Sankaran, K.S., and Bhaskaran, R., (1963), "Deformation and Failure Patterns in an Anisotropic Kaolonite Clay," Geotechnique, vol. 23, no. 1, pp 113-116.
- Schmidt, B., (1973), "Discussion on Soil Parameters for Design of Mt. Baker Ridge Tunnel in Seattle," Proc. Amer. Soc. Civil Engin. J. Soil Mech. and Found., vol. 99, no. SM8, pp 640-641, Aug. 1973.
- Schmidt, N.O., Tinoco, F.H., and Green, W.J., (1970), "The Effects of Organic Content, Temperature, and Stress Level on the Secondary Consolidation of a Clay," Proc. Eighth Ann. Engin. Geol. and Soils Engin. Symp., Pacatello, Idaho, pp 219-234.
- Schroeder, W.L., (1971), "Stress-Strain Time Relation for Compacted Residual Soil," Proc. Ninth Ann. Engin. Geol. and Soils Engin. Symp., Boise, Idaho, pp 107-118.
- Shackel, B., (1969), "A Nuclear Method for Detecting Small Variations in Density Within Soil Specimens," Australian Road Research, vol. 3, no. 9, pp 12-34, March 1969.
- Shepherd, R., and Charleson, A.W., (1971), "A Method of In-Situ Stiffness Measure," New Zealand Engineering, pp 97-101, April 1971.
- Sherif, M.A., and Strazer, R.J., (1973), "Soil Parameters for Design of Mt. Baker Ridge Tunnel in Seattle," Proc. Amer. Soc. Civil Engin. J. Soil Mech. and Found. Engin., vol. 99, no. Sml, pp 111-122, Jan. 1973.
- Shibata, T., and Karube, D., (1965), "Influence of the Variation of the Intermediate Principal Stress on the Mechanical Properties of Normally Consolidated Clays," Proc. Sixth Conf. on Soil Mech. and Found. Engin., Montreal, 1965, pp 359-363, pub. Univ. of Toronto Press.

BIBLIOGRAPHY (Cont'd.)

Shulman, A.R., (1970), Optical Data Processing, pub. John Wiley & Sons, New York, 710 pp.

Shumskii, P.A., (1955), Principles of Structural Glaciology, (Transl. by D. Kraus), Amer. Meteor. Soc., Lib. of Congress.

Skempton, A.W., (1961), "Horizontal Stresses in an Over-Consolidated Eocene Clay," Fifth Int. Conf. Soil Mech., Paris, vol. 1, pp 351-357.

Sloane, R.L., and E.A. Nowatzkt, (1967), "Electron-Optical Study of Fabric Changes Accompanying Shear in a Kaolin Clay," Proc. of the Third Panamerican Conf. on Soil Mech. and Found. Engin., Caracas, Venezuela, vol. 1, pp 215-225.

Smart D., (1966), "Optical Microscope and Soil Structure," Nature, London, pp 210, 1400.

Smith, D.C., et. al., (1968), "The Use of Nuclear Meters in Soils Investigations: A Summary of Worldwide Research and Practice," ASTM Special Technical Pub. No. 412, Amer. Soc. for Testing and Materials.

Smith, T.W., and Smith, R.E., (1968), Embankment Testing with the Menard Pressuremeter, State of Calif., Dept. Publ. Wks., Div/Hwys, Materials and Research Dept., Research Report No. M & R 632509-2.

Sridharan, A., Altschaeffl, A.G., and Diamond, S., (1971), "Pore Size Distribution Studies," Proc. Amer. Soc. Civil Engin. J. Soil Mech. and Found. Engin., vol. 97, no. SM5, pp 771-787, May 1971.

Steckley, R.C., (1972), Determination of Paleotectonic Principal Stress Direction, Including Analysis of Joints by Optical Diffraction, pub. U.S. Bur. Mines, Rept. Inv. 7706, 18 pp.

Stephen, I., (1960), "Pedology, Clay Orientation in Soils," Sci. Progress 48, pp 322-331.

Stokoe, K.H., II, and Woods, R.D., (1972), "In-Situ Shear Wave Velocity by Cross-Hole Method," Proc. Amer. Soc. Civil Engin. J. Soil Mech. and Found. Engin., vol. 98, no. SM5, pp 443-460, May 1972.

Stokoe, K.H., and Richart, F.E., (1973), "In-Situ and Laboratory Shear Wave Velocities," Proc. of the Eighth Int. Conf. on Soil Mech. and Found. Engin., pp 403-411, Moscow.

- Swanson, C.L.W., and Peterson, J.B., (1942), "The Use of the Micrometric and Other Methods for the Evaluation of Soil Structure," *Soil Sci.* 53, pp 173-183.
- Taylor, D.W., (1967), Fundamentals of Soil Mechanics, pub. John Wiley and Sons, Inc.
- Taylor, R.M., and Norrish, K., (1966), "Measurement of Orientation Distribution and Its Application to Quantitative X-Ray Diffraction Analysis," *Clays and Clay Minerals*, vol. 14, pp 127-141.
- Thorley, A., Calhoon, M.L., Zeman, Z.P., and Watt, W.G., (1968), "Borehole Instruments for Economical Strength and Deformation In-Situ Testing," Paper 13, Proc. In-Situ Investigations in Soils & Rocks, British Geotechnical Soc., London, pp 135-143, and 155-165, May 1968.
- Tchalenko, J.S., (1968), "The Microstructure of London Clay," *Q.J. Engin. Geol.* 1, no. 3, pp 155-168.
- Tobin, D.G., and Donath, F.A., (1971), "Microscopic Criteria for Defining Deformational Modes in Rock," *Geol. Soc. Amer., Bull.*, vol. 82, pp 1463-1476.
- Tovey, N.K., (1971), "Soil Structure Analysis Using Optical Techniques on S. E. Micrographs," Proc. Fourth Ann. Scanning Electron Microscope Symposium, PP 50-56, Chicago, Illinois.
- Tuffs, C.F., (1969), "The Application of Transmission Electron Microscopy and Electron Diffraction to Analysis for Materials Science," *Norelco Reporter* 16, pp 25-47, July 1969.
- Turner, F.J., and Weiss, L.E., (1963), Structural Analysis of Metamorphic Tectonites, pub. McGraw-Hill, New York, 545 pp.
- Uff, J.F., (1968), "In-Situ Measurements of Earth Pressure for a Quay Wall at Seaforth, Liverpool," Paper 18, Proc. In-Situ Investigations in Soils and Rocks, British Geotechnical Soc., London, pp 229-250, May 1968.
- Underwood, E.E., (1969), "Stereology, or the Quantitative Evaluation of Microstructures," *J. Microscopy*, vol. 89, p 2, and pp 161-180.
- Underwood, E.E., (1970), "Quantitative Stereology," Addison Wesley, 274 pp.



## BIBLIOGRAPHY (Cont'd.)

Uppal, H.L., and Gupta, S.K., (1971), "A Laboratory Study on the Measurement of Soil Density by Gamma Ray Backscattering Techniques," Indian Geotechnical J., vol. 1, no. 1, pp 37-52, Jan. 1971.

U.S. Army Corps of Engin., (1948), "Subsurface Investigation; Geophysical Explorations," Engineering Manuel - Civil Works Construction, Part CXVLLL, Chapt. 2, pp EM11102-1802.

Vesic, A.S., (1972), "Expansion of Cavities in Infinite Soil Mass," Proc. Amer. Soc. Civil Engin. J. Soil Mech. and Found. Engin., vol. 98, no. SM3, pp 265-290.

Wawersik, W.R., (1968), Detailed Analysis of Rock Failure in Laboratory Compression Tests, Univ. Minn., Ph.D. Dissertation.

Warne, S., (1962), "A Quick Field or Laboratory Straining Scheme for the Differentiation of the Major Carbonate Minerals," J. Sed. Petrol. 32, pp 29-38.

Weis, L.E., (1972), The Minor Structures of Deformed Rocks - A Photographic Atlas, Springer-Verlag, 203 Pl., 431 pp.

Werner, J., (1962), "On the Preparation of Fluorescing Soil Sections," Z. Pfl. Ernahr. Dung., Bodendunde, 99, pp 144-150.

Whiteside, E.P., (1953), "Some Relationships Between the Classification of Rocks by Geologists and the Classification of Soil by Soil Scientists," Soil Sci. Soc. Amer. Proc., bull. 17, pp 138-143.

P.A. Wichmann, (1971), "Neutron Activation for Elemental Determination in Boreholes," in SPWLA Twelfth Ann. Logging Symposium, Dallas, Texas, May 1971. See Nuclear Science Abstract No. 26-3347.

Wilkes, P.F., (1970), "The Installation of Piezometers in Small Diameter Boreholes," Geotechnique, vol. 20, no. 3, pp 330-333.

Willard, R.J., and McWilliams, J.R., (1969), "Micro-structural Techniques in the Study of Physical Properties of Rock," Int. J. Rock Mech. Min. Sci., vol. 6, pp 1-12.

Williamson, W.O., (1955), "Lineation in Three Artificial Tectonites," Geol. Mag., vol. 92, pp 53-62.

## BIBLIOGRAPHY (Cont'd.)

Wilson, G., (1968), "The Square Tube in Subsurface Exploration," Paper 11, Proc. In-Situ Investigations in Soils & Rocks, British Geotechnical Soc., London, pp 135-143, May 1968.

Wroth, C.P., and Hughes, J.M.O., (1972), An Instrument for the In-Situ Measurement of the Properties of Soft Clay CUED/C - Soils TR 13.

Wroth, C.P., and Hughes, J.M.O., (1973), "An Instrument for the In-Situ Measurement of the Properties of Soft Clays," Proc. Eighth Int. Conf. Soil Mech. and Found. Engin., Moscoe.

Wu, T.H., (1958), "Geotechnical Properties of Glacial Lake Clays," Proc. Amer. Soc. of Civil Engin., vol. 84, no. SM3, p 34.

Yong, R.N., and McKyes, (1969), "Advances in Consolidation on Theories for Clays," Proc. Spec. Session No. 12, Seventh Int. Conf. on Soil Mech. and Found. Engin. Pub. Soild Mech. Div., University of Waterloo, Canada, pp 81-98, Discussion pp 136-137.

Yong, R.N., Japp, and How, G., (1971), "Shear Strength of Partially Saterated Clays," Proc. of the Fourth Asian Reg. Conf. on Soil Mech. and Found. Engin., Bangkok, vol. 1, pp 183-187.

Yong, R.N., and McKyes E., (1971), "Yield and Failure of a Clay Under Triaxial Stresses," Proc. Amer. Soc. of Civil Engin., vol. 97, no. SM1, pp 154-176.

Yudhbir, and Prasad, B., (1973), "Discussion of Soil Parameters for Design of Mt. Baker Ridge Tunnel in Seattle," Proc. Amer. Soc. Civil Engin. J. of Soil Mech. and Found., vol. 99, no. SM11, pp 1023-1025.



TE 662

.A3

no. FHWA-RD- 74.

C-2

BORROWE

~~BDM~~

DOT LIBRARY



00054584

